THE UNIVERSITY
of EDINBURGH

This thesis has been submitted in fulfilment of the requirements for a postgraduate degree (e.g. PhD, MPhil, DClinPsychol) at the University of Edinburgh. Please note the following terms and conditions of use:

This work is protected by copyright and other intellectual property rights, which are retained by the thesis author, unless otherwise stated.
A copy can be downloaded for personal non-commercial research or study, without prior permission or charge.
This thesis cannot be reproduced or quoted extensively from without first obtaining permission in writing from the author.
The content must not be changed in any way or sold commercially in any format or medium without the formal permission of the author.
When referring to this work, full bibliographic details including the author, title, awarding institution and date of the thesis must be given.

MAPPING THE ECONOMIC POTENTIAL OF WAVE ENERGY: GRID-CONNECTED AND OFF-GRID SYSTEMS

A thesis submitted in partial fulfilment of the requirements for the award of an Engineering Doctorate

Ciaran Frost
The University of Exeter
August 2018

In memory of Louis Gillespie.

IDCORE

This thesis is submitted in partial fulfilment of the requirements for the award of an Engineering Doctorate, jointly awarded by the University of Edinburgh, the University of Exeter and the University of Strathclyde. The work presented has been conducted under the industrial supervision of Albatern Ltd. as a project within the Industrial Doctoral Centre for Offshore Renewable Energy (IDCORE).

Abstract

In recent times there has been a surge in renewable energy investment, as costs fall and the full danger of global warming is realised by policymakers. As well as more established industries, like wind and solar power, there is also high interest in pre-commercial technologies with significant potential. Wave energy fits into this category and has a number of advantages that make it a subject of ongoing research and industrial activity. An energy dense resource, it is easier to forecast than wind and fits the seasonal demand profile well. A global capacity of the order of hundreds of gigawatts has been estimated, with a particularly strong resource in the UK.

Despite these characteristics the industry has yet to reach a commercial level. No company has been able to demonstrate consistent energy production at a cost effective rate. Viable project locations must balance an energetic resource with conditions that allow devices to be accessed for maintenance, while also trying to minimise system costs. While utility scale farms are seen as the long term future for the technology, off-grid hybrid systems could supply cheaper and dispatchable energy at local levels. This market, while smaller, is made up of more costly forms of energy so provides a better entry market. Conventional economic analyses for both types of systems tend to be performed for single locations at a time. While useful for benchmarking the technology, these methods are of limited use for site scoping as energy production and costs can show large variation over relatively short distances (<10 km).

This research thesis describes a geospatial economic model that has been created to address the above issues. It was developed in collaboration with Albatern, a wave energy developer, who provided their expertise and helped to guide the research activities. The targeted application was to allow economic assessment of Albatern's "WaveNET" device, either as a power station for grid connection or an off-grid hybrid solution for aquaculture applications. The model has a number of aspects that are of significant interest to the industry. These include computational model design and geographic calculation of energy production, costs and Levelised Cost of Energy (LCOE). The spatial approach is valuable as a whole area can be evaluated at a time, indicating deployment locations particularly suitable for the technology at hand. Sensitivity analysis is also easily carried out, to build understanding of the cost drivers at specific locations.

The theory underpinning the model and its implementation is described. It

is then demonstrated with two representative case studies: considering grid-connected and off-grid WaveNET device demonstrators on the West Coast of Scotland. The results show the strengths of the approach as a way of identifying economically viable hotspots and the main cost drivers. For the grid-connected case, examining an area of 150 by 250 km, the model was able to identify a significant LCOE hotspot between the Isle of Skye and the Outer Hebrides. The potential for the device to power a fish farm, when combined with a battery bank and diesel generator, was then analysed. Two regions were examined and real fish farm locations considered. The output results allow easy comparison between the two system types, emphasising the advantages of investigating both to inform business activity.

Acknowledgements

Overall I greatly enjoyed this research, and feel like I have learnt a lot. I could not have done it without the help of many different people.

Firstly I want to thank my lead academic supervisor, Prof. Lars Johanning from the University of Exeter. He has been very supportive throughout, especially over the last year, and his wisdom has been invaluable. I would also like to thank my other academic supervisors, Dr. Ewen Macpherson and Dr. Phil Sayer. Their input was especially helpful in the early and mid stages of the project, and helped shape the structure of the thesis and direction of the work. Prof. David Ingram, the Programme Director of IDCORE, should also be thanked for his support and for playing such a key role in the IDCORE doctoral training centre. My thanks also extends to Energy Technologies Institute (ETI) and the RCUK Energy Programme for funding IDCORE (Grant Number EP/J500847/1).

Secondly I want to thank my old colleagues of Albatern. David Findlay, my Industrial Supervisor, played a pivotal role in guiding the model direction and research focus. Other key figures were David Campbell, Vivien Mavel and Danny McLaughlin, although everybody there imparted wisdom to me at some stage. My thanks also extends to my current employers at BVG Associates, who have given me the flexibility to get the thesis completed.

I also want to thank my fellow IDCORE colleagues: Steve Allsop, Enrico Anderlini, Leah Barker-Ewart, Claire Canning, Rob Clayton, George Crossley, Stephanie Mann, Scott McKirdy, Donald Noble, Simon Reynolds, Sunny Shah, Marco Sepulveda Gutierrez and Siobhan Vaughan. I could not have hoped for a better group of people to have gone on this journey with, and have enjoyed the fun that we have had over the last five years.

I would like to thank my friends and family. My parents, Richard and Marguerite Frost, have been extremely supportive, helping me with proof reading and sending me microwavable rice and dark chocolate to help cope with the writing! My girlfriend, Stephanie Lawrie, has also been extremely supportive by listening to my thesis-related issues and helping to proof read. My sisters, Aileen Frost and Louise Spencer, were also extremely helpful in this regard.

This has been a big part of my life, and I look forward to the next adventures in the exciting world of renewable energy.

Declaration

I declare that this thesis was composed by myself, that the work contained herein is my own except where explicitly stated otherwise in the text, and that this work has not been submitted for any other degree or professional qualification except as specified.

Parts of the work outlined in this thesis have been published:

- C. Frost, D. Findlay, E. Macpherson, P. Sayer, and L. Johanning, A model to map levelised cost of energy for wave energy projects, *Ocean Engineering*, vol. 149, pp. 438-451, 2018.
- C. Frost, D. Findlay, E. Macpherson, P. Sayer, and L. Johanning, Mapping Economic Performance of Wave Energy in *Proceedings of Renew2016*, 2016.
- C. Frost, D. Findlay, E. Macpherson, P. Sayer, and L. Johanning, "Global market potential for small scale wave energy." Presentation at the International Conference on Ocean Energy (ICOE), Edinburgh, 2015.

Ciaran Frost
26th of April, 2019

Contents

List of Figures

List of Tables

Nomenclature

Acronyms

BOEM Bureau of Ocean Energy Management

CAPEX Capital expenditure

CfD Contract for difference

COE Cost of energy

DECEX Decommissioning expenditure

EIA Environmental impact assessment

EMEC European Wave Energy Centre

EngD Engineering Doctorate

FMEA Failure mode and effects analysis

GIS Geographic information system

GUI Graphical user interface

IDCORE Industrial Doctoral Centre for Offshore Renewable Energy

LCOE Levelised cost of energy

MPA Marine protected area

NPC Net present cost

O&M Operations and maintenance

OOP Object-orientated programming

OPEX Operational expenditure

PTO Power take-off

PV Photovoltaic

R&D Research and development

RHIB Rigid-hulled inflatable boat

ROC Renewable obligation certificate

SARF Scottish Aquaculture Research Forum

SOC State of charge

SPA Special protected area

TRL Technology readiness level

UML Unified modeling language

WEC Wave energy converter

WSM Weighted sum method

Greek Symbols

Δt Length of time step for off-grid simulation

η Total device efficiency

η_i Input power conversion efficiency (battery)

η_o Output power conversion efficiency

η_{rt} Round trip efficiency of battery

ρ_{material} Density of mooring line material

ρ_{seawater} Density of seawater

τ_{ac} Average window length for a specific access significant wave height

Roman Symbols

b Scale parameter (3-parameter Weibull distribution)

c Capacity fraction that holds available charge (kinetic battery model constant)

C_{charter} Total vessel charter cost for a marine operation

C_{fuel} Total vessel fuel cost for a marine operation

C_{ns} Total non-spatial cost for a marine operation

$C_{\text{op total}}$ Total cost for a marine operation

C_{opl} Non-spatial costs defined within `MarineOperation` class instance

C_{port} Total non-spatial costs defined within `Port` class instance

C_{standby} Total vessel standby cost for a marine operation

C_{TMaP} Total cost for maintenance at port operation in a given month

c_c Vessel charter cost per day

c_d Vessel demobilisation cost per day

c_f Cost of vessel fuel per litre

c_m Vessel mobilisation cost per day

c_s Vessel standby cost per day

C_T Total count of sea states in given time period

C_v Total vessel cost for a marine operation for a given month

$C_{H_s>H_b}$ Count of sea states with H_s above bin edge H_b

D_{ch} Mooring chain diameter

d_{port} Distance from port to site

D_m Number of days in a given month

E_{d} Energy desired by the load at a given time step

$E_{\text{max, in}}$ Maximum energy that can be put into energy source (battery) in a given time step

$E_{\text{max, out}}$ Maximum energy that can be produced by an energy source

$E_{\text{min, in}}$ Minimum energy that an energy source must supply

$E_{\text{OG,m}}$ Monthly "useful" energy produced by the off-grid system (used to satisfy energy demand)

E_{OG} Total "useful" energy produced by the off-grid system (used to satisfy energy demand)

E_{out} Energy produced by an energy source at a given time step

F Fuel consumed by vessel for given number of hours

f_L Mooring line length multiplier (`Line` class)

h Displacement of mooring line fairlead from the seabed

H_{ac} Threshold significant wave height for a given marine operation

$H_{\text{cut-in}}$ Cut-in significant wave height

$H_{\text{cut-out}}$ Cut-out significant wave height

H_s Significant wave height of sea state

$I_{\text{c, max}}$ Maximum battery charge current

$I_{\text{d, max}}$ Maximum battery discharge current

k Rate constant (kinetic battery model)

k Shape parameter (3-parameter Weibull distribution)

L_{final} Final mooring line length as calculated by the `Line` class

l_{min} Mooring line length (minimum potential length)

m_{dry} Mooring line dry mass per metre

N_{ac} Number of days that site can be accessed in a given time period for a given significant wave height

N_{rt} Number of round trips to/from site

$P_{\text{i,j}}$ Device power for power matrix element (i, j)

$P_{\text{max, in}}$ Maximum power that can flow into energy source (battery)

$P_{\text{max, out}}$ Maximum power that energy source can generate (before losses)

P_{max} Maximum output power specified for device (grid-connected)

$P_{\text{min, in}}$ Minimum power that an energy source must generate

P_{rated} Rated power

P_h Probability of exceeding given significant wave height (exceedance probability)

$P_{m_{\text{i,j}}}$ Modified device power for power matrix element (i, j)

q Initial battery capacity at start of off-grid simulation time step

q_0 Nominal battery capacity

q_{max} maximum capacity of the battery (kinetic battery model constant)

q_{min} Minimum battery capacity allowed

r Discount rate

R_{min} Diesel generator minimum load ratio

R_{travel} Fuel consumption rate when vessel is travelling

R_{work} Fuel consumption rate when vessel is working

S_{min} Minimum battery state of charge allowed

T Mooring line tension tangential to mooring line

t Time period

t_{from} Time to travel from site

t_{MaP} Total time for maintenance at port operation

T_{max} Mooring line maximum resultant tension

t_{resting} Total time resting between multiple trips to site for a given operation

t_{site} Total time spent on site carrying out an operation

$t_{\text{task,d}}$ Total time spent carrying out a marine operation (in days)

t_{task} Total time spent carrying out a marine operation (in hours)

t_{to} Time to travel to site

t_{travel} Time that vessel spends travelling for a given operation

t_{waiting} Total time waiting for suitable weather window to carry out operation

t_{work}	Time that vessel spends working for a given operation
t_d	Number of days to demobilise vessel
T_E	Energy period of sea state
T_H	Horizontal mooring line tension
t_m	Number of days to mobilise vessel
T_p	Peak period of sea state
T_Z	Vertical mooring line force at the fairlead
V	Battery voltage
v_{av}	Average vessel speed considering journey to and from site
v_{from}	Average vessel speed from site
v_{to}	Average vessel speed to site
w	Mooring line submerged weight per unit length
X	Horizontal displacement of mooring line
X_0	Location parameter (3-parameter Weibull distribution)
X_{ac}	Length of weather window required for a given operation

Introduction

1.1 Motivation

All over the world, policymakers are seeing the importance of supporting the renewable energy industry. The effects of climate change are being seen and the danger is apparent in people's minds. This, combined with the plummeting costs of renewable energy technologies, means that the transition to a low carbon society is not only a necessity, but also contains a number of lucrative business opportunities. The wider industry is indeed growing and building momentum, as more and more organisations are divesting from fossil fuels.

Within the UK electricity sector, the brunt of development has come from the wind, solar and bioenergy industries. Along with hydro these generation technologies provided 26.6% of electricity generation in the first quarter of 2017 [1]. However, despite some progress, there is much work to be done in securing a low carbon future. One example that demonstrates this concerns the EU renewable energy directive, which targets 20% of energy from renewable sources across its member states by 2020 [2]. While several countries have exceeded their targets [3], the UK is lagging behind and is predicted to miss its 2020 target of 15% [4, 5].

1.1.1 Economic modelling: a research priority

Despite the resource size and potential advantages, wave energy as a concept is still in its infancy. The industry is currently in a pre-commercial, research and development (R&D) stage, with no company selling devices to produce energy or

turning over profits from selling electricity directly. The main reasons for this start at the technical challenge. The marine environment is a harsh one, especially in the high energy locations that are traditionally thought of as best suited for wave energy extraction. While the offshore wind industry has learnt from the onshore wind and oil and gas industries, (marine structures in the case of the latter), wave energy does not have a similar precursor. Tidal stream energy, once thought of at a similar stage to wave energy [6], has pulled ahead as it can take advantage of decades of learning in the wind energy industry due to similarities in the rotor design. To design a device capable of not only surviving but also generating suitable amounts of electricity in the marine environment is a difficult task. The industry is yet to converge on a specific device concept in the way that other industries have (for example the horizontal axis turbine in the wind industry) which makes developing industry standards difficult, although there have been attempts (for example [7, 8]).

While the technical challenge is clearly an overriding factor, dedicated computational tools are also a high priority for the industry. To make the transition to a viable commercial industry the main economic drivers need to be understood and quantified. Numerical modelling provides an invaluable, low cost way to determine these drivers by assessing the performance, costs and economic potential of a specific technology. These metrics are of great interest to multiple parties. For developers, it allows them to benchmark the progress of their technology and make informed design decisions in order to create the optimum energy capture system for a given project. It also allows them to see which project aspects incur the highest costs, informing future R&D activity. Additionally it will be easier for a developer to unlock further funding if they can demonstrate that they are actively working towards a market ready product, improving investor confidence and helping to inform future business direction (for example aiding market research). For investors, such modelling work can help to determine if a concept is worth investing in and can quantify the level of risk. For policymakers, vital insight can be gained into how the industry is progressing and the areas where public funding would deliver the best value.

Such an economic model has been developed for this thesis, designed to encourage the advancement of the wave energy industry. While there have been other models used in the literature, this research has a number of unique aspects that are of significant interest to the industry, including geographic calculation of energy production, costs, and Levelised Cost of Energy (LCOE) for both grid and off-grid systems. This spatial approach is particularly valuable as it allows

the most suitable sites for projects to be determined, indicating the locations and markets that would best suit the technology at hand. It also bridges the gap between the technical and non-technical aspects of the wave energy system. Consenting and Environmental Impact Assessment (EIA) are significant factors for wave energy, over which there is a lack of clarity over the processes that must be undertaken by the developer [9]. These will be location specific as they will be dependent on local environmental issues. Knowledge of the most suitable wave energy deployment locations would help policymakers choose suitable demonstration zones and streamline the consenting processes required for projects in those areas.

1.2 Industrial Partnership

1.2.1 IDCORE

This research was conducted to satisfy the requirements of an Engineering Doctorate (EngD). The EngD has been carried out at the Industrial Doctoral Centre for Offshore Renewable Energy (IDCORE). IDCORE is a doctoral training centre that is operated by a consortium of partners: The University of Edinburgh, the University of Exeter, the University of Strathclyde, the Scottish Association of Marine Science (SAMS) and HR Wallingford.

1.2.2 Albatern Ltd.

The industrial partner and sponsor for the research project was Albatern Ltd, a wave energy developer. Albatern are based in Roslin, just outside Edinburgh, and are currently developing the WaveNET device. This is an array based concept, made up of modular units known as "Squids". A central theme of the device is that that arbitrary numbers of these modules can be combined together to suit the desired application, with the quantity and array configuration optimised to minimise LCOE. The system can offer redundancy through utilising many Squids; individual units can be removed and swapped out for maintenance, leaving behind a fully functional array.

Figure 1.1 shows the main system components for the Series-6 WaveNET class and Figure 1.2 some photographs of the device. The device floats on the surface of the water and generates power via a hydraulic system. The power production is driven by the relative motion of the device anti-nodes and risers which activate the

pumping modules, pumping hydraulic fluid through a hydraulic motor/generator.

The Series-6 Squid was originally sized to fit on the back of an articulated lorry for ease of operations (as shown in Figure 1.2). The current device is small scale in nature, each Squid unit rated at 7.5 kW and weighing approximately ten tonnes. For comparison a single Pelamis P2 machine, one of the most well-known utility scale device concepts, was rated at 750 kW and weighed 1300 tonnes [10]. Two further device classes are in development, the Series-12 and Series-24, which are both physically larger. This is to increase energy capture, improve survivability in more extreme wave environments and take advantage of lower relative costs through economies of scale. Figure 1.3 shows the relative sizes of the three concepts. It is thought that these three standard sizes will together be able cover the vast majority of viable deployment locations and markets.

The WaveNET has undergone several rounds of testing to the present date; the main milestones are displayed in Figure 1.4. Arguably the breakthrough deployment was in 2014 at the Isle of Muck. This was the first major sea deployment for the current generation of Squid modules (the Squid 6.2) and resulted in Albatern gathering increasing interest within the wave energy community. This deployment has been followed by further testing at Kishorn Port in 2015 and early 2016, and most recently a pilot project in Glenmore Bay, currently ongoing.

Because of its small scale, it is thought that the Series-6 WaveNET is better suited to off-grid hybrid applications. Both these systems and more conventional grid-connected applications are incorporated into this research project.

During the research project the author was based at Albatern for approximately 30 months (June 2014 to January 2017), working as part of the company full time. As well as EngD research, work also involved commercially focused work and other day to day activities to support the business. The EngD focus evolved over time, being driven by both Albatern's business needs and developing knowledge

1.3 Research Aim and Objectives

The primary aim of the research was the following:

To develop an economic model capable of identifying the most suitable geographic locations for localised wave energy projects.

To meet this, the following project objectives were devised:

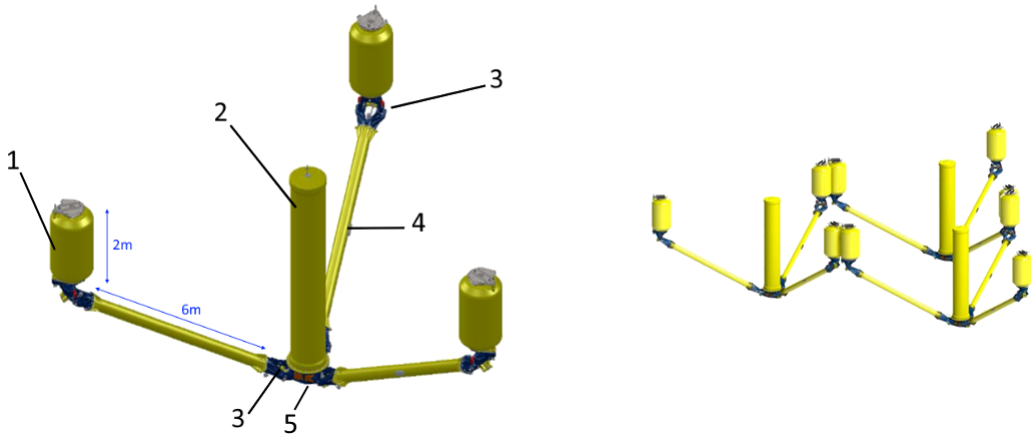

Figure 1.1: Left: A single Squid module for the Albatern Series-6 wave energy device concept, made up of: three floats or "anti-nodes" (1), a riser (2), six pumping modules (3), three link arms (4) and a central node (5). **Right:** A triangular array of three Squid modules joined together. Images provided by Albatern Ltd.

Figure 1.2: Photographs of the Albatern Series-6 WaveNET system. **Left:** Single Squid getting transported to site. **Middle:** Single Squid on the dock awaiting deployment. **Right:** WaveNET array being tested at the Isle of Muck (three Squids). Images provided by Albatern Ltd.

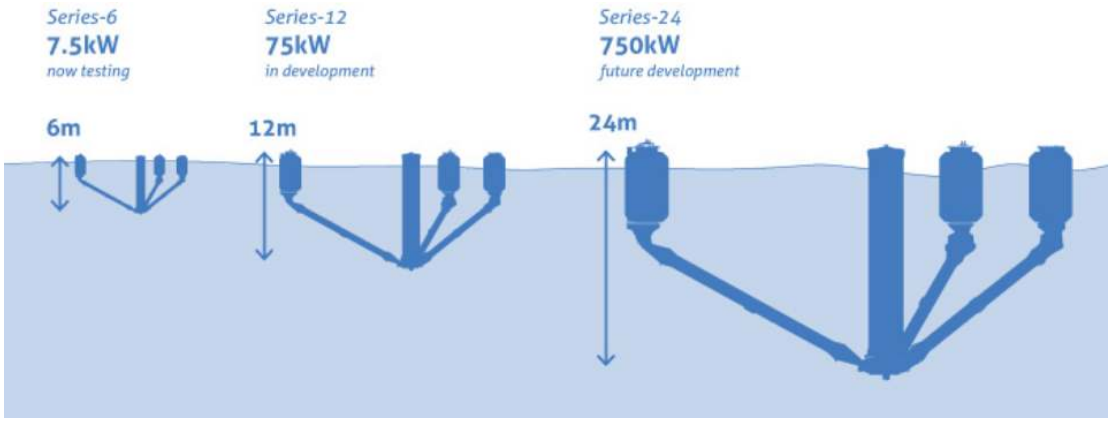

Figure 1.3: The three different classes of WaveNET envisioned by Albatern, with sizes aimed at different markets and applications. Image provided by Albatern Ltd.

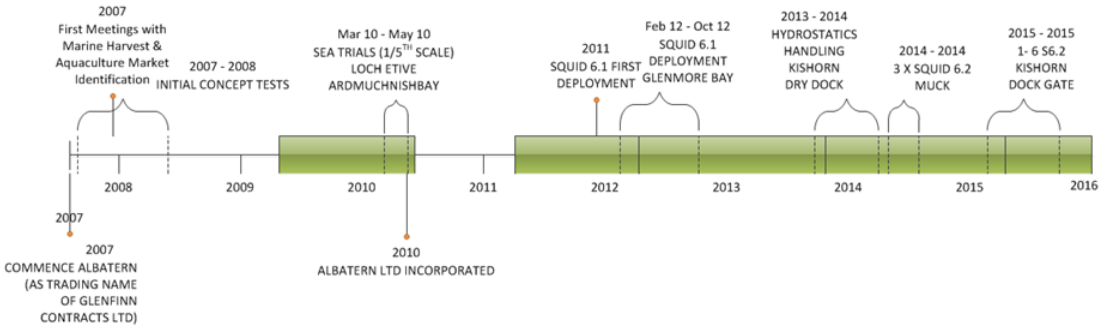

Figure 1.4: Historical device deployments and milestones related to the WaveNET Series-6 concept.

1. Review previous wave energy economic assessments and models to understand the major industry requirements and factors that such an economic model should include.

2. Develop a detailed, robust methodology that computationally applies the various theoretical aspects in a practical and structured way.

3. Develop a modular economic model, capable of estimating the performance and main costs of a wave energy project using spatial input data. Include the ability to consider both grid tied and off-grid wave energy systems, and build up the model in a generic way, so that it is of interest to the wider industry and not rigid to a single device concept.

4. Demonstrate the model by applying it to grid-connected and off-grid case studies, showing the potential of the approach and indicating suitable sites for small scale WaveNET arrays.

1.4 Contribution to Knowledge

The main contributions to existing knowledge from this work have been identified as the following:

- A practical application of object-orientated programming (OOP) methodology to marine energy economic assessment.
- A geospatial energy, cost and LCOE analysis tool, with focus on bottom up calculation methods.
- Spatial calculation of operation and maintenance (O&M) cost , including weather window calculation and transit considerations.

- Development and application of a hybrid energy "power balancing" algorithm to an off-grid system with wave energy input, to calculate LCOE of the system.
- Spatial hybrid LCOE analysis tool, designed to allow promising locations for off-grid wave systems to be determined.

1.5 Method Statement

To demonstrate the contributions to knowledge and address the overall research aim, the thesis is structured in the following way:

- **Chapter 2** provides the background context to the research, exploring previous LCOE modelling work. This includes techno-economic modelling, spatial economic assessments and off-grid hybrid energy systems.
- **Chapter 3** describes the core computational model that has been created to spatially model grid-connected wave energy systems. This covers theory, computational design and implementation. It includes the programming aspects, detailing the practices and assumptions as well as the main limitations that are present.
- **Chapter 4** describes the off-grid model that is used to simulate hybrid wave energy systems. This is considered a sub-module of the core model, extending the overall functionality to include niche wave energy applications. The content is similar in scope to the previous section, again focussing on module structure and implementation.
- **Chapter 5** demonstrates the core model, using the Albatern device as a case study. A baseline case study is presented, using estimates from the available data, to map the LCOE for an early demonstrator project deployed on the West Coast of Scotland. Sensitivities are examined to see the relative impacts of different model parameters on the costs and LCOE.
- **Chapter 6** demonstrates the off-grid sub-model. Again considering the West Coast of Scotland, a hybrid wave energy system to power a fish farm is considered. The LCOE is compared to a traditional diesel generator solution and sensitivities are considered.
- **Chapter 7** discusses the results, framing them in a wider context and in terms of the overall methodology.
- **Chapter 8** completes the thesis with some concluding remarks and ideas

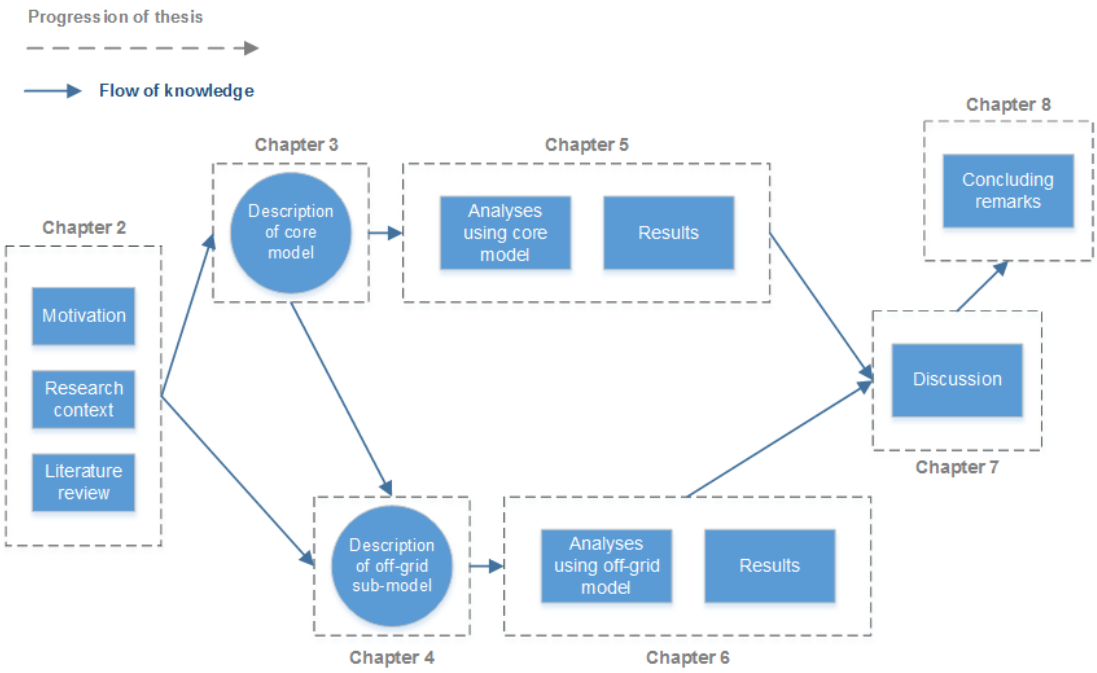

Figure 1.5: The structure of the thesis, with chapters working left to right. Blue arrows represent the flow of knowledge in the thesis. Circles denote the two chapters which describe the key modelling theory and implementation.

for future work.

This structure is represented pictorially in Figure 1.5. The chapters propagate left to right, the arrows denoting the flow of knowledge through the thesis. For example, the themes within the off-grid model theory section are guided by both the background context from Chapter Two and the previous modelling theory from Chapter Three.

Research Context and Literature Review

2.1 Wave Energy

Wave energy is a form of renewable energy which allows the kinetic energy of sea waves to be captured and converted into electricity. It is predominantly a third hand form of solar energy: the differential heating of the Earth's surface creates winds which transfer energy to the water surface [11]. While there are many device concepts at present, energy is typically produced by a device through a prime mover that is perturbed by the wave motion. While the concept of wave energy has existed for some time, with the first patent being filed as early as 1799 [12], the first offshore device to be grid-connected only occurred as recently as 2004 [13]. Since then there have been various demonstrators tested in the water, but no commercial projects.

One of the early wave energy pioneers was Yoshio Masuda. Working in Japan in the 1940s he developed a wave-powered navigation buoy which worked by forcing air through a turbine [14]. This is the same principle which modern oscillating water column concepts use. In Europe, the first serious wave energy funding programme was set up in the UK in the 1970s. This came as a result of the 1973 oil crisis, which saw the oil price dramatically rise, and the early work of Stephen Salter, whose nodding duck concept and 1974 publication in the journal Nature attracted attention in the scientific community [15, 16]. The UK government, with the aim of limiting the reliance on oil, supplied funding through an R&D

programme known as the Wave Energy Program [17]. This ran from the mid 1970s to the early 1980s, after which almost all funding was cut. This was due to the oil prices stabilising and the unrealistic, politically motivated, expectations of the government for wave energy, who did not see it as cost competitive as first anticipated [18]. After 1982, almost all government funding ceased until the 1990s, when interest was reignited by an increased awareness of climate change and the need to reduce CO_2 emissions. New policy was introduced, for example by the European Commission in 1991 who included wave energy in their R&D funding programme [14], and the UK government who introduced a small scale R&D programme of their own in 1999 [18].

As a concept wave energy has a number of advantages that would make it a useful contributor to electricity demand. Because the resource has a high energy density, output is more predictable than wind energy and solar energy, being less prone to temporal fluctuations and easier to forecast [19]. The resource is also not restricted by the diurnal cycle like solar, and follows seasonal demand much better: with more energetic waves in the stormier winter months where electricity demand is higher. Wave also has a number of environmental advantages compared to offshore wind and tidal stream. Generally it is thought that wave devices would be less risk to sea birds [20], as they tend to be on or below the water surface without a rotor, although collisions from diving birds would be possible [20, 21]. The visual and noise impacts are also lower, which could mean a more straightforward and cheaper consenting process. There are also potential positive environmental impacts not unique to wave, including habitat enhancement and the potential for environmental protected zones directly in the vicinity of the devices, although more research needs carried out to quantity the impacts [21, 22]. Lastly, wave energy could offer advantages to existing offshore energy systems; combined offshore wind and wave are commonly considered. Such systems could reduce costs (for example in the transmission network [23] or mooring system [24]), offer more consistent power with less variability [25] and the wave devices could offer some protection from challenging wave conditions to improve accessibility [26, 27].

2.1.1 Anatomy of a wave energy system

Unlike wind energy, wave energy is two dimensional, with reliance on both the wave height and the wave period. This, combined with the fact that there are six potential degrees of freedom for a body in the marine environment, means that there are many different ways that wave energy can be extracted. While the wind industry has overwhelmingly converged on a single design, the horizontal

axis wind turbine, the wave resource is more complex and hence many different approaches to energy capture still exist.

Despite this, there are some key systems which are fundamental to any device concept. An example of how these systems are defined and interlink with each other, as devised by DNV GL, is shown in Figure 2.1 [28].

1. **Hydrodynamic Subsystem**: This subsystem includes the main structure of the wave energy converter (WEC), including the hull. The structural elements must be designed to survive in the marine environment and hence are typically designed to be durable and heavy. The physical size of this system will influence how suitable it is for energy capture. It is anticipated that the industry will converge on a small number of device types, a similar trend as seen in the wind industry [29].

2. **Power take-off (PTO) Subsystem**: At the heart of the WEC is the PTO . Its role is to produce electricity from the relative movement within the hydrodynamic subsystem. There are various design concepts in development. These can be classified into two main types: linear systems and rotary systems, which are defined by the generator configuration that is used [30]. Historically rotary systems have been seen more frequently and is the method of choice for Albatern. They use a hydraulic system, converting the motion of the device into electricity by driving hydraulic rams. The advantage of this system is that components can be directly integrated

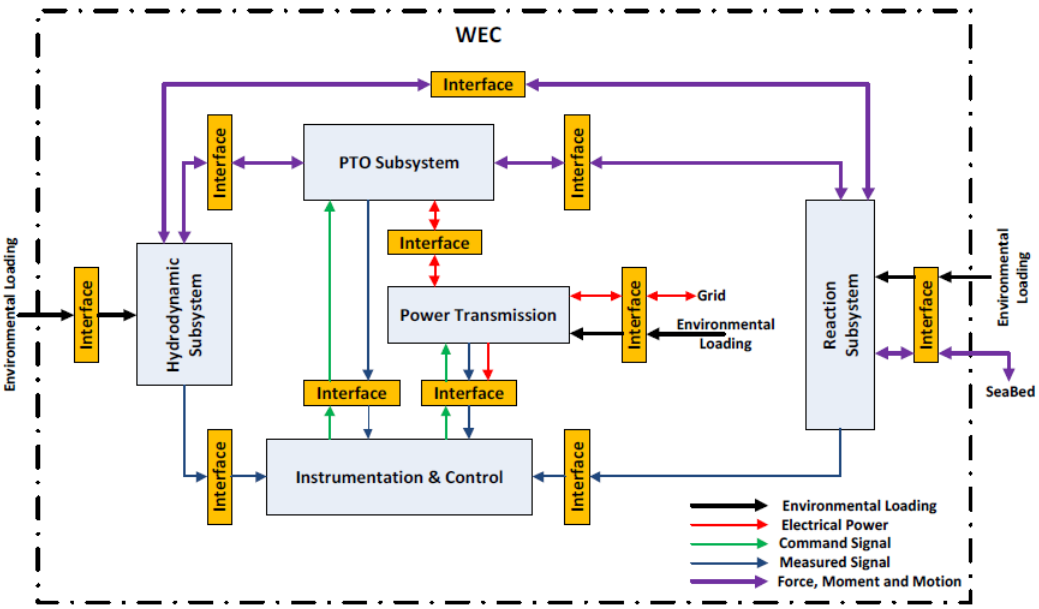

Figure 2.1: Main components of a wave energy system as defined by DNV [28].

to provide short term energy storage and passively smooth out the output power, for example high pressure accumulators. As they use common, off the shelf components [31], costs tend to be lower and supply chain issues are reduced. By contrast the linear PTO system is generally regarded as more efficient and requires less maintenance than hydraulic systems [31], thus is well suited for systems where accessing the PTO is more challenging (for example structures fixed to the seabed).

3. **Power Transmission**: Once power is produced it must be routed to shore. Multiple WEC units will be installed together in farms and connected with inter-array cables. In some cases, particularly for larger farms that are further from shore, an offshore substation might be required to boost the voltage and hence reduce electrical losses in transmission. As these platforms can be very costly many developers will avoid them in early farms, instead combining the inter-array cables within a junction box fixed to the seabed. The power is then sent to shore using an export cable. These tend to be AC cables, matching the electricity type produced by the PTO generators.

   For the Albatern device there are some notable differences to the conventional approach. As all of the Squid units are directly linked together there is no need for array cabling, and the junction box can be housed within one of the Anti Node floats. Additionally, rectification is also carried out within the PTO system: converting the voltage to 1 kV DC. This means that the export cable is a cheaper two-core DC rather than an AC cable.

4. **Reaction Subsystem**: This subsystem consists of the mooring system, and is designed to keep the device on station. It is an important element, as failure would be hugely costly in both financial and political terms. The specifics of the system again vary depending on the device concept, as well as the seabed conditions. For many device types, such as point absorbers, the system provides a reference point on the seabed for the device's movement. It is the movement of the device relative to this fixed point which drives the energy production. An alternative type of device is "self referencing", where energy is produced from the relative motion between elements of the WEC. The Albatern WaveNET is an example of this.

   For the mooring system the main cost drivers are the anchors and any mooring lines required to connect to the device. These costs are typically considered to make up 10-20% of the WEC capital cost [32]. For catenary mooring lines, often the length is considered to be 3-5 times the water depth

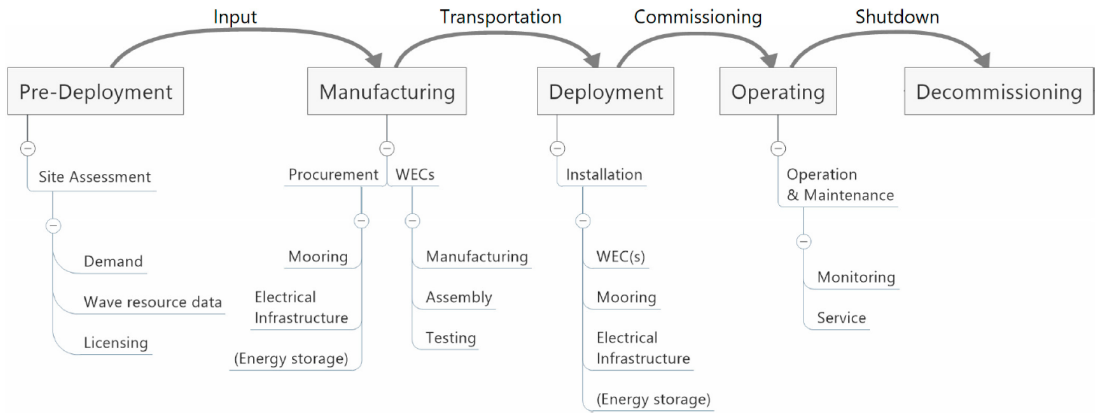

Figure 2.2: The five main stages that make up a wave energy project lifecycle. Taken from [34].

[33].

5. **Instrumentation and Control**: The primary purpose of this system is to monitor the status of the device to make sure that it is functioning as expected. For many devices there will also be a dual purpose of improving energy production, by controlling the response of the device.

Regardless of the type of WEC, there are specific stages that will make up the overall life cycle of a project. It is usually the job of economic modelling to estimate the costs incurred at each of these. One representation of the main stages is displayed in Figure 2.2, sourced from [34].

The first stage is to scope out a potential site. This will depend on the local resource but also political aspects, namely how receptive the government and local community are to the project and the investment and feed in tariff that can be secured. The consenting process can take a long time and might involve carrying out surveys and an EIA. The typical procedures required have been outlined in the literature, for example [35], however in general there is a lack of guidance on the issue which will need to be addressed as the industry moves forward [9].

Once a site has been selected and a marine license obtained, manufacturing can begin. This might involve manufacture from scratch, for the specific project at hand or, especially in the early stages, reusing infrastructure. While not suitable for all system components, reuse could reduce costs for demonstrator projects. This has been Albatern's approach, where the current Squid units have been deployed in three different locations for various levels of testing.

The ease of deployment of the WECs will depend on the nature of the device and location. Earlier projects will target locations close to shore so that the devices are easily accessible, as reliability is expected to be low. This also has

the advantage of keeping export cable costs low, a key cost driver particularly for smaller scale projects. Other environmental factors, for example strong tidal currents and rocky bathymetry will make installation more challenging [36] and might require the use of more expensive vessels.

After the WEC farm has been installed it will begin its operational life. The devices will require monitoring and maintenance, to increase the energy generated and maximise the revenue. Maintenance will be a combination of minor servicing carried out on site and more significant activities which will require bringing the devices back to port and carrying out work on land. At the end of the project the devices are then brought back to port and decommissioned. Resources might be kept for future projects, salvaged for income or scrapped.

2.1.2 Small scale wave energy

As well as larger, utility scale systems, wave energy also has significant potential at smaller scales. A so called "twin-track" development strategy, financial support for both large and small scale concepts, is an advantageous approach for the industry as it facilitates both deploying significant capacity and a rapid learning approach [37]. Smaller devices will lack the power producing potential of larger ones and cannot take advantage of the same economies of scale. It does mean, however, that the absolute costs will be much lower for early stage projects. This equates to lower financial risk for an investor, the lower costs also allowing fast innovation through learning, for example by being able to turnover multiple device iterations for a given monetary input. This approach of taking advantage of "learning-by-doing" has been seen historically for the onshore wind industry, as demonstrated in Figure 2.3. It shows the historical evolution of rotor diameter in the onshore wind industry, with commercial breakthroughs initially occurring for smaller devices [38].

For wave energy, a learning-by-doing approach is best suited for small scale devices to allow rapid expansion and demonstrate proof of concept [37]. It is a suitable strategy to promote early stage growth in the industry and build investor confidence. The best way to apply this kind of learning is through deploying devices in the water, gaining knowledge through the processes of operating and maintaining the devices. As this can be costly it does present problems for early TRL level concepts. It is for this reason that some instead promote a "learning-by-research" approach [39], whereby companies utilise research tools like tank testing and numerical modelling to lower costs and reduce risks before going into the

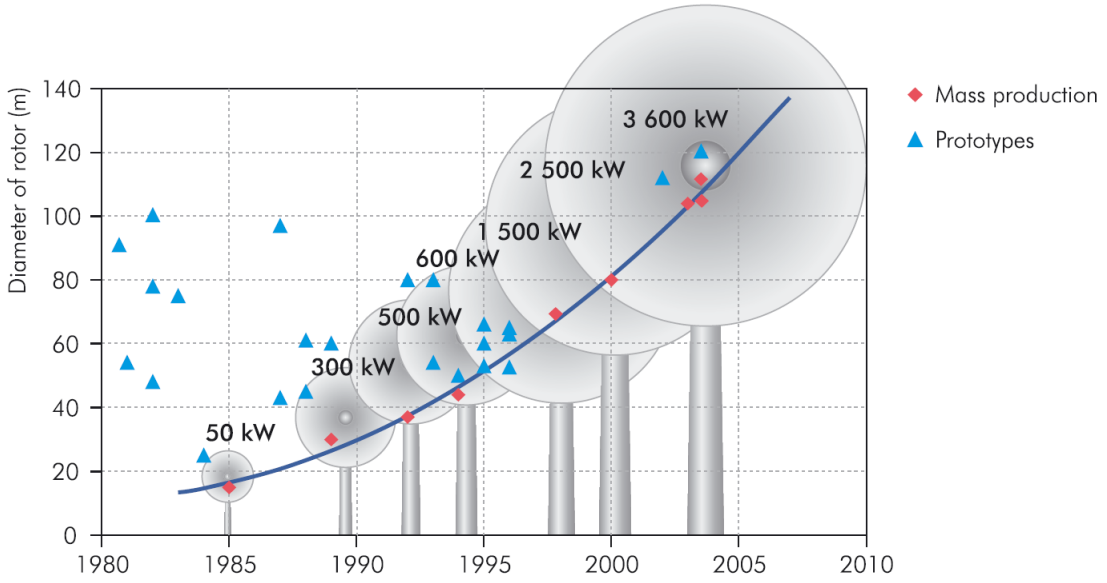

Figure 2.3: Evolution of wind turbine rotor diameter. Taken from [38].

marine environment. This is especially the case for larger devices, and also for more mature industries. For example research has suggested that there has been very little improvement attributes to learning-by-doing in offshore wind, where the technology concept is well understood and no two sites are the same [40]. Here, bigger improvement is obtained from technological innovations.

As the cost of energy is high for the emerging wave energy market, the best initial applications for these systems are thought to be off-grid. While the market is significantly smaller, electricity costs for existing systems are higher so wave energy would be better placed to compete. The solar PV industry trended to this market strategy, demonstrated in Figure 2.4, with a high proportion of off-grid installations in earlier years [41]. Examples of such off-grid applications include:

- Aquaculture (fish farms).
- Island communities.
- Oil and gas platforms.
- Military and defence.
- Oceanographic and scientific monitoring.
- Moored vessels.

While all of these have distinct energy demands, often the systems are located in remote areas and currently employ costly ways to supply energy. For example floating offshore salmon farms, the main application examined in this thesis, typically rely on diesel generators for electricity. The electricity requirements are

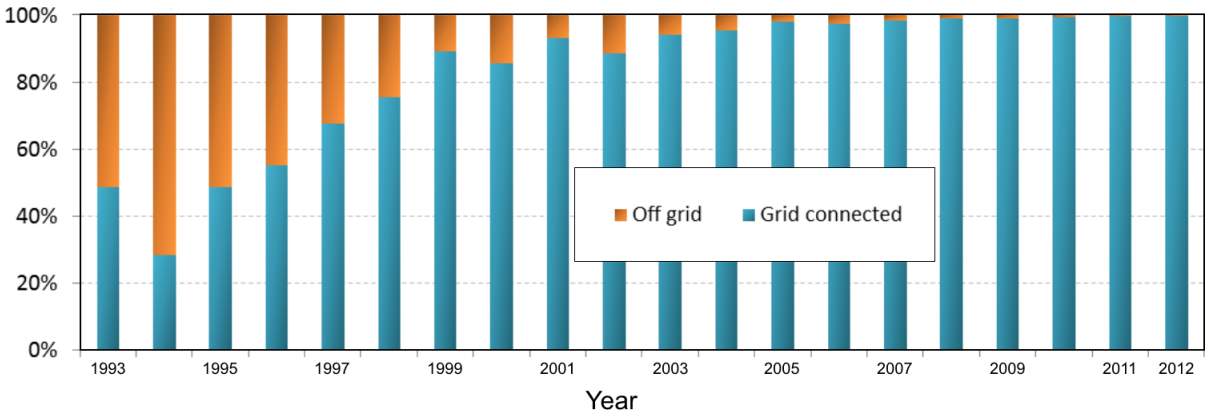

Figure 2.4: The ratio of off-grid to grid-connected solar PV system deployment from 1993 to 2012. Taken from [41].

typically at a modest level that utility, MW scale devices would be unsuitable for [42, 43]. The diesel price is higher than grid electricity prices, further realised by adding the logistical cost to transport the fuel to site. The potential synergies between wave energy and aquaculture are described further in Section 2.5.3.3.

2.2 Market Context

A wave energy industry could provide significant value to the UK, and indeed worldwide, electricity market. The theoretical resource has been estimated at two to four terawatts worldwide [44, 45]. The latter study, considering a Pelamis device, predicted that 96.6 ± 1.3 GW could be practically extracted, not considering tuning of the device for specific wave climates. By comparison the installed capacity of renewable electricity in the UK was 36.9 GW in the first quarter of 2017 [1]. The UK has a particularly favourable wave resource, with the practically extractable power estimated at 7-10 GW [11, 46]. This is primarily driven by prevailing Atlantic winds and the long fetch that allows powerful waves to build up, resulting in a resource that is thought to be 35% of the European total [47]. There would also be wider economic benefits, for example the industry could support 16,000 jobs into the 2040s [48]. Scotland has been noted as having a particularly suitable resource [49–51]. It also has a strong academic community, supply chain [48] and ambitious government renewable targets, for example to provide 100% of electricity from renewable sources by 2020 [52]. These factors mean that Scotland is a market of interest for future development.

Worldwide there has been significant interest in renewable energy of various forms. In Europe 30% of the energy generated in 2017 came from renewable sources [53], as shown in Figure 2.5. The renewable share has increased by ap-

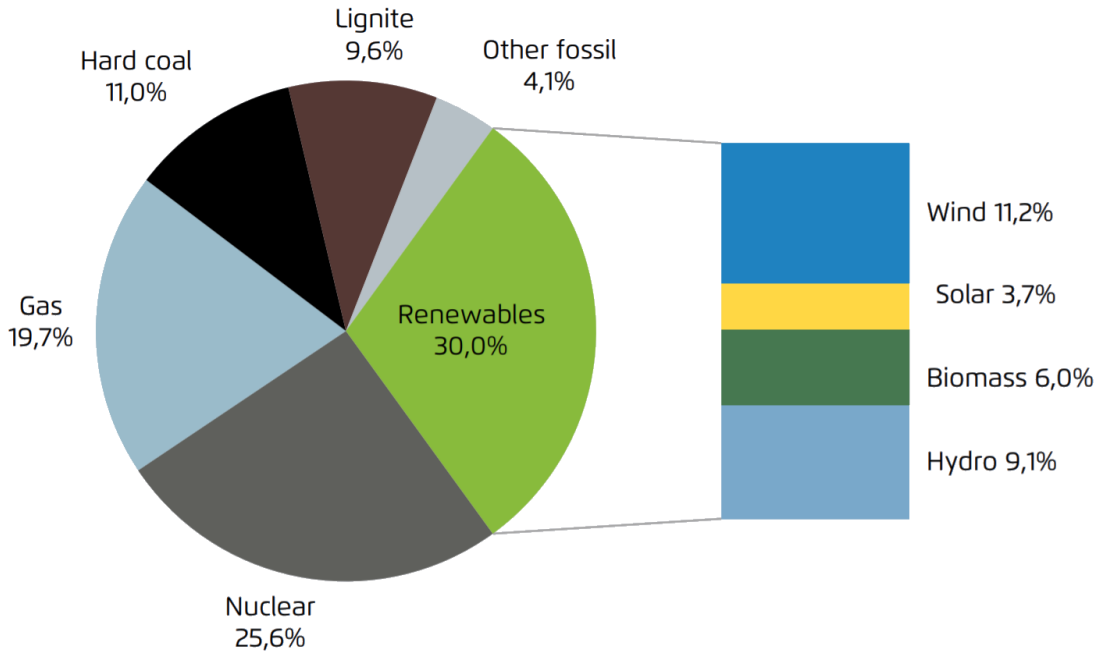

Figure 2.5: Electricity mix in Europe for 2017, by source. Taken from [53].

proximately 9.6% since 2010, with the majority from wind, solar and biomass. The main reason for this increase is down to the plummeting LCOE of the technologies, as visualised in Figure 2.6. The underlying data for this figure is from IRENA's Renewable Cost Database, their methodology meaning that the trends shown in the figure are comparable. The reduction has been facilitated by increased political and social acceptance of the industries, in the context of climate change, which has allowed increasing capacity to be manufactured and installed.

From the chart, it can be seen that solar PV and offshore wind are of particular interest because they have made the transition into the fossil fuel cost range. The equivalent learning rates are approximately 35% and 14% respectively [53]. Similar falling trends are also seen in other studies. For example Lazard's LCOE analysis presents LCOE reduction of 67% in wind and 86% in solar between 2009 and 2017 in the U.S [54].

While learning rate estimates can differ wildly depending on the worldwide location and time period considered, similar numbers are also seen in other works (for example [55], where a large number of studies are reviewed). For marine energy economic studies, learning rates in the range of 6-18% are usually considered [32, 56, 57]. Recent auctions have witnessed extremely low subsidies being awarded; for example the UK CfD Round 2 where offshore wind farms Moray and Hornsea 2 will begin generating at £74.75/MWh in 2021/22 and £57.50/MWh in 2022/23 respectively [58]. While this is highly encouraging for the renewable

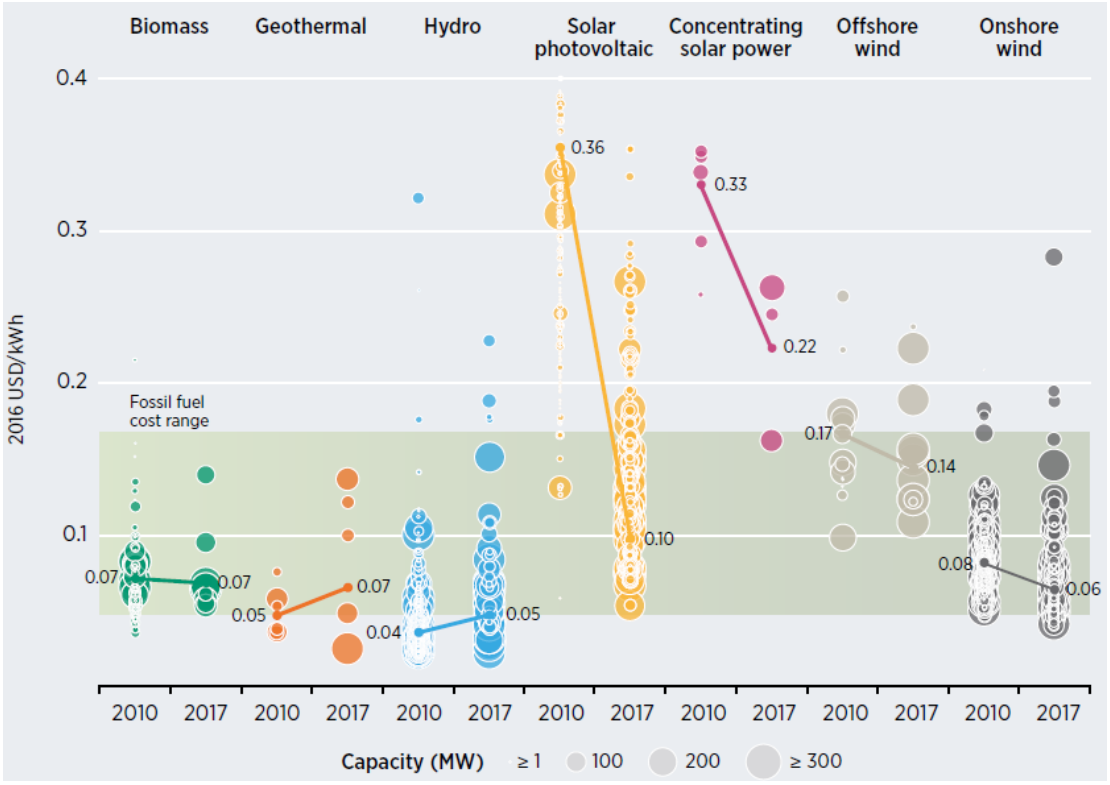

Figure 2.6: LCOE in 2017 compared to 2010 for seven renewable energy sources. These are for global projects, taking account of both project capacity and location. The thick lines show the trends in the global weighted averages across the two years. Taken from [53].

sector in general, it is problematic for less mature technologies like wave that will need more government support to get a foothold in the market. This was seen for the tidal stream Meygen project, which lost out in the same auction [59]. It was forced to compete directly with offshore wind as a higher subsidy rate "ring-fence" for marine energy projects was removed [60, 61].

A recent report, also published by IRENA, makes clear the global challenge ahead. They estimate that the deployment of renewable energy needs to see a "six to seven-fold increase" per year in order to limit global warming to 2°C by 2050, the upper threshold generally targeted by policymakers (for example the 2015 Paris Agreement [62]). It is clear that wave energy could provide meaningful contribution towards this target, despite the market challenges. This will also require the economic, business case to be established, an issue which the kind of research that is the subject of this thesis helps to address.

2.3 Elements of a Wave Energy Economic Study

While there are interesting advantages of wave energy over more conventional technologies, as previously introduced, the success of the industry will depend on

its ability to deliver at a competitive price. Understanding the performance and costs of a project are a crucial step towards building a commercial wave energy industry.

Estimating the economic potential of any energy technology should include a number of different aspects. Many of these are technology and project specific, and some can be problematic for wave energy due to limited operational experience and data availability. At the typical level, two criteria are required:

1. The total energy produced, and
2. The total cost.

This section describes the main themes which are included within these.

2.3.1 Levelised cost of energy

In the energy industry, the most common way to assess market potential is by calculating the LCOE. LCOE is defined as:

"The constant price at which electricity would have to be sold for the production facility to break even over its lifetime, assuming it operates at full capacity." [63]

Mathematically this is expressed as:

$$\mathrm{LCOE} = \frac{C_{\mathrm{PV}}}{E_{\mathrm{PV}}}\,, \tag{2.1}$$

where C_{PV} is the total cost incurred over the project lifetime and E_{PV} the total energy produced over the project lifetime. These are discounted to present values. Discounted costs are known as Net Present Costs (NPC). Discounting is a process commonly used in finance that involves reducing the values of cash flows that occur in the future by multiplying them by a time dependent factor, the discount factor. This is done to reflect the "time preference" of money: namely that cash in the present is worth more than the same value in the future, as it is subject to less uncertainty and could be invested sooner. The approach is also applied to energy with a similar logic: as it is more valuable in the present. The discount factor, D is expressed as:

$$\mathrm{D(t)} = \frac{1}{(1+r)^t}\,, \tag{2.2}$$

which is a function of the time period (commonly the year) the cash flow occurs in, t, and the discount rate r. This is a percentage that essentially represents

the level of risk in the project. It should reflect the market value of equity and debt [64]. There is a degree of subjectivity in its selection as it will depend on the return that an investor would hope to get. For wave energy the value chosen is typically in the range 5%-15% [26], depending on the commissioning date and technology maturity assumed for the project. More mature, commercial projects will have lower perceived risk and hence command lower discount rates [65, 66]. Considering D, Equation 2.1 can be expressed as a sum of the discounted cost and energy contributions for each discrete project period ($C(t)$ and $E(t)$ respectively):

$$\text{LCOE} = \frac{\sum_{t=0}^{n} C(t)/(1+r)^t}{\sum_{t=0}^{n} E(t)/(1+r)^t}. \tag{2.3}$$

It should be noted that the above equation assumes that the same discount rate is applied to every cost. In reality, different aspects of the project can be funded in different ways, with some investors willing to take more risk than others. This can be modelled by applying different discount rates for different elements of the project. One approach that is sometimes seen is using different discount rates for the capital costs and operational costs.

The calculation can be performed both in nominal (with inflation) or real (without inflation) terms by selecting an appropriate discount rate [67]. The main costs that are usually considered are introduced in the next section.

The main advantage of using LCOE as a metric is its simplicity, as it is well understood and used by developers, investors and policymakers alike. It also allows direct comparison between different sources of electricity to be easily made and the main cost drivers to be identified. Moreover, by incorporating the present value of the variables it allows risk to be introduced into the analysis.

LCOE does have drawbacks. It does not include revenue, which can vary depending on the business model chosen and could have a large impact on the potential of a given project. This is especially true for more established technologies like wind, which is moving to a zero subsidy market. In this context, where the relative costs are low, energy price and quality is a more significant consideration. For example, more dispatchable system types that can be switched on quickly to follow demand, may command a higher price in the market and thus would be more valuable to an investor in reality. For early stage wave technologies this also limits the application to business strategy. For example, competing business

models could be to directly sell devices or to keep ownership of the WECs and sell the electricity generated. Without examining the revenue the more competitive strategy could not be ascertained. Lastly, the focal point of the analysis is cost. While not a disadvantage in itself, it means that wider socio-economic and environmental factors can be neglected.

Despite these limitations, LCOE has been chosen as the main metric of examination for this research, due to the wide applicability of the method.

2.3.2 Energy analysis

The energy produced by a WEC is a function of the metocean conditions. This is often simplified to a two-dimensional dependency on the significant wave height, H_s, and the peak wave period, T_p. These are both statistical parameters that are moments of the variance density spectrum, a statistical description of the sea conditions over a short period of time (where the sea can be considered stationary) [68]. The most well known of these are the Pierson-Moskowitz [69] and JONSWAP [70] spectra, which were derived from physical measurements in the North Atlantic and North Sea respectively.

A common way of describing the power producing profile of a WEC over such wave conditions is with a power matrix. This defines power output by binning it at given sea states (combinations of H_s and T_p or energy period T_E) that can be arranged into a two dimensional table. They can be derived by developers by performing numerical simulations of the device in the time domain, by interpreting the resultant loads and movement of the simulated device. The power values can be verified experimentally, for example through tank testing or sea trials, and adjusted accordingly. The values can also be scaled by efficiencies in the device system, for example conversion efficiencies between the mechanical and electrical

Hsig (metres) \ Tpow (seconds)	5.0	5.5	6.0	6.5	7.0	7.5	8.0	8.5	9.0	9.5	10.0	10.5	11.0	11.5	12.0	12.5	13.0
0.5	idle	idle	idle	idle	idle	idle	idle	idle	idle	idle	idle	idle	idle	idle	idle	idle	idle
1.0	idle	22	29	34	37	38	38	37	35	32	29	26	23	21	idle	idle	idle
1.5	32	50	65	76	83	86	86	83	78	72	65	59	53	47	42	37	33
2.0	57	88	115	136	148	153	152	147	138	127	116	104	93	83	74	66	59
2.5	89	138	180	212	231	238	238	230	216	199	181	163	146	130	116	103	92
3.0	129	198	260	305	332	340	332	315	292	266	240	219	210	188	167	149	132
3.5	-	270	354	415	438	440	424	404	377	362	326	292	260	230	215	202	180
4.0	-	-	462	502	540	546	530	499	475	429	384	366	339	301	267	237	213
4.5	-	-	544	635	642	648	628	590	562	528	473	432	382	356	338	300	266
5.0	-	-	-	739	726	731	707	687	670	607	557	521	472	417	369	348	328
5.5	-	-	-	750	750	750	750	750	737	667	658	586	530	496	446	395	355
6.0	-	-	-	-	750	750	750	750	750	750	711	633	619	558	512	470	415
6.5	-	-	-	-	750	750	750	750	750	750	750	743	658	621	579	512	481
7.0	-	-	-	-	-	750	750	750	750	750	750	750	750	676	613	584	525
7.5	-	-	-	-	-	750	750	750	750	750	750	750	750	750	686	622	593
8.0	-	-	-	-	-	-	-	750	750	750	750	750	750	750	750	690	625

Figure 2.7: Example of a power matrix. This one is for the Pelamis P1 device, taken from [71]

system. An example of a power matrix is shown in Figure 2.7.

Given a time-series of wave elevation, a time-series of power can be obtained by using a power matrix as a lookup table, interpolating the metocean data at each time step. This interpolation is required when the metocean values of interest are given to a higher resolution than the power matrix bins (lying between the discrete sea state values that the numerical models have been run at). Another way that this can be achieved is by binning the input metocean data to the same resolution as the power matrix and directly multiplying the two. The timeseries interpolation is the superior method, however, as considering discrete metocean bins can introduce rounding errors [72].

The energy produced can then be obtained by summing the resulting over the time series, and can be discounted as described in Section 2.3.1 to form the denominator of the LCOE calculation.

2.3.3 Cost analysis

Costs are typically categorised into three types: capital expenditure (CAPEX), operational expenditure (OPEX) and decommissioning (DECEX) [73].

CAPEX items are those that are required to set-up a given project. They are often assumed to occur in year zero of the project (for example [57]), and as a result are not discounted, although this is not always the case (for example [74]). Installation of the wave energy device also falls under CAPEX, although is sometimes regarded within a separate category. Other examples of CAPEX include the cost to purchase the WECs, the mooring system and the export cable. The development cost is also an item of CAPEX. This is the cost associated with site surveys and obtaining a marine license, required to legally deploy the device. This cost is often very small, only a few percent, so is often assumed to be negligible

DECEX is the cost to uninstall and remove the system from the water at the end of the project. As there has been very limited decommissioning experience in the wave sector, it is often assumed to be equal to a percentage of the initial cost (for example [75]). As the costs occur very far into the future, they are heavily discounted. Components will also be salvaged, meaning that there will be some positive cashflow. Because of these factors this cost is typically assumed to be very low, for example estimated at 0.26% of the LCOE in [26], and sometimes will not be considered at all (for example [29, 74, 76]).

2.3.3.1 Operating expenditure

OPEX are the costs that are incurred during the operational lifetime of the WEC farm. These include both planned and unplanned O&M, and ongoing costs like labour and insurance. Because maintenance costs will depend on the state of the WECs and environmental factors, they have a time dependency that makes them more challenging to model.

For offshore wind, OPEX accounts for roughly 25% of the total project expenditure [77, 78]. Wave energy costs are expected to be higher than this, for example as considered in [32], due to lack of operating experience and reduced reliability from devices being deployed in more extreme environments. The aim would be to avoid winter for carrying out O&M, as accessibility is more difficult and there would be a greater loss of revenue from missing out on higher energy conditions [33].

A marine operation is a task that must be performed on the WEC out at sea. This could include deploying the WEC, accessing it to carry out maintenance or towing it back to port for maintenance on land. To carry out a marine operation the sea conditions must be suitable. If the conditions are too extreme, with high wave heights, wave periods or wind speeds, then the task cannot be carried out. This is due to safety concerns or technical limitations, for example a vessel is not stable enough to use certain equipment. The most influential factors are wave height and wave period, with wind speed also a factor if cranes are required [79].

These kind of extreme conditions are also linked to reliability. If the device is subjected to higher loads from the environment then this can cause failures in the device, possibly resulting in loss of energy production (known as downtime). Examples of failures include extreme snatch loads in mooring systems and end stop issues in PTOs, whereby a high force can cause a hydraulic cylinder to abruptly reach the end of its stroke [80]. Thus, in more energetic wave climates devices can be both more difficult to access and require more regular access for maintenance.

An early step towards understanding reliability for a particular technology is to undertake a Failure Mode and Effects Analysis (FMEA). This is undertaken by a developer, built up from device performance data, with the aim of documenting, quantifying and ranking by risk all of the potential failures that could occur in the system during operation. This analysis was undertaken for the Albatern device in 2017 by Kenny et al. [81]. Due to the poor data resolution the authors were unable to derive mean time to failure values, which can used to calculate availability [82]. They noted that relatively high occurrences of electrical and

instrumentation issues coincided with each new deployment of the Squids, hence could be attributed to the adoption of new innovations. They also anticipated that reliability will improve over time as "teething issues and design faults are addressed" [81].

Availability is defined as the proportion of time that the WEC is able to produce power. Availability is reduced by failures in devices, as well as planned downtime for scheduled maintenance. Quoted availabilities for onshore wind and offshore wind are 96.2% and 94.5% respectively [83]. There are limited data available for wave, due to the lack of commercial projects, but availability is generally regarded as being less than 90% [84] and as low as 60% for early stage technology in particularly energetic regions [65].

A weather window is a sustained period of time where conditions are suitable for the WEC to be accessed at sea. They are defined in terms of the maximum weather limits that the operation can be carried out in. These thresholds can be increased in different ways, for example using more stable vessels or simplifying O&M procedures. The length of the window that is required must be long enough to allow the desired operation to be carried out. Longer operations at sea will require longer weather windows. Usually maintenance will be carried out in the summer months, where possible, when the devices are easier to access [76]. For higher energy sites, generally more suitable for wave energy, there will be more waiting time for suitable windows [85]. In these waiting periods the vessel and crew will be on standby. For a chartered vessel this time will incur a fee; thus weather window analysis and waiting time estimation is an important part of the LCOE calculation.

There are two main ways that waiting time can be estimated: using frequency based methods or time based methods. Both of these require the maximum environmental limits to be defined, in which the operation could be carried out. Time based methods require a time series of the environmental quantities, typically the wind speed, H_s and T_p. Starting from an initial time step, the environmental data at each subsequent step are checked to see whether the maximum limits are exceeded. Consecutive time steps of non-exceedance form weather windows, of which those that are greater than the time required for the operation, can be identified. Because these methods often require large quantities of data, Markov chain methods can be used to create representative time series for a site [10]. This is achieved by using a transformation matrix, created from existing data, that allows the next sea state to be randomly generated from the current one.

Frequency based methods do not require such a detailed knowledge of the time series. Joint occurrence matrices, defining the frequency and probability of sea states occurring in particular bins of H_s and T_p, are used. This means that, when considering a specific time interval, the ordering of sea states within the interval is not important: the waiting time is calculated statistically. First formulated by Kuwashima and Hogben [86] the method is also described in [87] and [88].

Time series based methods are regarded as being more accurate and also allow multiple environmental limits to be simultaneously considered [79,87]. Anastasiou and Tsekos compared a Markov chain method with Kuwashima and Hogben's frequency based method, finding that their method provided a better fit to the observed data [89]. However in general the methods are more complex and a large quantity of time series data are required. Because the economic model developed for this research project is spatial in nature, with calculations needing to repeated over hundreds or thousands of time series, a frequency based approach was chosen to reduce run time and allow for smaller datasets of less than ten years. It can give a useful indication as to the most suitable time period for deployment, for example the month where the waiting time for operations will be minimised.

2.4 Previous Research

Understanding the previous research on the topic of wave energy economic assessments was important to this research project. This is so that the key methodologies and cost drivers could be determined and factored into the model framework created.

As computational power has increased, so has the capability of numerical modelling. The accessibility and usability of modelling tools means that they are readily available and of increasing interest both in an academic setting and within industry. Because wave energy lacks maturity the research topic is broad, and there has been significant work within the LCOE modelling theme. There is a strong need for research, with particular emphasis on bridging the gap between academic research and commercial application. The current status of wave energy, as well as high uncertainty over its future potential, means that there are numerous unanswered questions. The aim of this section is to introduce the literature that has been published on the research subject of wave energy economic modelling, so as to frame the wider context of this work and acknowledge the variety of research which it aims to contribute towards.

2.4.1 Economic evaluation

As economic modelling is such a broad subject area, with many underlying themes, there is a selection of material available. As wave energy has only recently generated interest again, the majority of relevant studies can be found in the 2000s.

One of the early pioneers in the field was Tom Thorpe. In 1999, Thorpe published a technical report for the UK government entitled: "A Brief Review of Wave Energy" [90]. It gives economic assessments of several of the most developed technologies at the time, including the Limpet and Salter's Duck, and also covers other aspects like environmental effects. The aim was to identify projects with the best potential for future government funding and development. At 200 pages, the methodology and cost breakdowns are detailed and consistent between the different technologies to allow direct comparison. For most of the devices, both LCOE and IRR are provided and the author highlights the high uncertainty in the calculations and the need for future research.

A limitation of the report is that it is very optimistic in nature. For example the majority of the devices are found to have LCOE of under 10 p/kWh, with some approaching 5 p/kWh. Based on these, wave power would be comparable with fossil fuels and almost certainly a commercial market by now. Thorpe does state that these costs are estimated based on the "predicted performances" of the devices and that there is "considerable uncertainty" with some of the cost estimates. As very few of these devices had actually been designed at full sea scale and deployed for any length of time, CAPEX and OPEX were based on proportional estimates and were potentially subject to bias from the companies who were keen to secure funding for their devices (indeed Thorpe states that "the inputs to the assessment are based on data provided by the teams working on these devices" and "it has not been possible to validate these data independently"). Nevertheless, the report was successful in applying simple and well understood economic evaluation methods to wave technology, paving the way for future work.

Into the early 2000s, interest in wave energy continued to grow. The creation of the European Wave Energy Centre (EMEC) in 2003 and the rise of the companies Pelamis and Aquabuoy were notable events [91], demonstrating that people were thinking more seriously about wave energy as a viable business opportunity. The need to assess the economics of the technology became more apparent: to help fuel industry growth, improve understanding and encourage investment.

An example of this wider interest, outside of the purely academic environment,

is a technical report that was led by Mirko Previsic [92]. The industrially focussed study was conducted by a consortium, with the aim of assessing the economic feasibility of creating a plant of Pelamis machines near San Francisco, California. Two projects are considered, an initial prototype of one unit and a commercial plant of 213 units, located further offshore to take account of the more favourable wave climate. It was found that the LCOE of a commercial plant of 213 units (300,000 MWh/y) was between 8.4 and 16.1 c/kWh. As this was higher than onshore wind, which they deemed as the main rival to the wave power scheme, they concluded that such a project was not financially viable. However, they then extended the analysis by applying learning rates to the WEC cost and energy production, as seen in the more mature wind sector. With these assumptions, even under their most pessimistic learning rate scenario, the wave energy plant was found to have a very similar cost of energy. Hence they conclude that a "Federal Government learning investment subsidy" was required for the technology to compete.

There are a great many strengths in this report that have led to it being cited in the majority of the proceeding literature, extending to the present day. The main advantage is in the fact that it contains very detailed cost estimates, obtained from Pelamis and using quotations from local suppliers. As commercial interest in the industry grew, technology developers became much less willing to put these kind of data in the public domain, to prevent losing ground to competitors. This is reflected by the fact that the data still form the basis of many economic studies, for example [57, 74, 93, 94]. This attention to detail extends to wider aspects, for example the site assessment. In this area solid rationale is provided for project decisions (for example landing the export cable through an existing waste water outfall pipe to reduce cost). The methodology is particularly rigorous. Estimates of the wave resource come from a nearby wave buoy, at approximately the depth of the proposed plant and using 21 years of data. Availability and conversion efficiency are justified and applied to the power. Costs are highly detailed, for example shipping prices from Edinburgh to San Francisco were incorporated. Interesting was the way that uncertainty was considered, by estimating it for each component and performing Monte-Carlo simulation.

As the report is assessing a specific project it does have limitations. While the results for the commercial plant are comprehensive, giving LCOE and IRR and including inflation and subsidies, the same level of detail is not provided for the prototype project. This makes their results hard to compare to alternative WECs. Additionally some of the financing aspects seem quite specific to the

USA and California, making the context of their results in the wider wave energy market less clear. Detailed breakdown of the actual uncertainties used for each component and how they were chosen is missing, as well as the choice of cost distribution that they must have used. Finally, as this study is somewhat old, care needs to be taken as there has been development in the market outlook. While wave energy is still in a pre-commercial place, the wind industry has seen huge cost reductions, and so the conclusions are dated.

In the years following Thorpe and Previsic there has been further work in the area. As the theoretical framework is somewhat established, the general research motivations have been to enhance specific aspects of the methods, attempt to predict economic viability for various combinations of devices and locations, and to suggest alternative economic metrics to simplify the evaluation processes.

Due to the availability of data for the Pelamis device (as used by Previsic), there are a large number of studies which use this technology as the centre point of the analysis. A notable example was published by Allan et al. in 2011 [74]. The authors estimate the LCOE for both wave and tidal stream in the UK and make comparison with the LCOE of mature technologies. These include offshore wind, nuclear and combined cycle gas turbine (CCGT). The results are used to discuss the banded Renewable Obligation Certificate (ROC) scheme for renewables (where different renewable technologies are awarded different amount of ROC subsidies depending on their relative maturity). Examining baseline, high and low CAPEX estimates, the LCOE for wave energy was estimated between 11-22 p/kWh, with a baseline estimate of 19 p/kWh. This was for a relatively large farm size, with bulk discounting included. It was the most expensive out of the twelve technologies that they examined. They also found that the amount of ROCs available had an impact, although even in the optimistic case wave power was expensive: three times greater than CCGT.

The economic analysis considered sensitivities in CAPEX, discount rate and the ROC subsidy. LCOE was broken down into components for CAPEX, fuel and OPEX among other things. The LCOE for eleven additional technologies were also obtained using similar methodology as for wave, giving strength to their comparisons. The inclusion of several fossil fuel sources retrofitted with carbon capture and storage is also useful, as when developed this industry could rival the wave sector in terms of mitigating CO_2 emissions. A weakness in the approach is in the power estimation, which assumes a constant capacity factor of 33% for the project. Although it is justified, the choice is obviously quite device and location specific and has a large influence on the economic potential.

Generally the subject of subsidies is a common theme in the literature. Another prominent paper was published by Dalton et al. [93]. It was a feasibility study of the Pelamis device for three locations. The economic viability was assessed using an in house Excel model developed by the authors (NAVITAS). They followed a similar methodology to Previsic, but estimated the majority of costs as percentages of the initial device cost. They included revenue from salvage and a 10% learning rate, examining device quantity as a sensitivity. At 2004 prices, to compare with Previsic, they found that the Irish site had the lowest LCOE, tailing off to 0.05 EUR/kWh as the number of devices approached the hundreds. Considering more recent 2008 prices, where the cost of steel had tripled, the LCOE was much less favourable and a subsidy of €0.20/kWh required to get a positive NPV. For an IRR of 10%, deemed acceptable by the authors, a higher subsidy of €0.30/kWh was required for Ireland, the best location of the three examined.

An extension to this analysis was published in 2012, with the aim of investigating the impact of installing 500 MW of wave energy in Ireland over a ten-year period [75]. Again Pelamis was chosen and the NAVITAS Excel model was used. To adjust for falling costs of the WEC over the ten-year period, the authors consider learning rates. Three different rates are examined, and applied with combinations of multipliers to account for potential variations brought about by constraints in the supply chain. The authors considered ten projects of 50 MW installed within the ten years and investigated different feed in tariffs. They found that CAPEX had a very large impact on economic viability: a cost reduction of 50% was required to get to a 10% IRR. The future cost of cash was also a big driver and this combined with negative supply chain aspects had the potential to outweigh benefits from learning. The authors acknowledged the need to apply the methodology to different device concepts and different locations, as the results were very sensitive to these factors which limited the applicability of the analysis to the wider industry.

Because the authors relied on top down, proportional cost estimates in the last two studies mentioned, there is notable uncertainty in the results. More recent studies have tried to improve confidence by applying more rigorous methodologies. Farrell et al. addressed high uncertainty by using a probabilistic based, Monte-Carlo method in order to estimate the distribution of LCOE and IRR [57]. While the cost estimates are based on similar sources to Dalton, they are accompanied by uncertainty bands, with different distributions considered for the various project elements. Considering Ireland as a case study, the authors obtained distributions of LCOE. They found that LCOE reduced for larger farms sizes, as infrastructure

could be shared between multiple devices, with an LCOE of €0.456/kWh at the 95th percentile. It was found that the current FIT was not suitable, supporting the conclusion of Dalton. A positive IRR was only likely at the largest, 100 unit farm size. However there was a less than 1% chance of achieving a 10% IRR. While there are limitations in the work, for example uncertainty in energy yield is not considered, the methods demonstrated a more thorough approach, with particular interest for investors.

A different approach, focussing more on the uncertainty in the resource rather than the costs, was published by Guanche et al. [95]. This considered a heaving buoy in Spain, using hindcast wave data as input to the study. To account for uncertainty in the resource a Monte-Carlo technique was applied, pre-processing the input data to select random data samples representative of the time of year. Costs were obtained using rough material mass estimates with some industrial correspondence. Considering a four WEC farm, the authors found that the mean NPV was positive, however negative NPV was also possible. In general they found that the inter-annual variability was a key factor and arguably the greatest source of financial uncertainty, as climates with less variability give more stability for investors. The baseline results demonstrated a low IRR of 5.6%, however still more optimistic than Farrell who also considered larger farm sizes. While this indicates that there might be more merit in the device and location combination, Guanche was also working with less detailed cost data and so the estimates are likely to be more optimistic. Considering sensitivities, the authors found that a FIT of €0.40/kWh was required to achieve a mean positive IRR, however there was large variation in the FIT required due to the resource variability. At the Irish FIT of €0.22/kWh it was found that a learning rate of 48% and 20 device farm was required to get to a 10% IRR. This supported the conclusions of Dalton and Farrell, namely that the Irish tariff was too low to encourage suitable investment.

The majority of previous studies, which includes all of those discussed above, have calculated OPEX by considering it as an annual percentage of the initial cost. This is because there are significant unknowns in the maintenance requirements, due to both a lack of operating experience in the sector and data in the public domain. As wave energy components tend to be bespoke and vary between different device concepts, the impact on the marine environment on system reliability is a difficult question to answer.

There have been a number of notable papers which attempt to more robustly estimate OPEX. One example, by Teillant et al., involved creating an operational simulation tool which functioned as part of a wider economic model ("Wave Farm

Productivity and Financial Calculator") [76]. The tool used FMEA analysis to estimate device reliability, and hence determine when operations needed to be scheduled. A "Deployment Model" looked for the first available weather window and calculated the time taken to install each device, based on the distance of the farm to port and the towing speed of the vessel. Two O&M procedures were considered: onsite service and a mid-life refit. Frequency rates of failures for six components were considered, and all of the necessary expenses calculated (for example the cost of parts and hourly rates of the engineers). The authors examined a 100 unit farm in Ireland, considering a heaving buoy. They found that the Irish FIT of €0.22/kWh produced a negative NPV and hence did not look financially viable. They also examined sensitivities in the model inputs. Varying the number of devices in the farm, a positive NPV was only found when considering a more optimistic FIT scheme involving ROCS. Variation of the operation task durations had negligible impact, while improvements in CAPEX had a much larger effect. This led to the conclusion that a more promising business case could be found for cost reduction than for streamlining operational aspects.

A second example was published by O'Connor et al. The key focus of this paper was on accessibility, to see how availability could impact financial returns [65]. A 75 MW farm of Pelamis devices was considered and the NAVITAS model again used, as in [93]. Two locations were considered: Ireland and Portugal. The main device cost was from [92] but modified to 2011. The rest of the project costs were generally taken as percentages of the device cost or overall initial cost. The authors considered sensitivities in OPEX and insurance cost, both as an annual percentage of CAPEX. They also considered a more detailed OPEX cost scenario, with 10% of the device cost incurred every four years for maintenance and a 90% replacement cost after ten years. Such a midlife refit was also considered by Teillant, described above. Availability reduction in harsher locations was applied by considering a function from the literature which mapped accessibility to availability for offshore wind [96]. This means that O'Connor et al. do not consider weather windows or the timing of operations directly, which represents a significant simplification of the calculated availability.

Calculating the NPV and IRR, the authors found that only the Irish site exhibited positive NPV values, with the resource at the Portuguese site too poor. An IRR of 10% was only achieved when considering larger farm sizes in the 200-500 MW range. In general the accessibility had a big impact, reducing the energy output by 10% and 40% at the Portuguese and Irish sites respectively. For the more detailed OPEX scenario they found that adding the four-year maintenance

had very little impact on the cash flow, while the impact of the midlife refit on NPV had a big effect: making all of the NPVs negative over the lifetime. A general conclusion from the work was that the FIT needs to be tailored to the site, as the conditions seen could be very different.

A further source of uncertainty which the literature tries to address is in the device selection. The industry is yet to converge on one or several optimal designs, and so any studies which can indicate the most promising technologies are of significant interest: so that investment can be more focussed and comparison methodologies can be improved.

Another paper by O'Connor et al. examined the economic potential of the Pelamis and Wavestar devices at six European locations [97]. The aim was to examine how they compared to each other, with particular focus on applying site specific factors to account for differences in availability and accessibility. They considered three different device scales for each technology, 0.25, 0.5 and 1 MW, with a total farm size of 100 MW. The results indicated that smaller devices had better economic potential, although they acknowledged that this was partly due to the way that the device scaling had been applied. Comparing the technologies, they found that the Pelamis was better at the higher energy sites but the Wavestar was more consistent over the six sites, a main conclusion being that siting is very important to get the best value solution. While only two device concepts were considered, the results also implied that the industry might not see the same kind of convergence as wind energy, with very different device concepts sensitive for particular sea conditions. While the accessibility was modelled in a crude way, the authors found that it had a big impact on NPV. This was especially true for the more exposed sites like Ireland and Scotland.

Another study of this form was conducted by Archetti et al. Considering two promising locations in the Mediterranean, the authors considered three device concepts: Pelamis, AquaBuoy and AWS. Costs were mainly derived from [92] and [93], with energy production estimated using device power matrices. Energy production for the three devices was low, the maximum capacity factor calculated was 8.5% for the Pelamis at the more promising site. Only the Pelamis was considered for the economic analysis. For a 21 MW farm the authors calculated the LCOE at €0.64/kWh, in line with similar studies released at the time (for example the North American case study conducted in [93]). The fact that this analysis was not performed for the other devices is a weakness of the study, although due to a lack of data in the public domain. While AWS was found to be much worse, Aquabuoy was almost on a par with the Pelamis device for energy production and

could have demonstrated cost advantages. The authors conclude that the devices are not well suited to the wave climate, as they are designed for longer waves, and a device better suited for shorter waves might yield better potential.

A more recent study comparing Wavestar and Pelamis was conducted by Biyela et al. in 2016 [94]. The location for this study was South Africa; while not renowned as an area of significant wave resource the author notes that there is strong political motivation to progress from an energy mix that is mainly coal. As for previous studies, top down cost data come largely from the literature, with OPEX estimated as 6% of the CAPEX per year. The authors found that the devices were not at all well suited to the site: both having capacity factors less than 15% and very poor LCOE, \$4.50/kWh for Wavestar and \$7.50/kWh for the Pelamis. While this supports the broad conclusion of O'Connor, that the Wavestar is better suited to low energy wave sites, both numbers are far higher than other studies and thus seem anomalous. This can be explained both by the poor resource and the fact that the authors only considered single devices (not a farm). Because of this the results are interesting as they are more representative of a present day scenario, unlike the majority of the literature which focusses on very large and somewhat commercially mature farms. The authors state that if learning effects and economies of scale were considered then they would expect the values to reduce considerably.

Another study which includes consideration of an early stage project looks at the SEAREV device [31]. It documents the evolution of a particular device concept over a twelve year period. While the paper is a general history of the device, it includes descriptions of the economic modelling that was carried out to guide the design progression. The first stage of design involved optimising the shape and examining different control methods. However the payback period was calculated at over 50 years for just the device CAPEX, with a very high tariff required for the device to be affordable. After improving the design the economics were examined in more detail using a dedicated economic model. This included CAPEX and OPEX estimates, with consideration of the device lifecycle. Considering a 20 device farm and sensitivity in several high level areas, it was found that the CAPEX and energy production were the key economic drivers. The former conclusion mirrors that found in [76]. Applying a 10% learning rate and a starting point at the 100th machine the LCOE was found to be high, with the device requiring a FIT of €421/MWh to be financially viable. The low learning rate compared to other studies was applied to take account of the lack of convergence of wave energy into a dominant device concept. Despite the high

LCOE, it was found that the tariff required reduced by a factor of 2.5 and the energy production increased by 90% from the first design. While the economic analysis was not as sophisticated as some of the others that have been described, the fact that it was applied to a prototype stage device, directly informed research activity and allowed cost reduction areas to be identified makes it notable in the overall literature context.

Lastly, there have been other studies which delve into specific aspects of the economic analysis. Beels et al. presented a methodology which incorporated array configuration aspects [98]. Considering the Wave Dragon overtopping device and three different array layouts, numerical modelling was used to simulate the devices and quantify the impact that inter-array shadowing losses had on the energy production and LCOE. The cost of inter-array cabling was calculated for each configuration. The authors found that the the cost of inter-array cabling was fairly negligible and that energy production should be prioritised where appropriate. They also found that a farm showed promise as a breakwater. While there were limitations with the study, for example installation and O&M cost as functions of array layout were not investigated, as the CAPEX is the most dominant cost element one would expect the conclusion to be broadly representative.

Contestabile et al. also considered a breakwater application [99]. The device modelled was the Overtopping BReakwater, an overtopping device that is designed to be built into harbour walls. Considering Australia as a case study, the authors used hindcast simulated wave data and estimated the energy production at several different coastal locations using a derived power matrix. To study payback period and NPV a subsidy rate of 40 AUD cents per kWh was considered. Two different turbines were considered: a simpler design requiring semi-regular replacement and a more expensive screw turbine with a longer lifetime but higher upfront costs. Comparing a harbour wall with WECs built in compared to a traditional solution, it was found that the WEC was actually cheaper in some cases. For the simple turbine payback costs were very short, less than two years across the nine sites examined. The performance was generally found to be better at lower energy sites.

Lastly, worthy of mention is a study carried out by Astariz et al [32]. The aim was to provide LCOE estimates for offshore wind, wave and tidal and compare the values. This work was in the style of a review paper, with the authors using an extensive catalogue of literature to derive best estimates of costs. Using these high level costs, the LCOE for a generic wave energy device was estimated at €325/MWh, higher than the generic tidal and offshore wind systems. The au-

thors quoted that 20-50% capacity factors are used in the literature, however it was not explicitly stated which was chosen to get to the LCOE. As the LCOE is very sensitive to the energy, and will be highly site specific, the value chosen would have been of interest. Additionally, due to the large number of different device concepts available, the notion of a generic device has limited usefulness. The authors also discuss the impact of externalities on LCOE. These are socio-economic factors which have an indirect impact on the cost of energy. Examples include job creation, security of supply and CO_2 emissions. Including these factors made the wave energy system much more competitive, halving the LCOE difference with conventional forms of energy generation. The authors also advocated combined wind and wave systems as a way to reduce the costs of both systems, by sharing project infrastructure.

2.4.1.1 Alternative methodologies

One of the main disadvantages of conventional economic analyses like LCOE or NPV are the amounts of input data required in order to formulate an accurate representation. To mitigate this problem there have been several studies published which propose alternative methodologies. While these can have advantages, for example being faster to compute or reducing bias [33], they are generally considered to be inferior as they include higher uncertainty.

An older example, published in 2004 by Stallard et al., studied a selection of point absorber concepts with the aim of investigating how the energy production and cost of energy varied at eight different UK locations [33]. A data envelopment analysis (DEA) was used, a technique that allowed different design decisions to be analysed with the aim of maximising energy output (or "technical efficacy") by minimising a selection of inputs. The advantage of this method is that it is not sensitive to the input units and allows both physical (e.g. installation time) and non-physical parameters (e.g. jobs created) to be incorporated. The authors considered four different types of point absorbers, defined by their control system. One was based on the Waveswing device and used a real power matrix. Considering seven weighted independent inputs, including the quantity of devices, inter-array cable length and device failure probability, the DEA method aimed to minimise them while maximising energy outputs for each device. The results were ranked, to get to 100MW of rated capacity while minimising maintenance expense. The results found that the unrealistic, ideal point absorber was the only one to reach the required technical efficiency. The passive and tuned devices performed better at medium energy than the maximum energy sites, indicating

the location specific nature of the technology. Different sensitivities, e.g. O&M and transmission cost, had the effect of improving the outlook at different sites. This was particularly apparent for lower energy site, where the technical efficacy saw marked improvement when O&M was considered.

An advantage of the method is that it is independent of "expert costs", useful when wanting an unbiased outlook. However, when costs are well known and understood, it adds another layer of complexity and hence has not seen widespread usage in the literature. While the author considers relatively simple input variables, the method is more difficult to scale to large problems with many variables to be incorporated.

There have also been studies which aim to indirectly estimate LCOE by using simplified methods. One of these, published by Okamoto et al., attempted to create an index to estimate LCOE from WEC design parameters [100]. The motivation for the methodology came from a need to quickly assess different sites and device options in order to predict combinations with the best economic potential. A generic heaving buoy device is considered with a power matrix obtained from frequency domain simulations. The device width and generator capacity were incrementally varied, both with energy and cost implications, and an index created taking both factors into account. This was then compared to the LCOE, calculated using a more traditional method. They found that the index better matched the LCOE for lower energy sites and smaller farms, with the index not properly scaling for larger farm sizes. While broadly similar trends were seen, the index lacked the resolution of the traditional LCOE method.

Two further studies which have discussed using alternative metrics to estimate LCOE are [101] and [102]. The former created numerical models of eight different wave converter concepts and examined three design metrics: the absorbed energy per mass, per km^2 of footprint and per root mean square of PTO force. The aim was to see how these varied across the device classes; as all of the metrics relate to physical parameters of the device they could be linked to cost. While full cost analysis is not conducted, the resulted showed that there was surprisingly little variation between the devices. This was despite the fact that the absorbed energy saw a high variation. This provided a typical target metric that an early TRL level device should be aiming for, however the low variation also implied that such a metric is not well suited for estimating economic potential.

The second study presented a methodology to optimise sizing of a WEC, considering both LCOE and other metrics. A point absorber was considered, the

technology being developed by CorPower. From an initial power matrix, power matrices for several different sizes of devices were obtained, from 25 kW to 2 MW, by using Froude scaling (similar to [97]). Costs were also scaled depending on the nature of the subsystem. Five sites across Europe were considered, with costs obtained from correspondence with CorPower and other economic parameters chosen according to the literature. Two different O&M schemes were considered: high level based on a percentage of CAPEX and a more detailed estimate based on the life cycle of the device. This latter strategy included one major repair every two years. The authors discovered that the annual energy production was higher for smaller devices, a similar result to [97] and due to the way the power matrix scaling was performed. Due to learning discount applied to multiple devices, the best LCOE was found for the smallest size of device when considering the simplified O&M. Considering the more detailed O&M strategy, which scaled the O&M more accurately with increasing device quantity at lower ratings, the authors found that the larger devices were better. However this considered the same size vessel for all device scales, in reality larger vessels would be required for the larger devices which would incur greater cost. Accessibility and weather windows were also not considered.

The authors also examined the CorPower device with respect to the metrics that were detailed in [101], including discussion on how closely they followed the trends in LCOE. While the trend with LCOE for most of them was unclear, the Average Climate Capture Width per Characteristic Capital Expenditure (ACE) metric as advocated by the Wave Energy Prize showed the most promise as it had a clear functional form for the technology over all five sites. Despite this, no analysis was conducted considering other devices. As the purpose of such a metric is for early TRL level, comparison how it fares across devices is crucial and unclear.

In a different study, de Andres et al. considered a reversed LCOE calculation [29]. This method starts with a target LCOE. The energy and cost components that are required to get to the LCOE can then be derived. The benefit of the method is that it gives the technology developer an idea of the costs that they should be targeting to reach the LCOE, hence allowing research activity and relevant supply chain aspects to be focussed on. The authors considered five types of devices and a target LCOE of 15 p/kWh, as identified in the literature. From a target array capacity, an AEP was calculated for a farm. The costs were then derived in order to get to the LCOE, calculated considering typical cost breakdowns as seen in the literature. Categories with higher costs were considered

more restrictive, with less flexibility to get to the LCOE. Comparing with offshore wind, the authors found that the wave devices showed much greater variation in CAPEX, supporting the notion that the technology is in a less mature stage and yet to converge on a concept. Comparing the cost categories it was found that, while some costs were not too far away from floating offshore wind expectations (for example the mooring system), the majority of categories were far away from the trends seen in offshore wind. This was partly driven by the relatively high OPEX calculated. While the overall method is interesting, it is really only useful to technology developers. Moreover, the cost breakdowns seen in the future would vary significantly between device concepts and are not necessarily relevant to the devices in the present, which are largely in the prototype stage.

2.4.2 Spatial economic analysis

What the studies from Section 2.4.1 have in common is that they all only consider a single or a small selection of locations to conduct the analyses. While this is suitable for getting a general feel of the economic potential, it is not so useful to a developer as metocean conditions can show large variation over relatively small areas. Additionally there will be a balance between energy and cost which is not so apparent when only considering single locations at a time. For example locations further from shore will typically be in more exposed locations, benefiting from higher energy waves which can improve yield. However this also means that accessing the devices for maintenance will be more difficult, increasing downtime and OPEX. It also means that transmission costs will be higher, as a longer export cable is required. Analysing multiple locations at a time means that it is easier to identify any sweet spots that arise because of specifics of the WEC design.

While spatial analysis methods do have limitations, requiring large amount of data and relying on spatial approximations that may not always hold in reality, they are very useful for initial site screening. As all devices will be better suited for some locations than others, the ability to perform economic evaluations over multiple locations allows the best sites for the technology to be determined. These will not necessarily be in the highest energy locations [45, 99]. For example, for early stage devices this might involve leaving the most promising sites for future, more technically advanced devices that can fully utilise the economic potential [33]. This methodology could be advantageous to developers, investors and policymakers, and as a result has garnered interest in the literature.

2.4.2.1 Resource assessments

There are a large amount of studies which focus on spatial aspects of the resource. Using numerical models, the aim is to characterise the resource and identify the highest energy locations in particular regions that are suited to wave energy application. This is regarded as the first step to obtaining estimates of energy production. While some of the studies do include qualitative cost aspects, this is not typically a feature.

Earlier studies relied more on physical measurements, due to low computational capabilities. One example, conducted by Mollison et al., used three years of data from the UK Met Office hindcast wave model to estimate the energy resource at the Azores [103]. They discovered some areas with reasonable energy, of the order of 30-40 kW/m, and concluded that there was a long term potential of "tens, possibly hundred of megawatts". A difficulty was in estimating the nearshore resource, as the wave model was a deep water model, hence these areas were subject to higher uncertainty. A second major limitation was in only using three years of data, as inter-annual variability in the resource means that the full wave resource is not accurately reflected. In more recent studies it has been recommended that no fewer than ten years of data are used so the full effect is captured [51].

More recent studies mitigate these limitations by utilising more advanced wave models and considering more years of data. Examples include [104], which considered the Australian shelf, and [105], where a WAM model was used to characterise the resource at Galicia (Spain). The former study found that the Western and Southern shelf offered the greatest potential, with some nearshore areas demonstrating 25-35 kW/m at the 90% percentile. As the study considered the entire area around Australia, the data resolution was somewhat poor that limited its applicability for detailed wave energy siting. The latter generated 11 years of wave data at a temporal resolution of three hours. The initial resource over the area was characterised at 18 points, before applying a finer resolution model at a selected area of coastline in the north west. This was selected by discussing the results in the context of practical considerations like aquaculture locations, shipping routes and local ports. A conclusion was that there was high spatial variability, seen due to nearshore aspects such as shoaling and bottom friction, which should be taken into account when deciding on the location of a wave farm.

Other papers have also incorporated specific wave energy aspects. E. Rusu and Guedes Soares considered Peniche (Portugal), investigating how a small wave

farm could impact the resource at the nearshore [106]. Considering the Pelamis device and using two local buoys for data validation, SWAN was used for the numerical modelling. They modelled two farm sizes: one row of five devices and two rows of five devices. These were not fully hydrodynamically simulated, but considered by applying a transmission coefficient to the selected farm area within SWAN. They found that H_s decreased a lot directly behind the farm, however this change was not significant at the shore. As well as this, the farm also caused a change in wave direction, due to diffraction around the farm, and a minor change in spectra shape at the shore.

Rather than just considering the resource, other studies around this time incorporated device power matrices, to determine the direct power producing potential. The devices commonly considered were Pelamis, Aquabuoy and Wave Dragon as the power matrices were in the public domain. All three were considered by Aoun et al., who considered wave energy potential in Lebanon. Being in a particularly sheltered part of the Mediterranean, they found that capacity factors were very low for all three devices: not exceeding 7% using local buoy data. Using spatial altimeter data improved the capacity factors seen, however results were still at the lower bound of what was deemed "technically viable". The authors recommended expanding the buoy network around Lebanon in order to better characterise the nearshore resource, as only 1.5 years of buoy data were available for the research. Bozzi et al. also considered these three devices but examined the energy at two energetic Italian locations [107]. Buoy data were again used, however much more data were available (15 and 17 years for two buoys). A power matrix method was again used, however timeseries bilinear interpolation was applied rather than just multiplying by the scatter plot, improving accuracy as the power between bins of the power matrix can be captured. The authors also used Froude scaling to consider smaller device scales, more suitable for the relatively sheltered Mediterranean resource. As in Aoun, they found that capacity factors for the full scale devices were low, never exceeding 10%. However, looking at smaller devices they found that capacity factors of 15-20% were possible at a device scale of 1:2.5, with device scales at tens rather than hundreds of kW. Importantly this also saw reduced variation in the power output, to about 20% of the full scale devices. This more constant energy production is particularly useful for making an investment case [95]. Another power matrix based assessment was carried out by L. Rusu and Guedes Soares [108]. They considered the Azores, an area with decent potential as indicated in [103], and the Pelamis device. They used two years of altimeter data to define the resource, before narrowing down the area of interest

by carrying out a simulation using WAM and SWAN wave models for a three month winter period. While they found some high energy potential, 40-80 kW/m for some nearshore areas and daily average energy of 4.6 MWh for the Pelamis (approximately equivalent to a capacity factor of 25%), it should be noted that this was only applied to the three winter months and would reduce when averaged over larger time periods. Other studies published around this time have focussed on discussion of the practical areas in which wave energy could be deployed, rather than examining the energy specifically. Two examples, by Veigas et al., examine the offshore wind and wave resource around Tenerife [109] and Fuerteventura [24]. Both studies, using a 44 year hindcast dataset, found that the spatial distribution of the wave resource was much more significant than that of the offshore wind resource, meaning that correct siting was a much more important issue. The authors combining the resource with a discussion of the bathymetry, distance to shoreline and port and suitable offshore zones as described by the Spanish Ministry of Agriculture and the Environment. From this they established the main areas around the Island where wind energy would be best utilised.

In the last few years there have been several notable studies which apply the resource assessment in a wave energy context. Another study undertaken by L. Rusu aimed to find the highest energy locations worldwide and consider the energy performance of different WECs [110]. Considering fifteen years of hindcast data at a relatively coarse resolution, 30 worldwide locations were chosen which exhibited high mean power per crest length and were within a practical distance to the shore. Ten WECs were then examined, with the power matrices applied to the scatter matrices to determine which WECs were most suitable. The authors found that significant inter-annual variability was seen, especially at the European and Northern Hemisphere points, due to storm events. The devices were better suited for different areas, as one would expect, with no overall concept dominating. A distinction was seen between the larger devices (>2.5 MW) and the smaller devices in terms of the best locations. Another study that compared WEC technologies considered the Mediterranean [111]. Six devices were examined, to see how well they matched the resource. A relatively coarse dataset was applied over the whole sea, with SWAN used at four promising areas of Italy that were close to ports and grid infrastructure. It was found that the variability was high over the region, although low compared to more energetic sites from the literature (such as Bellmullet in Ireland). A maximum crest energy of 16.4 kW/m was found between Corsica and Sardinia. Comparing four offshore devices at 50 m water depth, capacity factors were all below 10%, indicating that the devices were

poorly matched to the resource (in agreement with [107]). The two nearshore devices, Oyster and Wavestar, fared better: with the Wavestar achieving 16% off the coast of Sardinia. Despite the poor capacity factors, the authors compared the best locations with results for the more energetic Azores Islands, taken from the literature. Comparing the relative power available in the resource with the power captured by the devices, it was seen that the conversion efficiency was generally higher for five out of the six devices examined. While the absolute power capture was lower, the devices were able to convert a greater proportion of the available energy, implying suitability for demonstrating proof of concept.

Lavidas and Venugopal also investigated a relatively benign region, the Aegean sea, to investigate what opportunities could be available for wave energy [112]. SWAN was used to generate a 35 year hindcast, which was validated against a buoy network dispersed between the Greek Islands. Five different devices were considered, again multiplying their power matrices against representatives scatter matrices to determine the most suitable locations. A so called "Wave Energy Development Index" was defined as the ratio of mean and maximum wave power within a time period, to assess the potential. A lower index indicated that extreme events outweighed energy potential and so the location was less suitable. Presenting eleven points, the authors found that there was not significant variation in the index, and that the values were much lower than other areas examined (such as Scotland). As in [111], this has implications for survivability, although obviously does not represent the absolute energy potential. As in the previous study, the Wavestar was found to be the best suited device: with capacity factors of 10-20% possible. While this is a higher estimate than some of the other studies considered, the data were also particularly high resolution (0.025°). As the energy production is very sensitive to geographic location, this demonstrates the advantages of using higher resolution data. Gallagher et al. considered Ireland, aiming to identify promising, potentially overlooked locations for wind, wave and combined systems [113]. This study also considered accessibility, examining the percentage of time that a jack-up barge could operate given operating limits in H_s, T_p and wind speed. It was found that, while the west coast had a more energetic resource it was also much less accessible: with many areas available less than 20% of the time at the required duration. They found that the wind resource was much less variable than the wave resource around the coastline, as also concluded in [24], implying that from an energy perspective there is a greater consequence of incorrectly siting wave energy farms.

2.4.2.2 Multi-criteria studies

Multi-criteria analyses can be thought of as the next step on from resource assessments as they combine the wider technical, economic and social aspects. The methods are used to aid decision making, by maximising benefits and minimising costs of a technology to arrive at an optimal solution for the issue being examined [114]. This involves a scoring methodology: weighting and ranking the relevant aspects which are then combined into a final metric. As the literature is extensive, this section focusses on studies that are directly concerned with wave energy. As siting is such a key issue, as demonstrated in Section 2.4.2.1, typically the analyses are conducted using GIS software and incorporate geospatial aspects.

As the ranking aspect is arbitrary in nature, attempting to quantify factors which are usually more qualitative in nature, caution must be exercised in the results [115]. This is especially the case with wave energy, where there are still significant unknowns. To attempt to mitigate these effects the scoring is usually conducted through collaborating with experts in the industry (e.g. [115–117]) and sensitivity analysis of the scoring is carried out (e.g. [117–119]).

In the wave energy context, there are two general stages that are carried out for the analysis:

1. Exclude any areas where deployment of wave energy is not deemed possible, for example due to very low energy or overlap with heavily used sea areas.

2. Rank any issues that are more subjective in nature (for example distance to ports or grid infrastructure) and combine these to arrive at an overall index.

The way that the spatial factor are ranked and combined depends on the method chosen, descriptions of these can be found in [114] and [120]. One of the more common methods is the weighted sum method (WSM). This involves combining each individual judging criteria with an arbitrary weighting factor and summing the contributions. The final criteria is typically normalised to a value between 0 and 1. Because of the simplicity it has been considered several times in the literature.

Galparsoro et al. considered the Basque continental shelf [121]. They examined seventeen criteria, covering commonly considered aspects like water depth and distance to port and lesser known effects like sediment transport and bathing zones. A very high resolution grid of 20 m was considered for the criteria, with coarser layers re-sampled to match the resolution (for example the energy resource). Some exclusion zones were applied, for example covering 500 m around

harbours to allow access. The results found that one particular stretch exhibited strong potential. Higher indices were generally in shallower waters and were found not to greatly coincide with environmental protection areas. However the authors do note the limitations in the method, particularly regarding aspects like fishing and recreational use of the sea where data are limited.

A paper published by the Bureau of Ocean Energy Management (BOEM), based in the USA, applied WSM to the coastline of Oregon [116]. Eight different criteria were selected, including the energy in the resource, distance to port, seabed geology, water depth and distance to grid infrastructure; these were weighted through engagement with 21 wave energy stakeholders. Three different WEC classes were considered: nearshore, mid and offshore devices. The only difference between these was the water depth constraint considered, a large simplification being that the WEC energy was characterised by the resource energy rather than device power production estimates. The results found that a very small number of sites, less than 1%, were suitable for the nearshore technology, driven by the poor resource. A more recent study by Flocard et al. performed a WSM analysis considering the south Australian coast [117]. This was more detailed than the BOEM study, with eighteen criteria incorporated. This included all of those from the BOEM study, as well as extreme wave conditions, protected environmental areas, fisheries and areas for military activity. Sites deemed unfeasible, with average H_s less than 1 m, were filtered out of the analysis before performing the multi criteria aggregation. Using a high resolution SWAN model to create the metocean data, the authors found a best resource of about 30 kW/m at the 100 m depth contour, in agreement with other studies (e.g. [104]). Applying the different criteria, the best area was determined to be South of Portland. Minimal variation for this area was found when applying sensitivity analysis to the criteria weightings, indicating the resilience of the method. As in the BOEM study, the WEC power production was not directly incorporated, and criteria such as extreme wave height and seabed geology would be very device specific and so might have the adverse effect of driving attention away from areas suitable for specific device concepts.

Another recent paper, by Cradden et al., considered a large area of encompassing most of Northern Europe [122]. They examined two combined wind and wave platforms, using a GIS focussed approach which included development of a tool as part of the EU funded MARINA Platform project. For the resource data, ten years of hindcast data were used at a 0.05° spatial resolution. Plug-in tools were created for QGIS software which included a GUI (Graphical User In-

terface) and PostgresSQL database to store the data layers. Exclusions included wind speed, MPAs and a relatively high energy density of 20-30 kW, depending on the platform. Unlike other studies an exclusion was also applied to depth for cable installation; 250 m was applied although it was indicated that 100 m was more commonly considered by industry. The results found that the North West of Europe looked particularly promising, especially Scotland and Ireland. This was largely based on the energy, suitable water depth and distances to port. Five points were examined in more detail, considering specific ports and weather windows to the sites. The accessibility was not considered over the full domain, which would have a great impact at many of the more exposed locations [113].

Two final studies that presented more limited WSM methodologies were [123], which introduced the methodology for a region in the South of France and [124] who considered Morocco. The former considered very similar criteria to BOEM, while also considering several exclusion criteria. Considering offshore devices, some of the best areas were found relatively far from the coast, at 50 km and greater. As costs would be high at these relatively large distances, it indicates that the results are potentially biased towards energy production and do not reflect the economic picture. The main focus of the latter study is in resource assessment. A 44 year hindcast was used, created using a WAM model, at a relatively coarse spatial resolution of 0.25 degrees. Along the Atlantic facing coast, the 23 nearest points to shore were considered for the analysis (varying between five and 52 km from shore). Relatively high resource was seen over the central stretch of coastline of 25-30 kW/m. Only five criteria were considered for the multi criteria analysis including water depth, distance to shore and resource energy as seen previously. Unlike previous studies, they considered power output from two WECs, the Wave Dragon and Pelamis, which were obtained from the power matrices. Despite only considering two physical criteria to represent the site, it was enough to rule out the most promising energy producing site which was located at a very large 500 m water depth.

Another common multi-criteria approach is Analytical Hierarchy Process (AHP). The weightings of n different criteria are considered in a pairwise manner, defined by a n by n square matrix [114, 125]. A matrix of normalised weightings is calculated by dividing each matrix element by its column sum, the relative weightings for each criteria then derived by computing the average for each row [119]. The method can be assessed by computing an "inconsistency index", a key advantage of the method as it allows the robustness of the pairwise values to be judged [114].

Vasilou et al. applied the AHP method to combined wave and wind systems in the Aegean sea, to determine the most suitable locations [119]. The method was implemented in GIS, and made use of a GIS database. Areas excluded from the analysis included those designated for military exercise areas, oil and gas exploration, areas already designated for offshore renewables and marine protected areas. In the case of the latter, the authors assumed that any areas within Natura2000 sites were unfeasible. Additionally, areas with wave resource below 5 kW/m were excluded, a lower threshold than that considered in [122]. Eight criteria were chosen for the AHP analysis, covering the main aspects with the exception of actual device power (as also seen in previous studies). Twelve suitable areas were identified and examined with AHP, with the waters to the east of Crete found to be particularly suitable. Sensitivity in the weighting parameters was examined, with the authors finding that, while the suitability values for the sites changes, the order did not. However the new values were not included, so it is unclear the extent to which they were actually varied.

Two further studies using AHP for spatial assessment are [125] and [115]. The former considered Tasmania, combining AHP with the Technique for Order Preference by Similarity to Ideal Solution (TOPSIS) method, which defines the best solution as that which is furthest from the ideal negative solution and closest to the ideal positive solution [114]. Ten factors were chosen for the analysis, areas that were filtered out included those which coincided with aquaculture areas and commercial shipping areas. The south coast was generally deemed to be the most suitable location, however the results were somewhat sensitive depending on whether the ocean features (e.g. energy and bathymetry) or marine user features were selected as dominant. The second study was applied at two selected points, one in the UK and one in Jamaica, rather than over a domain using GIS. An artificial neural network was used to assess and predict the relationships between the input criteria and the output suitability index, to identify the key drivers. Ten input criteria were considered, with the most important found to be the wind speed and site characteristics. Interestingly wave energy was not directly considered, as in the majority of previous studies: instead the wave height and distances between waves were considered which makes the results less clear in an energy context. The shipping density and water depth were two relatively insignificant factors, the latter also at odds with other studies where this is given higher weighting (for example it was the third highest factor in [119] and had a big influence in [124]).

Lastly, there have been other studies which have applied the methodology in

different ways. Maulud et al. applied a simplified methodology study considering Malaysia [126]. After considering eight exclusion types, the energy resource was used to visually assess the most suitable areas. As objective aspects like distance to shore were excluded, rather than incorporated into the analysis, the range of potential locations was limited. Such subjective factors were considered in a more qualititave way in [127]. This considered the North Sea and a combined wind and wave platform, pre-screened the most suitable locations by calculating an energy based index. A total of 60 points all along the North Sea coastline were selected, with water depths greater than 50 m considered. Subjective criteria such as distance to port and shipping traffic were considered in a qualitative manner, as well as indicative LCOE which was obtained from a somewhat dated European energy roadmap from 2010. The authors judged the most promising points to be off the Danish coast, as these were close to shore and exhibited lower LCOE. Another study which dealt with the criteria in a more qualitative way was [128]. They considered Northern Italy, with resource data coming from hindcast data validated by buoy measurements. A very fine grid with 30 m spatial resolution was considered along the coastline. The criteria included heavy emphasis on environmental protected areas, including the specific species at risk from heavy use of the marine environment. Generally the nearshore wave resource was found to be very low, the annual average typically less than 4 kW/m, but some resource hotspots were detected near some harbours. As well as not considering WEC power or quantitative assessment, a key limitation was the absence of shipping traffic or fishing considerations which would likely impact the optimal site suitability.

Two final studies with key spatial elements are [129] and [118]. The former study was focussed on the export cable for a WEC farm, using multi criteria analysis to estimate the most suitable farm locations and optimise the cable route. The main exclusion criteria was the cost of the cable infrastructure, calculated as a function of cable length. Areas of high connection cost were excluded, with the potential cable path subjected to eighteen environmental exclusion zones that included unsuitable onshore locations (for example where cliffs greater than 50 m high were present). Sites shallower than 50 m and with a wave resource of less than 15 kW/m were also initially filtered out. The results found that the exclusion areas had a large impact on the viable sites, especially for the sites closer to shore which were more likely to coincide with the exclusion areas. In the final study, Monds considered a different type of multi criteria analysis: the PROMTHEE method. This method essentially uses preference functions to define the different criteria, which are specified by using input threshold values. Unlike the majority

of studies examined, three WEC technologies were directly investigated: Wave Dragon, Aquabuoy and Pelamis. Three point locations in Canada were considered for the analysis, heavily relying on input data from [72]. Seven criteria were examined, including capacity factor, rated power, LCOE and more subjectively treated "maturity" and "survivability". In the baseline case, considering equal weighting across the criteria, Wave Dragon was found to be the most suitable at all three sites. Applying sensitivity and different weighting criteria, Wave Dragon was still found to be the best, with relatively low variation seen in the results. A disadvantage of the method is that, due to the relative complexity of the method, only three locations were chosen rather than applying the method over an area as seen previously. This makes the initial site selection much more of a key issue.

To summarise, several multi-criteria studies have been examined in the literature. Due to the spatial nature of the analyses they are worthy of mention in the context of this research. The methods are useful for building a high level, quantifiable picture of the local region. They are also useful in the absence of specific device data and are especially relevant for stakeholders as they often utilise environmental data and government records. However, because the analysis method fundamentally contains subjectivity, it is too general and inflexible to the needs of a developer. While the environmental aspects will be increasingly critical, earlier projects are likely to be smaller in scale and hence conflict with other marines users will be less of an issue and secondary to the economics. The weighting between environmental, technical and economic aspects is highly subjective and hence of limited usefulness. Lastly, the majority of studies do not consider a technology directly, but instead consider the energy resource as representative of the wave energy potential. As the WEC operation is very sensitive to the environmental conditions this is not the case in reality, for example as demonstrated in [45, 97, 110].

2.4.2.3 Levelised cost of energy

Sections 2.4.2.1 and 2.4.2.2 described studies that performed analyses of wave energy devices over geographic areas. This section describes spatial studies that calculate and map LCOE directly. This is a novel topic, and hence has not had much attention in the literature. The large amount of data required means that more advanced computational processes must be adopted to perform calculations over large arrays of points.

Dunnett and Wallace calculated the LCOE for three devices, considering 116 locations around the Canadian coast [72]. This involved loading CSV files of

metocean data, calculating the capacity factors for the devices and screening out sites with values below 20% and further than 15 km from shore. Five sites were then extracted for the LCOE analysis, considering a mooring system cost that scaled with water depth, an export cable length estimated from Google Maps and CAPEX per kW as specified by the manufacturers. OPEX costs per kWh were also used directly within the LCOE calculation, and the study also calculated the LCOE required to achieve a ten year payback period. The lowest value was found for the AquaBuOY device, at \$0.10/kWh.

Behrens at al., focussed on the wave energy potential around Australia [130]. They considered three different device types and determined LCOE around the coast using data from the US National Oceanic and Atmospheric Administration's (NOAA) WaveWatch III. Combining a ten year hindcast with power matrices, they produced maps of the energy produced by each device for a large area encompassing the whole of Australia. The LCOE was then calculated for the coastline around Australia using cost data from [72]. Only locations 5 km from the coast were considered. This, combined with using fixed CAPEX and OPEX estimates across all of the points, limited the analysis.

A more recent study conducted by Castro-Santos et al. calculated and mapped the LCOE around Portugal using GIS [131]. They also filtered out restricted zones, in a similar way to the studies identified in Section 2.4.2.2 (for example [117,121]). This involved using 11 different data layers, for example environmental protected areas, seismic fault lines and submarine electrical cables. To obtain power at each location they used a wave resource atlas (giving average theoretical wave energy per crest length) and combined it with capture width ratio, availability and PTO efficiency. Costs were estimated using CAPEX per kW and OPEX as 1% of total CAPEX per year. The LCOE was calculated considering three sensitivities: in CAPEX, in capture width ratio and in discount rate. The authors found that the best areas for wave energy were on the north-west coast, reaching €81/MWh for the most optimistic scenario.

The work does suffer from a number of limitations. As for [130], the cost calculations contained no spatial dependence. The spatial LCOE trend only comes from the energy calculation, which is biased towards far from shore locations. In reality these would incur higher costs in aspects like the export cable [129] and operations due to challenging wave conditions at the higher energy locations [97]. The energy is also based on the annual average wave resource, which means that inter-annual variability is not captured.

There have been other studies focussing on different areas. The Carbon Trust published a report in 2012 detailing as a wave energy resource study [46]. This also included a map of LCOE, derived by modelling empirical costs curves for the mooring system, export cable, vessel transit and availability. The mooring system was a function of water depth, while the other three were linear with distance to shore. Guanche et al. published a global analysis of O&M costs [132]. This used a global hindcast and time domain method to predict weather window occurrence. These were used to estimate global O&M costs for device corrective maintenance, using a Monte-Carlo technique to randomise the time periods for maintenance. Almost 1,200 points were considered along country coastlines. The authors calculated OPEX of €0.01-0.06/kWh, with the highest in Chile and Australia.

There have been spatial LCOE studies carried out for other marine renewables. Vazquez and Iglesias developed a MatLAB based spatial model for analysing tidal stream projects [133]. They considered CAPEX only, deriving rotor cost from rotor diameter, export cable cost from the distance to shore, and using an empirical relationship to express foundation cost (including installation) as a function of water depth. Sites were categorised in three ways: viable sites up to 21 p/kWh, future sites between 21-42 p/kWh and sites that are not economic, above 42 p/kWh. They also compared their results to a standard case, which assumes the same cost over the whole area and is only based on the power. Two points which look identical in this second study are found to be an order of magnitude different using their new approach (14 p/kWh vs 100 p/kWh), demonstrating the power of the spatial cost approach.

Cavazzi and Dutton examined offshore wind around the UK [134]. They created a GIS tool which included empirical spatial cost calculations for foundation, transmission, OPEX, installation. These were linked to factors like distances to port, cable length, vessel costs and associated timescales. They also included exclusions, and created maps for the different spatial elements. Sensitivity analysis was performed across the geographic domain for six parameters to see how they influenced the final results, as a way of including uncertainty.

2.4.3 Other models

In terms of economic modelling software, there are several commercial level tools that are in various stages of development:

- **WaveFarmer**: This software was created by DNV and is part of a wider suit

of tools including WindFarmer and TidalFarmer. It is commercial software that allows the user to determine the most optimum array layout for a wave farm. They allow yield and economic feasibility to be examined for different array configurations, including the effects of interactions between devices. While the software does offer site assessment capabilities it is primarily focussed on yield calculations on localised scales. The fact that DNV GL have released this software commercially demonstrates an industry need for wave energy assessment tools.

- **Exceedance**: A spin-out from University College Cork, Exceedance Ltd. was set up in 2014 and produce economic modelling software for industries including onshore and offshore wind, tidal and wave. The software allows calculations of LCOE, as well as other financial metrics such as internal rate of return (IRR) and net present value (NPV). It takes in a number of inputs and allows sensitivity of the results to these inputs to be examined. To the authors knowledge, the software relies on point metocean data for analysis, so is not capable of performing the kinds of spatial analyses previously described. The cost of €999 per month for the standard package might be somewhat prohibitive to wave developers, although it is also targeted at investors.

- **Wave Venture**: Wave Venture are another spin-out company, from Maynooth University. They specialise in wave energy consultancy and software. Their consultancy services include resource assessment, cash flow projection, LCOE estimation and technical due diligence.

  The company is still in its early stages. It aims to release commercial software to perform wave energy techno-economic analysis in 2018. Functionality will include detailed engineering and hydrodynamic analysis, weather window analysis, and failure modes and effect (FMEA). The company specifically mentions a software advantage as being "designed for deployment on High Performance Computing clusters", highlighting the complexity of the calculation procedures that this kind of modelling can require.

- **DTOcean project**: This was a collaborative project between eighteen organisations including the University of Edinburgh, Vattenfall and Ocean Energy Europe. The aim was to create a series of work packages to aid in the design of both tidal stream and wave energy arrays. The centrepiece is a piece of open source software to aid stakeholders in wave and tidal industries make key technological and business decisions [135].

It assesses the cost of an ocean energy array project, incorporating reliability and environmental analysis which can be applied as constraints to a project. Distinct optional modules can be used to enhance the analysis, including optimising array layout and cable layout. The cost is optimised with a "global decision tool" which uses a combination of user specified data and data from a global database. The project is now finished and the tool available to download online.

A follow on project, DTOceanPlus, was announced in May 2018 [136]. The aim of the €8m project is to build on the first generation of tools, this time working with a software developer to improve the usability of the tool. New modules will also be added, including a stage gate design tool (that can compare model outputs against industry benchmark standards) and a technology assessment tool that will analyse a given technology at TRL level 5.

All of the software described consider slightly different aspects of wave energy economic analysis. What they all demonstrate is that there is an industry need for these kind of tools, to allow the transition to a commercial market to be made. What they all have in common is that they have been designed with more conventional grid-connected farms in mind. As introduced in Section 2.1.2, there are more niche applications for wave energy which require different aspects to be incorporated.

2.5 Hybrid Energy systems

All of the previous studies examined have considered devices at utility scales, feeding into the grid. This section considers the other, off-grid application for small scale wave energy, as introduced in Section 2.1.2.

2.5.1 Features of a hybrid energy system

A hybrid energy system is where a combination of multiple electricity generation sources are utilised to provide electricity output. These are well suited for renewable energy, where the output power is variable, as it can provide more consistent power output. This is desired by the end consumer as it gives them the flexibility to use the energy at the times that they want. This is not an issue when connected to the grid, but for off-grid locations. The worldwide population who live off-grid has been estimated at 1.2 bn, the majority in sub-Saharan Africa and

South East Asia [137]. Hybrid energy systems can provide a cost effective way to supply energy to remote areas, for example the applications listed in Section 2.1.2.

The conventional way to supply energy to these off-grid markets is using diesel generators. According to IRENA, the global installed capacity has been estimated at 400 GW for diesel systems over 500 kW and could be as high as 1000 GW including smaller systems, although data do not exist [138]. About 60% of the market is for systems less than 20 kW and 15% for systems higher than 220 kW. Currently hybrid systems only equate to 2-3% of the diesel market size and hence have high potential.

A wind-based hybrid system will typically contain the following components [139]:

- One or more renewable energy sources. These are usually small, mirroring the energy requirements (as larger commercial consumers would be located on-grid).
- An energy storage device. This can store excess energy and provide energy when the renewable energy source is not producing power.
- A charge controller. This is to control the charging and discharging processes of the energy storage device.
- An uninterruptable power supply, which is dispatchable and can supply energy when the other systems are unable to.
- Rectifiers (AC to DC) and inverters (DC to AC) to covert the energy from the various energy sources into AC as typically required by the consumer.

The configuration of these components will depend on the electricity requirements and options available. Figure 2.8, taken from [140], shows examples of two wind and solar systems: one with DC side storage and the other with a diesel generator. These kinds of systems have been implemented all over the world. Examples include the Island of Eigg in Scotland [141], which combines hydro, wind and solar; Utsira Island in Norway, which uses wind and converts excess energy to hydrogen [142]; and Nabouwalu in the Fiji Islands which used wind and solar [143]. As of 2012 this latter system has apparently fallen into disrepair, with energy now supplied by the diesel generators only [144]. This highlights a disadvantage of the systems: they are more complex and more effort is required to keep them maintained.

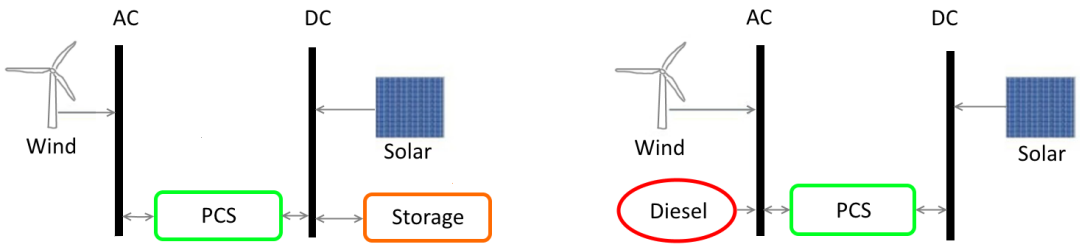

Figure 2.8: Examples of wind and solar hybrid system configurations. Taken from [140].

2.5.1.1 Energy storage

There are various storage options suitable for hybrid systems including batteries, flywheels and hydrogen fuel cells. Battery storage has many advantages. Batteries are portable, easy to scale to system size and provide instant response to the energy system [145]. The most common option is lead acid batteries [139], as they are a mature technology and especially cost effective [146, 147]. As of 2018 they have the largest global market share in terms of both sales value and storage capacity [145]. Other types of batteries, for example lithium ion and flow batteries, can also be used. However these are more expensive, especially at the larger scales required for use in an energy system.

There are two main types of lead-acid batteries: flooded (FLA) and valve-regulated (VRLA). FLA batteries contain a liquid electrolyte that need regularly replenished. They also release hydrogen gas during charging and so the storage location needs actively ventilated [148]. VRLA batteries contain a solid electrolyte and are sealed. While the costs are higher and lifetimes typically shorter, they only need passive ventilation and require less maintenance [145].

The lifetime of a battery will vary depending on the type and how it is used, but is typically in the range of 4-7 years [149,150]. Deep discharges of the battery will reduce the lifetime, as will higher operating temperatures. Some batteries are specially designed for deep cycle applications, which means that they can regularly be discharged by 80% of their capacity with a reduced impact on lifetime. The charge going in and out of the batteries must be carefully regulated, to protect them from damage. The charge controller monitors the battery charge to ensure that the state of change does not drop too low.

2.5.1.2 Diesel generators

Regardless of the scale of the renewable energy systems and battery bank, almost all systems will need a backup power option to supply power when the need is critical. This role is served with a diesel generator [140]. The major advantages

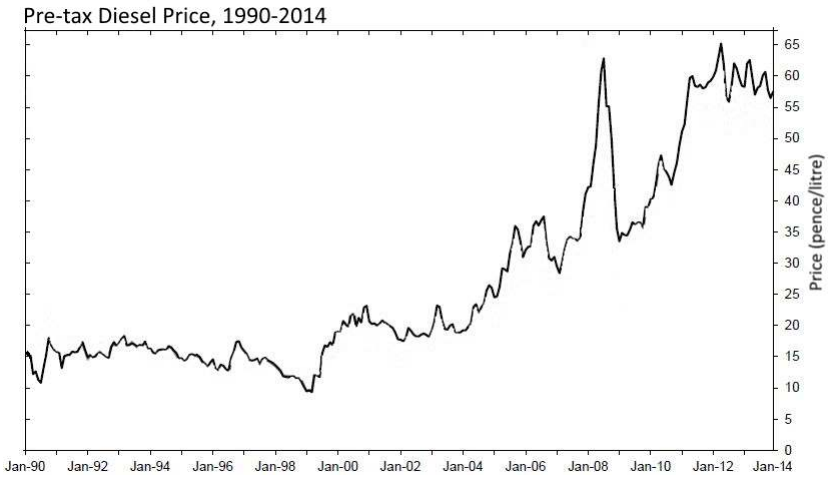

Figure 2.9: Historic pre-tax diesel price in the UK. Taken from [153].

of using diesel generators are cost and convenience, and for this reason they are the most common way to provide power for off-grid markets.

Diesel generators typically run at efficiencies of 30-35% [146] and have a lifetime of 20,000 hours [151, 152]. They are subject to fluctuating diesel price, subject to geopolitical factors and outside the control of the consumer. Examples of this long term variation are shown in Figure 2.9 for the UK from 1990-2014 [153]. They are noisy and pollute the local environment. These issues mean that the general aim of the hybrid system is to minimise the reliance on the generator, but in a cost effective way.

2.5.2 Hybrid system modelling

It is important to be able to model the performance of a hybrid system, to judge whether it would be beneficial for the proposed application and ensure that it is properly designed. The systems are more complex to model than just a single energy source [154], as the energy provided is obtained from a combination of the systems. These have different operational modes that depend on the load requirement and energy available [139].

There are various software options available to simulate hybrid energy systems, for example nineteen are described in [154]. These can be classified into four types [155]: pre-feasibility, for high level economic analysis and rough sizing of components; sizing, to optimise the components used; simulation, which perform in depth simulations using detailed system parameters; and open architecture, where the user can specify their own control algorithms.

The Hybrid Optimization Model for Electric Renewables (HOMER) is an ex-

ample of this software [156, 157]. First developed in 1993, this is the most widely used software [154], claiming over 100,000 users in 192 countries [158]. It is numerously used in research, recent examples include [159–162]. HOMER takes both technical and economic input parameters and simulates the system by balancing the power produced with the electricity demands over a series of timesteps. It should be noted that HOMER does not perform full analysis of the electrical system, (for example simulating currents and voltages) but deals with the average energy produced over discrete time-steps. The energy inputs from the various sources are optimised to minimise the total NPC. Sensitivity analysis can also be performed by modifying the system components (for example considering different generator models or costs).

HOMER is a powerful tool, underpinned by years of research, and is generally regarded as being sophisticated and realistic [158]. There are two key issues with the model which motivate this research. The first is that it does not support wave energy. The second is that, as a commercial tool, the software is difficult to integrate into other tools used by industry. The user is reliant on the control systems and optimisation process as specified by HOMER.

2.5.3 Application to aquaculture

2.5.3.1 The aquaculture market

The main market that Albatern are pursuing for their technology is the Aquaculture sector. Aquaculture is the process of farming aquatic organisms for human consumption. The industry is well established and expected to grow into the future due to pressure on food supply from overpopulation. In 2007 it provided 43% of aquatic animal food for humans and in 2008 was worth $98.5 billion, producing 52.5 million tonnes of produce [163]. The largest world market is Asia, which made up 89% of the volume and 79% of the value. The two main facilities suitable for wave energy development are coastal ponds/tanks and offshore cages. This is because they are located closest to the resource and are often off-grid, relying on diesel generators and fuel imports for power.

Scotland is renowned for its aquaculture industry. In 2017 the gross value added (GVA) of the sector was £620 m [164]. The majority of this, £540 m, was in the salmon farming trade. This fish also account for 95% of the finfish produced. From 2005 to 2015 the amount of salmon produced per annum increased from 130,000 to 170,000 tonnes, a 30% increase. This is smaller than Norway and China, the leading producers, who produced 1.3 m tonnes and 600,000 tonnes

in 2015 respectively [165]. While the market is largely domestic [166], Scottish salmon is one of the UK's largest food exports [167] and there are ambitious plans to grow the sector. By 2030 it is anticipated that total finfish production could reach 300,000 to 400,000 tonnes, doubling the economic value of the sector and increasing the number of indirect jobs from 8,800 in 2016 to 18,000 [168]. Because floating cage Scottish salmon farming is the primary market of interest for Albatern, no other types of aquaculture are considered further.

2.5.3.2 Salmon farming

The salmon farming process is split into six distinct stages:

1. Fish eggs are fertilised and incubated in freshwater hatcheries.
2. The fish grow up to 100 g in mass in freshwater tanks. These fish are known as parr.
3. The fish mature and undergo "smoltification", giving them the ability to survive in saltwater. They are then are transferred to sea.
4. The fish continue to grow to a mass of 4-5 kg over a period of 12-24 months. The specific time period depends on the practice of the fish farm operator.
5. Once of sufficient mass, larger fish are collected and slaughtered.
6. The fish produce is then processed and sold.

These are illustrated in Figure 2.10, taken from [166]. The overall process, from egg to processing, takes about three years. Of interest to this thesis is the growth stage at sea, as this is where wave energy could directly contribute to the farms energy requirements. Generally the facilities used for the first two stages are grid-connected [169] and hence of less interest for the hybrid system application.

An offshore fish farm comprises of three main elements:

- **Floating offshore cages**: These are used to contain the fish. They are generally constructed from HDPE [170], with layers of netting to prevent the fish from escaping. There are multiple units per site, the cage specification depending on the site conditions. An individual cage interacts with the environment and other cages in various ways, as shown in Figure 2.11.
- **Mooring system**: This is designed to keep the cages on station. The cages are arranged in a rectangular grid, interconnected with mooring lines, and

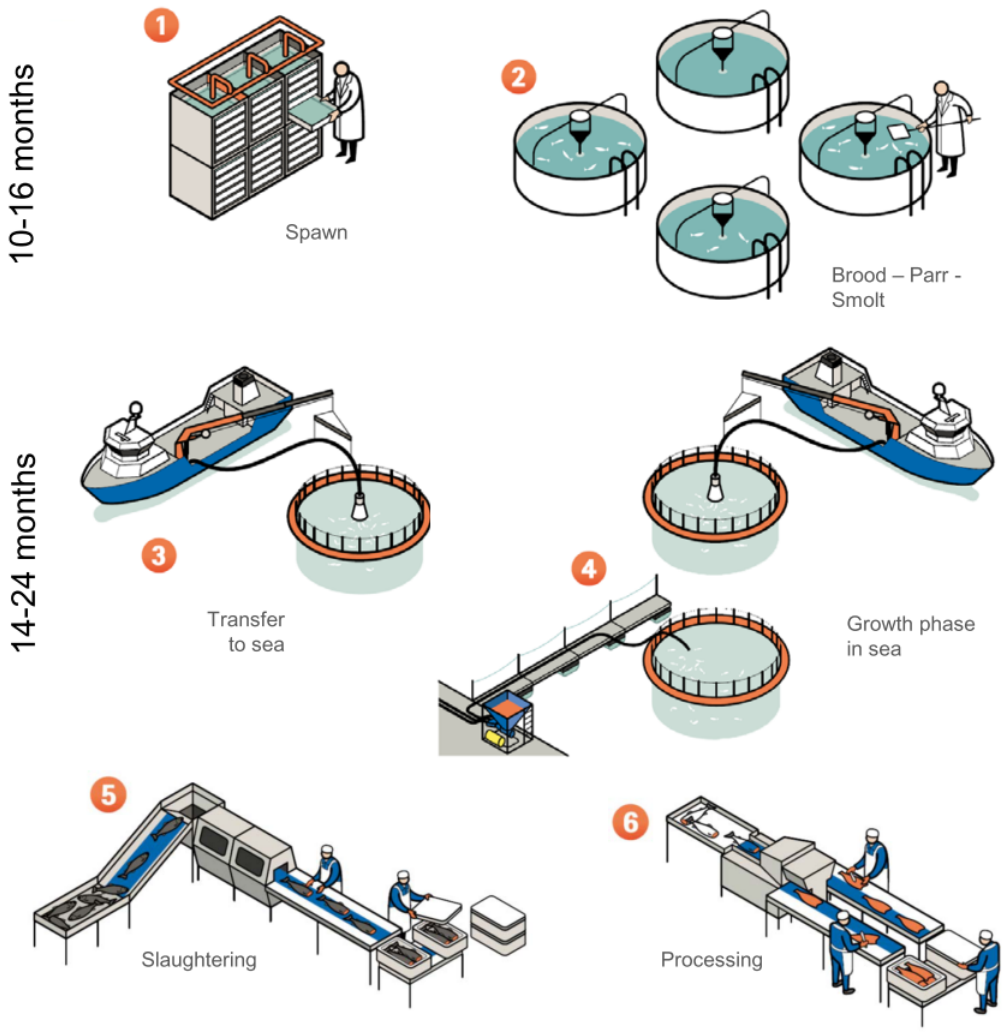

Figure 2.10: The six stages of the salmon farming production cycle. Taken from [166].

anchored to the seabed at multiple points using drag embedment or gravity anchors [170]. The number and strength of the lines will depend on the site conditions.

- **Feed system**: There are various ways that the fish can be fed. A common option is a feed blower (or cannon), which blows high volumes of feed from a hopper into the cages [169]. This can be automated. Larger or more modern sites might instead use a feed barge: a dedicated vessel which houses the necessary feed. This serves as a centralised store, often with lines which run to the individual cages [170]. These systems can be costly, and are less suitable for more exposed locations [170].

There are many factors that need to be considered at this stage. The most significant cost to the fish farm operator is in fish feed, which makes up 50-75% of the total production cost [166, 170]. Minimising the feed requirement not only

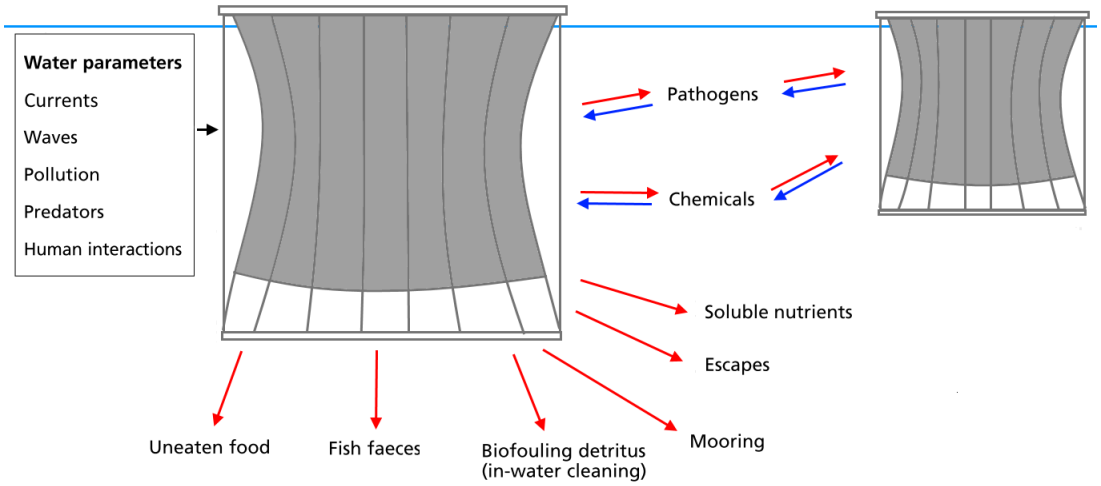

Figure 2.11: The mechanisms by which an offshore fish farm cage interacts with the environment (red arrows) and other cages (blue arrows). Adapted from [170].

reduces cost but also reduces the environmental impact, as uneaten feed falls below the cages and damages the benthic environment [171]. A current at the site is generally desired, to disperse the waste and reduce the impact.

Of the salmon seawater farm sites, 83% of them produced over 1000 tonnes of fish in 2016 [172]. The majority of these are also off-grid [169], with power supplied by a diesel generator. This trend is also seen in other countries, for example half of the fish farms in Norway rely on diesel generators [173]. These generators are subject to the disadvantages as introduced in Section 2.5.1.2. The typical size of a generator is 150 kW [169], with a cost of energy between £190-260/MWh [169].

2.5.3.3 Synergies with wave energy

Wave power could offer a number of advantages to the aquaculture industry. As part of a hybrid energy system it would reduce the operating hours of the generator, reducing the fuel consumed and improving its lifetime. This would not only reduce fuel cost and CO_2 emissions but also make the project less sensitive to fuel prices, which are governed by external factors and can hence be unpredictable. Producing the fish in a more environmentally sustainable way could improve the image of the aquaculture developer, making their produce more marketable and allowing them to add a price premium [174].

One of the biggest dangers in salmon farming is fish escapes. These events can cause lost revenue, ecological damage from farmed salmon interacting with wild salmon stocks [175] and potential negative publicity for the operator (for example [176]). A large scale wave energy system could act as a breakwater and take

significant energy out of the sea, reducing the damage to nets and moorings. Such damage does occur. For example in 2015 16,000 salmon, worth approximately £250,000 escaped from a farm operated by Marine Harvest due to storm damage [177].

Generally the industry in the EU is trending towards more exposed farm locations, a requirement to meet 2030 industry targets [178, 179]. These sites have better water circulation that mitigates environmental impacts, improves fish welfare and results in a better quality product [170]. This could also benefit WECs, the more energetic resource leading to better energy capture.

There are similarities in the types of components that are required, especially for small scale WECs. This includes the mooring systems and the vessels required for manoeuvring around site. If the wave industry could access these items at a cost reduction then it could benefit both industries. There is also the possibility that small wave devices could be directly connected into the fish farm mooring system, again saving cost, although this would require detailed feasibility analysis [169].

Lastly, there are numerous lower power ancillary applications that a small scale WEC would be well suited for. Any excess energy could be used for non critical, low power applications like sensors, underwater cameras, net cleaning robots or heating site office space [42]. There are also more novel applications, such as equipment to remove sea lice from the fish (for example [180] or [181]). This is of particular interest as sea lice, parasites that prey on salmon, are a major concern for fish farm operators and their prevention is a priority going forward [168]. As farms move to more exposed locations, more automated systems are required to counteract reduced accessibility issues [170].

2.5.4 Hybrid system research examples: aquaculture and wave energy

Using a hybrid energy system to power a fish farm is not a new idea. However it is one which has been seldom examined in the literature, even without considering wave energy.

A study by the Scottish Aquaculture Research Forum (SARF) examined the different renewable energy options that could suit an aquaculture site [169]. Largely a qualitative approach, they identified salmon farming as especially suitable, with more passive types of fish farming such as for shellfish generally unsuit-

able due to the very low energy requirements. They identified wave energy as an option with "possible suitability", with the main barrier in the short term being a high LCOE. From this, they concluded that small scale wave would be unlikely to be suitable, although just compared an LCOE number from the literature and did not carry out a full economic evaluation.

Syse carried out a more in depth study, also comparing different renewable sources [173]. A quantitative analysis was carried out for a wind-solar-diesel system at an off-grid aquaculture site, using HOMER. The energy demand was estimated from visiting a fish farm and noting the components used; this included domestic usage and assumed a period of one year, with variability applied on a daily and timestep basis. The hybrid system was found to have a lower NPC than the diesel only system. A renewable only system was also examined, however this was found to be uneconomic with a LCOE of £0.81/kWh compared to £0.491 for the conventional diesel system. The author did consider wave energy at the start of the project, however again excluded it as an option due to higher LCOE, which was not quantified, and lack of data regarding OPEX.

Botne Sandberg et al. investigated both technical and non-technical factors critical to the viability of wave energy to power luxury resorts and small utilities. It included an LCOE analysis. A point absorber, currently being developed by CorPower, was used for the analysis. Considering an availability of 90% and using a device power matrix, an array of 1-4 WECs was found to be able to supply 7.5-22% of a hotels energy demand, although the time dependence of this was not accounted for in the calculations. The LCOE of a wave-battery system was found to be €240-430/MWh, with a battery lifetime of ten years assumed.

There have been other studies examining various lower power applications in the aquaculture industry. Erwin et al. used HOMER to examine hybrid biomass and wind systems for a shrimp pond in Indonesia [182]. They found that a renewable option was feasible for the small system (with peak energy demand of about 15 kWh). Prasetyaningsari et al. considered a solar powered aeration system for an onshore fish pond, again with a lower energy requirements (2kWh per day average). Both of these studies demonstrate the applicability of hybrid energy systems to aquaculture, however are too small to be of interest for wave energy at Albatern's scale.

2.5.5 Summary

Despite references to wave energy for hybrid system applications, there has been very little research in quantitatively examining them. A key reason for this is the complexity of modelling required, lack of data and the fact that it is too niche to have caught the attention of large software developers like HOMER Energy. This thesis aims to contribute to knowledge in this area by describing a model capable of performing such hybrid system analysis. Because it calculates LCOE it is highly desirable for early stage feasibility analysis. Moreover it incorporates spatial analysis methodology, as described in Section 2.4.2. To the authors knowledge this kind of analysis has never been carried out before in the literature.

The Computational Model: Structure and Implementation

In order to perform the in-depth calculations required to assess the economic potential of a wave energy project, a dedicated computational model has been created. Because there is a large variety of both input data required and output data generated, a key part of this research has been concerned with designing the model in an organised, flexible way. Emphasis has been placed on modularity of the underlying code, to make the model easy to interpret, adapt and expand into the future.

This section begins with an overview of the overall model structure and the calculation which is being performed. This is followed by a summary of the input data required and more detailed descriptions of each of the various sub-modules, including how they are organised and the functionality that they contribute.

As well as the code used directly in the model, more generic modules have been designed to aid with particular processes. Descriptions of these can be found in Appendix B.

3.1 Overall Calculation Procedure

While the model has the ability to analyse different wave energy systems and probe a large number of system sensitivities, in all cases the overall computational procedure follows an identical logic. This is made up of well defined, ordered calculation stages which are interspersed with several key decisions which dictate

the elements of the model that need to be utilised. A high level flow diagram describing this calculation sequence from start to finish is shown in Figure 3.1. Programmatically this is executed by a top level function, `spatial_analysis`, which calls sub-functions to achieve each process in the chain. This analysis is contained within a distinct module, `spatial_analyses.py`. It contains all of the top level functions and scripts that define the overall calculation process.

First the input data, stored in configuration files, are loaded into the model environment. This includes metocean data, a device power matrix and costs, as well as optional system components like an export cable and mooring system. The model is fully coded using the Python (2.7) programming language [183]. This decision was taken for multiple reasons: the relative ease of use, high level of support available and the fact it is free to use. A further advantage of Python is that it is very well suited for OOP [184]. OOP is a popular software development approach, based around the idea that real world objects can be categorised and represented programatically using a distinct data type, or *class*. OOP was applied to this project to keep the underlying code modular and flexible, providing consistency and making it easy to modify specific parts of the model without worrying about impacting the rest of the code. Basic definitions of the Python terminology used in this section can be found in Appendix A.1.

After loading the data, a default discount rate of zero is set if not specified in the configuration file. The function can then follow two different paths, depending on the application for the wave energy system. The more typical grid-connected analysis, the subject of this chapter, follows the high level methods previously outlined in Section 2.3. The off-grid analysis obtains a wave energy time series for each point in turn, using this as an input to an energy balancing algorithm. This employs a specially created off-grid analysis module, similar in principle to HOMER software (as introduced in Section 2.5.2). It requires additional system components to be specified; these, along with the other facets of the off-grid module, are discussed in Chapter 4. Whichever application is considered, the key output is the total energy produced by the device. This is the denominator in the LCOE calculation, Equation 2.1 from Section 2.3.1. If the time series data do not cover the lifetime of the system that is being modelling (for example ten years of data but a WEC lifetime of 20 years) then the calculated energy can be projected forwards in time to cover the full lifetime.

Next the costs analysis is undertaken for every system component. The specific calculations, discussed within the proceeding sections, depend on the nature of the component but all create the same output: discounted cash flows which are

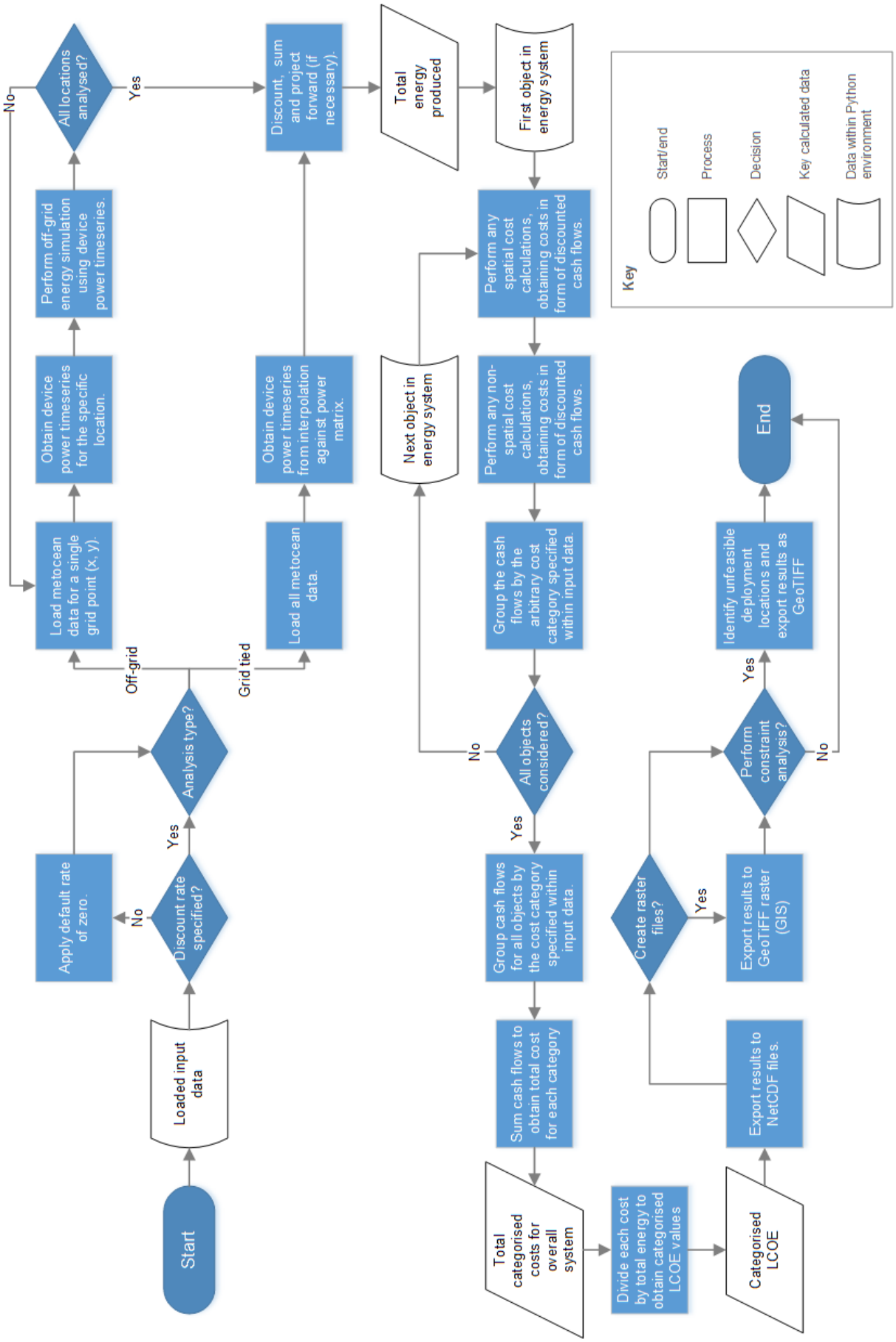

Figure 3.1: The main processes and calculation steps that are used in the model. The decisions that are taken depend on the energy system and modelling inputs being examined, specified by the user in the configuration file.

grouped according to arbitrary cost categories defined within the input data. Once all of the cash flows are calculated for all of the input objects, identical categories are summed together to obtain one cash flow per category. This is then summed along the time dimension to get total categorised costs. These form numerators of the LCOE calculation, allowing LCOE values to be obtained for each user-defined cost category using Equation 2.1.

The two-dimensional energy, cost and LCOE results are exported to NetCDF files. The merits of this file type, as well as the other data types used, are discussed in Section 3.3. Output maps can also be created if an option is specified in the input configuration file. These maps are GeoTiff raster image files and allow the data to be visualised in GIS software (e.g. ArcGIS). Vector files, for example port locations or the export cable paths across the domain, can also be created from the output data.

Lastly, an optional constraint analysis can be performed. This allows invalid deployment locations for the device to be defined and identified by examining the values of physical site parameters. Raster files are created for each individual constraint which can be laid over the previously created result maps in GIS. A raster showing combinations of constraints is also created.

Figure 3.2 shows the structure of the calculations steps, as categorised within the three high level analyses from Section 2.3. While there are clear data dependencies between the calculations, they have been designed with modularity in mind: so that the key analyses can be isolated and run independently if necessary. The environmental data includes the water depth, required for some of the cost calculations. The model outputs are converted to GIS raster formats and exported, as previously mentioned. The only GIS data imported into the model are for the constraints analysis, the rest of the data are contained in NetCDF or text files (these data types are discussed in more detail in Section 3.3). As the constraints analysis is an optional, secondary model application it is not shown on Figure 3.2.

3.2 Module Structure

As mentioned in the previous section, to achieve the research objectives an OOP philosophy has been used. This resulted in the creation of approximately 40 classes, designed from scratch specially for the project. To keep the overall model manageable, it is organised into eight distinct sub modules. These are summarised

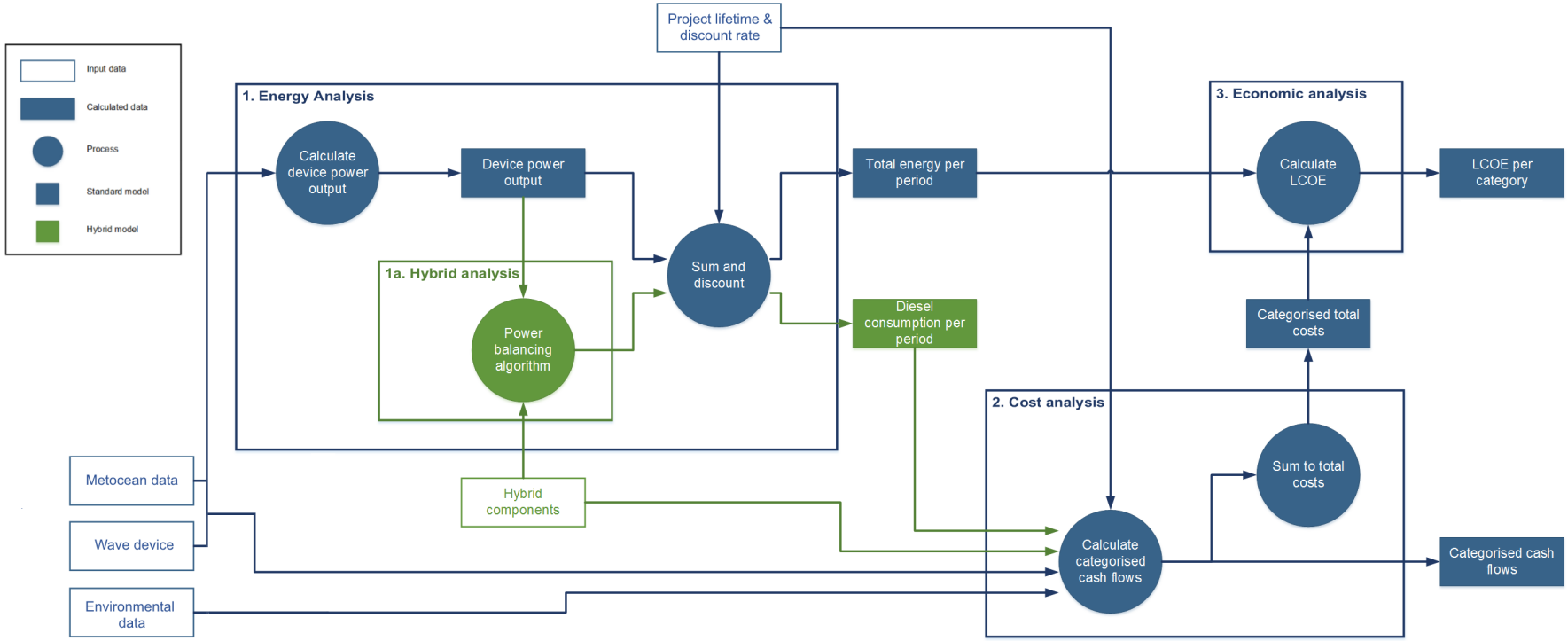

Figure 3.2: The main input data and processes associated with the model calculations. Blue objects apply to both hybrid and grid-tied systems, green objects the hybrid system only. White filled boxes are the input data, filled boxes represent calculations (circles) and calculated quantities (rectangles).

in Table 3.1.

Module	Main purpose	Section/Chapter
Base classes	Provide top level classes with attributes and functions that are inherited by classes within other modules.	3.4.
Wave site	To define the geographic area and extract metocean data. These data are required for energy calculation, weather window estimation and pathfinding for spatial cost estimation.	3.5
Wave device	To calculate energy yield and costs for the wave energy device (excluding balance of plant).	3.6
Operations and maintenance	To allow O&M tasks to be defined and the costs estimated.	3.7
Export cable	To calculate export cable capital and installation cost.	3.8
Mooring system	To calculate mooring system CAPEX.	3.9
Constraints	To identify invalid wave energy deployment locations in the geographic area.	3.10
Off-grid sub-model	To allow hybrid wave energy systems to be modelled and their performance and economics assessed.	4

Table 3.1: The eight different modules that make up the model.

The first seven of these make up the main grid-connected model. The final module, the off-grid sub-model, extends the core functionality to niche off-grid energy systems. It is designed to be relatively standalone, only directly requiring the `base_classes` module, but utilises the other modules when considering spatial wave energy systems. Further discussion of this module is provided in Chapter 4; this chapter is only concerned with the core functionality.

The way that the classes link together across the first six core modules is shown in Figure 3.3. This is a simplified Unified Modeling Language (UML) diagram, with the class attributes and methods omitted. While the specifics of the modules are discussed in the later sections, the figure alone makes apparent some of the key benefits of the approach. At the top, the `base_classes` module is acting as the foundation for the whole model. The vast majority of child classes inherit from a single class, `Base`, as this allows key metadata and database integration abilities to be defined once and propagated down via inheritance. The

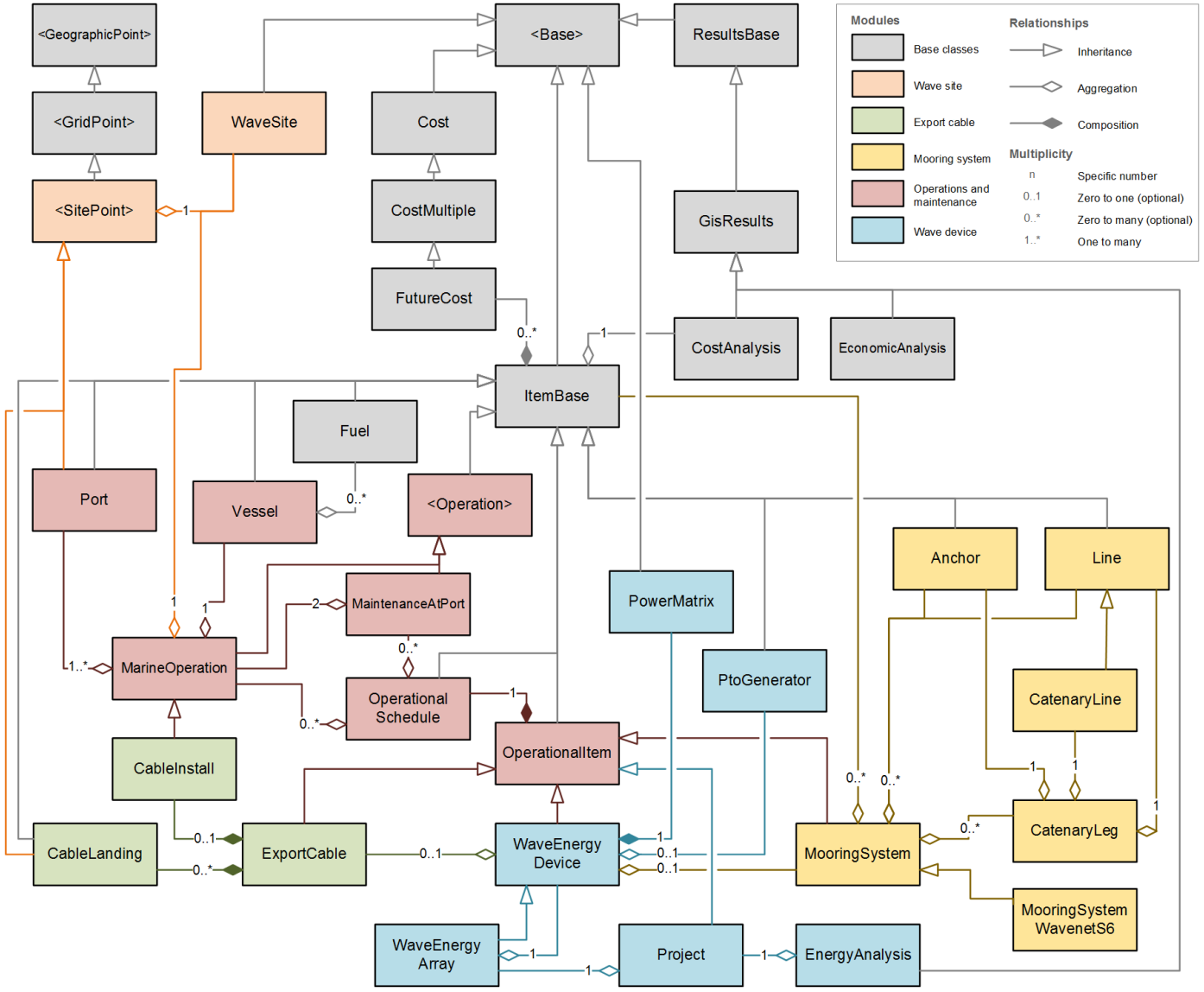

Figure 3.3: The relationships between the different modules and classes that make up the overall model. Six of the seven classes from Table 3.1 are depicted (the hybrid module is omitted to improve readability). Classes that are enclosed in chevrons (e.g. <Base>) exist but are not directly initialised during running of the model; they are used to pass down attributes and methods only.

`ItemBase` class is arguably the most important in the model, defining any cost item and allowing combinations of cost components to be easily calculated under a uniform methodology. The `WaveEnergyDevice` class represents the culmination of the various different system components: the export cable, mooring system and operational activities.

It is worth noting that these modules occupy very specific spaces within the overall structure, with very few interdependencies between them. This is particularly advantageous as it allows new functionality to be easily added with little to no modification of existing modules required. Version control is also straightforward, as each module can be tracked separately. Care has been taken to limit the usage of multiple inheritance, as this can be a source of bugs as the complexity of the class hierarchy increases [185].

The constraints module is not included in the diagram. This is because the classes are more abstract in nature and do not represent physical aspects of the wave energy project.

To complement Figure 3.3, more detailed UML diagrams for each module are presented in the relevant sections. Each is used to guide the flow of text within the section, and hence should be used by the reader as a reference to the attribute and function names and descriptions that are presented. Descriptions of the terminology used in the UML diagrams can be found in Appendix A.3.

3.3 Data Types

There are various types of input data that are required. Metocean data, namely H_s and T_p, are stored as NetCDF (.nc) files [186]. Because the data required by the spatial model are three-dimensional (time by latitude by longitude), these file types are advantageous as they allow different portions of the data to be easily queried and loaded separately. This is useful when analysing smaller datasets, so that the necessary data can be easily extracted from the full dataset without incurring the memory issues from having to load all the data. Within a NetCDF file multiple data variables can be stored and defined over the same dimensions. Specific portions of data can be easily queried using Python packages like Pandas or xarray [187]. The data can also be chunked, either when creating the file (using a tool like nccopy) or upon reading (using xarray). This essentially allows the data to be loaded in bite-size chunks, rather than in one go, which is much less memory intensive.

Class instances that represent physical objects, for example devices and export cables, are stored in text (.txt) files. These files are two column, with attribute names on the left and the attribute values on the right, separated by a tab delimiter. The attributes can point to further text file paths, defining other class instances. The files are read with a specially created function, which iterates down through the directory tree and creates a class instance in Python from the attributes specified in the file. This way of storing objects is useful, as it is relatively simple for the user and does not require the use of any further software or python packages. It also allows class instances to easily be nested inside each other, and the attributes are straightforward to modify on the fly. Examples of these text files can be found in Appendix C.

An alternative method that was examined was using a datebase. The advantage is that it enforces organisation and allows the data to be easily queried. NoSQL was considered rather than the more conventional SQL database approach. This is because NoSQl has no constraints on structure, allowing different types of data to be stored together. Setting up a SQL database requires good knowledge of the schema and more preparation upfront to avoid future issues associated with large quantities of data [188]. Having no limitations on schema would be useful for this type of research as the object classes and functionality has evolved on an iterative basis, and hence there is no need to constantly re-evaluate the database design. The specific NoSQL software considered was MongoDB. This is because it has good integration with Python, lots of support available (including tutorials and a free online course) and can be downloaded free of charge. While a more elegant solution, the text file storage method ended up being used. This was for two reasons: project time constraints and because the learning curve associated with using databases would make the model harder to use for other people within the sponsoring company.

Lastly, some input data sources are stored as GIS files. This mainly applies to constraint layers: layers which limit the potential deployment locations of the wave energy device. Storing these data as GIS files allows them to be externally visualised in GIS software (for example ArcGIS) as well as loaded into Python to use in analyses. These constraint layers are discussed in more detail in Section 3.10.

3.4 Base Classes Module

The `base_classes` module provides the foundation to the model. It is used across both the core model and off-grid sub-model. Figure 3.4 shows the UML diagram representation of the module. Advice on the notation and how to interpret all of the UML diagrams in this work can be found in Appendix A.3.

The only dependencies which it has are to standard Python libraries, for example NumPy, SciPy and Pandas. The module contains three "families" of classes: the cost classes, results classes and geographic classes. It also contains the fundamental `ItemBase` class, which defines any item used in the code with attached costs.

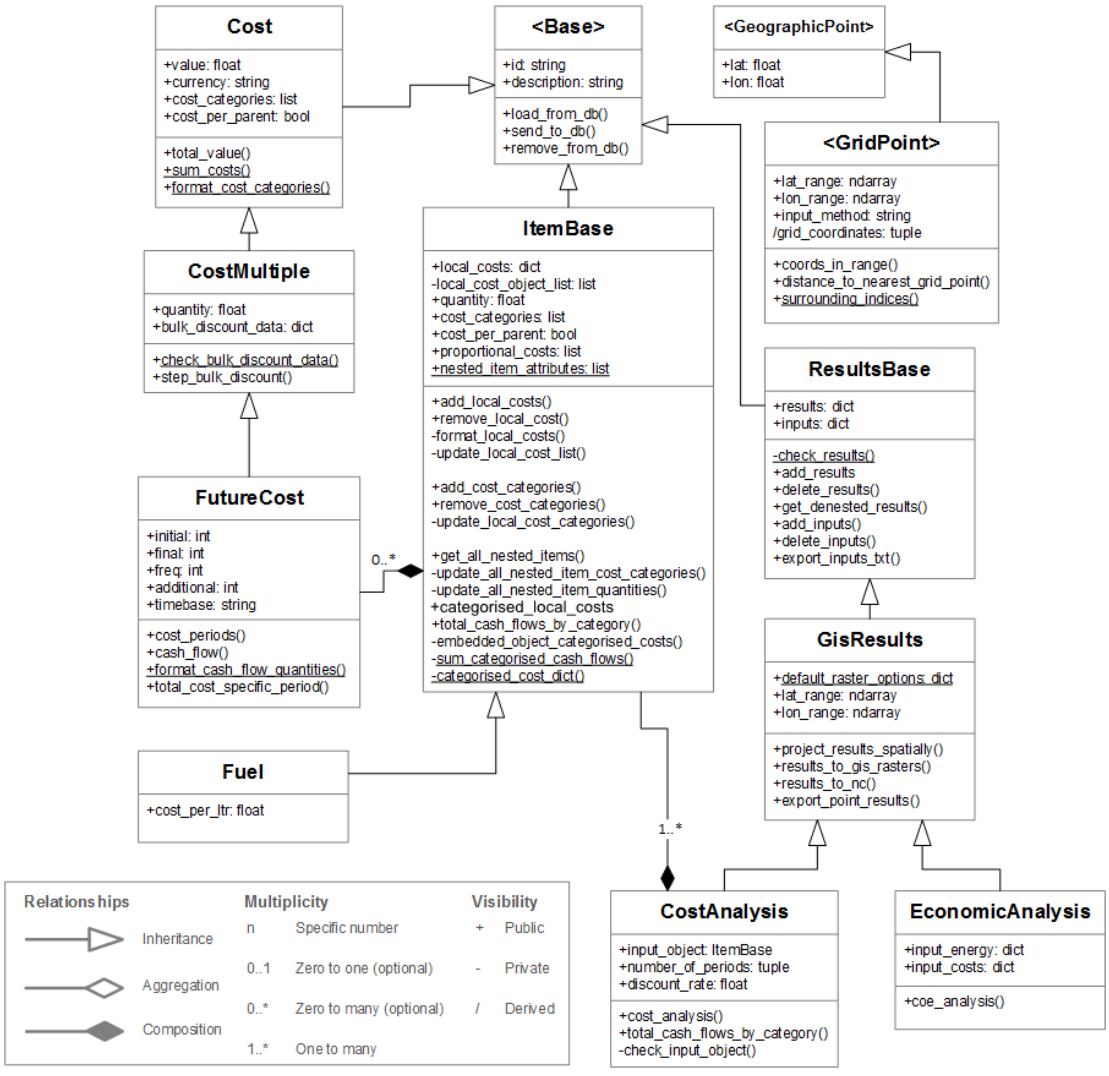

Figure 3.4: The main attributes and methods for the classes making up the base class module, and the relationships between them.

3.4.1 The Base class

The `Base` class serves as a parent class to every class that represents a physical object. Objects have an `_id` attribute, an id tag that allows the object to be identified and, in theory, stored as a unique database entry. This can either be specified by the user or automatically created using the MongoDB ObjectId class. The class also has methods for exporting the current object to or from a MongoDB database, although these are not used in the implementation described and are included for completeness. As well as an id, base class objects also contain a `description` and `comments` attribute that can hold basic information.

All of the base class attributes can be exported to a csv file, using the instance method `export_attributes`. This allows the user to view the attributes outside of the Python environment, and is particularly useful for documenting the inputs going into the model. Within the method, the user can choose specific attributes to export by name and/or by data type. Additionally, the user can decide whether to export the attributes of nested objects. These objects are class instances themselves, typically incorporated into the instance within specific attributes. An example is the wave device class (`WaveDevice`), which includes an export cable attribute. This attribute is an instance of another class, `ExportCable`, and is embedded within the device instance.

3.4.2 Costs

These classes were created to allow the model to properly handle costs. Because there are a large variety of objects that have costs associated with them, a base cost class allows the uniform treatment of costs across the model.

The base cost class, `Cost`, represents a single cost. Its attributes include the cost value itself, the currency of the cost and description and comments, as in `Base`. A method `in_currency` allows the cost to be represented in a different currency, using the third party Python package *CurrencyConverter* [189]. This is useful when aggregating costs that are provided in different currencies. A key attribute to aggregate multiple costs is the `cost_categories` attribute. This is essentially a list of tags, representing the categories that the cost fits into. These are designated arbitrarily. Examples could include "device CAPEX", "mooring system" or something lower level like "delivery cost". All of the costs that fall under a certain category can be grouped together for cost analysis, and hence different costs easily compared (see Section 3.4.3).

The `CostMultiple` class builds on this by introducing a quantity attribute, to define times when a cost is incurred multiple times. The `bulk_discount_data` attribute allows bulk discount factors to be applied to the items, occurring after discrete quantities. This is specified as a dictionary, for example `{0.8: 10, 0.6: 20}` would indicate that the cost value falls to 80% of the original cost after ten items and to 60% after 20 items. The total cost value, calculated using the `total_value` function, is hence the cost value multiplied by the quantity, with any bulk discount factored in.

The `FutureCost` class represents costs that are incurred in the future. Costs are defined not only with a value, but with attributes that allow the future time periods where the cost occurs to be defined. The `initial` and `final` attributes are integer values defining the first and last time period where the cost is incurred. The `freq` attribute sets the frequency of the cost. For example, a frequency of two tells the class that the cost is incurred every second time period from the start period to the end period. The `additional` attribute allows any additional periods not covered by the frequency attribute to be specified. The time period definition can be specified to either an annual or monthly base. This is only relevant if a discount rate has been specified for calculating the final cost, to ensure that the costs are appropriately discounted into the future (see Section 2.3.1 for a description of discounting). Linking the base cost with a time element means that capital costs and operational costs are properly discounted and can be distinguished. Capital costs are assumed to occur in time period 0.

3.4.3 Cost items

The `ItemBase` class is one of the most important in the model. It is used to represent objects that have one or many costs associated with them. It is a parent class to many objects and provides methods which allows costs to be easily grouped and summed according to their cost category attributes.

At the heart of the class is the `local_costs` property. This is where all of the individual costs related to the object are stored, each converted into a `FutureCost` instance upon input using the method `format_local_costs`. The actual property is a dictionary made up of these cost instances, with each key defined by the cost's `_id` attribute. Using a dictionary makes it easy to remove specific cost items and prevents identical costs from being accidentally duplicated within the `ItemBase` instance. Methods to add or remove individual local costs are coded into the class, improving usability when working within Python.

Like the cost classes previously discussed, the class also has `quantity` and `cost_categories` attributes which work in the same way as previously described. They are both implemented by composition, via a private embedded `Cost` instance. This allows only these attributes to be copied from the `Cost` instance without requiring an unrealistic inheritance relationship. The quantity is multiplied by the constituent cash flow totals to obtain an overall cash flow for the instance as as whole.

At a local level, this is achieved using the method `categorised_local_costs`. The method iterates through the local costs and obtains a cash flow for each cost instance, based on an input number of time periods and discount rate. As the `total_value` method of the cost classes is used, it means present values and any bulk cost reductions are automatically included. The totals are then multiplied by the instance `quantity`, if the `cost_per_parent` attribute of the cost is set to *True* (otherwise the assumption is made that the cost is only incurred once despite the quantity of `ItemBase`). The cash flows are then linked to their cost categories using a dictionary. The `cost_categories` defined at the `ItemBase` level are automatically added to the individual cost instances at the beginning of the cost calculation. This follows the logic that the embedded cost items can be considered part of the wider system.

More useful than calculating cash flows for the costs within `local_costs` is the ability to calculate cash flows for all of the embedded cost objects contained within the instance. The method `_embedded_object_categorised_costs` does this by examining all of the instance's attributes, searching for other instances of `ItemBase`. This process is achieved by a specially coded algorithm, `get_nested_instances`, which is contained within the extra utilities library (introduced in Appendix B). Any additional `ItemBase` instances that are found are saved into an output dictionary and appended to the loop, the algorithm working down through all of the embedded objects recursively until all `ItemBase` instances are identified. As these items are found, the higher level quantities and cost categories are filtered down to them to ensure the correct item quantities are used.

One final point is that the `_embedded_object_categorised_costs` searching algorithm also finds instances contained in lists, by searching each list entry in turn. This allows multiple `ItemBase` instances to be grouped together within a single attribute, preventing class hierarchies from getting too complex. The method is not compatible with `ItemBase` instances contained in dictionaries. This decision was made because the dictionary data type is typically used for larger data within the model (e.g. graphs from path finding algorithms) which would greatly

slow down the code. The dictionary exclusion does not apply to the `local_costs` attribute, this achieved using the `local_cost_list` private attribute. This is updated automatically and contains identical data to the `local_costs` dictionary. As a list type it can be found by the algorithm.

After the embedded `CostItem` instances are found, the `categorised_local_costs` method is run on each one. In the most basic case this just performs as previously introduced, although some child classes modify this method to perform other calculations that are required. For example, the `ExportCable` class version of the method contains an initial stage which calculates the cable length prior to cost calculation.

The `_embedded_object_categorised_costs` method is private, not meant to be directly used. The whole cost aggregation process described above is achieved with the `total_cash_flows_by_category` method. This internally runs the aforementioned function, combining this with the private functions `sum_categorised_cash_flows` and `categorised_cost_dict` to format the output in a more user friendly way.

The final thing that this function does is create any proportional costs defined by the user with the `proportional_costs` attribute. These costs are different to local costs because, rather than absolute values, they are defined in terms of specific cost categories. They are still instances of `FutureCost` but with an additional attribute, the `master_category`. Once all of the cost category totals categories are obtained, all of the proportional costs enclosed in the top level item are extracted. For each, the cost category which matches the master category field is identified and the proportional cost value obtained by multiplying the cost category total by the proportional cost's user-defined `value` field. Because the proportional cost is an instance of `FutureCost`, time values can also be assigned to them. This is useful when considering high level costs that are incurred at regular intervals; A common example in the literature is expressing O&M cost as an annual proportional of CAPEX (for example [57,93])

3.4.4 Analysis results

Output results of any kind can be stored together using the `ResultsBase` class. The data type of each result element can be anything, although two-dimensional numeric NumPy arrays are most commonly used for spatial data. They are grouped together as a dictionary within the `results` attribute and methods are defined to add and remove specific results using the underlying dictionary

keys. These keys can be used to define the name of the result and are linked to the output data file names. The attribute also supports nested dictionaries, allowing a way of creating sub result groups. The `get_denested_results` function reduces this multilevel dictionary to a single level by joining the keys together. This is desired as it means that unique output file names can be created from the data within a single results instance. It should be noted that `ResultsBase` is an abstract class, hence does not contain methods to export the data. Instead, data export is left to child classes where the data types will be more specific. Lastly, the `inputs` attribute is also a dictionary to accompany the results set. This is implemented so that the inputs used to generate the results are remembered. As most of these inputs are typically strings or single numbers (as the more complex inputs can be linked to specific class instances) they are suitable for storing in a simple text file. This is done with the `export_inputs_txt` method.

Locational results are stored within a `GisResults` instance. This class adds methods to export results to NetCDF files and GeoTiff raster images. Each pixel in these images represents a location in the domain. To create the raster, functions from a separate module, `gis_utilities`, are imported. This module is summarised in Appendix B.1.

The results contained in this class are typically two-dimensional arrays which define some quantity over a geographic domain of latitudes and longitudes. This means that the class requires knowledge of the geographic system so that the locations of results are correctly interpreted. The attributes `lat_range` and `lon_range` are included for this purpose; they are Python lists which together define the (x, y) pixel locations. Single numbers can also be mixed into the results dictionary; typically these define parameters that are static across the geographic domain (for example cost aspects which will be the same regardless of location). The function `project_results_spatially` takes the values and, using NumPy array methods, projects the number across the whole range: so that it is the same shape as the spatial domain

3.4.5 Analysis classes

The aim of these classes is to group functions and class methods together that define specific spatial calculations. Uniting different aspects of the code in this way improves usability, providing functionality which would otherwise be difficult without an in depth understanding of the inner module workings. While the model functionality could also be achieved using functions instead of classes, the class

based approach offers a convenient way of grouping different functions under a unifying concept. For example, the economic analysis class could include distinct methods to perform LCOE, IRR and NPV analyses. These could be calculated independently, but grouping them enforces consistency in the input and output data by design.

Within the overall model there are four analysis classes: `CostAnalysis` and `EconomicAnalysis`, within this module; `EnergyAnalysis`, within the `wave_device`; and `OffGridAnalysis`, within the off-grid module.

Both `CostAnalysis` and `EconomicAnalysis` inherit from `GisResults` and are designed to obtain spatial costs and spatial LCOE. They are contained in this module because they are relevant to both the hybrid and non-hybrid system configurations. `CostAnalysis` calculates total costs and output cash flow from an input instance of `ItemBase`. This instance is embedded within the `input_object` attribute. The total number of periods to consider for the analysis (months or years) and discount rate are also required. The main class function, `cost_analysis`, uses the `total_cash_flows_by_category` method, as defined in Section 3.4.3, to obtain both categorised cash flows and total costs for the input object. These results are saved within the `results` attribute, and can hence be exported as NetCDF files or GIS rasters when paired with the necessary spatial dimensions.

The `EconomicAnalysis` class takes in energy data and cost data as input, the latter as can be created from a cost analysis. From these data, cost of energy is simply obtained by dividing each of the costs by the energy. This class does not apply discounting for the COE analysis, assuming that the input data have already been discounted. This is advantageous as it makes the class flexible and generic in nature, not fixed to data of any particular type. It also means, however, that a degree of care must be taken to ensure that the energy and cost input data are both defined according to the same discount rate and project lifetime assumptions. The output of `coe_analysis` is COE (LCOE if discounting is applied) for each input cost. Using spatial results as inputs allows total COE to be calculated across the domain and the results exported to GIS rasters. It should be noted that only LCOE analysis is coded within the class. This decision was taken due to the research project time constraints, with the sponsoring company instead prioritising different model aspects.

3.4.6 Geographic classes

Single spatial points that are used within the analysis, namely ports and cable landing points, derive their geographic properties from two base classes. The purpose of these classes is to provide a framework that allows any single location, defined by a latitude and longitude, to be defined. This uniform way of representing locations is useful as it allows core attributes and functionality to be present, regardless of the point's place in the overall model.

The first class, `GeographicPoint`, simply defines a pair of coordinates. It is initialised with a longitude and a latitude value, which must be given in decimal degrees. A method `export_as_vector` uses functions from the aforementioned `gis_utilities` module to create a vector layer of the point which can be viewed in GIS software.

Functionality is added to this class with the child class `GridPoint`. This class provides the link between a single point, as described by its parent class, and an array or "grid" of points which is the level that the desired analyses are performed over. As well as coordinates, this class also takes in latitude and longitude dimensions in the form of one dimensional NumPy arrays or lists. The user can choose to input the coordinates in the form of indices using the `input_method` attribute, in this case the coordinates are selected from the input dimensions. This is particularly useful for debugging, to ensure that valid coordinates are always chosen regardless of the input dimensions.

This class has several methods which are useful for the physical object child classes. The point coordinates can be checked against the latitude-longitude grid to see if the point lies within the input dimensions, using the `coords_in_range` method. This check is required because if the point lies outside the grid then pathfinding analysis cannot be safely conducted. In addition, the class provides methods to determine where the point lies in relation to the grid. The `surrounding_indices` static method returns the nearest grid points to the input coordinates, with distances calculated using the haversine equation. These neighbouring points are required for pathfinding, discussed in more detail in Section 3.5.2. Lastly, using similar methods the `grid_coordinates` for the grid point instance can be obtained. These are the coordinates of the nearest grid point to the input coordinates, and are useful to know as they can be substituted for the input coordinates in child class pathfinding methods to ensure that a solution can be found.

3.4.7 The Fuel class

This base class is used to describe a combustible fuel source. Inheriting from `ItemBase`, it is used to define vessel fuel in the `operations_and_maintenance` module and fuel consumed by a diesel generator in the off-grid sub-model.

The class is designed so that fuel cost can be easily considered within the economic analyses. It is a simple class, inheriting most of its behaviours from `ItemBase`. The main addition is the `cost_per_ltr` property, which defines the cost paid per litre of fuel. As this is a cost, the data are stored as a `FutureCost` instance within the `local_costs` attribute. As a cost instance, `cost_per_ltr` has a quantity attribute of its own. This is where the quantity of fuel that is consumed is defined, when calculated by other classes.

3.5 Wave Site Module

This module contains two classes: `WaveSite` and `SitePoint`. These classes are concerned with the hindcast metocean data that is used for estimating energy and pathfinding. These classes used to be part of the overall `wave_device` module described in Section 3.6. However, as the overall model grew the decision was taken to form them into a distinct module, to keep the structure modular and prevent any confusing circular module dependencies from forming between the `wave_device` and hybrid system modules.

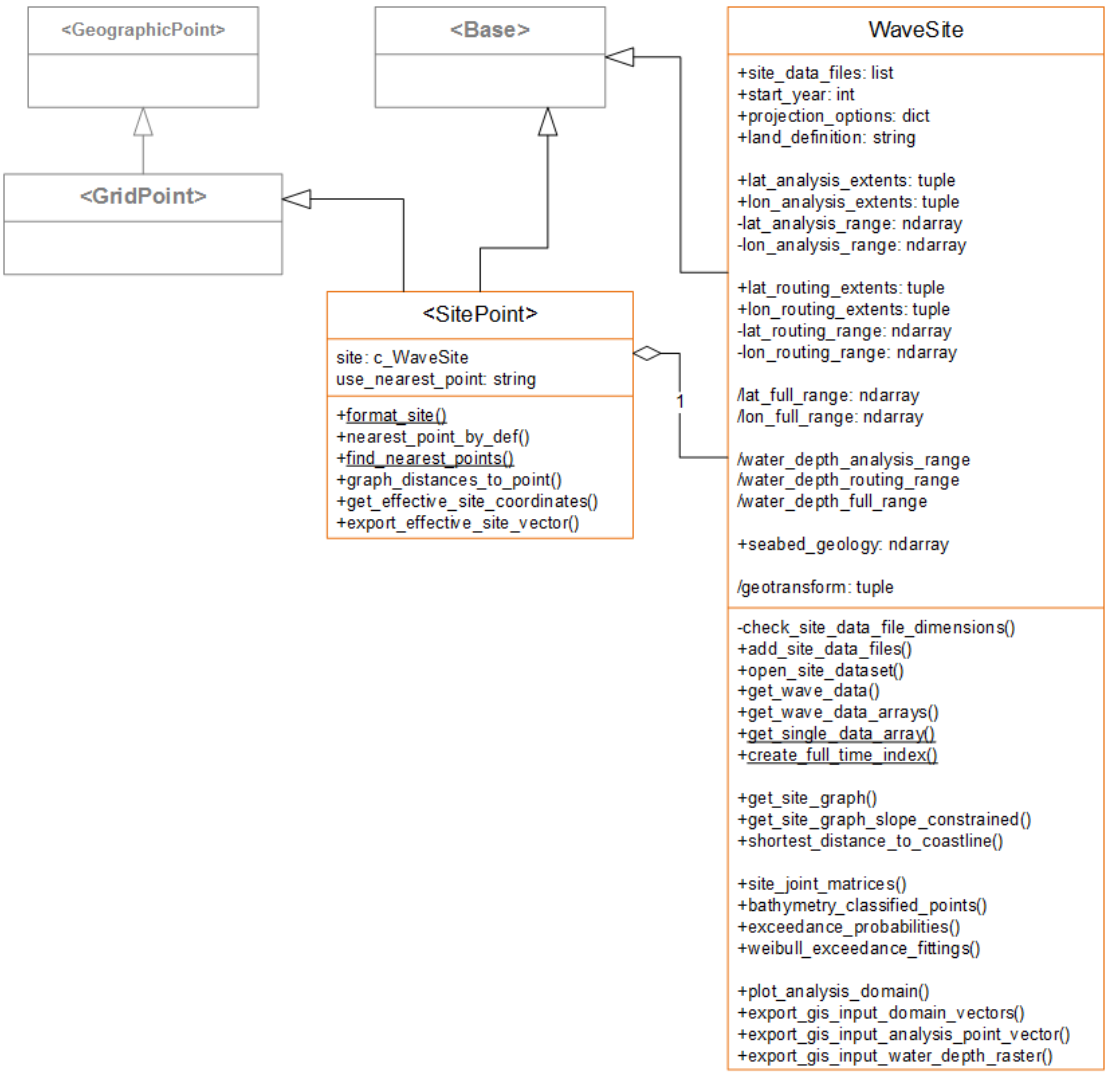

Figure 3.5: The two classes that make up the `wave_site` module: WaveSite and SitePoint. The base class parents are coloured in grey. Notation is the same as used for Figure 3.4.

3.5.1 The spatial domain

The class `WaveSite` is one of the most important in the model. It is a representation of a physical geographic area, over which is defined some gridded hindcast metocean data. Its main purpose is to facilitate the easy import and handling of the metocean data into the model for analysis.

The actual metocean data are stored within NetCDF (.nc) files, prior to being loaded into Python. For an instance of the class, the directories where the NetCDF files are stored must be defined within the `site_data_files` property. For convenience, entries can be added with the `add_site_data_files` method. Typically each year of hindcast data is stored within its own NetCDF file, a good balance between convenience and memory[1]. Either a single string is specified, defining a single file, or a list defining multiple files. Each list entry can either be a string or a dictionary containing the string accompanied by two further keys: a 'time range' key to allow a specific time range in the file to be isolated and a 'rank' key that controls the ordering that the data files are loaded in. This latter functionality was provided to allow the user to mix and match data files, for example one could combine the most low energy months from a series of data files to examine a pessimistic energy scenario. By default the whole time range is chosen, and the rank set to one more than the previous highest. Within the property setter a function also checks that all of the files are defined over the same spatial range and at the same resolution, and returns an error if this is not the case.

The NetCDF files are three-dimensional, containing time series of H_s and T_p specified over latitude and longitude dimensions. The default geographic area defined by the area is known as the "full domain". The extents of this domain are extracted using the `open_site_dataset` method, which opens a single file within the `site_data_files` attribute; by default this is the file with the lowest rank although the user can specify a rank to open a certain file. Usually the user will not be interested in the whole geographic area, as it will include many unsuitable locations and the more points that are included the slower the subsequent analyses will take to run. To avoid this issue, data extraction can be limited to a specific rectangular subset of the full domain. This is known as the "analysis domain" and can be specified using the `analysis_extent` attributes. The analysis range can be defined either in terms of coordinates, the format of the

[1] A single file containing all of the data would be preferential but there would be significant memory overheads when accessing the data, even after chunking.

Purpose: To extract metocean data in a form suitable for spatial analyses.
Required: A `WaveSite` instance (defined as self below) with site data files defined.
Returns: Metocean data variables, that can be projected and used to estimate device power and weather windows.

```
def get_wave_data(self)

# Get the spatial domain
lat_range = self.lat_analysis_range
lon_range = self.lon_analysis_range

nc_filepaths = self.site_data_files
nc_filepaths_sorted = sort_data_files(nc_filepaths) # Sort the data
    files according to rank key.
D_files =[] # Pre-allocate list of arrays.
for file_dict in sorted_data_files:
    # Open the dataset.
    filepath = file_dict['path']
    ds = open_dataset(filepath)
    time_range = ds['time_range']
    ds_subset = ds.sel(time_range, lat_range, lon_range) # Set the data
        extents.
    ds_subset_no_leap = remove_leap_day(ds_subset) # Remove leap day
        from subset.
    D_files.append(ds_subset_no_leap)

D_wave = concatenate(D_files) # Combine the data from each file.
start_year = self.start_year
t_i = create_full_time_index(D_wave, start_year) # Create a new time
    index.
D_wave['time'] = t_i # Assign the time index.
return D_wave
```

Algorithm 3.2: Extract metocean data, defined within external NetCDF files.

dimensions in the file, or in terms of the indices in the array. This latter functionality is useful for debugging. Two functions `analysis_extent_coordinates` and `analysis_extent_indices` return the analysis domain extents in terms of coordinates or indices, again primarily for debugging purposes. If analysis extents are not defined then the analysis domain defaults to the full domain.

With the data files and the spatial domain defined, the user can extract the actual data. This is achieved using the `get_wave_data` instance method. This is used twice: to get both H_s and T_p variables. The procedure for this method is shown in Algorithm 3.2.

First the analysis domain extents are obtained in terms of coordinates, and the site data file strings are sorted according to the rank key. A *for loop* iterates

through the dictionary entries that define each file: opening the dataset, selecting the dimension ranges and removing the leap day. A list, `D_files`, stores the intermediate datasets which are then concatenated together into a single dataset, `D_wave`. Lastly a new time index is created for the dataset, `t_i`, using the `start_year` attribute of the `WaveSite` instance. This allows the user to normalise the data to a starting year and is required so that the data are defined over a constant period of time (as gaps could otherwise occur from mixing and matching input data files).

It should be noted that the data has not been directly loaded into memory. The output dataset, created using the xarray Python module, effectively serves as a link to the data in memory. This can then be loaded for analysis by looping over the array, as typically the dataset will be too large to load in one go.

The fundamental use of the metocean data is to calculate the energy produced by the device. This part of the model is introduced in Section 3.6. The second major use of the metocean data is for pathfinding, to allow distances and spatial costs to be estimated. The variable that is used for this is the bathymetry. As several wave models require the use of bathymetry data, such as SWAN, this is easy to package with the output metocean time series results. The model relies on the user saving the bathymetry data as a variable within every metocean NetCDF file using a predefined variable name. The `open_site_dataset` method is used to get the bathymetry data; because all of the files will contain the same bathymetry any of the files can be used. A private method, `_set_water_depth_full_range` is initiated within the `site_data_files` property setter to effectively set the bathymetry data automatically. The method loads the bathymetry data from the file and assigns them to the attribute `water_depth_full_range`. The data are contained within a `ConstraintData` class to allow water depth based constraints to be considered; this is discussed in more detail in Section 3.10.

With the bathymetry data contained within the `WaveSite` class instance, pathfinding graphs can be created from the data. The data are a two-dimensional array: water depth in metres as a function of latitude and longitude. Points that coincide with points on land are denoted by NaN values. These serve as obstacles and can be identified using simple inequality statements. The `get_site_graph` method is used to create the graph. This uses methods from an external module created specially for pathfinding, `path_finding`, details of which can be found in Appendix B.3. The graph itself is a dictionary which maps each point to its nearest neighbours. By default a third domain is used to create the graph, the "routing domain". The reason for this is so that points outside of the analysis

domain can still be considered. By default the routing domain is set equal to the full domain. For very large datasets it might not be desirable to run the pathfinding analysis over the whole dataset as the computation time may be very high. The routing domain hence is designed to lie between the full and analysis domains, just big enough to enclose the infrastructure locations and outermost point of interest, and any paths for routes. This is illustrated in Figure 3.6

While the default graph obstacles are land points in the bathymetry data, the function does allows different obstacle categories to be specified. Key to this is the ability to classify the points in the domain. In the simplest case three categories are present, defined by the bathymetry:

1. Sea: These are the points associated with a water depth and where metocean time series are defined. They represent potential locations for wave energy devices.

2. Land: Wave energy devices cannot be located at these points. They also represent obstructions to vessel and export cable routes.

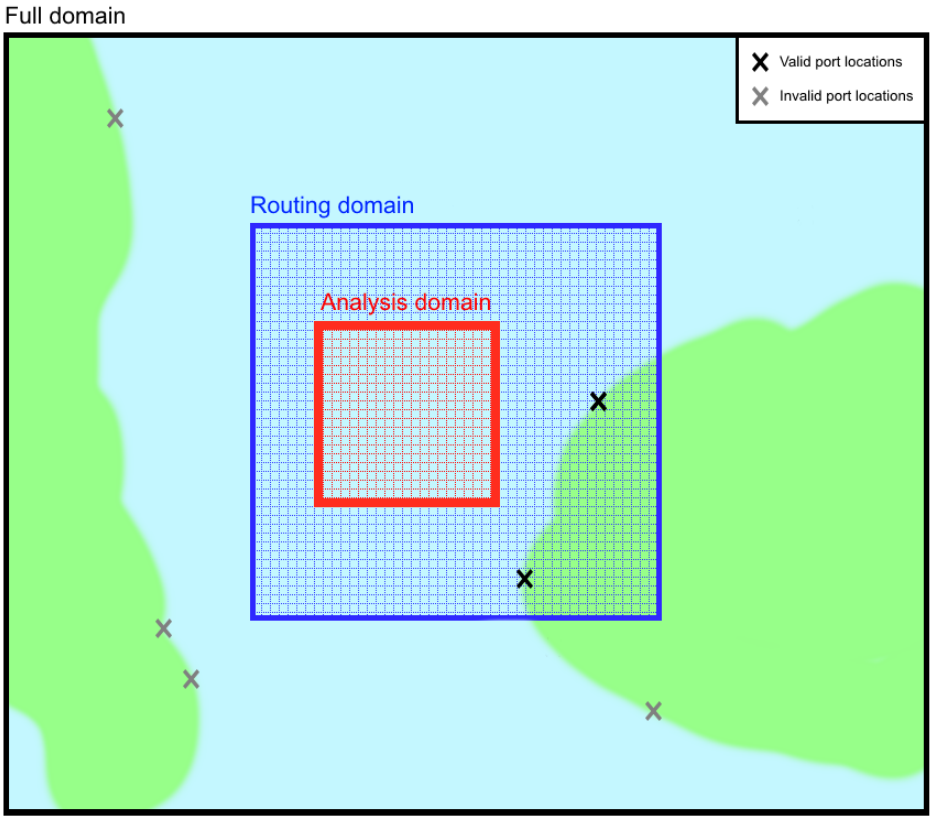

Figure 3.6: The relationships between the three different domains that define the overall site. The full domain contains the whole dataset, while the analysis defines the specific wave device deployment locations. The routing range is used for pathfinding and should encompass all of the supporting infrastructure desired (the example of ports is presented).

3. Coastline: These are land points that are nearest to the sea. They are determined by iterating through the land points are looking for any that have at least one sea neighbour.

These point classifications are stored in a global dictionary within the module, allowing them to be easily used for different pathfinding applications and added to. The ways that the point definitions are used to facilitate graph creation and pathfinding are discussed more in the next section.

3.5.2 Point locations

Within the model there are a number of objects which represent single geographic points in the domain, namely ports and cable landing points. It is useful for these to have access to the parameters that define the overall site (contained within a `WaveSite` instance) so that they can use the underlying data for pathfinding and distance calculation. As the nature of the pathfinding calculation is the same for these different elements, it follows that they should be grouped by a parent class.

The site point class, `SitePoint`, inherits from both `GridPoint`, discussed in Section 3.4.6 and the `Base` class. It takes advantage of multiple inheritance. Inheriting from `GridPoint` allows the point coordinates to be defined, and existing methods utilised in order to constrain the coordinates to the specified site grid, where appropriate.

At initialisation, the coordinates defining the point location are defined. As well as these, the user defines a `site` property; this is formatted upon input to ensure that it is an instance of `WaveSite` and to try and convert it it is not. The `site_range` attribute is a string which must correspond to the potential range options that can be selected within `WaveSite` (namely the analysis range, full range or routing range). This allows the point's grid ranges to be set to the coordinate ranges of the site. Using only the analysis range will decrease computation time, however often points outside the direct analysis range are of interest so the routing range is the typical range that is chosen.

3.5.2.1 Calculating distances

The main reason for the class is to provide a framework for calculating distances from a single point to all of the analysis points in the domain, defined by the analysis extents of the input site. The instance method `graph_distances_to_point` makes this possible through the following process:

1. **Get the effective point coordinates**: While any coordinates within the site extents are technically valid for pathfinding, sometimes it is necessary to use coordinates which explicitly lie on the site domain grid. This is because the input point needs at least one neighbour that is not an obstruction, or else it is blocked in and cannot link up with the other graph nodes. A common example is sheltered ports at coarser grid resolutions; the real world coordinates might have no sea neighbours and hence vessel paths cannot be resolved.

   To use the nearest coordinates on the grid, the `use_nearest_coordinates` property is specified. This is a string which must match one of the bathymetry categories introduced in Section 3.5.1. In this case, the coordinates used as the starting point for the pathfinding (the "effective coordinates") are those nearest to the input coordinates of the desired category.

2. **Check that the coordinates are in the analysis range**: The user-defined coordinates must lie within the graphing range of the site, otherwise the point's position relative to the site cannot be determined. If this condition is not met then a custom error is returned.

3. **Get the site graph**: The graph is obtained from the embedded site instance using its `get_site_graph` method.

4. **Add the effective coordinates to the graph**: If the effective coordinates are not contained within the graph then they must be added to allow pathfinding. This is necessary when the user has arbitrarily defined coordinates not on the grid. This point is added by finding the nearest grid coordinates surrounding the point. These are stored as neighbours if they match existing nodes in the graph, or else it is assumed that they are obstacles. The effective coordinates and its neighbours are then added to the graph dictionary in an identical format to the rest of the graph.

   If the coordinates are already present in the graph, perhaps due to using the `use_nearest` property, then this stage is skipped.

5. **Perform the pathfinding**: Using the effective coordinates as the starting point, the pathfinding operation can be performed by applying Dijkstra's algorithm to the modified site graph. Two dictionaries are returned, with the analysis coordinates as keys. The first contains the distances from the analysis point to the effective point, which is converted into a NumPy array by comparing the coordinates values with the embedded site analysis ranges

and getting the corresponding indices. The second dictionary stores the successful paths, pairing each analysis point with its predecessor along the resolved path.

With the distances to the analysis points obtained, spatial costs can be derived. These processes are discussed in the proceeding sections. One final comment on the `site_point` class is that both the input and effective coordinates can be exported as vector point layers, for visualisation in GIS.

The functions have also been extended to consider multiple input points. The static method `find_nearest_points` performs Dijkstra's algorithm for each in turn, using a *for loop*. Each loop obtains an array of distances, which are then compared at the end, and the NumPy package used to find the minimums.

3.6 Wave Device Module

The purpose of this module is to group together all of the main classes that are related to the WEC system. The main outputs are the costs and the energy produced, which can be fed into the LCOE calculation. The UML diagram showing the main properties of the classes is displayed in Figure 3.7.

3.6.1 The power matrix

As introduced in Section 2.3.2, a power matrix is the typical way of estimating wave energy production as a function of sea state. The actual values in the power matrix will differ considerably, depending not only on the specifics of the physical wave device but also the simulation method. A power matrix class is required in order to ensure the consistency between different power matrices for analyses and also to provide functions to allow the user to modify a given matrix to satisfy more detailed device design criteria.

The power matrix class, `PowerMatrix`, inherits from `Base`. Four more parameters can be specified by the user at initialisation: the power matrix data and three factors to constrain the power, based on physical device properties.

Making up the power matrix are the actual power values and the H_s and T_p ranges over which the power values are specified. The default behaviour is to load the data from a CSV file, the user specifying the file location. CSV was preferred to a database to keep consistency with practice at Albatern. Upon loading the power matrix, the data are then formatted into the desired type, a Pandas DataFrame, using the `format_power_matrix` static method. Originally the power matrix was formatted as a dictionary, with each key holding one of the matrix attributes (the H_s range, T_p range and values). This was changed to a DataFrame, as the DataFrame allows more convenient methods for modifying specific subsets of the matrix.

The first way that the power matrix can be modified is by applying an overall efficiency factor, i.e.:

$$P_{m_{\mathrm{i,j}}} = P_{\mathrm{i,j}} \cdot \eta \,, \tag{3.1}$$

where $P_{m_{i,j}}$ is the modified power, $P_{\mathrm{i,j}}$ an element of the initial power matrix and η the overall efficiency. This concept was introduced to allow hydrodynamic conversion efficiencies to be applied to the raw power values, as often hydrodynamic

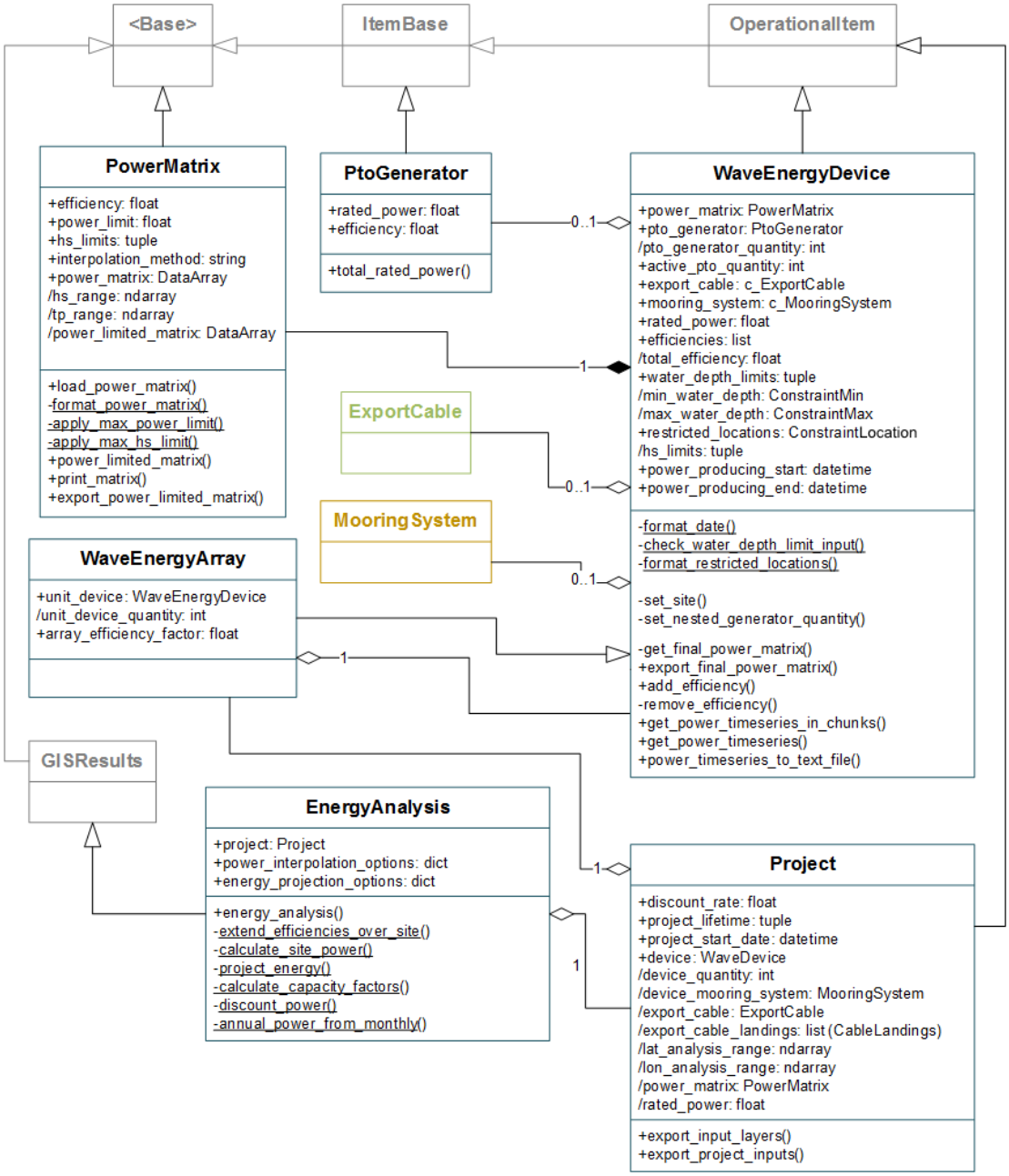

Figure 3.7: The classes that make up the `wave_device` module. The base class parents are coloured in grey. The export cable and mooring system are optional sub components of the wave device and are defined in their own respective modules (described in Sections 3.8 and 3.9). Notation is the same as used for Figure 3.4.

simulations are performed under somewhat idealised conditions. In this case, the device will be unable to capture all of this energy in reality as there are losses in the mechanical system. Programatically the factor is a property of `PowerMatrix`, so that only valid values can be set (between 0 and 1). This approach is mimicked for other efficiencies also defined in the model (for example for the device and PTO generator classes described in the proceeding sections).

Secondly a maximum power limit can be applied to the power matrix data. This is useful when considering a specific PTO generator, which will only be able to extract power up to its rated value. If a power matrix value exceeds the maximum specified then it is curtailed and set to the maximum:

$$P_{m_{\mathrm{i,j}}} = \min\left\{P_{\mathrm{i,j}}, P_{\max}\right\} . \tag{3.2}$$

The condition applies the maximum power, $P_{\max}$, in an element-wise manner to the whole power matrix.

The last way that the values can be modified is by defining the range of H_s over which power can be extracted. This is achieved by defining power extraction limits: cut-in and cut-out H_s values. For matrix values outside of these limits ($H_{\text{cut-in}}$ and $H_{\text{cut-out}}$), the power output is set to zero:

$$P_{m_{i,j}} = \begin{cases} 0 & \text{if } H_{s_i} \leq H_{\text{cut-in}} \vee H_{s_i} \geq H_{\text{cut-out}} \\ P_{\mathrm{i,j}} & \text{otherwise} . \end{cases} \tag{3.3}$$

Hence, putting the three expressions together leads to the overall modification being applied:

$$P_{m_{i,j}} = \begin{cases} 0 & \text{if } H_{s_i} < H_{\text{cut-in}} \vee H_{s_i} > H_{\text{cut-out}} \\ \min\left\{P_{\mathrm{i,j}} \cdot \eta, P_{\max}\right\} & \text{otherwise} . \end{cases} \tag{3.4}$$

The unmodified input power matrix values are permanently stored within the class instance. This means that the efficiency values can be easily changed when working within Python, safe in the knowledge that they are always being applied to the original input data. The method `power_limited_matrix` returns a copy of the power matrix with the power constraints applied; this is the matrix used for estimation of the energy yield (the implementation of this calculation is discussed in Section 3.6.2). Figure 3.8 gives an example of how the factors affect the values in practice.

There is one final attribute that influences the energy calculation: the

Hs (m) \ Tp (s)	5	6	7	8	9	10
7	0.0	0.0	0.0	0.0	72.5	57.5
6	0.0	0.0	0.0	81.2	61.8	47.1
5	0.0	0.0	74.9	64.8	47.8	35.3
4	0.0	68.3	61.5	46.8	34.7	25.5
3.5	0.0	67.4	50.1	38.2	27.6	20.3
3	71.1	51.1	40.3	29.4	21.6	15.7
2.5	49.9	38.9	29.3	22.2	16.0	11.4
2	37.4	27.4	20.3	14.9	10.5	7.1
1.5	24.3	17.4	12.3	8.3	5.3	3.4
1	12.0	7.8	4.9	2.9	1.6	1.0
0.8	7.4	4.4	2.6	1.6	0.8	0.5

Hs (m) \ Tp (s)	5	6	7	8	9	10
7	0.0	0.0	0.0	0.0	0.0	0.0
6	0.0	0.0	0.0	45.0	45.0	40.1
5	0.0	0.0	45.0	45.0	40.6	30.0
4	0.0	45.0	45.0	39.7	29.5	21.6
3.5	0.0	45.0	42.6	32.5	23.5	17.2
3	45.0	43.5	34.2	25.0	18.4	13.3
2.5	42.4	33.0	24.9	18.8	13.6	9.7
2	31.8	23.3	17.2	12.6	8.9	6.0
1.5	20.6	14.8	10.4	7.1	4.5	2.9
1	0.0	0.0	0.0	0.0	0.0	0.0
0.8	0.0	0.0	0.0	0.0	0.0	0.0

Figure 3.8: Example of applying power adjustments to a power matrix. Left: An input matrix. Right: The input matrix with an efficiency of 85%, maximum power output of 45 kW, cut-out at 7 m and cut-in at 1 m.

`interpolation_method`. This determines the way that power values are obtained for sea states between the matrix rows and columns. Valid options include linear, cubic and nearest neighbour interpolations. For Albatern's devices this parameter was found to have a negligible influence on the energy yield (especially after discounting of future contributions) and so linear is set as the default to reduce computation time.

3.6.2 The wave device

The `WaveDevice` class, combines a power matrix with device costs and wider properties to create a representation of a single WEC. It inherits from the `OperationalItem` class, a child of `ItemBase` which allow O&M tasks to also be defined. This class and the O&M cost calculation methods are described in the next section, Section 3.7. The class also includes embedded class instances that represent other objects which are required to complete the overall WEC system (the `mooring_system`, `export_cable` and `pto_generator`). The export cable and mooring system are discussed in more detail in Sections 3.8 and 3.9 respectively.

3.6.2.1 PTO generator

The `pto_generator` attribute is an embedded instance of a further class, `PtoGenerator`. This represents the generator item used to harness the wave energy. The rated power and the efficiency of the PTO can be specified. Here the assumption is made that the PTO efficiency is constant over the power range. In reality the efficiency will vary with the power output, and hence sea state, however this is not considered in the model as the overall impact on power produced is thought be to low if an appropriate efficiency value representative of the system is chosen.

Within `WaveDevice` the number of PTO units can be specified. This would not be a factor of interest for all device types. Some classes, for example point

absorbers, might only contain one generator per device. The Albatern WaveNET is capable of supporting up to three generators per Squid (one in each anti-node) and for an array could contain extra units for redundancy. The two relevant class attributes are `pto_generator_quantity`, which is a handle to the quantity attribute of the embedded PTO object, and `active_pto_quantity`. This latter number determines the device rated power; it is the number of PTOs that produce power and must be less than the total PTO quantity. Lastly, sometimes a higher level approach is desired without needing to think about the specifics of PTO units. This can be achieved by defining the rated power attribute directly within `WaveDevice`, which overrides the rated power calculated for the `PtoGenerator` instance. This is useful for sensitivity studies, so that arbitrary rated powers can be easily considered without needing to delve into the embedded object.

3.6.2.2 Energy production

To calculate energy production, the device requires two key attributes: a power matrix and a site instance. Both of these are embedded objects, within the `power_matrix` and `site` attributes, the reason so that the relevant methods can be easily exploited. Other optional attributes that can be specified are the start and end times for the power production (`power_producing_start` and `power_producing_end`) and any power conversion efficiencies in the PTO system. An arbitrary number of efficiency values can be specified (optionally they can be accompanied by strings describing the nature of the value, e.g. "hydraulic losses"). Values can also be designated as "pre" or "post" generator depending on where in the conversion process they occur. Values occurring before the generator are multiplied into to the power matrix efficiency value, to be applied before the power matrix is constrained by rated power. Post values are applied after the power matrix is created, representing losses between the generator and connection point.

The first step towards getting to energy is to obtain a power time series. This process is achieved using the instance method `get_power_time series_in_chunks`. First, H_s and T_p time series are required. These can be obtained from the embedded site instance for the time period of interest using the methods described in Section 3.5.1. Once these are obtained, the data are chunked according to the time axis. If the input metocean time series gets large, the model will experience memory issues if it tries to load it all into memory at once. This can range from large lag to completely crashing the running model. The function allows the data to be chunked by year or by month, year is the

default as this has been sufficient for the examined datasets.

A *for loop* iterates through the chunks, loading each in turn and interpolating the sea state values against the power matrix. The interpolation is handled by a separate function, `get_power_time_series`, to keep the code modular and function length manageable. This takes in the H_s and T_p chunks, interpolates the values against the constrained power matrix from the embedded power matrix object to obtain the power time series. Device-level efficiencies are applied to the matrix prior to interpolation. Various NumPy operations are utilised here to reformat the input arrays into the desired shape. The interpolation itself is achieved using the griddata function from the SciPy interpolation package. While there are alternative function options (notably the interp2 function from the same module), griddata was found to be computationally quicker. The interpolation method that is used is extracted from the power matrix's `interpolation_method` attribute. Once the data are obtained they are reshaped into a new array to match the dimensions of the original input data. If any of the array elements in the metocean data are NaN then these are set to NaN in the power array too. Lastly a new DataArray is created, linking the power values with the time and geographic dimensions.

Once the power time series is obtained for the chunk then any time steps that occur before the power producing start time or after the power producing end are set to zero. For the resulting array there are two options available, specified by the user with the boolean variable `sum_to_base`. In the default *True* case, the power values are summed for the chunk along the time axis to obtain a two-dimensional energy. For example, a monthly chunk will lead to an array of monthly energy production. Alternatively, no summation will take place and a power profile will be returned. This latter functionality is more suitable for smaller datasets where the power time series could fit comfortably in memory. Its main use is to obtain a time series to be used as an input for the off-grid sub-model; this application is discussed more in Section 4.4.2.

The monthly energy time series can also be projected into the future, required when the project lifetime exceeds the amount of metocean data available. This process is achieved within the overall analysis by using another class, the `EnergyAnalysis` class, which is discussed in Section 3.6.4.

3.6.2.3 Calculating costs

Because the class inherits from `ItemBase`, local costs can be defined and calculated in the way described in Section 3.4.3. Device cost categories and quantities

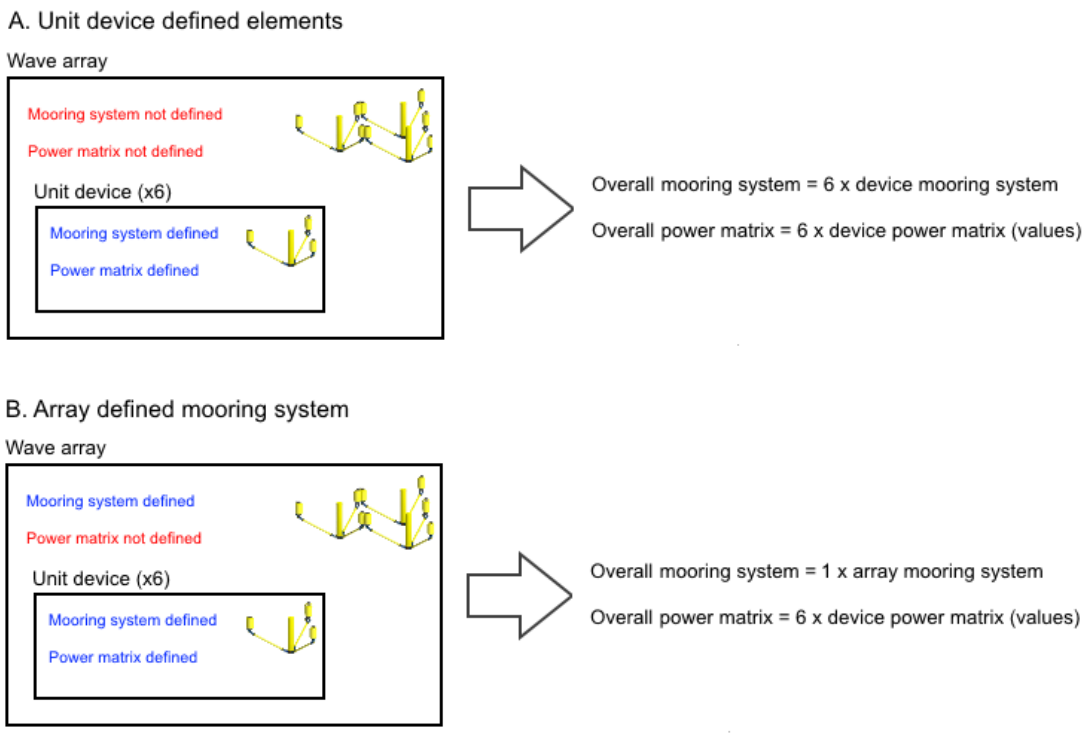

Figure 3.9: Behaviour of setting attributes in the wave array class that are defined in the unit device embedded object. In the upper figure both mooring system and power matrix are set in the unit device and not the array, leading to the unit device properties being used. However, in the bottom figure the mooring system is now defined at array level too, meaning that this replaces the existing device level mooring system.

are filtered down to the embedded mooring system, export cable and PTO generator.

3.6.2.4 Arrays of devices

For arrays of wave energy devices there are various options that might be available for a developer. Some components might be specified per device, whereas others are shared between multiple devices.

The `WaveEnergyArray` class offers an extra level to the overall device system, at which alternative systems and costs can be specified. The class inherits from `WaveDevice`, as an array of devices can be thought of as a device in its own right. The key difference to the parent class is the introduction of the `unit_device` property. This is a `WaveDevice` instance, a representation of a single array member. The array class and device class hence share a composite based relationship, as they are linked by both inheritance and composition. The quantity of devices is also specified with the `unit_device_quantity`, this is a handle to the quantity attribute of the embedded unit device. The way that this works in practice is that, by default, the array attributes are obtained from the unit device. The

exception to this are array level local costs, which are considered in addition to any local costs within the unit device. With the unit quantity specified, the parameters are equal to the unit device parameters multiplied by the number of devices. For a single parameter, this behaviour is changed if it is explicitly set on the array instance level. In this case the model uses the array level parameter, as demonstrated in Figure 3.9. The properties that can be set at array level are the mooring system, power matrix, export cable, rated power and generator quantity.

This array level is of particular significance to Albatern because the device modules are directly connected. They share a mooring system which reduces costs, but also the power capture per unit has been shown to increase for smaller arrays. This is because the characteristic length of the unit increases, improving the power capture across a range of sea states. The result is a different power matrix that represents the whole array.

A limitation with considering the power calculation on the unit device level is that it assumes that all devices are exposed to the same input metocean data at a given location. In reality, particularly for a large and spread out farm, the devices will see different wave conditions which will result in more smoothed out power. There are ways around this, for example by specifying an overall power matrix at the array level with an assumption about smoothing built in. As the Albatern device is very small relative to the metocean grid resolutions examined previously this has not been an issue, but should be noted for larger devices, farms or smaller data resolutions

3.6.2.5 Constraints

The physical properties of the wave device or array will have an influence on the potential areas that it can be deployed in. The model allows constraints to deployment to be examined and plotted in GIS. Within the device itself there are two constraints built in: water depth limits and restricted locations. These, as well as a description of how the overall analysis is carried out, are described in Section 3.10.

3.6.3 Wave energy projects

The purpose of the `Project` class is to represent the entire grid-connected wave energy project. It is essentially a container for the various objects that are required to form estimates of energy, cost and LCOE. Keeping all of these elements together in this way is beneficial, as it gives a convenient way to define and load

up different case study scenarios. Having a level defined above the device class, which contains almost every model aspect within it, is also good as it means that external costs can be defined which do not explicitly fit into the device system (for example project management or site assessment and consenting costs).

Central to the project definition are the `discount_rate` and `project_lifetime`. These are fed through into the analysis, and determine the present values of energy and cost that are calculated (as introduced in Section 2.3.1). It is assumed that the device is capable of producing power during the whole project lifetime, unless power producing start and end dates are specified within the device instance as described in Section 3.6.2.2 above.

The main source of data within the class is the `device` attribute. This embedded `WaveEnergyArray` instance contains the specifics of the operations, export cable and mooring system, as previously described. The derived methods relating to device quantity, export cable, mooring system and the analysis range are simple there to improve usability of the model, they link to the relevant properties inside the device object which allows the main parameters to be set at the top level. Additional costs not considered part of the device can also be added, as the class inherits from `OperationalItem` and hence contains its own local cost attribute.

Lastly the class contains methods which allow all of the vector input data to be exported to GIS shape files. This includes things like port and cable landing locations, cable routes at specific points and the relative site domain and grid locations.

3.6.4 Energy calculation

The `EnergyAnalysis` class encapsulates the full energy calculation process. It is similar in principle to the two analysis classes introduced in Section 3.4.5, bringing together the necessary functions and classes to get spatial energy estimates. While the energy itself is obtained within the `WaveDevice` class, as described in Section 3.6.2.2, this class controls the whole process including extracting and feeding in the metocean data and projecting the resulting energy time series forward over the project lifetime. A high level representation of this is presented in Figure 3.10, including the main input data that are required and the primary calculation steps. The final output is the energy at each time period of the device lifetime.

The main input to the class is the `project` attribute, an instance of `Project`. This contains the `Site` and `WaveDevice` instances that are directly required to obtain energy, as well as other attributes like `project_lifetime` and

`discount_rate` which discount the data according to the detail of the project. The `energy_analysis` method performs the actual analysis, calling the other six static methods within its scope. Segmenting the overall function in this way keeps the code clear and modular, making the processes easier to debug and modify going forwards.

Once the energy time series is obtained it can be projected forward in time. This is required when the duration of the input metocean data is less than the project lifetime. As typical device lifetimes considered are quite long, 15 or 20 years are commonly assumed, to match this would require a large amount of input data. These might not be available, as the simulations to get them can be complex and costly to run. For the projection, the power time series is first summed to a monthly timebase, as previously seen. There are then two options implemented to stack the data: either the monthly data are replicated or the monthly means used for the remaining duration. The ways that these work in practice are depicted in Figure 3.11, applied to an example of a four year lifetime where only two years of data are defined. While the replication approach is generally preferred for multiple years of data, as it can better capture inter-annual variability, both methods are crude in nature and could be improved in future work. To account for datasets that contain partial years of data, more sophisticated functions have been created which allow the data to be trimmed or extended to get to complete

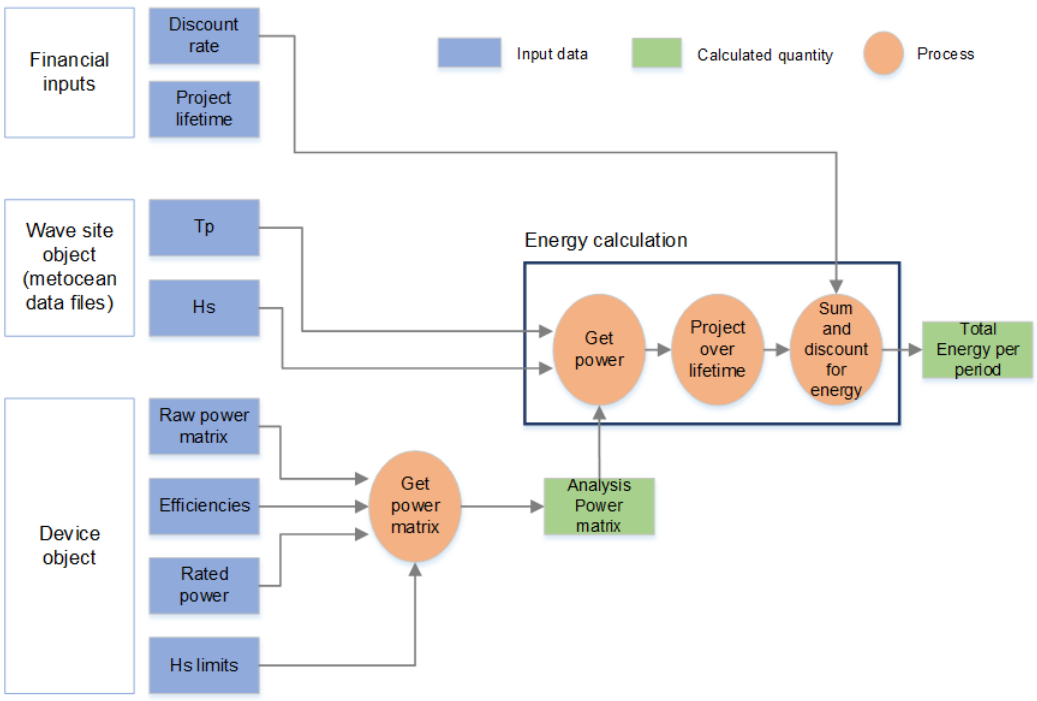

Figure 3.10: The energy analysis procedure, including the main input data and calculation steps to get to the energy production for each time period.

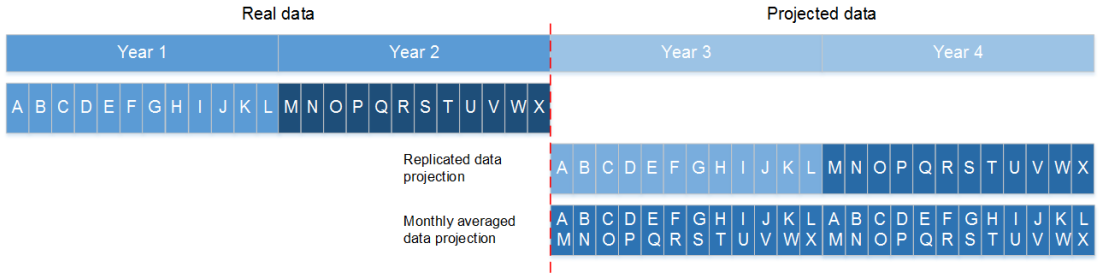

Figure 3.11: The two main methods that allow monthly power data can be projected over the full project lifetime. Each month is represented by a different letter. The replicated projection reuses the data, keeping the ordering the same. The monthly averaged projection finds the mean of similar months (for example all of the Januaries), building up a mean year which is used for the remaining duration.

years. However, as all of the metocean data used for this research project are in complete years, these are not directly implemented into the function. This was not deemed a priority, as such pre-processing of data can be achieved outside the model environment (highlighting an advantage of using the NetCDF data type).

3.7 Operations and Maintenance Module

The aim of this module is to allow the timescales and costs that are associated with specific O&M activities to be calculated. These could include things like installing the mooring system or recovering the devices to carry out scheduled maintenance. The classes that have been created to facilitate this are displayed in Figure 3.12. The module is only directly linked to two other modules: the `base_classes` and `wave_site` (previously described in Sections 3.4 and 3.5). The `ItemBase` class is required for cost calculations. Two classes from `wave_site` are required: `SitePoint` to define ports and `WaveSite` to define the grid and wave climate necessary for the calculations. The main O&M cost calculation is performed within the `MarineOperation` class, the other classes providing input data and methods to extend the functionality and improve usability.

It should be noted that the O&M module only supports planned operations. Unplanned operations, required to fix WECs, are not directly supported. If the time periods where failures occur were known then the `MarineOperation` class could be used, however the model offers no way to calculate these. This and other limitations of the research are presented and discussed in Section 3.11.

This section continues with a discussion of each class, detailing how each has been structured and how they fit into the overall cost calculation.

3.7.1 Vessels

The vessel is an important consideration for any marine operation, to ensure that it can be carried out in a safe and cost effective way. The properties of the vessel will have a significant impact on how well O&M tasks can be performed and the weather windows that are required. Within the model the physical vessels are represented by the `Vessel` class, containing a number of attributes that are important for the cost calculation performed within `MarineOperation`.

As for previous classes, `Vessel` inherits from `ItemBase`. This means that local costs can be defined, for example the cost required to fit equipment onto the vessel to carry out its duties. These are one-off costs (unless cost periods are specified by the user); costs that recur for each operation must be defined within the overall charter rate.

This charter rate, `charter_cost`, is one of four unique cost attributes that can be defined, the others being `standby_cost`, `mob_cost` (mobilisation cost)

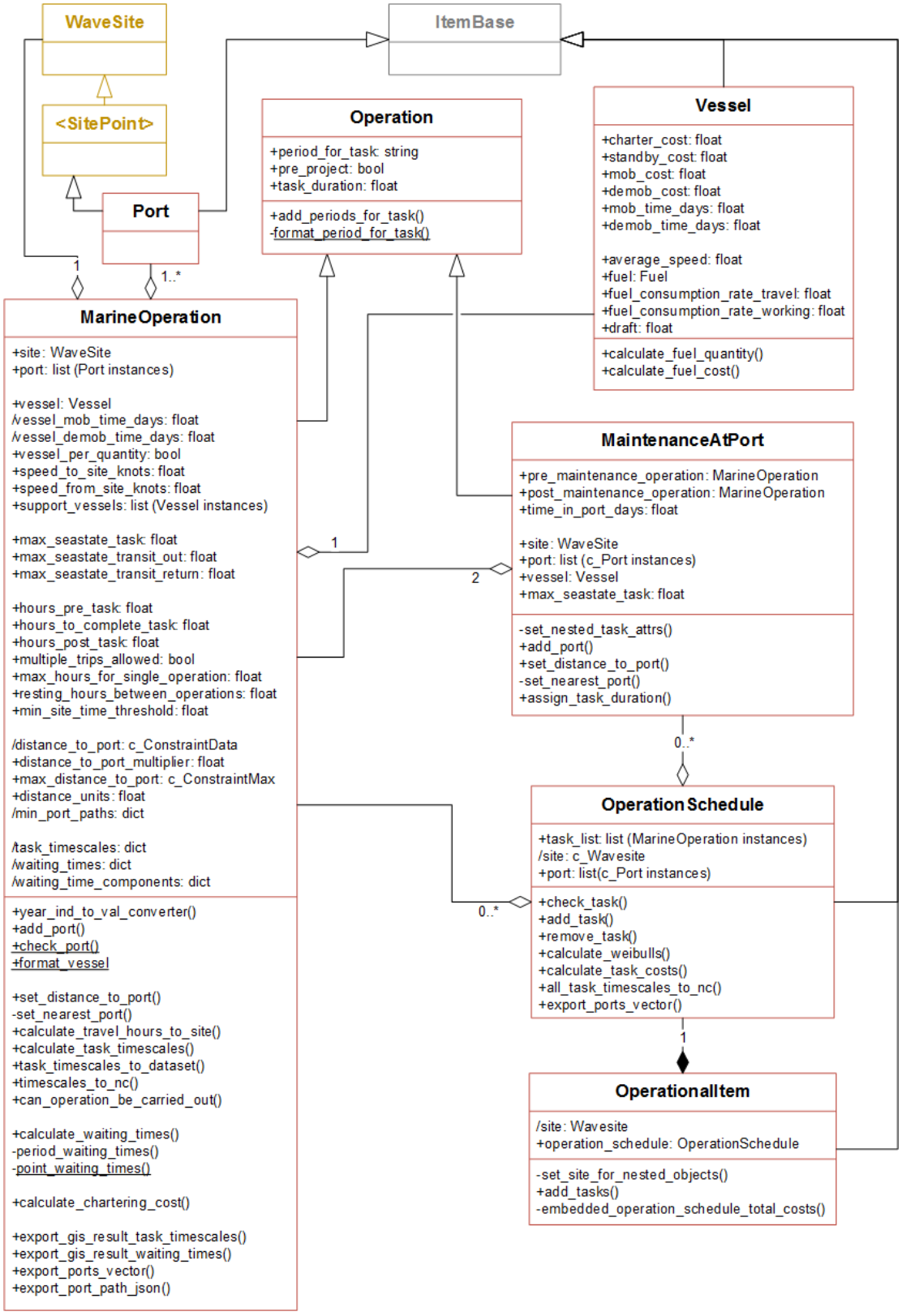

Figure 3.12: The classes that make up the `operations_and_maintenance` module. The module requires classes from `base_classes` and `wave_site`. Notation is the same as used for Figure 3.4.

and `demob_cost` (demobilisation cost). They are all properties, formatted prior to being set using the `add_local_costs` method from the `ItemBase` parent class. This means that they are stored within the instance's local costs attribute, so that they can be included in the cost category aggregation as described in Section 3.4.3. They are all specified in units of days. Longer term options, for example monthly or annual charter, can also be defined but would be specified as recurring local costs.

The charter and standby costs are important as they are multiplied by task timescales calculated within the `MarineOperation` class to obtain charter cost estimates. This differs to the the mobilisation and demobilisation costs, where the times are specified within the vessel directly (`mob_time_days` and `demob_time_days`) and are considered to apply equally across the whole domain. While spatially varying numbers could be estimated using pathfinding algorithms over a global dataset, it would be a largely trivial improvement in functionality as better estimates could be supplied by vessel hire companies themselves (for given ports).

The `average_speed` attribute defines how quickly the vessel can travel to site. This also feeds into the calculated charter time, discussed in Section 3.7.4. The fuel consumed by the vessel while performing its duties is split into two components: `fuel_consumption_rate_travel` for the fuel used while travelling and `fuel_consumption_rate_working` for the fuel used while working. The latter attribute could include aspects like vessel station keeping, vessel movement around the site and the fuel required to operate any on-board machinery. The fuel quantity consumed for a given number of hours, F, can be calculated with the `calculate_fuel_quantity` method. This takes the travel and working times, t_{travel} and t_{work}, and multiplies by the relevant fuel consumption rate directly:

$$F = R_{\text{travel}} t_{\text{travel}} + R_{\text{work}} t_{\text{work}} \,. \tag{3.5}$$

Using this and the `fuel` attribute, an instance of `Fuel`, the fuel cost can be calculated using the `calculate_fuel_cost` method. The calculated fuel quantity is assigned to the quantity attribute of the fuel instance's `cost_per_ltr` attribute, ensuring that the categorised costs propagate through. To provide flexibility the `fuel` and two fuel consumption rate attributes are optional. Within the `MarineOperation` class the fuel consumption will only be calculated if both are specified. This allows fuel cost to be ignored if not of interest or if it is considered within the overall charter cost.

The final attribute for the vessel class is the `draft`. This is the physical length of the vessel below the waterline, and effectively defines the minimum water depth that the vessel can traverse on its journey to site. This is considered when creating graphs from the ports to the sites.

3.7.2 Ports

The port is the second main element associated with the operation. This representation of the physical port is where the operation vessel (or vessels) is harboured, and assumed to contain the main workshop where onshore repairs are carried out. As different port instances can be specified for different tasks, distinction can be made between a major port for installation activities and smaller operations ports which might be set up closer to the device deployment site.

The `Port` class, inherits from the `SitePoint` class from the `wave_site` module and the `ItemBase` class from the `base_classes` module. This multiple inheritance is required so that local costs can be defined for the port (for example workshop rental and equipment hire fees) and path finding algorithms can be used to determine distances to the sites using methods defined in `SitePoint` (introduced in Section 3.5.2.1).

The only modification to the port child class is in the `graph_distances_to_point` method. If the port is in a particularly sheltered location, the parent method might fail as the neighbouring grid points are land and there is no path to the wider graph. This occurs as a consequence of the data resolution. To avoid this problem the method is contained within a try/except block. If a path cannot be found, a graphing error is returned and the nearest coastline point will be considered as the port location instead. This process is demonstrated in Figure 3.13, considering Stornaway Port and some sample site data. The actual location of Stornaway port is isolated in relation to the domain, surrounded by points in the domain that are defined as land. Because the four nearest neighbours are land, routes to the sea points cannot be resolved. Hence, in this circumstance the port class uses the nearest coastline point for any pathing analysis, a point which is linked to the wider dataset by the bottom left most sea point. For the example this is only 1.4 km away from the original point, a negligible distance in terms of both time and fuel consumption. Something to note is that this reassignment of the port location is only necessary if the data resolution is not sufficient. If higher resolution data are used then this issue would not arise.

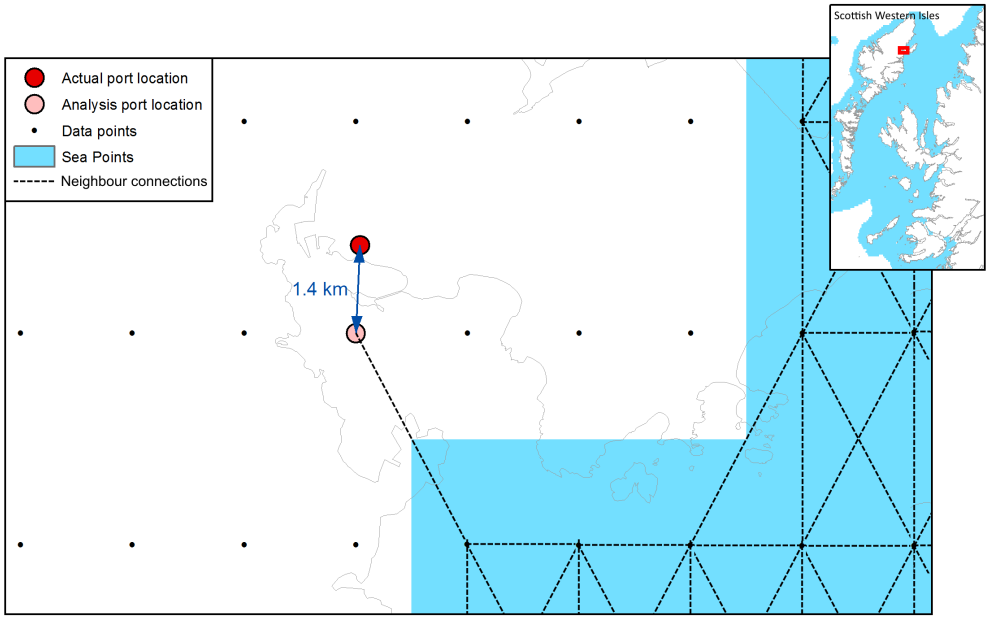

Figure 3.13: Example of how port location is modified for points that lie away from the main data grid. As the actual port location is surrounded by points in the domain that are considered land, the location is routed to the nearest coastline point. In this instance the point is only 1.4 km away from the original location.

3.7.3 The Operation class

This class serves as the base for the different O&M procedures that can be carried out on the WEC. It is designed to be built on by child classes, not used itself. While only three such classes have been created, `MarineOperation`, `MaintenanceAtPort` and `ExportCableInstall`, `Operation` is designed to cover other possible operations. Examples could include land-based operations, for example transporting the devices to port from the place of manufacture or installing the onshore electrical components. These were not considered for this research project as the costs are regarded by Albatern as a relatively low proportion of the total cost. They also rely on land-based knowledge and pathfinding which are considered outside the research scope.

The class has three attributes. The `period_for_task` attribute defines the period or periods that the task is carried out in. As the statistical analysis is typically conducted to a monthly base, each individual period is defined as a string in the form 'yyyy-mm' (e.g. '2000-06'). Operational costs that occur in the future are discounted. However this is not always desired, for example for installation costs that occur pre-project. To account for these the boolean attribute `pre_project` can be defined. If this is set to *true* then the final cost will be calculated using the specified month but will be assigned to month zero and not discounted in the

subsequent cash flow analysis. The two class methods, `add_periods_for_task` and `format_period_for_task`, give a convenient way to add new periods into an initialised class instance and ensure that the data formatting is consistent.

The `task_duration` is the total time to complete the operation. Is it a dictionary, with a value defined for each time period that the task occurs in. For the `Operation` class it is just a placeholder, but is used in the child classes.

3.7.4 Marine operations

The `MarineOperation` class is the most important in the module, as it contains the attributes and methods that are used to calculate the timescales and hence costs associated with specific tasks. It defines a single operation that involves making a trip out to site, made up of the following stages:

1. A vessel waits in port for a suitable weather window to carry out the task (in standby).
2. The vessel travels to the site.
3. Some operation is carried out on site.
4. The vessel returns to the original port.

Tasks that involve maintenance in port require two trips out to site: recovery and redeployment of a device. These are modelled using the `MaintenanceAtPort` class, which builds on the methods presented in this section and is described in Section 3.7.5.

The spatial aspect of the class is in calculation of the vessel standby and charter costs, generally regarded as major components of the overall operation cost. As it inherits from `ItemBase`, additional costs can be added as local costs. Examples could include costs of spare parts or project management overheads.

To calculate the spatial costs, first the timescales associated with the task are calculated. For each analysis point in the domain this is the time to travel to and from the point, and the time to wait for a suitable weather window to perform the operation. From these, the charter costs are calculated by multiplying the task time required by the vessel charter rate and the waiting time by the vessel standby rate. These processes are achieved using methods within `MarineOperation` and are discussed in more detail in Sections 3.7.4.3 to 3.7.4.5.

3.7.4.1 Key attributes

There are five compulsory attributes that must be specified to obtain spatial cost estimates for the task:

- The site of interest (a `WaveSite` instance).
- A vessel to carry out the operation (a `Vessel` instance).
- One or more port options, where the operation starts and finishes (`Port` instances).
- The time to complete the task.
- The time period (or periods) when the operation is carried out.

The site is used for two purposes: to determine the distances from the port to the sites and to provide the metocean data for weather window estimation. The relevant methods are coded within the `WaveSite` class (see Section 3.5.1). The distances are stored within the `distance_to_port` attribute.

While only a single vessel is used to compute the task timescales, multiple ports can be specified using a list of `Port` instances. This is to preserve the model applicability over large areas, by allowing ports to be defined for localised regions of the domain. The model effectively optimises the task port by distance, for a given point choosing the closest port for the cost analysis using the `find_nearest_points` static method described in Section 3.5.2.1. Future behaviour could be to optimise by cost instead, as different ports will charge different rates for usage, however this is not deemed a key feature (and would be straightforward to achieve by comparing output results for single ports) so has not been considered for this research.

At site, the time to complete the task is defined by three attributes:

1. The time on site required to set up any equipment prior to commencing work (`hours_pre_task`).
2. The time to carry out the actual task (`hours_to_complete_task`).
3. The time that it takes to prepare the vessel for travel back to port (`hours_post_task`)

While the pre and post times could be incorporated into the overall task completion time, they are kept separate to allow for greater flexibility. This is especially useful for the export cable installation class, `ExportCable`, where the task

time is spatially dependent but the pre and post task times generally would not be. This class is discussed in Section 3.8.2.

The waiting time for weather windows is calculated using the `max_sea state_task`. As this calculation is the slowest part of the code it is not a compulsory element, however is recommended to get an overall reflection of the site specific metocean conditions.

The attribute defines the maximum sea state that the operation can be performed in. For real operations there are many factors that would be taken into account, including wave period and wind speed. However, the weather window analysis for this model only considers significant wave height as a metric. This decision was taken because it is usually regarded as the most significant factor [85,87] and the thresholds are better understood (in Albatern's case the wind speed and period thresholds have not been quantified and would be largely hypothetical).

Any locations where the weather window required exceeds the time available in the month are filtered out of the analysis, as it is physically impossible to perform the necessary operation. This is carried out when calculating the costs, and is discussed more in Section 3.7.4.5.

The `task_timescales` and `waiting_times` attributes store the results of the timescale calculations. They are dictionary types, and hence the data can be easily exported to NetCDF or raster files.

3.7.4.2 Other attributes

As well as those described above, there are also minor attributes that influence how the task timescales and costs are calculated.

In the default case the vessel instance's `average_speed` is used to compute the timescales. Different speeds can also be specified with `speed_to_site_knots` and `speed_from_site_knots`. These are required when the vessel speed might be limited, for example when towing a device to site, and also have implications for operation waiting time calculation.

The `vessel_per_quantity` attribute has implications for multiple operations defined within a single `MarineOperation` class instance. This is set through the `quantity` attribute, inherited from `ItemBase`. Multiple operations in a single time period could mean one of two things:

1. One vessel is used for all the operations.

2. Each operation is carried out by its own vessel.

While the options are assumed to have the same cost associated with them, there is a difference in the time available for the operation. Using the example of six identical operations in the month of January, one vessel would have 31 days to complete all six tasks. Alternatively, six vessels would each have 31 days to do one task, a more relaxed deadline. This influences which points are excluded at the cost calculation stage and also the mobilisation costs (as this is incurred for each vessel assumed).

As well as the main vessel, support vessels can also be defined by specifying a list of `Vessel` instances. These represent smaller vessels like Rigid-Hulled Inflatable Boats (RHIB) that are chartered to assist the task at hand. They are treated differently to the main vessel. Timescales are not calculated for these vessels, they use those calculated for the main vessel. For example if the main vessel is found to require two days of charter and three days of waiting then the support vessel will also assume these times, using its own cost rates to obtain overall costs.

There are two further sea state thresholds that are optional. The `max_sea state_transit_out` and `max_sea state_transit_return` attributes allow H_s thresholds to be set for transit to and from site. The main application for this is for operations where the wave device is towed to site, as this will require calmer conditions. Following the methodology of Walker [88], weather window analysis is performed for each component separately and the results summed. Results are stored in the `waiting_times_components` attribute. More information on these is provided in Section 3.7.4.4.

There are several attributes that control how the task timescales are calculated. The `max_hours_for_single_operation` quantity defines the maximum number of hours that are available to carry out the task, including travel to and from the site. If the task cannot be completed in this time (excluding waiting time) then there are two different options. The `multiple_trips_allowed` attribute determines whether or not the operation can be carried out over multiple trips. If False then the task must be carried out in a single journey; it cannot be carried out if the time required for the task exceeds the maximum number of hours. If True then the task can, in theory, be carried out all over the domain (subject to waiting time), although might require multiple round trips. In this case, the time that elapses between arriving back at port and heading back out to the site can be set with the `resting_hours_between_operations` attribute which adds to the charter time that is required. Finally, the `min_site_time_threshold` attribute can be specified to screen out sites at more extreme distances. Without this attribute, for longer multiple trip operations the issue arises where valid

sites furthest from the port would require very large numbers of round trips to complete the task, as once the vessel has travelled it has very little time to actually complete the task at hand. Such situations are both unrealistic and increase the computation time. The attribute screens out these sites when calculating the task timescales: if the time available for the task after travelling is less than the attribute then it is filtered out.

Lastly, there are two attributes which concern the port distances stored within `distance_to_port`. The `distance_to_port_multiplier` attribute is a modification factor that is applied to the calculated distances prior to the calculation of task timescales. This can be used to account for uncertainty in the distances calculated but is set to a value of one by default. The second is a distance constraint, `max_distance_to_port`. This can be assigned to the operation class which allows points that are too far away to be easily identified and filtered out in GIS (see Section 3.10 for a description of constraints).

3.7.4.3 Calculating task timescales

As previously stated, the calculations that underpin the cost analyses require calculating the timescales associated with distinct tasks. The main cost drivers incorporate a time dependence, i.e. vessels are commonly chartered on a daily rate, which allows cost estimates to be built up. The method `calculate_task_timescales` is used to calculate these timescales, with the exception of weather window waiting time that is described in the next section.

For a particular operation, the total time required to carry out the task at a particular point (x, y) is expressed as:

$$t_{\text{task}}(x, y) = t_{\text{travel}}(x, y) + t_{\text{site}} + t_{\text{waiting}}(x, y) + t_{\text{resting}} \,. \tag{3.6}$$

Here t_{travel} is the total time to travel to and from the point, t_{site} is the time spent on site carrying out the task and t_{waiting} is the average time spent waiting for a suitable weather window. t_{resting} is the time resting between operations if multiple trips to site are required. All quantities are considered in units of hours.

The travel time is estimated by calculating the time to get to and from site, t_{to} and t_{from} and multiplying by the number of round trips needed until the task is completed, N_{rt} :

$$t_{\text{travel}}(x, y) = N_{\text{rt}} \left[t_{\text{to}}(x, y) + t_{\text{from}}(x, y) \right] \,. \tag{3.7}$$

The parameter N_{rt} depends on the number of hours that are available for a single operation. In the default case, the variables t_{to} and t_{from} are calculated by multiplying the distance from a specified port, d_{port}, by the average transit speed of the vessel that is carrying out the task, v_{av} :

$$t_{\text{to}}(x, y) = t_{\text{from}}(x, y) = v_{\text{av}} d_{\text{port}}(x, y) \,. \tag{3.8}$$

As the vessel speed is the same in both directions they are considered equal. Alternatively, if the `speed_to_site_knots` or `speed_from_site_knots` attributes are defined, v_{to} and v_{from}, then the timescales are calculated as:

$$t_{\text{to}}(x, y) = v_{\text{to}} d_{\text{port}}(x, y) \tag{3.9}$$

$$t_{\text{from}}(x, y) = v_{\text{from}} d_{\text{port}}(x, y) \,. \tag{3.10}$$

The port distances are calculated using the `set_nearest_port` method, which runs Dijkstra's algorithm on the site instance with the port locations as starting locations (as described in Section 3.5.2.1).

As the time on site required to carry out the operation, t_{site}, is defined directly, it is independent of location in the current model. This could be made spatially dependent in future to account for the fact that operations may take longer in more exposed locations, where conditions could be more challenging.

Within the class, the task timescale results are stored together as a dictionary within the `task_timescales` attribute. This includes the following components:

- The travel hours to site.
- The total hours on site.
- The total hours travelling.
- The number of round trips.
- The total hours required for the operation, excluding waiting time.
- The window lengths that are required at each location, for each trip required to site.

The window lengths are used to calculate the waiting time for each individual trip required out to site. This procedure is discussed in the next section.

3.7.4.4 Calculating waiting time

To calculate waiting times the model incorporates the frequency based approach of Kuwashima and Hogben [86], as introduced in Section 2.3.3.1. This process first involves creating a joint occurrence matrix for every point in the analysis domain for every month of interest (as defined within the `period_for_task` attribute). For each ascending H_s bin with edge value H_b, the probability that a given sea state will exceed the bin, P_h, is calculated as:

$$P_h(H_b) = \frac{C_{H_s>H_b}(H_b)}{C_T}\,, \tag{3.11}$$

where $C_{H_s>H_b}$ is the number of recorded sea states in the matrix above the bin and C_T is the total number of sea states in the time period. P_h is known as the exceedance probability and can also be approximated by a 3-parameter Weibull distribution for a given threshold significant wave height, H_{ac}:

$$P_h(H > H_{\mathrm{ac}}) = \exp\left(-\left(\frac{H_{\mathrm{ac}} - X_0}{b}\right)^k\right)\,. \tag{3.12}$$

The parameters k, b and X_0 are the shape, scale and location parameters respectively. From initial values (by default $k = 1.5$, $b = 1.5$ and $X_0 = \min(H_s) - 0.05$), they are then adjusted to get as good a fit to the raw distribution as possible (Equation 3.11). This is done using using an iterative least squares method from the *SciPy* statistical Python package.

Once they are obtained, the average window length at a particular H_{ac} can be found:

$$\tau_{\mathrm{ac}}(H_{\mathrm{ac}}) = \frac{1 - P_h(H_{\mathrm{ac}})}{P_h(H_{\mathrm{ac}})} \cdot \frac{A}{[-\ln(P_h(H_{\mathrm{ac}}))]^\beta}\,, \tag{3.13}$$

where the constants A and β are functions of a separate factor γ, calculated from the Weibull parameters:

$$A = \frac{35}{\sqrt{\gamma}} \tag{3.14}$$

$$\beta = 0.6\gamma^{0.287} \tag{3.15}$$

$$\gamma = k + \frac{1.8X_0}{(\bar{H} - X_0)} \tag{3.16}$$

$$\bar{H} = b\Gamma\left(1 + \frac{1}{k}\right) + X_0\,. \tag{3.17}$$

Given these quantities, the probability that wave conditions less than the threshold will persist for at least a desired duration X_{ac} can be calculated:

$$P_t(X_i > X_{\mathrm{ac}}) = \exp\left(-C_{\mathrm{ac}}(X_i)^{\alpha_{\mathrm{ac}}}\right) , \tag{3.18}$$

where:

$$C_{\mathrm{ac}} = \left[\Gamma\left(1 + \frac{1}{\alpha_{\mathrm{ac}}}\right)\right]^{\alpha_{\mathrm{ac}}} \tag{3.19}$$

$$\alpha_{\mathrm{ac}} = 0.267\gamma\left(\frac{H_{\mathrm{ac}}}{\bar{H}}\right)^{-0.4} . \tag{3.20}$$

The value X_{ac} can be thought of as the length of weather window required, which is calculated using the `calculate_task_timescales` method from the above section.

The overall probability of a weather window occurring in the time period conforming to both the H_s threshold and duration required is equal to:

$$P(T > \tau_{\mathrm{ac}}) = P_h(H > H_{\mathrm{ac}}) \cdot P_t(X_i > X_{\mathrm{ac}}) . \tag{3.21}$$

Hence, the number of days that the site can be accessed in the time period, N_{ac}, and the average number of days required to wait for a suitable weather window, $t_{waiting}$, can be determined by also considering the total duration of the time period in days, D_m:

$$N_{\mathrm{ac}} = D_m \cdot P(T > \tau_{\mathrm{ac}}) \tag{3.22}$$

$$t_{waiting} = \begin{cases} \frac{D_m - N_{\mathrm{ac}}\tau_{\mathrm{ac}}}{N_{\mathrm{ac}}} & t_{waiting} \leq D_m \\ D_m & t_{waiting} > D_m \end{cases} \tag{3.23}$$

Of these quantities $t_{waiting}$ is the main output of interest, as it represents the average time that the vessel will be on standby to carry out the operation within the month. The number of waiting days cannot exceed that available in the month; in this case $t_{waiting}$ is set to D, with these locations filtered out of the analysis in the cost calculation step.

The above formulae are coded into the class within the `calculate_waiting_times` method. The joint occurrence matrices are created for each time period and analysis location using the `site_joint_matrices` method of the embedded `Site` instance. Next the Weibull fitting parameters are calculated as above. From these, the waiting time for each time period and

point are found by calling the private functions `period_waiting_times` and `point_waiting_times`.

If H_s thresholds are specified for the transit to and from site, `max_sea state_transit_out` and `max_sea state_transit_return`, then the above process is repeated for each of these. This gives three components of the waiting time. The resulting waiting times are then added to that for the task itself to get the total waiting time, as recommended in [88]. For the transit operations the metocean conditions at the site are used to estimate the weather window, assumed representative of the journey to site as a whole.

The total waiting times for each time period are stored together in the `waiting_times` attribute. This is a dictionary: each key being a different time period and each corresponding value a NumPy array of the waiting times. For locations where multiple trips to site are required to carry out the operation in a given time period, the waiting times are calculated for each trip required and summed to get a total waiting time.

The three waiting time components are stored within the `waiting_times_components` attribute. This is so the final results can be dissected and the most influential factor determined.

3.7.4.5 Calculating task costs

Once the task timescales are obtained, the vessel charter costs are calculated. The method `calculate_chartering_cost` carries out this step and also calls the other two calculations automatically if no timescales have been set (i.e. the `task_timescales` attribute is *None*). The standby cost for the operation in a given month m is calculated by multiplying the waiting time (rounded down to the nearest day) by the vessel standby cost per day c_s:

$$C_{\text{standby}}(m, x, y) = c_s t_{\text{waiting}}(m, x, y)\,. \tag{3.24}$$

The working charter cost is equal to the vessel charter cost c_c multiplied by the time that the vessel is working (i.e. the sum of t_{travel} and t_{site}):

$$C_{charter}(x, y) = c_c\left[t_{\text{travel}}(x, y) + t_{site}\right]\,. \tag{3.25}$$

The total fuel cost is calculated from the transit and working contributions:

$$C_{\text{fuel}}(x, y) = \sum_{b=1}^{B} c_f\left[R_t(b) t_{\text{travel}}(x, y) + R_{\text{work}}(b) t_{\text{site}}\right]\,. \tag{3.26}$$

Here c_f is the fuel cost per litre. For each vessel b involved in the operation (the main vessel and any supporting vessels), the fuel consumption is calculated using the relevant timescales, where R_{travel} and R_{work} are the fuel consumption rate attributes for travelling and working respectively.

Both $C_{charter}$ and C_{fuel} are spatially dependent, however are assumed to be the same for each operation time period. This means that the cost associated with vessel hire in a given month is equal to:

$$C_m(m,x,y) = C_{\text{standby}}(m,x,y) + C_{\text{charter}}(x,y) + C_{\text{fuel}}(x,y) \tag{3.27}$$

$$C_v(m,x,y) = \begin{cases} C_m(m,x,y) & t_{\text{task,d}}(m,x,y) \leq D_m(m) \\ \text{inf} & t_{\text{task,d}}(m,x,y) > D_m(m) \end{cases}, \tag{3.28}$$

where $t_{task,d}(m,x,y)$ is the total time that the vessel is required in the month, in days, as defined in Equation 3.6. If the total time exceeds that available in the month then the operation cannot physically occur, and is assigned a value of *Inf*. This value can be detected in the GIS raster outputs, so these regions can be easily identified.

For operations carried out over multiple periods it is useful to be able to see, for a given point, the time period where the maximum task times occur. This is because particularly stormy months might significantly shrink the size of the domain. The maximum task times over the periods are calculated within `calculate_chartering_cost`, as well as the specific time periods where the maximums occur. These can then be visualised in GIS, as demonstrated in Figure 3.14. In this example the time periods (19, 3) and (10, 3) incur the longest time penalties to the west of Lewis and Harris. From this information these months could be manually substituted for other months to see if the domain could be made larger.

The monthly vessel totals are then summed and added to any non spatial costs C_{ns} to obtain the total cost for all of the months specified:

$$C_{\text{op total}}(x,y) = C_{ns} + \sum_{m=m_0}^{m_T} C_v(m,x,y)\,. \tag{3.29}$$

Examples of non spatial costs include vessel mobilisation and demobilisation costs, c_m and c_d respectively, any local costs of the `MarineOperation` instance (C_{opl}) and any local costs of the port instance (C_{port}):

$$C_{\text{ns}} = c_m t_m + c_d t_d + C_{\text{opl}} + C_{\text{port}}\,. \tag{3.30}$$

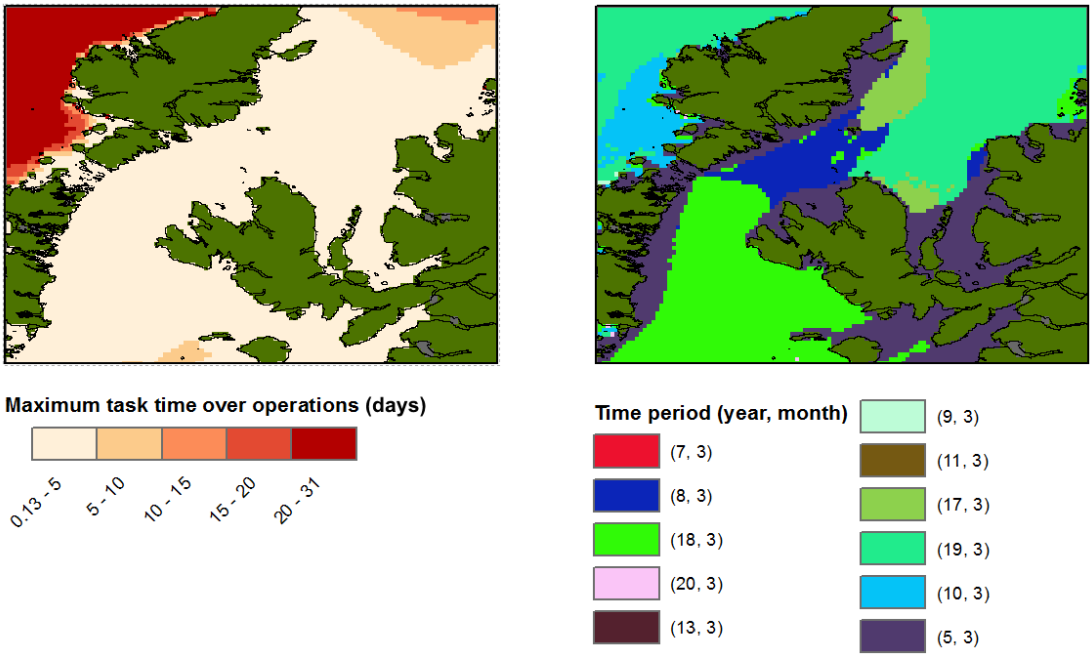

Figure 3.14: The maximum time to perform an example task over several different time periods (in days) and the corresponding time period that these are incurred in. This functionality makes it easier to identify particularly stormy time periods that might curtail the output data domain.

It should be noted that this cost aggregation process occurs for cost categories defined at the `MarineOperation` level. Individual cost elements are also be grouped by their `cost_categories` attributes and filtered through the cost analysis as described in Section 3.4.3, meaning that every individual operational cost can be tracked.

3.7.5 Maintenance at port

The `MaintenanceAtPort` class represents an operation where the device is brought into port for maintenance. The operation is treated as three separate tasks and requires two trips to site:

1. The vessel travels from port to site, collects the device and returns to port.
2. Some maintenance is carried out on the device.
3. The device is towed back to site and redeployed. The vessel then travels back to port.

The first and third tasks are each identical in principle to a single `MarineOperation`. Costs associated with the second task can be included within the local costs attribute.

To model the three tasks, the class contains three unique attributes. The `pre_maintenance_operation` and `post_maintenance_operation` attributes define tasks 1 and 3 above. These are `MarineOperation` instances, taking advantage of all the existing class functionality.

The `time_in_port_days` attribute, t_{port} defines how long the port maintenance takes. This is used to apply the operation time constraint. As for the `MarineOperation` class, the maintenance at port must be carried out in a single month. The total time to carry out the operation is:

$$t_{\mathrm{MaP}} = t_{\mathrm{task1}} + t_{port} + t_{\mathrm{task2}} \,. \tag{3.31}$$

As for the `MarineOperation` class, the total time to carry out the three tasks, t_{MaP}, cannot physically exceed the time available in the month. This means that the total cost in a given month, C_{TMaP} is calculated as:

$$J(m,x,y) = C_{\mathrm{task1}}(m,x,y) + C_{\mathrm{local}}(m) + C_{\mathrm{task2}}(m,x,y) \tag{3.32}$$

$$C_{\mathrm{TMaP}}(m,x,y) = \begin{cases} J(m,x,y) & t_{\mathrm{MaP}}(m,x,y) \leq D_m(m) \\ \mathrm{inf} & t_{\mathrm{MaP}}(m,x,y) > D_m(m)\,, \end{cases} \tag{3.33}$$

where C_{task1} is the cost of the operation to site, C_{local} the class instance's local costs, including port maintenance costs, and C_{task2} is the cost of redeploying the device at site.

To achieve the cost calculation, the inherited `categorised_local_costs` class method is modified, calling the `categorised_local_costs` method for the two embedded `MarineOperation` classes and then applying the time constraint as described above. The four remaining class attributes, as shown in the UML, are included for convenience (`site`, `port`, `vessel` and `max_sea state_task`). They can be set at the class level and are then assigned to the two embedded `MarineOperation` classes at runtime with the `_set_nested_task_attrs` private method. This is also the case for the `period_for_task` and `pre_project` attributes inherited from `Operation`.

3.7.6 Operation schedule

When considering larger arrays or more complex operational tasks it is not practical to have to define the inputs for each individual task, especially where input quantities like the vessel or port are shared among multiple tasks. In addition, repeating the task timescale calculations among similar tasks can greatly increase

the computation time. The `OperationSchedule` class is essentially a group of tasks and has been developed to mitigate these problems.

The most important attribute of this class is `task_list`, a list containing all of the task instances. Tasks can be instances of `MarineOperation`, `MaintenanceAtPort` or other instances of `OperationSchedule`, this latter ability allowing schedules to be easily combined. Tasks can be added or removed from the list using dedicated instance methods (`add_task` and `remove_task`), which can be useful when scripting or debugging within Python. The real advantage in storing multiple tasks together is that certain operation attributes can be defined in the schedule which are then applied to all of the `task_list` members at calculation runtime. These attributes are:

- The site.
- The vessel.
- The port.
- The time period that the operations take place in.

It is mandatory that the same site (`WaveSite` instance) is defined for every task. The schedule class gives a convenient way of ensuring that this is the case, using the private method `_assign_site_to_tasks` which is initiated upon setting the `site` property. The other three attributes do not have to be the same across multiple task instances but commonly might be. Examples of these scenarios could include a group of installation tasks that occur in the same time period or a single operational port from which all tasks are carried out from.

For a single operation, calculating the Weibull parameters is a particularly time consuming part of the task timescale calculation process. For tasks that are carried out within the same time period it does not make sense to perform these calculations multiple times. The `calculate_weibulls` method reduces the computation time in these situations. The time period for each task within `task_list` is extracted into a list, with any duplicated entries removed. The function then iterates through these time periods, obtaining the joint matrices and Weibull parameters as described in Section 3.7.4.3. A dictionary of the form $\{<$ `period` $>:<$ `weibulls` $>\}$ allows the parameters to be matched to the corresponding tasks prior to calculating the waiting times.

The `calculate_task_costs` method gives a straightforward way to calculate all of the task costs: looping through each task and performing the calculations described in Sections 3.7.4.3 to 3.7.4.5.

3.7.7 Assigning operations to items

The operational item class, `OperationalItem`, combines the important `ItemBase` class with an operation schedule instance to define a cost object which has some operational tasks associated with it.

As a child of `ItemBase` it inherits all of the methods related to embedded cost calculation. The main difference is that there are two new inputs to be specified at initialisation: a `site` attribute and an `operation_schedule` attribute. Both of these must be instances of the respective classes. Setting the `site` property for the operational item will automatically set it for the embedded operation schedule too.

To prevent double counting of task costs, the `get_embedded_costs` method is modified. Because the `categorised_local_costs` method of the operation schedule calculates task costs, the risk is that the default function would get the task (and task embedded object) costs twice. To mitigate this problem, the function uses the following process:

1. The usual local and embedded cash flows within the operational item object are calculated and extracted (as in Section 3.4.3), but with the the embedded operation schedule and operation items omitted.

2. The operation schedule's embedded costs are obtained with the private method `embedded_operation_schedule_total_costs`. This uses the methods described in Section 3.7.4 and 3.7.6 to obtain cash flows for all of the operational tasks specified. The function makes sure to only get operation schedule or operation embedded instances, to prevent items from the last step being included again.

3. Both sets of cash flow outputs are combined to get all of the embedded costs. This means that the overall categorised cash flows can be obtained as previously described in Section 3.4.3.

3.8 Export Cable Module

The export cable module contains classes to calculate cable routes and costs for the export cable system. This includes the cable CAPEX and the installation. The UML diagram for this module is shown in Figure 3.15. While there are only three separate classes present, the decision was taken to create distinct module, rather than using the device module, to prevent any circular dependencies occurring between the device and hybrid system modules.

3.8.1 Export cable

The export cable is defined by the `ExportCable` class. This inherits from `OperationalItem` to allow the cable installation cost to be embedded and calculated.

The main property of the export cable is its cost per metre. This is specified at initialisation and is defined as the capital cost required to purchase a metre of cable. Typically this will just be defined as a float (e.g. 20.0), and is formatted into a cost type and saved as a local cost within the property setter (under the description 'cost_per_m'). The quantity attribute of this local cost is where the

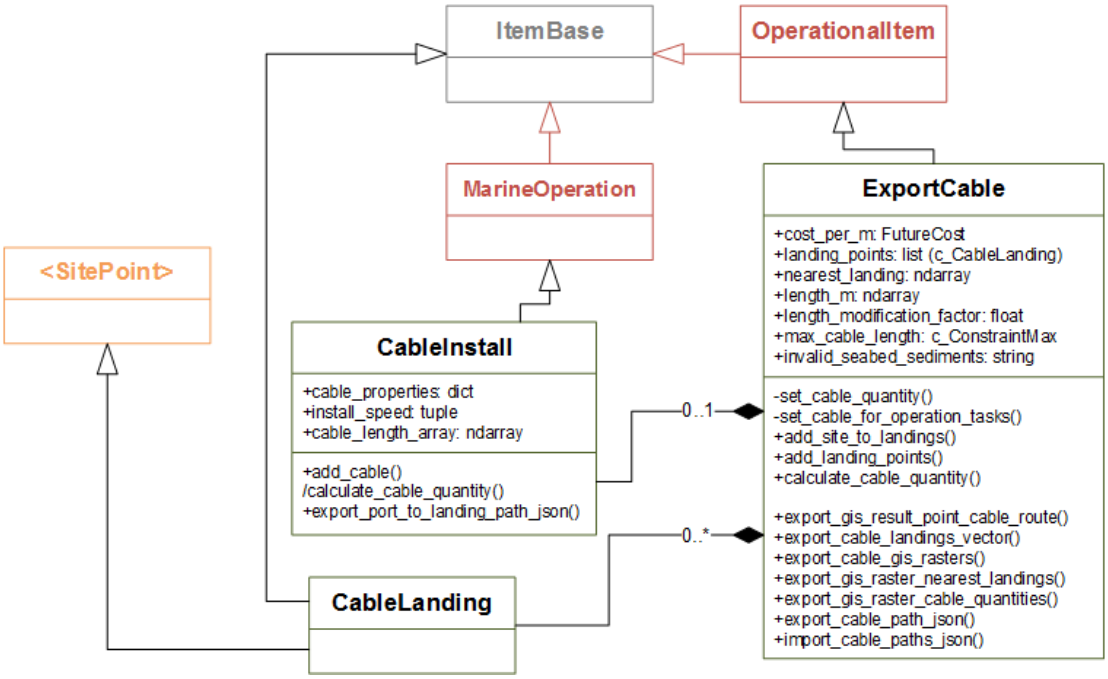

Figure 3.15: The properties and relationships between the three classes contained in the export cable module (outlined in green). Parent classes are obtained from three other modules: the `base_classes` module (grey), `wave_site` module(orange) and the `operations_and_maintenance` module (red). Notation is the same as used for Figure 3.4.

actual length of cable is stored and used for calculation. This is not set but rather calculated from the site and cable landing properties.

Cable landing points on shore are defined within the attribute `landing_points`. There are two options for landing points. If no points are specified (i.e. the landing point attribute is set to None) then the model will assume that the cable travels the shortest distance to shore for each site analysis point. This approach is seen in the literature (for example [133]) and gives a useful way of assessing site viability in the absence of more detailed information. The alternative is to explicitly state the coordinates of potential landing locations. In reality this will depend on factors such as geology and topography along the coastline and, in the case of grid-connected systems, the distance to potential grid connection points.

The suitable landing points are input as a list of coordinates (in decimal degrees). The landing points property then iterates through these, converting each into an instance of the `LandingPoint` class. This class inherits from both the `ItemBase` and `SitePoint` classes (from Sections 3.4 and 3.5.2 respectively). This is so that the distances from the landing point to the analysis points can be calculated and so that, if the user desires, different costs can be applied to different landing points.

The cable lengths are calculated using the instance method `calculate_cable_quantity`. This considers the analysis domain points from the embedded `site` attribute. When specific cable landing points are specified the function is almost identical to the distances to port calculation, using the distance calculation framework introduced in Section 3.5.2.1. This really highlights the benefits of using an object-orientated approach for such a model: inheritance means that code only needs to be written once and can be used for similar applications, making it easier to understand and debug. Using the `find_nearest_points` static method for all of the cable landings results in an array of distances, from each analysis point to its nearest cable landing. Something to bear in mind is that the function optimises for distance, not for cost. In reality it is possible that a further away cable landing might require more cable but be easier to excavate and connect to, leading to a lower cost. This kind of cost optimisation is of interest for future work but is not considered for this work.

If the shortest distance to coastline is desired then an alternative function is employed. This function, `shortest_distance_to_coastline` is coded within the

site instance and was briefly introduced in Section 3.5.1. Originally it was located within the `ExportCable` class, however was shifted to the `Site` class as it only uses underlying site data and could, in theory, be extended for other applications. The first step is to identify all of the inland points in the routing range, i.e. points that are land but not coastline (do not have a sea point neighbour). These points serve as the obstacles. A graph containing the sea and coastline points is created using the `get_site_graph` methods, as described in Section 3.5.2.1. All of the nodes in the graph are then classified according to if they are sea or coastline. From the analysis nodes the valid sea points are identified. The algorithm then iterates through these points, carrying out Dijkstra's algorithm for each in turn. This modified version of the algorithm finishes when it encounters a coastline point: the first point that it finds is the nearest coastline point in the routing domain. The distance value and path are then extracted as for the pathfinding methods described previously.

The main output of interest is the array of cable distances, one for each analysis point. Points in the analysis domain that are land are automatically screened out and assigned values of *NaN*. The distances, the calculated cable quantities, are stored within a new attribute: `length_m`. This is not used directly for the cost per metre quantity. Instead, it is first combined with an arbitrary modification factor, `length_modification_factor`. The purpose of this factor is to allow cable length to be easily adjusted or examined as a sensitivity. As the pathfinding algorithm calculates the shortest path, this also allows contingency to be added to the cable lengths to account for divergence from this path on the sea bed. The factor is multiplied by the calculated length to obtain an effective length. This is the value used as the cost per metre quantity and is set automatically whenever the length modification factor or `length_m` are set by calling a function within the property setters.

As well as cable distances, the other outputs to the algorithm are the cable paths (stored within a dictionary as described previously) and, when considering specific landing points, an array showing which landing point is nearest for each analysis point.

All three of the outputs can be exported as raster files for visualisation in GIS, using instance methods within the class. A multi-point vector layer showing the landing locations can also be exported.

Lastly, there are two constraints associated with the cable class. The first is maximum cable length; analysis points which require cables over a certain length

can effectively be screened out of the analysis. This is useful if only nearshore sites are to be considered, or if a particular cable needs to be used but must not exceed a certain length to keep losses within a desired limit. The second constraint is seabed geology. Invalid seabed geologies can be specified as input to the class (these must match up with the definitions within the site's seabed geology attribute). This is considered as a constraint in the traditional sense (i.e. a device cannot deploy where the geology is invalid) and is also input as an obstacle into the pathfinding function. This latter process is achieved by defining the geology as a new point classification, adding to the default bathymetry based classifications described in Section 3.5.1. It means that cables will route around unsuitable geologies. The main purpose for this is if the cable is being trenched. Cheaper cable ploughs will not be suitable for rocky seabed types, and so these locations can be considered as obstacles to the pathfinding (in the same way that land is).

3.8.2 Export cable installation

The export cable installation class, `ExportCableInstall`, inherits from the `MarineOperation` class but with changes to reflect the nature of the operation. While the standard operations are assumed to occur at a single point in the domain, for example installing the mooring system, the export cable is different because it must be installed over a number of locations.

The class contains two additional properties that must be specified to perform the necessary calculations: `export_cable` and `install_speed`. The `export_cable` is simply a `ExportCable` class instance, or a dictionary of `ExportCable` attributes that is used to initialise an export cable instance. Definition of the export cable is required as this is where the cable distance and pathing calculation is conducted (see Section 3.8.1). The install speed is used to estimate the length of the weather window required for the whole cable installation procedure. The default units are metres per hour. Different units can be specified by the user by inputting a tuple of the form (<`install speed value`>, <`units`>).

The costs are estimated using a similar procedure, but modified methods, from the standard `MarineOperation` class. A simplified representation of the function to obtain the timescales that feed into the cost calculation is shown in Algorithm 3.3.

First the export cable lengths are calculated at every location in the analysis

Purpose: To spatially estimate timescales associated with export cable installation, including waiting time.
Required: An `ExportCableInstall` instance (denoted as self below) with `site`, `export_cable` and `install_speed` properties defined.
Returns: The transit time, time required to install the cable and the waiting time to carry out the installation for each analysis point.

```
def calculate_task_timescales(self):
vessel = self.vessel
v_transit = vessel.average_speed
v_install = self.install_speed
d_cable, p_cable = self.calculate_cable_quantity() # Cable lengths and
    paths.
t_install = v_install / d_cable # Times required to install cable.
self.set_distance_to_port()
t_to_site = self.distance_to_port / v_transit
for site_coords, path in p_cable:
    # Cable start and end locations.
    landing_coords = path[-1]
    end_coords = site_coords
    # Assign basic timescales.
    t_to_start = t_to_site[landing_coords]
    t_to_end = t_to_site[end_coords]
    t_transit = t_to_start + t_to_end
    t_on_site = t_install[end_coords]
    t_window = t_on_site # Weather window required.
    waiting_times_along_path = [] # Preallocate for point waiting times.
# Waiting time calculation
    for coords in path:
        # Calculate individual waiting times and store in list.
        waiting_for_coords = get_waiting_times(coords, t_on_site)
        waiting_times_along_path.append(waiting_for_coords)

    t_waiting[end_coords] = max(t_w_points) #Use maximum waiting time.

return t_transit, t_install, t_waiting
```

Algorithm 3.3: Calculate task timescales associated with export cable installation.

domain, utilising the `calculate_cable_quantity` method in the embedded export cable object. Crucially, as well as lengths the paths of the cables are also returned. With the quantity of cable and the installation speed, the time to install the cable can be obtained. This is important as it determines the weather window that is required. Next the distances from the installation ports to the analysis points are obtained, as for a standard `MarineOperation`. With these data the task timescales can be calculated. At a given WEC deployment location, the total operation is considered in three stages:

1. The vessel travels from port to the cable landing point that is associated with the location. The port nearest to the landing point is assumed.

2. The vessel begins the installation. Using the export cable path dictionary as a reference, the vessel travels from the landing point to the deployment location.

3. The vessel completes the installation, and travels from the deployment location back to port.

Whereas in the standard marine operation the time to and from the site are assumed to be the same, this is not the case for the cable installation. The time to the site is represented by the first part of the operation and the time back the third part. The second part is the hours on site; this is calculated rather than being specified by the user, as in the standard case. This is equivalent to the window length required for the operation.

There is a possibility that two different ports will be used for the operation, as the port nearest to the cable landing is assumed for the first part of the operation and the port nearest to the deployment location for the final part. As the installation is a single operation, with the vessel returned to the operator upon completion of the task, the discrepancy between initial and final port is not deemed to be a significant issue and will only have a minor influence on the charter time.

Once the task timescales are calculated the waiting time can be estimated. The main assumption underpinning this is that the export cable must be installed in a single operation. This is the typical approach for small to medium projects from Albatern's experience, and was corroborated from correspondence with Leaske Marine, a marine contractor who specialise in vessel charter. The waiting time is calculated for every point along the path, using the standard methodology from Section 3.7.4.4, using the metocean data at that point along with the window length. The total waiting time is then set to the maximum value that was calculated along the path. Essentially, this assumes that the metocean conditions along the whole path are equal to the most extreme conditions seen along the route. This is a somewhat pessimistic approach, as for particularly long routes the vessel would see calmer conditions at certain stages of the installation, for example when very close to shore.

With the task timescales and the waiting times, the cost for the operation can be calculated as for a standard marine operation.

3.9 Mooring System Module

The `mooring_system` module contains the classes and functions that are used to represent mooring system components and perform calculations. The UML diagram in Figure 3.16 shows the relevant classes and how they are structured. The `ItemBase` class is at the centre of the module, imported from the Base Classes module. Components inherit from this class, allowing local costs to be defined for them and cost calculations performed.

3.9.1 Theory

Because the Albatern WaveNET employs a catenary mooring system, similar to that described in [190], a simple inelastic static calculation is utilised in order to estimate catenary length, and hence cost for a given line tension. This system configuration is shown in Figure 3.17. While more complex methods exist, for example quasi-static analyses or inelastic analysis incorporating elasticity such as [191], the static method has been chosen due to its simplicity. While the aforementioned methods would give more accurate results, they would also have a computational cost that was not deemed worthwhile for such a low cost part of the overall device system (in monetary terms). Examining sensitivity of the cost or LCOE to catenary parameters would allow any discrepancy in results to be considered. It should be stated that mooring analysis is not a major focus of the tool; it assumes high level, prior knowledge of the system. More detailed analysis could be performed by the user in dedicated software like Orcaflex if mooring system design was desired.

To obtain line length, the line tension is the starting point. This quantity, specified at the fairlead, can be defined in two ways: either as the resultant tension tangent to the line, T or the horizontal tension, T_H. The relationship between these quantities is:

$$T_H = T - wh\,, \tag{3.34}$$

where h is the displacement of the fairlead from the seabed (the water depth minus the fairlead displacement from the water surface) and w is the weight per unit length in water. As the water depth gets larger, the factor wh will get larger and can exceed T, giving a negative T_H. Because of this typically T_H is considered as the line tension attribute, which avoids this issue as it means that T will be positive.

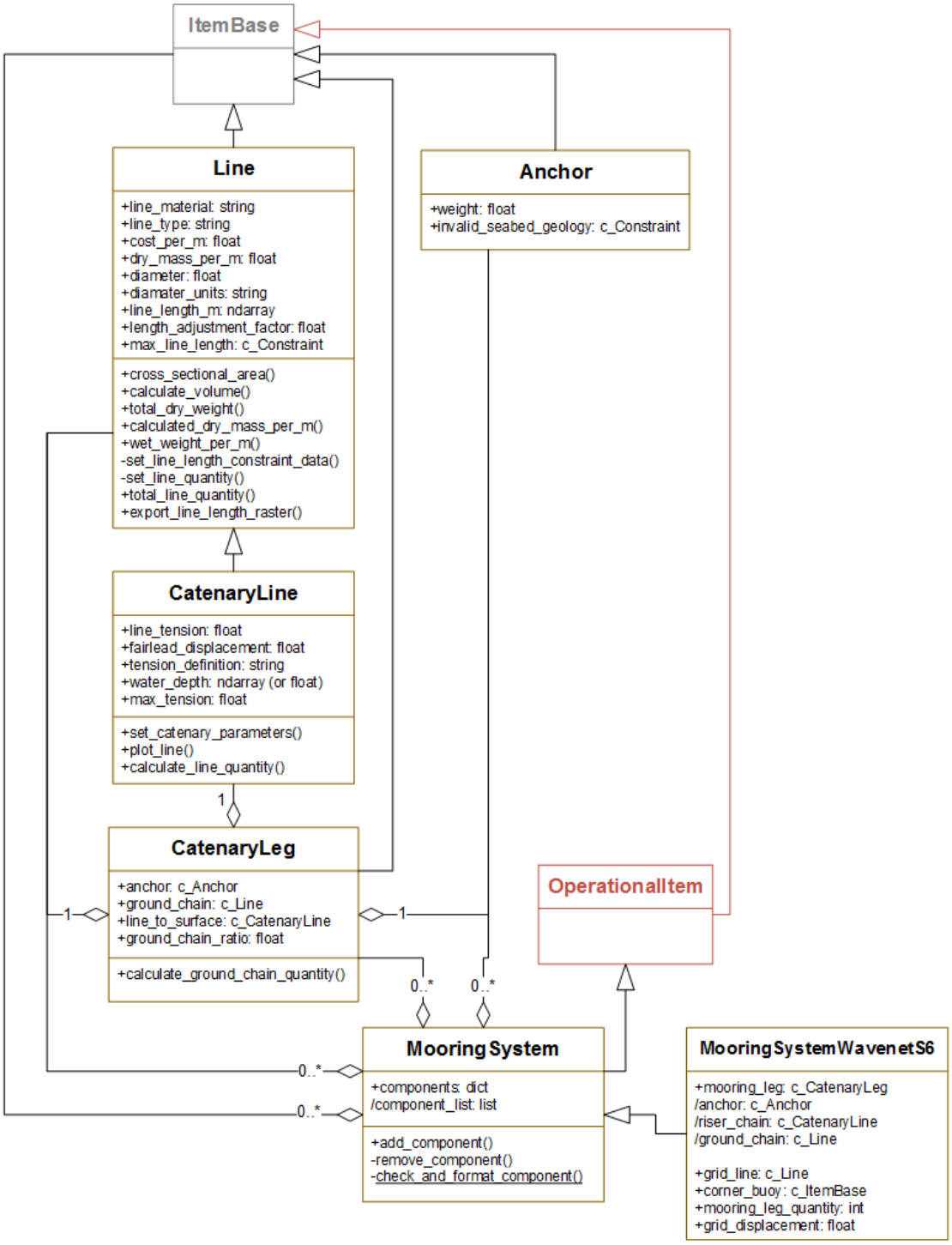

Figure 3.16: The structure of the `mooring_system`. There are only two external parent classes used: the `ItemBase` class from the `base_classes` module and the `OperationalItem` class from the `operations_and_maintenance` module. Notation is the same as used for Figure 3.4.

Given a maximum resultant tension $T_{\max}$, the line length, l_{min} can be found:

$$l_{\min} = h\left(\frac{2T_{\max}}{wh} - 1\right)^{\frac{1}{2}} . \tag{3.35}$$

This length represents the minimum potential length of the line and is what is used for the line quantity, and hence cost, calculations. In addition to l_{min} two further output quantities can be calculated: the horizontal displacement of the line, X, and the vertical fairlead force, T_z:

$$X = \frac{T_H}{w}\sinh^{-1}\left(\frac{wl_{\min}}{T_H}\right) \tag{3.36}$$

$$T_Z = wl_{\min} . \tag{3.37}$$

3.9.2 Anchors and lines

For the purposes of the model, the mooring system is considered to be made up of two main types of components: the anchor and any lines. These form the building blocks of the subsequent mooring system classes. The anchor is a simple child of `ItemBase`. It contains a weight attribute, which can help inform the user about the suitability of the installation vessels that are being considered. In the model, the only impact that the anchor type would have would be on costs, which the user has to define. For example, the anchor instance could be a drag embedment anchor or a gravity anchor; the anchor specifics are not factored into the mooring system analysis or design.

Mooring lines are instances of the `Line` class, which also inherits from `ItemBase`. The line is defined by seven main attributes:

- The line length.
- A length adjustment factor.
- The cost per metre of line.
- The line material.
- The dry mass per metre.
- The diameter of the line.
- The line type (for example studless chain, wire or rope).

The line length can be defined by the user, but is more typically calculated within the model to obtain a cost dependency based on the water depth. Total

cost of the line is calculated by multiplying the line length by the cost per metre attribute and adding any local costs. The cost per metre is a cost instance, stored within the local cost attribute. This is similar in principle to the `ExportCable` class. The final line length, used for the cost calculation, is stored within the quantity attribute of the cost instance. This is not set directly, but is the product of the line length attribute, L and the length adjustment factor f_L:

$$L_{\text{final}} = L_{\text{min}} f_L \,. \tag{3.38}$$

It is set when either the line length or line adjustment factor is varied, using a private method. The length adjustment factor is a contingency factor of sorts, arbitrarily set by the user to take account of uncertainty in the length. This could provide a mechanism for Monte-Carlo analysis, allowing different lengths to be considered without changing the underlying input data.

The line material, dry mass per metre, line diameter and line type are used to calculate the submerged weight of the line in water, required to estimate the line length for catenary lines. Including these parameters in the class could also be useful for estimating breaking loads in the line, although this is not a consideration in the current model. The line material is defined by a separate class, `Material`, denoted as an aggregation in the UML. This class is primarily defined by a density attribute that the user must specify in units of kg/m^3. A method, `seawater_density_factor`, calculates the ratio of the material density to that of seawater. This allows the submerged weight for that material to be determined. If a dry mass per metre is specified, m_{dry}, then this is used to calculate the submerged weight:

$$w = m_{\text{dry}} F \,, \tag{3.39}$$

where F is the submerged density factor:

$$F = 1 - \frac{\rho_{\text{seawater}}}{\rho_{\text{material}}} \,. \tag{3.40}$$

If the user does not specify a dry mass per metre then the class will attempt to calculate it, using an external function contained in the module (the `calculate_dry_mass_per_m` function). This provides a default value which is useful if the user is lacking specific data for the line. The formula to calculate the mass depends on the type of line, specified by the `line_type` attribute. For chains,

it is estimated using the same empirical formulae as used by OrcaFlex [192]:

$$m_{dry} = \begin{cases} 0.0199 D_{\text{ch}}^2 & \text{if line type is studless chain} \\ 0.0219 D_{\text{ch}}^2 & \text{if line type is studlink chain}\,, \end{cases} \tag{3.41}$$

where D_{ch} is the chain diameter, in metres. The output is in units of kg per metre. If the line type is not a chain then the mass is calculated using the material density, assuming a solid circular cross sectional area:

$$m_{dry} = \pi \left(\frac{D}{2}\right)^2 \rho_{\text{material}}\,. \tag{3.42}$$

This is a simplification for most wires and ropes as these are typically made up of strands of material. However, it is anticipated that the majority of users would define the line mass per metre directly, as this is commonly provided by manufacturer, which would bypass these assumptions. Other empirical relationships would be very easy to add into the model, by adding the relevant options to `calculated_dry_mass_per_m`.

A key ability of `Line` is to allow calculation of the line length, based on the water depth at the location of interest. The class contains a method to enable this calculation, `calculate_line_quantity`. As `Line` is a base class that does not require any kind of water depth dependency, the method is blank. It acts as a place holder for child classes, for example the `CatenaryLine`, to inherit and build on.

`CatenaryLine` is a class to represent a catenary line, hanging between some point in the water column and the seabed. As well as the attributes from `Line`, the class has the following attributes:

- Line tension
- Tension definition
- Fairlead displacement from the water surface.
- Catenary parameters

The line length for a given line tension is calculated using the theory introduced in Section 3.9.1.

If the user does not define a T_{max} then it is assumed to be equal to T. A main assumption in the calculation is that the design T_{H} is constant across the domain. In reality this tension will also be influenced by the water depth at the site and

the extreme conditions that are likely to be seen. It would be simple for the user to include such data; as the underlying functions utilise the NumPy package a 2-dimensional line tension would be compatible with the calculations.

Within the class, the calculation of the catenary parameters is facilitated by the `calculate_catenary_parameters` method. The parameters calculated, namely T, T_H, $l_{\min}$, X and T_Z, are stored in the `catenary_parameters` attribute. The `calculate_line_quantity` method for the catenary line class takes water depth as an input, calculating the catenary parameters using the aforementioned method and assigning the value of $l_{\min}$ to the line length attribute.

Lastly, a method has been created that allows the catenary profile to be plotted. This works by calculating the vertical positions of the catenary line for discrete x values along the horizontal scope, at a user-defined resolution:

$$z(x) = \frac{T_H}{w}\left[\cosh\left(\frac{w}{T_H}x\right) - 1\right] \quad . \tag{3.43}$$

3.9.3 Mooring systems

Mooring systems are defined by the `MooringSystem` class. This inherits from the `OperationalItem` class, allowing operational tasks to be explicitly defined for the mooring system instance. The class itself is relatively simple: containing an embedded `Site` instance, as required by `OperationalItem`, and a `components` attribute. This latter attribute is a dictionary, containing all of the anchor and line instances that make up the overall mooring system. The dictionary key is the component description by default. This decision was taken to make it easier to include duplicate components, which might have the same `_id` attribute. Components can be added or removed from the mooring system when working in the Python console using the instance methods `add_components` and `remove_component`. An alternative key to the description can be specified when adding a component. This is useful for child classes that must contain certain components, allowing consistency in the approach across different class instances.

In order to correctly extract the nested components for cost analysis, the component objects are also stored in a private attribute as a list. This is because dictionaries are not searched when extracting nested objects (see Section 3.4.3 for clarity). A `calculate_line_quantity` is used to calculate the line lengths for the various `Line` type components: by iterating through the component objects and attempting the `calculate_line_quantity` on each. Non `Line` objects will

return attribute errors, which allows them to be skipped over. Because the class contains the site as an attribute, this means that it directly contains the water depths over the range of interest. This is specified as an input when calculating the nested line lengths, as it is a required input for the catenary line class.

Using the `MooringSystem` class as a parent class, it is possible to define custom mooring systems. Requirements can be made about the components that they must contain, and they can also be designed in order to include specific calculations that might only be relevant for that system. The mandatory components are defined as distinct properties that must be defined for the object to be successfully intialised. The actual component objects are still stored in the mooring system component dictionary, the property providing a direct link to the dictionary entry for the user. Currently two such mooring systems have been designed that are, in general, more specific to the Albatern WaveNET.

The first mooring system is the `MooringLeg` class. This class must contain an anchor and a catenary line at a minimum and describes a simple catenary mooring from fairlead to anchor inclusive. An optional component can also be specified: the ground chain. This ground chain, typically heavier than the catenary chain in the real system, runs between the anchor and the catenary chain. Connectors between these components, such as shackles, are not compulsory and can be defined by the user in the usual way. The mooring leg also contains an additional attribute, the `ground_chain_ratio`. This ratio is the ratio of ground chain length to water depth and gives an approximate way of calculating the spatial quantity of ground chain. While in reality the amount of ground chain would be determined from dynamic mooring simulations, Albatern have found that, at small array sizes, a suitable footprint for the device is typically three to four times the water depth. As the aim of the `mooring_system` module is to obtain preliminary cost estimates, not rigorous design of the system, such an approach is useful to get an indication of the spatial variation in costs which also lends itself well to sensitivity and uncertainty analysis. While this class has been designed with the Albatern wave energy device in mind, it is a fairly generic catenary system that would be well suited to any floating WEC that requires one of more catenary lines.

The second custom system is the `MooringSystemWavenetS6` class. This is based on the real mooring system that is used for the Series-6 WaveNET. Figure 3.18 shows a plan view of the mooring system for a triangular shaped array. The basic mooring system is made up of the following components:

- Mooring legs, each made up of an anchor, ground chain and riser chain (the

catenary line to the surface) as previously described.

- Corner buoys, used to support the mooring grid.
- A mooring grid. This connects the array to the mooring legs and is positioned below the water surface.

Other low cost components such as shackles and intermediate grid lines can be added as additional components. The mooring grid is typically made from rope, with the length a function of the array size and shape. This should be specified by the user as an input, although could be approximated for given configurations in future work (because of the low cost nature of the component this calculation is neglected here). The properties of the mooring leg, for example the specific components and the ground chain ratio can be set within the class itself, properties providing a direct link to the embedded leg properties.

3.9.3.1 Calculation procedure

The process to calculate the spatial costs associated with a particular mooring system is as follows:

1. **Define the system**: The desired mooring system is defined in a class configuration text file. This includes specifying all of the components, which can be done either directly in the configuration file or by providing a database query or file path to the necessary class text file (see Section 3.3). The path of the site NetCDF file is also required to calculate water depth dependent costs and any operational costs that are specified.

2. **Load the system**: The configuration file is read and the class instance created.

3. **Calculate quantities (line lengths)**: The `calculate_line_quantity` method is executed for each component (any non line components are automatically skipped). If the site attribute is defined, the water depth for the analysis range (`water_depth_analysis_range`) is used to calculate spatial quantities with water depth dependence, primarily catenary lines and ground chain.

4. **Calculate costs**: Categorised costs and cash flows are calculated for the whole system, including the embedded component instances, using the embedded cost method as previously described.

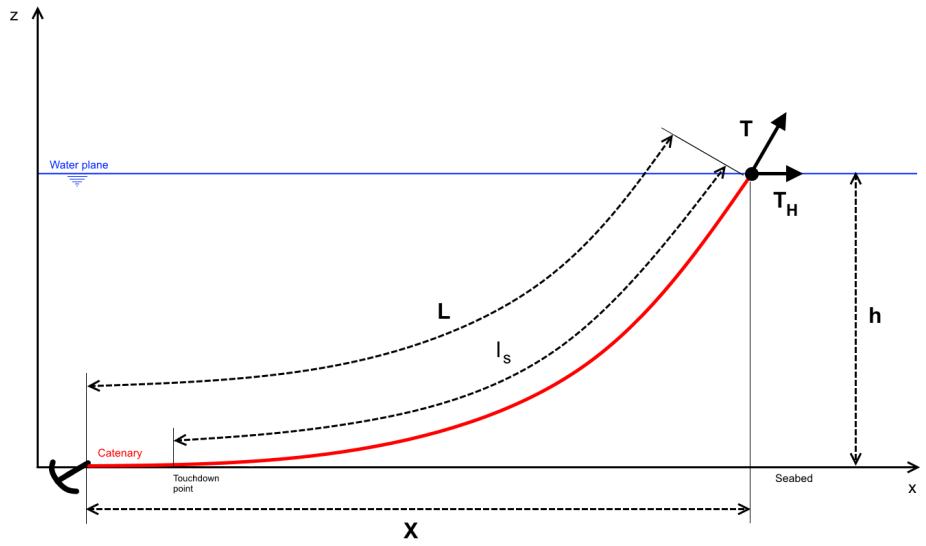

Figure 3.17: The catenary system configuration and geometry that is considered by the `CatenaryLine` class. Adapted from [190].

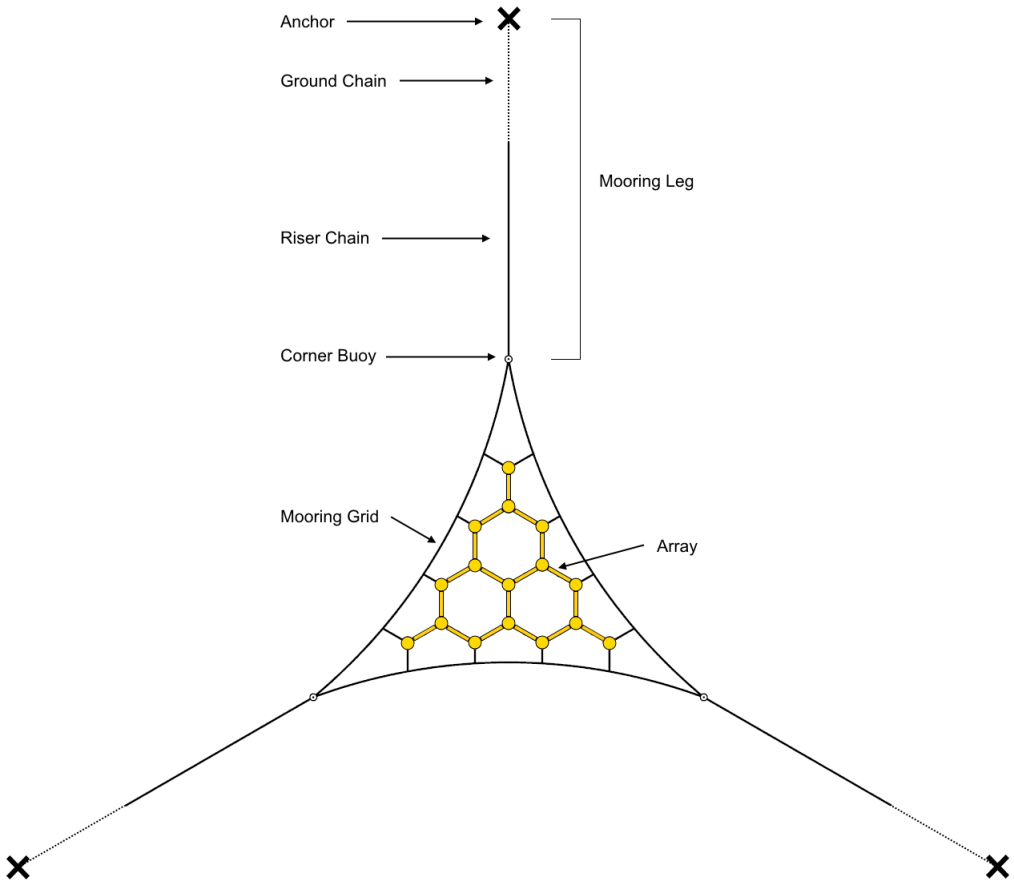

Figure 3.18: Plan view of the Albatern Series-6 WaveNET mooring system for a triangular array made up of six Squid units. Dimensions are not to scale, for illustrative purposes only.

3.10 Constraints Module

In the context of the model, constraints are defined as conditions that limit the potential deployment locations for the wave energy device. These factors are important to consider, as not including them can give unrealistic expectations of device performance and deployment capability. They help to narrow down the data domain to only suitable areas, saving time and helping the model user to build up an accurate picture of the opportunities and limitations of the device design.

To include an individual constraint in the model, two pieces of information are required:

1. The condition (typically an inequality) used to define the constraint.
2. The data that the condition is applied to.

The module defines constraints as classes, with several different options existing. These constraint classes, inheriting from a base class to provide a uniform structure, each effectively define a different conditional statement that is applied to the input data. Data values that meet the conditional can be masked, and hence excluded from the output data. The modified data can also be exported as a raster file, so the invalid data locations can be seen in the context of the data domain. Table 3.4 shows examples of some of the conditions that can be applied to arrays of data.

Class Name	Effect	Example of Usage
`ConstraintMin`	Exclude values below a specified value	Exclude shallow water depths.
`ConstraintMax`	Exclude values above a specified value	Exclude locations too far from shore.
`ConstraintLocation`	Exclude values at specific geographic locations	Exclude locations that fall within protected areas.

Table 3.4: Examples of the constraint classes, and hence conditions, that can be applied to different data arrays used by the model.

Within the model itself, the constraints are contained within attributes of the higher level objects that they are being applied to, for example the wave energy device. All of the constraint instances contain a special attribute, the `constraint_variable` attribute, which is a string. This allows the constraint instance to be linked to the data which is it applied to, by matching this string to

the description attribute of the data. All of the data arrays that are required by constraints, such as the 2D array of water depths across the domain, are stored as instances of a unique class, the `ConstraintData` class. This is a simple class, inheriting from `Base` but with an additional attribute to store the data. The purpose of this different class for the data is so that references to the instances can be easily obtained using with the `Base` instances attribute (see Section 3.4.1).

The desired outputs of the constraints analysis are individual raster layers, presenting the invalid locations calculated for each constraint, and an overall raster containing all of the constraints. These can be used as overlay layers for the output results from the model analysis, and formatted within GIS software to the wishes of the user. For the overall raster, each constraint is assigned a different pixel value which allows them all to be identified. At some locations, multiple constraints can apply. For example, a point could have a water depth of less than 30 m and also be located within the boundary of a Marine Protected Area (MPA). For such combinations of constraints, new pixel values are created and assigned.

Figure 3.19 gives an example of how the constraint layer data can be visualised in GIS, considering an area in the Inner Hebrides, to the South of the Isle of Rum. Four project constraints were specified, with the data and export cable landing location arbitrarily chosen to demonstrate the output capabilities:

- Water depth must be greater than 30 m.
- Water depth must be less than 150 m.
- Cable length must be less than 5 km.
- Locations within Special Protected Areas (SPA) are not valid for deployment.

The main map, in the top right, shows the combined constraints. The four input constraints yield five unique categories of constraint over the region when combinations of constraints are taken into account (for example, the purple area signifies locations that both lie in the SPA and where the cable is too long).

The locational data used to define a constraint are specified in a GIS file. This could be a vector file, where restricted areas are defined by polygon features, or a raster file, where restricted areas will depend on pixel values. Some constraints are instead defined by calculated quantities within the model.

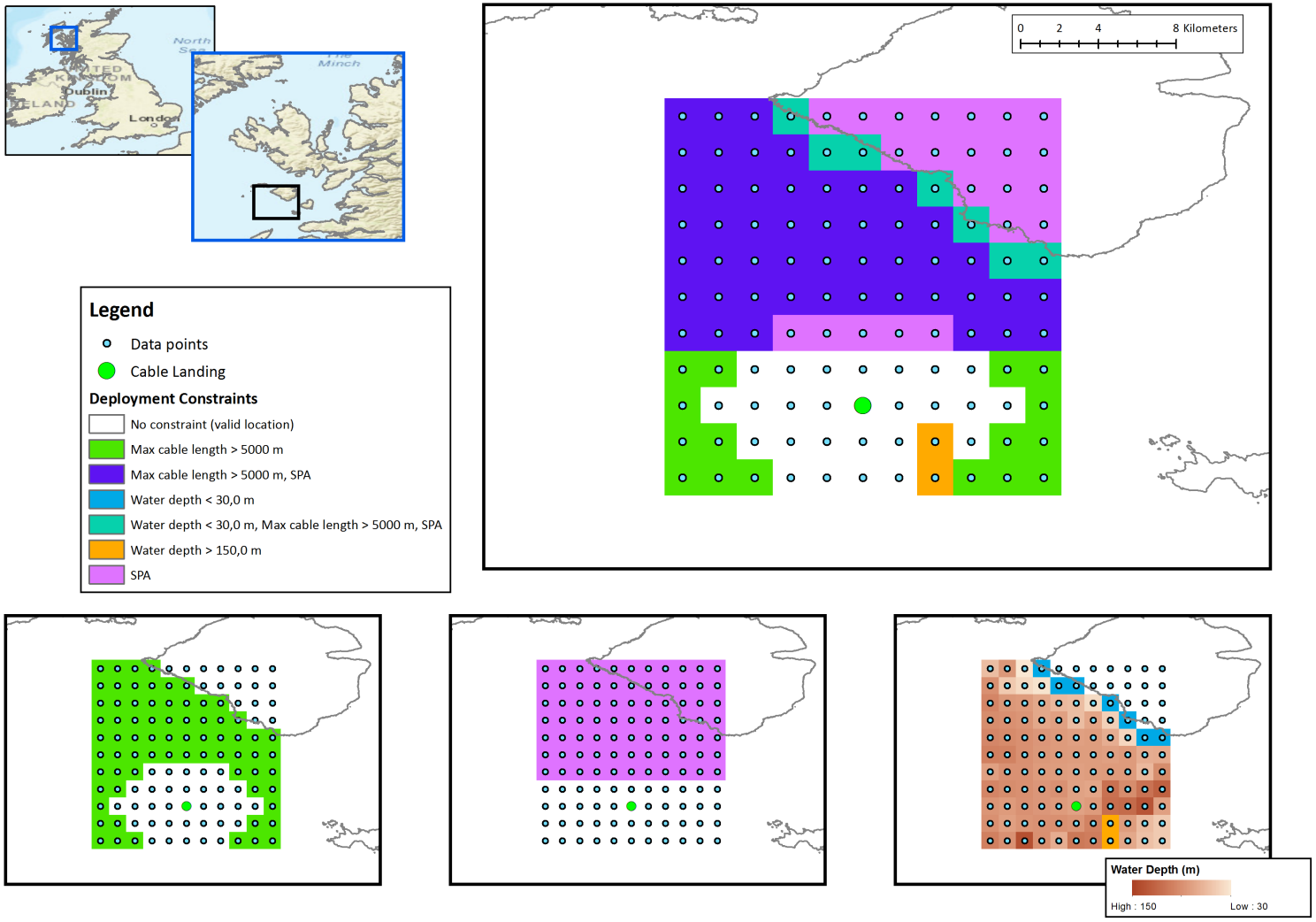

Figure 3.19: Demonstration of the data that can obtained from the model constraint analysis, considering an area in the Inner Hebrides. Four input constraints were considered, shown at the bottom (water depth constraints combined into a single map). These yield five unique types of constraint, when combinations are taken into account.

3.11 Limitations and Assumptions Summary

As has been demonstrated by the material presented so far, there are a large number of factors that influence the economic viability of a wave energy project. Due to the time constraints associated with this project it was not feasible to include every aspect in the research. The key functionality of the model was driven by the wishes of the industrial sponsor, primarily centred on the theme of spatial mapping. The future for the model, designed and created completely from scratch, is to follow an iterative process and be built upon over time. Eventually it is hoped that it can form a key part of Albatern's project scoping, development and business strategy.

The main limitations and assumptions that are present in the model are summarised in Table 3.5. These vary from missing functionality to limitations in the modelling approach. The table also provides some justification as to why the identified areas were not covered in the detail described.

Arguably the most significant omission is regarding unplanned O&M. As stated in the introduction of Section 3.7, while unplanned operations could be defined if the months that they occur in are known, the model offers no way to directly simulate these. This could be done by using Monte Carlo based analysis to simulate component failures, allowing the timing of the failures, and hence timings of operations, to be derived. Following this, the associated costs could be calculated as described within the relevant subsections of Section 3.7. The decision to leave out this cost aspect was due to the scope of this project relative to other R&D activities within the sponsoring company. As reliability was the research focus of another doctoral research engineer, the decision was made to keep the work packages distinct but keep open the possibility of a unified model for the future.

Rather than leaving out unplanned O&M it can be modelled as a proportional cost (Section 3.4.3), equal to a fixed percentage of the total CAPEX per year. While this is an inferior treatment of the cost, the method is an approach used numerous times in the literature (for example [57, 65, 99]) and is hence deemed suitable to complete the overall wave device cost picture.

A related feature missing from the model is downtime calculation for operational tasks (planned or unplanned), which will impact availability. To include this would require feeding the time series of energy production from the device directly into the cost calculation. There was not time in the project to accomplish

Limitation	Justifications	Priority
Reliability/unplanned O&M cost not directly implemented in model.	• Reliability analysis research was being undertaken by another EngD student at the sponsoring company, thus was not a priority for this project. • Unplanned O&M can be included using proportional costs (e.g. % of CAPEX), a common approach in the literature.	H
O&M downtime not spatially included.	• Lack of reliability analysis limits usefulness of downtime inclusion. • For planned O&M static availability factor deemed sufficient, as for a given location operations could be streamlined.	H
Lack of tools to easily calculate impact of learning rates on future costs.	• Costs with learning can be calculated outside the model and used for model inputs. • Learning rate analysis would not contribute to the spatial aspect of the model. • Learning rates could be applied to results.	M
Lack of tools to perform analysis of revenue aspects (e.g. NPV, IRR).	• LCOE is the most common metric and allows easy comparison with other forms of technology. • Device technology readiness level (TRL) is at a stage where revenue analysis would be largely hypothetical. • Model primarily designed for internal usage, where revenue calculation is less of a priority.	M
Lack of spatial/temporal efficiencies (e.g due to length of export cable or speed of PTO generator).	• Electrical system could be designed to the point where the efficiency variations would be low. • The export cable length constraint can be set to prevent unrealistic cable lengths (and hence efficiencies) being considered.	L
Lack of tools to perform in depth uncertainty analysis.	• Current O&M module calculation process is too slow for Monte Carlo analysis. Would need some aspects recoded. • Simpler uncertainty estimation methods judged to be sufficient, given project time constraints.	L
Multiple discount rates not supported.	• Not the typical approach for marine energy analyses as specifics of project financing are less clear	L
Defining farm locations at points when in reality they might traverse multiple points.	• As the Albatern device is very small relative to the dataset spatial resolutions that have been examined to the present date, this is not deemed a high priority issue.	L

Table 3.5: The main assumptions and limitations that exist within the core spatial model and the reasons why they were not fully addressed.

this, as it would require a restructuring of the overall spatial analysis calculation function. Availability can be incorporated into the model using the `efficiencies`

attribute of the wave device, although this applies the value over the whole spatial domain. In the absence of detailed reliability and downtime estimation this is considered a suitable approach, especially when examining more localised regions as the variation in the parameter will be reduced.

Two omitted analysis types analyses that are sometimes seen in the literature are revenue based analyses (for example NPV and IRR) and learning rate analysis to examine future LCOE potential. The latter of these can be applied manually, by selecting input data with learning cost reduction built into the values. This is demonstrated in the case study in Chapter 5. While the ability to do this within the model itself would improve usability, it was not regarded as a research priority. This was because it was not judged to fit so well into the spatial analysis theme.

The final four limitations are more minor. The first two, electrical efficiencies and uncertainty, can be partially achieved by the model and mitigated by careful selection of input data, but more sophisticated modelling approaches are desired for future work. Uncertainty analysis is less of a concern over time, as better data are collected from real projects.

Multiple discount rates, the ability to set different discount rates for different costs, would be a useful addition to the model. It would be possible by defining the discount rate as an attribute of the `ItemBase` class rather than at the `Project` level. It is not deemed a key limitation as using a single discount rate is overwhelmingly the accepted method in the marine energy context (for example [57, 92, 93, 95]).

The final point concerns data resolution. For larger devices and fine metocean data resolutions the model may not give an accurate representation of a farm: as the farm is considered at a single point. As the Albatern device is very small this is not an issue for the current model application. Even for large devices, where array footprint is comparable to the data resolution, the analysis can still give valuable information on siting at a first pass. This could be followed by lower level, bottom up modelling at more localised regions where aspects like array layout could be explicitly taken into account.

The Off-grid System Sub-Model

This chapter describes the module that is used for analysing off-grid wave energy systems. As this is a more niche wave energy application it is considered as a distinct entity, a sub-model of the core grid-connected model as described in Chapter 3.

Given an electricity demand time series (or load profile) and an arbitrary selection of energy sources, the aim of the module is to determine the useful energy input and time dependent costs. This is achieved by simulating the energy flow in the off-grid system in the time domain, using an algorithm which attempts to balance the energy production and demand. This involves calculating the energy contributions that are required to meet the demand at each time step. This allows cost contributions over the system lifetime to be determined, that can then be filtered into a wider cost analysis using the methods from Chapter 3.

4.1 Overview

Three different types of energy sources have been coded into the model: a WEC, battery bank and diesel generator, represented by Python classes. The component combinations that can be theoretically examined are listed in Table 4.1, along with justification of which have been presented in the case studies for this body of work.

Of the six system types, two are considered. Because the Albatern device considered in this thesis is so small, the systems would struggle to economically support the fish farm loads, even with storage. To put this into context: a load of

Energy sources	Considered in research?	Justification
Diesel generator only	Yes	Conventional approach
WEC, battery and diesel generator	Yes	Proposed hybrid configuration
WEC and diesel generator	No	Cannot meet load economically
WEC only	No	Cannot meet load for array size
WEC and battery	No	Cannot meet load for array size
Diesel generator and battery	No	No wave energy present

Table 4.1: The off-grid renewable energy systems that the sub-model is capable of simulating, along with the ones that have actually been simulated for this research project.

100 kW would require 67 Squid units (assuming a 20% capacity factor), the capital cost of this alone is over £5m. For comparison the CAPEX of a 160 kW diesel generator is approximately £20,000. While the generator would also require a large amount of fuel, the total cost would still be far lower than the capital cost of the WEC units (for example the total NPC for the energy system of a Norwegian diesel-only fish farm with a 20 year lifetime was estimated at £838k in [173]).

The aim of the WEC is not to supply these loads and replace the diesel generator completely, but to ease the burden on the generator at lower loads. The battery/diesel system, while interesting, is not considered because it is outside the wave energy research focus. The WEC and diesel system is not considered as it was found to be uneconomic from unpublished work conducted in-house for Albatern [193].

The high level configuration of the typical WEC/battery/diesel generator is shown in Figure 4.1. On the AC side it consists of an electrical load, a wave energy device and a diesel generator which is required as backup and to support times of peak demand. The load is depicted by a fish farm, the wave energy application examined in this research. These components are supported by a battery bank on the DC side, which is used to store excess wave energy and provide energy to reduce the diesel consumption at lower loads. Facilitating the transfer of energy between the AC and DC bus is a converter. For sophisticated hybrid systems a controller will be integrated into it, to regulate the power flow between the different system components and monitor the voltage levels to make sure that the correct amount of power is routed to the load. These can take advantage of complex algorithms to optimise the performance of system, in this example to minimise diesel consumption and hence reduce cost and environmental impact.

Such an energy balancing algorithm is the heart of this module. The aspects of the module are designed to represent the real physical system, integrating with the previously described modules to allow the LCOE for the overall system to be calculated. Keeping compatibility with the spatial elements of the grid-connected model means that the most promising locations around the energy consumer to deploy a wave energy device can be obtained.

The module UML diagram is shown in Figures 4.2 and 4.3; the first of these shows the characteristics of the main energy system classes while the second shows the make up of the final `OffGridProject` class, used to define the overall system. As can be seen, the majority of this module is self contained, with low dependency on other modules, although the `ItemBase` class is required for hybrid components that have associated costs. It can also be seen that it is arguably the most complex module. While the physical wave energy system is split between four modules (wave device, export cable, mooring system and O&M), all of the hybrid components are contained in the one class. While the functionality could have been split in a similar way, for example a "diesel generator" module or a "battery" module, in the wave energy context the constituent parts have little applicability outside of the hybrid system scope. As they are designed to function as a unit rather than as individual elements, an optional addition to the wave energy device, the decision was made to package them together.

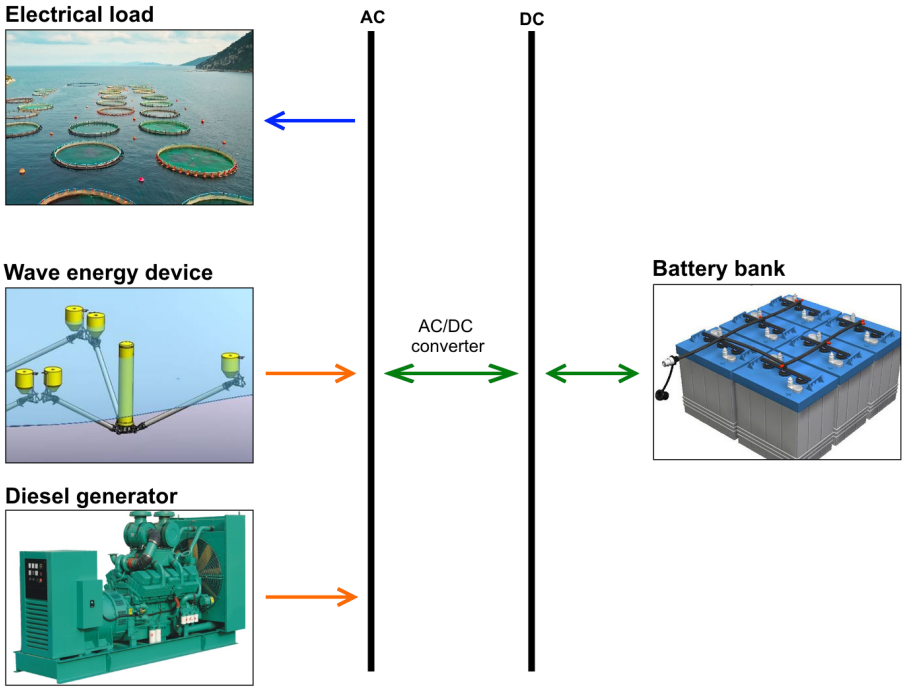

Figure 4.1: Typical configuration of a small scale renewable energy hybrid system, in this case consisting of a wave energy device, battery bank and diesel generator. These supply an AC load (depicted as a fish farm).

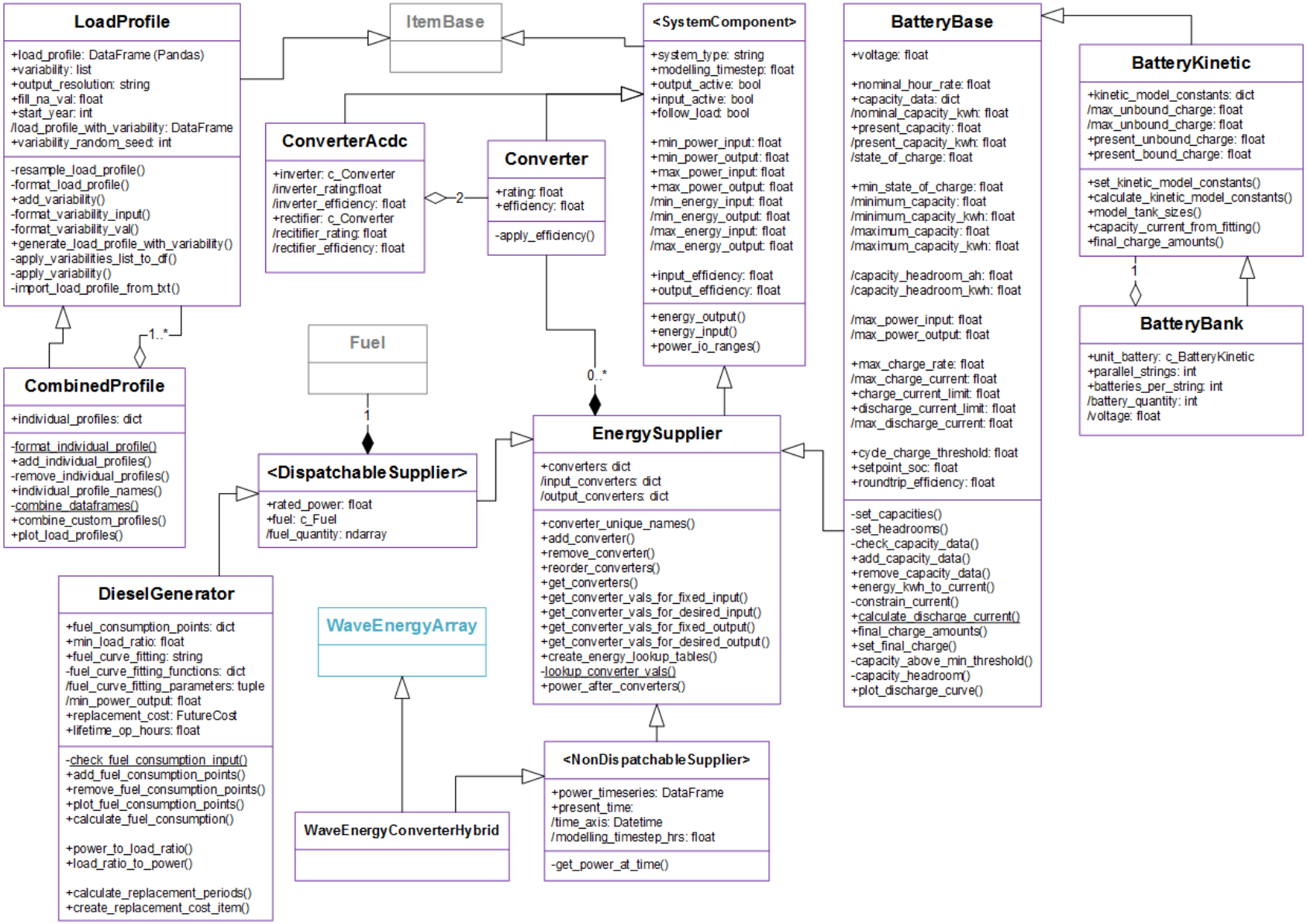

Figure 4.2: The energy system classes that make up the hybrid energy module. They include both real energy components (diesel generator, batteries and wave device) and classes to define load profiles of energy usage. Notation is the same as used for Figure 3.4.

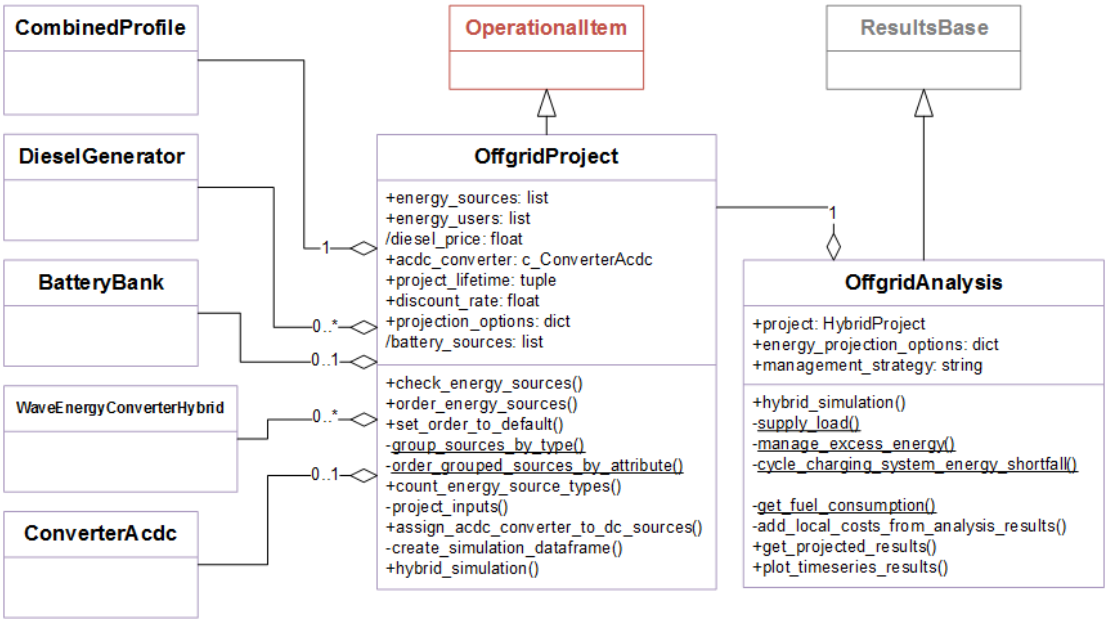

Figure 4.3: The class defining the off-grid project as a whole. The aggregated off-grid module classes making it up are presented in the previous figure. Notation is the same as used for Figure 3.4.

4.2 Off-grid System Analysis

4.2.1 The off-grid project class

This class is analogous to the `Project` class that was used to define the grid-connected analysis (Section 3.6.3), providing a way to define the different elements of the project in a single object. Some of the attributes are seen again in this new context, for instance the `discount_rate`, `project_lifetime` and `projection_option` which behave in the same way.

The constituent load profiles and hybrid components are stored within the `energy_users` and `energy_sources` attributes respectively. The embedded energy sources are stored as a list. The `check_energy_sources` method is applied when adding energy sources, to check that they are children of the `EnergySupplier` type. This is required as this class, introduced in Section 4.4, contains the supporting energy calculation methods. The order of this list is important as it is the order in which the sources will supply power to the load. A typical wave system will have the wave device activated first, followed by a battery bank and then the diesel generator. This default ordering is embedded into the model and can be set using the `set_order_to_default`, improving the usability of the class. A further function, `order_energy_sources` allows the order of the energy sources to be changed manually. They can be automatically sorted by

class type and/or size, this latter ability useful when considering multiple objects of the same type. For example two generators could be put into the system: a smaller one and a larger one, the larger one only used if the smaller one fails to meet the necessary demand.

The `diesel_price` attribute gives a way of setting the fuel price for all of the embedded diesel generators at the same time, by iterating through the energy sources list. This is useful as it prevents the user from having to set this parameter for multiple objects, which could lead to errors. The `acdc_converter` is required to link any DC components to the load and components on the AC side.

4.2.2 Algorithm overview

Once the project is fully defined a hybrid system simulation can be executed. This is carried out by using another class: `OffGridAnalysis`. The class itself is similar in application to those previously described (Sections 3.4.5 and 3.6.4) and serves as a convenient structure to group the various algorithm sub functions together. While not directly spatial in nature, it also inherits from `GisResults` (described in Section 3.4.4) which forces consistency in the output data that are generated.

The overarching methodology employed is a hybrid energy balancing algorithm, similar in principle to those found in the literature and commercial software (the main example being HOMER [156]). The requirements are an input load profile, defined over a number of discrete time steps, and a selection of energy sources; both of these are embedded within the off-grid project. Essentially the algorithm loops through the load, at each time step seeing if each energy source in turn can supply the full load. If it cannot then the responsibility falls to the next energy source in line to make up the shortfall. Costs can be deduced from the results, the primary one being the fuel cost consumed by any diesel generators.

An example of the flow of logic for the algorithm that has been created is shown in Figure 4.4. This is for a wave/battery/diesel generator system, the same as depicted in Figure 4.1.

The first phase of operation is to attempt to supply the load with the energy from the wave energy device. If this is possible then any excess energy is routed to the battery bank and the simulation continues to the next time step. Conversely, if there is energy required after the WEC input then the battery bank attempts to supply the remaining load. In this example the energy that can be supplied by the battery bank is constrained by two conditions. First the capacity must not

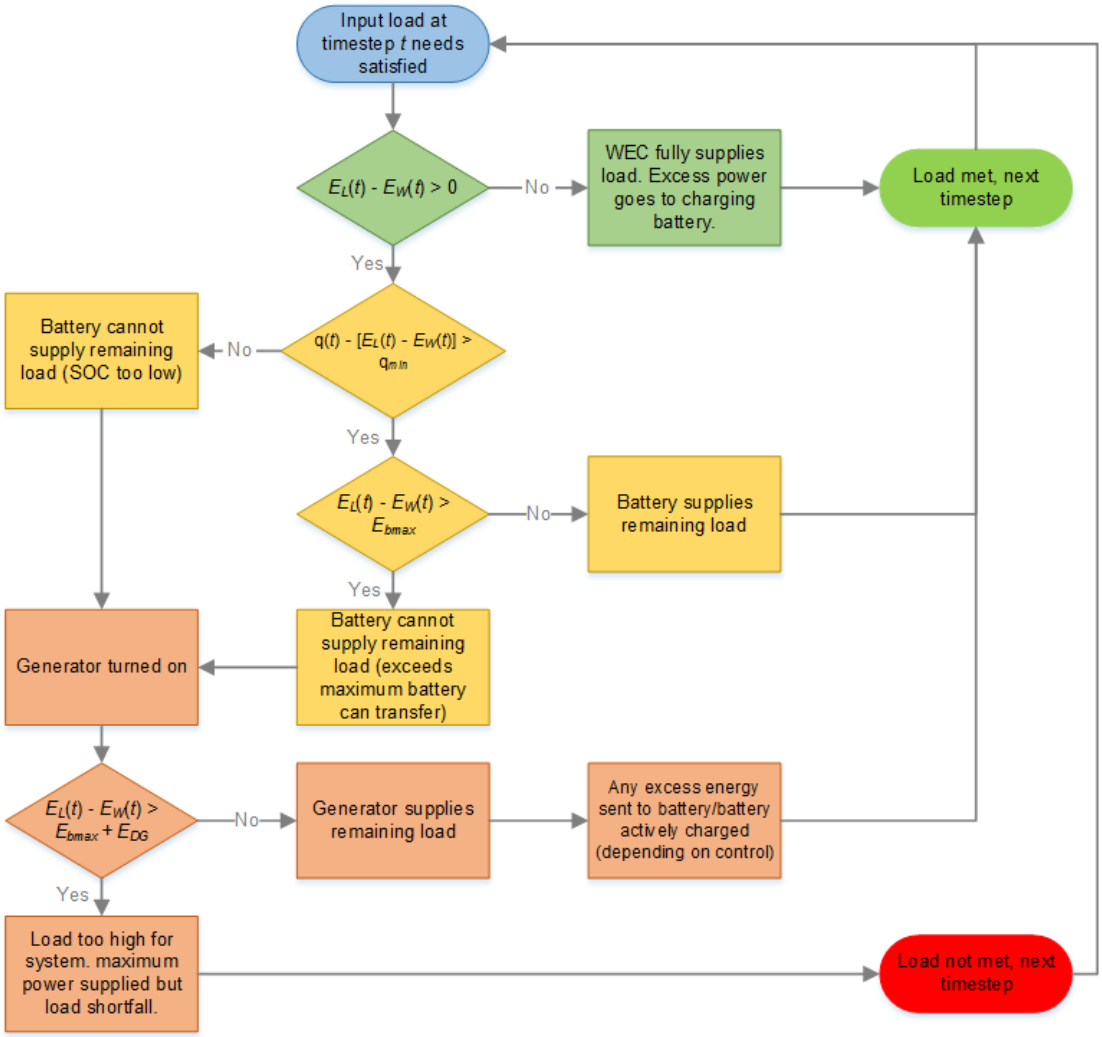

Symbol	Definition
$E_L(t)$	Energy load required at time t.
$E_W(t)$	Energy supplied by the wave energy device at time t.
$q(t)$	Battery bank capacity at time t.
$q_{\min}$	Minimum capacity of the battery bank which is allowed.
E_{bmax}	Maximum output of the battery bank.
E_{DG}	Maximum energy supplied by the diesel generator.

Figure 4.4: The high level processes that are carried out for each time step of the hybrid algorithm for a wave/battery/diesel system (as seen in Figure 4.1). Using three energy sources leads to three defined phases of operation: these are coloured in green, yellow and orange respectively. The variables are defined in the supporting table, with all units in kWh.

drop below a threshold state of charge, arbitrarily defined by the user. Second, the energy is limited by the absolute capacity and, for the kinetic battery model, the charging history of the battery. These aspects are discussed in more detail in Section 4.4.3, where the battery classes are described. If the battery bank cannot supply the load then it falls to the diesel generator. If the generator is properly sized for the application, with rated power exceeding the peak demand, then the load will always be met. Depending on the battery bank state of charge and the input parameters for the simulation, the generator may be operated at a higher load than necessary to recharge the battery. Once the algorithm has worked through all of the time steps then the simulation is completed. For each energy component the input and output power values at each time are obtained. These can then be summed for each month to get seasonal trends and can subsequently be projected forward in time using the same methods as previously described in Section 3.6.4.

It should be noted that Figure 4.4 describes the algorithm for just one potential configuration. Different systems can be examined by varying the types and order of the energy sources and by specifying different inputs to guide the overall process.

4.2.3 The off-grid analysis class

Together `OffGridProject` and the hybrid algorithm work to define the hybrid system and run the simulation. In a similar way to the conventional `EnergyAnalysis` (Section 3.6.4) the hybrid project is directly embedded within the analysis so that all of the objects needed for the simulation can be easily accessed. While the hybrid analysis can be thought of as a type of energy analysis the classes are not linked to each other, for example through inheritance. This decision was taken for two reasons: first to reduce the dependencies between the modules and allow the off-grid module to function in a standalone way, and second because the hybrid algorithm is applied in a non-spatial way. The algorithm uses single time series, the application to spatial modelling achieved using a higher level function. This is described in Section 4.2.6.

As well as the project, the only other inputs defined directly at the class level are the projection options, as in `EnergyAnalysis`, and a new parameter: `management_strategy`. Directly following the logic used in HOMER commercial software [156], two different control strategies have been implemented: load following and cycle charging. The difference between these concerns the diesel generator behaviour. In the load following case it will only supply the load required and will

not produce any excess energy to recharge any battery bank present; the battery bank is only charged by the wave energy device. In the cycle charging case, when the battery state of charge falls below a certain level the generator will operate at a level exceeding the peak load and charge the battery.

4.2.4 Energy balancing algorithm implementation

The method `hybrid_simulation` executes the hybrid simulation. Programatically this is made up of the following stages:

1. Copies are made of the energy sources, to prevent any time dependent parameters from being overwritten. This is particularly important when applying the algorithm spatially to ensure that the same initial conditions are used each time (the spatial process is described in more detail in Section 4.2.6).

2. The initial capacities of any battery banks are set. The capacity depends on the number of batteries in the bank and the discharge current profile of the battery (discussed further in Section 4.4.3).

3. The output data structure is created, using the `create_simulation_dataframe` private method within the project. This is a Pandas DataFrame, with each column representing a time dependent property of the simulation. The columns that are created for each system component are summarised in Table 4.2. The unique `_id` attribute of the component is assigned to the column names, so that the object can be linked to the output data after the simulation has completed.

4. The analysis load profile is obtained: this is the load profile as defined by the user but modified to include any time based variability factors (see Section 4.3).

5. The algorithm then begins to iterate through the time steps using a *for loop*:

   (a) The duration of the current time step is calculated by finding the time difference with the next time step.

   (b) The `supply_load` private method in the `OffGridAnalysis` class is called, to determine which energy sources are required to meet the load.

   This method iterates through the energy sources in order, until a solution is obtained. For each it calculates the energy which could be

supplied to the load, taking account of the length of time, any constraints on power output and power reduction due to any converters between the energy source and the load. After each stage the reduced load is calculated. Once the load is fully satisfied this part of the simulation is complete.

If any battery banks have supplied load then their capacities are recalculated. If the SOC is below the cycle charging threshold (arbitrarily defined for the battery, see Section 4.4.3) then the battery bank is "turned off", flagging up to the simulation that the system must create more excess power on the next simulation run.

(c) The `manage_excess_energy` function then routes any excess energy to the battery banks. For a WEC, this is simply that left over from supplying the load (assuming that the WEC is first in the list of energy sources).

For the diesel generator, excess energy can only be created for the `cycle_charging` strategy. In this case, the maximum amount of energy that can be put into the battery bank in the present time step is back calculated within the battery bank class. The diesel generator will then attempt to supply this. If the resulting bank capacity exceeds a setpoint state of charge, again an arbitrary attribute of the battery, then the battery will be "turned on" again and can supply energy to the system as before. If not, the battery remains in an off state and the excess energy requirement is carried over to the next time step.

(d) At the end of the time step all of the results are saved into the respective columns of the preallocated results DataFrame.

6. Once all of the time steps are complete the simulation is finished. For any diesel generators the fuel consumption is calculated by using the output energy profile and input parameters defined within the class. New columns in the DataFrame are created to store these data.

7. Finally the output results are projected over the specified `project_lifetime` defined within the `OffGridProject` instance, as previously described. The resulting data are then restructured into a dictionary and saved within the `OffGridAnalysis` instance.

Component	Time series data columns
Load	Required load (*required*); energy sent to load (*input*); unmet load (*unmet*), excess energy dumped (*dump*)
WEC	Output energy (*output*); excess energy created (*excess*)
Battery	Input energy (*input*); output energy (*output*); capacity (*capacity*); state of charge (*soc*)
Diesel generator	Output energy (*output*); excess energy created (*excess*); fuel consumed (*fuel_ quantity*)
Converter	Incident energy into converter (*input*); energy out of converter (*output*)

Table 4.2: The time series data that are incorporated into the simulation and extracted for the different system components. The names in brackets are shortened column names as used in the simulation.

4.2.5 Calculating LCOE

From the monthly results the system LCOE is calculated. For the energy part of the equation it is the useful energy that goes into the system that is used, i.e. the input column of the load profile in the *DataFrame* $E_{\mathrm{OG,m}}$. The useful energy is discounted and summed over the months of the project, i.e.:

$$E_{\mathrm{OG}} = \sum_{m=1}^{n} D(m) E_{\mathrm{OG,m}}(m)\,. \tag{4.1}$$

This is similar to the discounted energy in the conventional case, as was introduced in Equation 2.1 from Section 2.3.1.

The system cash flows are categorised and calculated using a `CostAnalysis` object, as previously described in Section 3.4.5. This is possible because all of the hybrid components inherit from `ItemBase`. As for some of the `ItemBase` child classes described in the preceding sections, some extra calculation steps are required in addition to the parent class `ItemBase`. This is because there are some time dependent costs, for example the fuel consumption, which depend on the output from the hybrid simulation. These costs can be calculated after the hybrid simulation has finished using the `calculate_item_cost_results` function. The details of these costs can be found in the respective energy sources sub sections within Section 4.4. The `set_item_cost_results` function performs the time dependent calculations and reassigns the results back into the `local_costs` attribute of the respective embedded objects (as the time dependent cost outputs are instances of `FutureCost`). This means that cost categories and quantities are

properly filtered down to the costs from the parent objects.

4.2.6 Extension to spatial modelling

As previously explained, the hybrid algorithm is only performed for a single input time series. Extending the analyses over multiple points is achieved within the overall `spatial_analyses` module that was introduced in Section 3.1. The analysis is carried out using a dedicated function, `spatial_hybrid_simulation`. All that this requires is an instance of `OffGridAnalysis`, as this contains all of the necessary spatial data within the embedded wave energy device instance. The spatial functionality that is being provided stems from this object, namely the three-dimensional metocean data. As the load, battery bank and diesel generator do not depend on this resource, the spatial modelling only applies to systems that contain a WEC.

Algorithm 4.3 describes the main calculation steps for the spatial algorithm. First the hybrid analysis object is copied so that the original object is kept unmodified. From the `site` attribute the metocean data are extracted, as seen previously within the `EnergyAnalysis` class. Then the function iterates through the energy sources, creating a power time series for each instance of `WaveDevice` using the class methods described in Section 3.6.4. The data are stored in a dictionary, linking the `_id` of the object to the three-dimensional Pandas data structure. This part of the algorithm is coded in a fairly generic way, so that it could be applied to other time dependent energy classes in the future (as long as they contain a `get_power_time_series` function. Also any energy lookup tables are created within the energy sources; these speed up the algorithm when chains of converts are specified for individual sources (described further in Section 4.4).

Once the initial data are set up, the spatial *for loop* is executed. Looping through each latitude and longitude, the power time series data are extracted for each time dependent energy source in the dictionary and stored within the object. A temporary copy of the hybrid analysis is made and the hybrid simulation is run, as described in Section 4.2.4. The projected results are stored in the result dictionary, each key representing the latitude/longitude dimension indices. Once all of the points have been analysed, each result can be restructured into a NumPy array into the position defined by these keys. This fairly standard process is represented by the `combine_results` function within Algorithm 4.3, not explicitly included to make the algorithm easier to follow.

The time dependent cost results are dealt with in a similar way. At

each loop the costs are set within the relevant class instance using the `set_cost_results_to_items`. The amended cost items are then stored within a separate dictionary, again keeping the link to the spatial indices with the dictionary key. These are then formed into three-dimensional `FutureCost` items which are stored within the source object's `local_costs` attribute. As above, the full details of this are not displayed in Algorithm 4.3. Using the cost class allows the values to be picked up by the cash flow algorithm within `ItemBase` as described in Section 3.4.3. As before the cost analysis can be achieved using the dedicated `CostAnalysis` class, using the off-grid project as the input object, and from this the LCOE determined.

4.3 Load Profile

A new component required for the hybrid analysis is a load profile. While the conventional analysis assumes that all energy is exported into the grid, to be dealt with by the network operator, the hybrid system has a specific, time step by time step local energy demand. It is the overall system objective to meet this demand, by balancing the different energy sources available at that time. The `LoadProfile` class allows the energy demand to be defined at every time step.

The actual load profile time series is represented by a Pandas DataFrame embedded within the `load_profile` attribute. The DataFrame class is used as it contains in-built methods for advanced indexing, grouping and resampling of data. The load profile time series data are typically stored in text files and loaded into the model, using the `import_load_profile_from_txt` attribute. Text files were chosen as the default because they are easy to work with, match the data type used previously at the sponsoring company and match the load profile data type used by HOMER, allowing data to be reused and analysis methods compared. The files are arranged into two columns: the first containing the time dimension and the second the accompanying power requirements.

Within the class, random variability can also be added to load profiles. This allows natural, systematic variations in the data to be applied and the uncertainty associated with the load profile to be incorporated into the analysis, opening up the potential for Monte Carlo analysis or similar. Multiple variabilities can be defined and are stored as a list within the `variability` attribute. Each individual variability is defined as a tuple within the list: containing the time base over which unique random values are applied (e.g. hourly, three-hourly, daily) and the variability proportion. The value is chosen so that the load values in each time

Purpose: To perform the hybrid analysis spatially.
Required: A `HybridAnalysis` instance with a WEC defined within the embedded `OffGridProject`.
Returns: A modified `HybridAnalysis` instance with spatial energy flow metrics and costs defined within it.

```
def spatial_hybrid_simulation(hybrid_analysis_obj):

hybrid_project = hybrid_analysis_obj.project
site = hybrid_project.site
wave_data = site.get_wave_data()

source_power_time series = {}
for index, source in enumerate(hybrid_project.energy_sources):
    # Create any lookup tables, for chains of converters.
    source.create_energy_lookup_tables()
    # Get power time series for WEC.
    try:
        power_time_series = source.get_power_time series(**wave_data)
        source_power_time_series[index] = power_time series
    except AttributeError:
        # Will be skipped if not a DispatchableSupplier type.
        pass
# Get all combinbations of coordinates.
lon_range = site.lon_analysis_range
lat_range = site.lat_analysis_range
all_coords = [(lt, ln) for lt in lat_range for ln in lon_range]

point_results = {}
# Iterate through each point in turn.
for lat, lon in zip(lon_range, lat_range):
    analysis_copy = copy.deepcopy(hybrid_analysis_object)
    # Assign power time series to energy sources.
    for index, power_ts in source_power_time_series.iteritems():
        hybrid_project.energy_sources[index].power_time series =
            power_ts.loc[:, lat, lon]
    # Run simulation.
    analysis_copy.hybrid_simulation()
    point_results_out[(lat, lon)] = analysis_copy.results
    # Set simulation dependent costs (e.g. fuel cost).
    hybrid_project.set_cost_results_to_items()
# Convert results to array, using the indices.
results_out_3d = combine_results(point_results)

analysis_out = HybridAnalysis(results=results_out_3d,
    project=hybrid_project, lat_range=lat_range, lon_range=lon_range)

return analysis_out
```

Algorithm 4.3: Perform spatial hybrid energy analysis.

group are modified by plus or minus the load value. For example, for a load value of 10 and variability of 0.2 the modified load value will be between 10 ± 2.

The `variability_random_seed` attribute allows the seed to be chosen for generating the random numbers, so different scenarios can be run for the same random variabilities. The actual output load profile from the class is the derived attribute `load_profile_with_variability`. This applies the method `generate_load_profile_with_variability` to the input load profile. The two private methods below this in the hybrid UML (Figure 4.2) are just used to apply the variabilities. The final load profile with variability attribute can then be propagated into any subsequent hybrid system simulations. If the `output_resolution` is specified then the output load profile will be resampled to a new time base. This step is carried on in a straightforward manner, using the inbuilt `resample` method of Pandas.

The second load profile based class, `CombinedProfile`, contains multiple `LoadProfile` instances and provides a way to combine then into a single profile. This is useful for situations where the overall energy demand can be clearly compartmentalised into distinct, independent components. For a fish farm energy system, two examples might be the feed system (active during the morning and early afternoon) and underwater lighting (which might be active 24 hours per day during winter months).

In a similar way to `WaveDevice` and `WaveArray` from Section 3.6.2, the load profile classes are linked by a composite relationship: as a combined load profile can also be thought of as a load profile in its own right. To generate the combined load profile the class resamples all of the constituent load profiles, with any variabilities applied, to the same time base, defined by the inherited `output_resolution` attribute. As a child of `LoadProfile`, variabilities can also be defined at the combined profile level. These are then applied, the output load profile consistent in type to that generated by the parent class.

4.4 Energy Sources and Converters

All of the system components that define the hybrid system and are used directly in the algorithm inherit from a common class: `SystemComponent`. This includes diesel generators, batteries and the wave energy converter. While the nature of the energy provided by these objects differs, the parent class contains attributes and methods that are applicable to all of them, and provides the nec-

essary blueprint for creating components compatible with the hybrid algorithm.

For a given system component, four generic attributes dictate the upper and lower limits of power transfer, in units of kW:

- The maximum power that can be output (`max_power_output`).
- The minimum power that must be output (`min_power_output`).
- The maximum power that can be input (`max_power_input`).
- The minimum power that must be input (`min_power_input`).

The convention is for output to be positive and input negative. In some cases the values are constants, indirectly set by the user (for example the maximum power output of the diesel generator is set equal to its rated power). For other classes, the values will vary in time and will essentially be reassigned for each time step of the simulation; includes the battery where the energy output depends on the battery capacity at that time step. The `input_active` and `output_active` attributes allow the component to be turned on and off within the simulation. This is primarily used for the battery class to allow it to build up charge over multiple simulation time steps without being expected to supply load. This functionality could be extended to other components, to allow them to be forced on or off at specific periods in time, however this is not a fundamental feature and so is considered as future work.

The `modelling_time step` attribute is the length of the algorithm time step in hours. It is set within the hybrid simulation, and allows the extents of energy output and input to be determined through multiplication with the above attributes. For example, the maximum energy output that is possible, $E_{\text{max, out}}$, is given by:

$$E_{\text{max, out}} = P_{\text{max, out}} \times \Delta t \times \eta_o \,, \tag{4.2}$$

where $P_{\text{max, out}}$ is the maximum power output attribute, Δt the `modelling_time_step` attribute and η_o is the `output_efficiency` attribute. The `energy_output` and `energy_input` methods calculate the actual energy values that can be obtained, given the values that are desired. They are calculated by limiting the energy to the energy ranges:

$$E_{\text{out}}(t) = \begin{cases} E_{\text{min, in}}, & \text{if } E_d < E_{\text{min, in}} \\ E_d(t), & \text{if } E_{\text{min, in}} \leq E_{\text{d}} \leq E_{\text{max, out}} \\ E_{\text{max, out}}, & \text{if } E_d > E_{\text{max, out}} \,, \end{cases} \tag{4.3}$$

where E_d is the energy that is desired from the energy supplier by the load. Similar equations are specified for energy input considering the power input limits; this includes an `input_efficiency` attribute. Both this and the output efficiency are considered to be inherent properties of the physical component, although might not be relevant for all child classes. The energy output and input functions are used at each time step of the hybrid algorithm, to see how a given system component interacts with the energy flow.

As for the efficiency attributes, the decision was taken to have both energy input and output contained within the same object, even when input is not relevant (for example, in the case of the diesel generator). This ensures that all of the objects look identical to the energy balancing algorithm previously introduced. While there are a small number of potential components that can be considered, enforcing this typing and coding the objects in this generic fashion means that additional energy sources, for example wind turbines or solar PV, could be easily introduced in the future.

The `EnergySupplier` class represents objects that produce power and can supply energy to reduce the load requirements. The main distinction between this class and its parent is the introduction of the `converters` attribute. This is added to account for any physical electrical power converters that are required to obtain the necessary energy form. Examples could include transformers, rectifiers and inverters. By essentially considering the converter and energy source as one system, while not a true representation of the physical system, means that the impact on the final energy due to losses in the converter are straightforward to apply internally.

Individual converters are defined by the `Converter` class. This adds the `rating` attribute to the `SystemComponent` parent, which acts as an upper limit to power output. The `efficiency` attribute is directly linked to the `output_efficiency` attribute inherited from the parent class. The class also contains a modified `energy_output` method. This allows two potential variations of energy output to be obtained: the output for a desired output value (post efficiency) and the output where the output value is fixed (pre efficiency). For example, considering a 20 kW converter with efficiency of 90%, the output power could be defined in the following ways:

- 15 kW is *desired* from the converter. The maximum power output is 18 kW (20×0.9) so $E_{\text{out}} = 15$ kW.
- A *fixed* power of 15 kW is send to the converter from a component further

up the chain. The input power cannot be modified, and so the output power is $E_{\text{out}} = 15 \times 0.9 = 13.5$ kW.

The approach chosen depends on the level of control that the system has on the power flow. For example, wave energy converter output is non-dispatchable and so a converter for this system would use a fixed approach. Conversely, the hybrid system can provide feedback into a diesel generator so has control over the generator power to obtain a certain amount of energy. Here a converter's energy output would use the desired method, to back-calculate the generator power.

Within the `EnergySupplier` class, multiple converters can be chained and stored within the `converters` attribute as entries in an ordered dictionary type. The dictionary key is set to the converter's `_id`. As well as the converter the direction of the converter must be specified, i.e. whether it applies to output power, input power or both directions. For multiple converters, due to the rating parameter the order of the converters in the system is important. For example a low rating converter at the beginning of the chain would limit the power flowing into subsequent converters, acting as a power bottleneck. The converters can hence be reordered, using `reorder_converters` which creates a new ordered dictionary based on the key order specified.

The modified energy values due to the converters can be obtained using four methods:

- `get_converter_vals_for_fixed_input`
- `get_converter_vals_for_fixed_output`
- `get_converter_vals_for_desired_input`
- `get_converter_vals_for_desired_input`

These methods essentially supersede the `energy_output` and `energy_input` functions, giving breakdowns of the energy flow across the converter components.

For each function, an algorithm cycles through each converter in the chain of converters in turn. It calculates the resolved power, constraining by rating and multiplying by efficiency as described above, and sends this though to the next converter. Each function outputs the input and output power for every converter in the chain for the initial power value specified. The fixed functions start at the beginning of the converter chain, whereas the desired functions perform a similar calculation but considering a reversed chain which starts at the desired value. For longer chains of converters this process can increase the hybrid algorithm calculation time if it needs to be done at every time step. The solution for this

is the `create_energy_lookup_tables` function. This calculates the energy input and output at discrete energy values, storing the resulting functions within the object so that the energy can be looked up rather than needing to be calculated.

While all of the child energy sources inherit from `EnergySupplier`, the main distinction between them is how they define and calculate their power limits. The next sections describe the components and the properties that they have which facilitate these considerations.

4.4.1 Diesel generator

For the majority of hybrid energy applications a conventional energy source will be required in some form to ensure that energy can be supplied at crucial times. For smaller hybrid systems, like the fish farms that are the subject of this research, a diesel generator is the primary source of energy. The main output of the diesel generator class in the model context is the fuel quantity that must be consumed by the generator to supply the necessary energy to the required load. This allows fuel cost to be calculated. As fuel cost is one of the biggest components of a conventional off-grid energy system, it is vital to quantify this number and see how the introduction of renewable energy can reduce it.

The diesel generator functionality has been split up into two classes: `DispatchableSupplier` and `DieselGenerator`. The `DispatchableSupplier` class is to represent energy sources which run off a fuel source, and hence can be turned on and off at will when the energy user desires. The base `Fuel` class is reused for the fuel in this context, as described in Section 3.4.7 and previously used for the vessel fuel in Section 3.7.1. This is to provide a uniform framework for fuel cost definition and calculation. The fuel quantity is denoted as a derived attribute in the hybrid system UML as it can be set at the dispatchable supplier level using a dedicated method.

The `DieselGenerator` class inherits from `DispatchableSupplier`. It is the sole child; the classes were separated to allow dispatchable sources to be easily added to the model in the future if desired. As well as costs and rated power (inherited from the parent classes) the class is also defined by its fuel consumption properties. On diesel generator data sheets, it is common for the manufacturer to quote the amount of fuel that is consumed when the generator is providing different levels of power, typically in units of litres or gallons per hour of operation. An example of these data is shown in Figure 4.5.

The `DieselGenerator` class stores these data as a dictionary within the

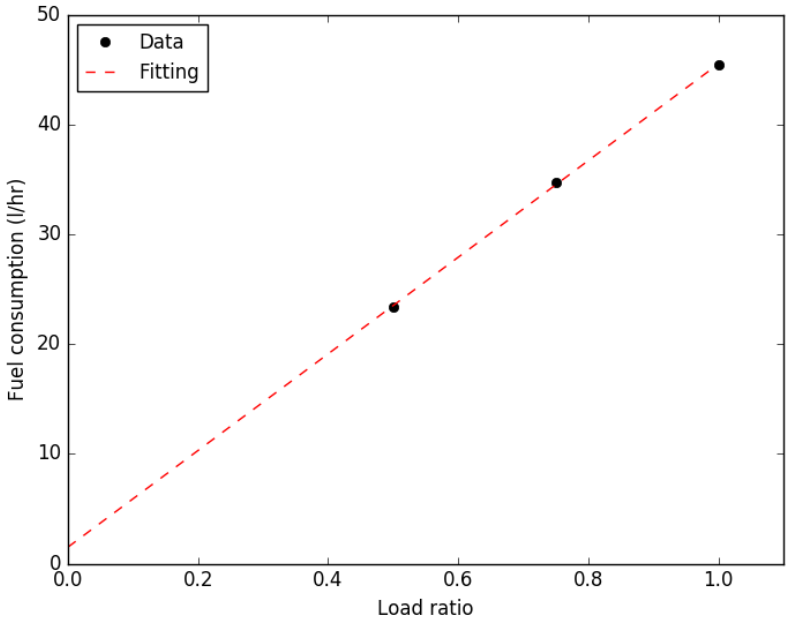

Figure 4.5: Example of fuel consumption as a function of load ratio for a real diesel generator, the FG Wilson P220-1 (160 kW rated) [194]. The full datasheet for this generator can be found in Appendix E.

`fuel_consumption_points` property, mapping each benchmark load ratio to its fuel consumption value. A dictionary is advantageous as it prevents ratios being defined multiple times. The data are formatted prior to being set, using the `_check_fuel_consumption_input` static method, to ensure data type consistency. Additional functions also allow points to be easily added or removed within Python.

Using the defined points, the fuel consumption is estimated from a function fitted through the data. This fuel curve fitting function is calculated internally. The function type is defined by the `fuel_curve_fitting` property and can be set at class initialisation. Currently only linear fitting is supported, as in HOMER; as this has always looked reasonable for the input data examined (as demonstrated in Figure 4.5) no further function types have been coded in. The constants required by the fitting are derived and saved within the instance in the `fuel_curve_fitting_parameters` attribute, this allowing the fuel consumption for a given output power to be obtained using a further method, `calculate_fuel_consumption`. In the hybrid simulation this process is carried out after the power balancing algorithm has been run and the generator output powers are known. Applying it at the end, rather than at every time step, speeds up the code by limiting the number of calculations performed.

As well as the rated power, the output of the generator can also controlled with the `min_load_ratio` attribute, setting a lower limit on the output power

can be produced. This feature, also used in HOMER, copies a real generator management strategy that might be followed in situations where the generator is oversized for the application. Some generators will have minimum loads specified by the manufacturer. At other times it might be desirable to prevent damage to the generator, for example to limit "wet stacking" (where fuel is not completely combusted and hence can clog up and reduce the lifetime of the generator). In reality, a minimum load could be applied by connecting the generator to a bank of resistors to dissipate power. The attribute is represented as a proportion of the rated power, defined as a *float* between 0 and 1, and overwrites the inherited `min_power_output` property:

$$P_{\text{min, in}} = P_{\text{rated}} \times R_{\text{min}} \,, \tag{4.4}$$

where R_{min} is the minimum load ratio and P_{rated} the generator rated power.

Lastly, in addition to any local costs, a dedicated replacement cost can be set. This is represented by the `replacement_cost` attribute. This can be used in combination with the generator lifetime, defined in units of hours within the attribute `lifetime_op_hours`, to calculate the cost periods that the generator needs to be replaced in.

The method `calculate_replacement_periods` takes in a time series of generator operating hours, either as a NumPy array or Pandas DataFrame. This is the number of hours that the generator is operating per time period and works irrespective of the time units (although monthly data is used in the main hybrid algorithm to keep consistency with the other components of the cash flow analysis which tend to consider a month base). The function iterates through the array, calculating the cumulative sum of the operating hours. The time period where replacement is needed is found when the hours exceed the lifetime. In this case the cumulative sum is reset (starting from the time remaining in the period) and the index of the period is stored. This algorithm continues until it has iterated through the whole array, the output being a list containing periods where generator replacement is required.

With knowledge of these replacement periods, a new cost instance representing the replacement can be created. This process is achieved using the method `create_replacement_cost_item`. After getting the replacement periods above, the method creates a new `FutureCost` instance: with a value set to that specified in the `replacement_cost` and cost periods defined as in the periods (see Section 3.4.2 for a description on how these are specified). This output instance can then

be assigned to any object as a local cost and filtered into the cash flow analysis using any `cost_categories` defined within the generator replacement cost.

4.4.2 Hybrid wave device

To incorporate wave energy devices into the algorithm, a class is required which combines the `EnergySource` class characteristics with the wave device classes defined in Section 3.6.2. It is assumed that, while not all of the grid tied project costs will apply, the nature of the device structure itself will remain the same. The hybrid wave energy device class, `WaveEnergyConverterHybrid` hence inherits from both the `wave_device` module's `WaveEnergyArray` class and the `EnergySource` class, through the intermediate `NonDispatchableSupplier`.

The class `NonDispatchableSupplier` is the opposite of the dispatchable supplier class from Section 4.4.1. It is a representation of intermittent renewable energy sources, which generate power according to physical resource and hence contribute to the load at will. Whereas the latter class can be simply defined by constant minimum and maximum power limits over all time steps, `NonDispatchableSupplier` instances have limits which fluctuate according to the power output at the desired time.

The key attribute for this class is `power_time_series`. This power profile is a *Pandas DataFrame* (as used for previous time series), the time dimension allowing the power value at a specific time to be easily queried. The `time_axis` property is directly derived from this embedded *DataFrame*.

To obtain the energy output for a particular time step in the hybrid power balancing algorithm, first the instance attribute `present_time` is set to the same time as the current time step of the hybrid algorithm; this is the start time of power production. The end time of power production is equal to the start time plus the length of the `modelling_time step` attribute (this is set from the load profile time dimension as described in Section 4.3).

If both start time and end time are defined in the power time series (i.e. the load profile and power time series are defined over the same time dimension) then the energy is just obtained by multiplying the power at the start time step by the time difference. Computationally this is the fastest method. If the power time series dimension is different then the energy is calculated by looking at the power values between the start and end time, calculating the energy for each portion of the time series in turn. This functionality is useful as it means that the power can be provided at a different time dimension, however it is also slower to execute

as there are more calculations required to resolve the energy factors between the time displacements.

In this class there is no distinction between maximum and minimum energy output: the energy is always defined by the relevant portion of the time series, which is then modified to account for any embedded converters.

The `WaveEnergyConverterHybrid` class contains no additional methods, only using those inherited from its two parents. To prepare the wave device object for the hybrid analysis, the `power_time_series` attribute needs to be set. This is done within the overall spatial analysis function (described in Section 3.1). The modular nature of the code makes any modifications to the embedded items within the wave device easy to define, without needing to define the whole system again. For a fish farm system, this might include specifying a cable landing point to the feed barge location and reduced mooring costs due to being able to share some of the fish farm infrastructure.

4.4.3 Batteries

The energy storage is a crucial part of the wave energy hybrid system, both reducing the amount of excess energy produced when the wave energy input exceeds the load and picking up any shortfall to reduce diesel consumption.

There are three classes that have been created to model battery systems. These all inherit from `EnergySupplier`, allowing power input and output limits to be defined and set at each simulation time step set. The first two classes, `BatteryBase` and `KineticBattery` are representations of individual batteries. The third, `BatteryBank`, represents a bank of batteries, with the batteries connected in series and parallel. This is the class that is most commonly used as it allows larger amount of energy to be stored.

4.4.3.1 Battery base class

The class `BatteryBase` represents a very basic battery. While it can be used in the model, the main purpose of the class is to define fundamental battery parameters, serving as a foundation for more complex battery child classes (for example the `KineticBattery` described in Section 4.4.3.2). Whereas in a real battery the maximum amount of energy that can be input or output will depend on the charging history of the battery, in this system the limits are defined arbitrarily by the user.

As for the energy sources previously introduced, this class seeks to determine

the power limits, and hence energy, that the battery can contribute towards the load profile in a given time step. To achieve this the class has three key properties:

- The battery capacity (the `nominal_capacity_kwh` attribute). This defines the nameplate energy that is stored in the battery.
- The maximum current that is applied to charge the battery (calculated using the `max_charge_current` function).
- The maximum discharging current that is applied to get energy out of the battery (calculated using the `max_discharge_current` function).

Whereas the diesel generator and hybrid wave energy converter classes are only concerned with energy production, the battery system also must be able to calculate the maximum energy that can be put into it.

At a given time step, the power limits are calculated using the `voltage` attribute, V, and respective charge current limit:

$$P_{\text{max, in}} = VI_{\text{c, max}} \tag{4.5}$$

$$P_{\text{max, out}} = VI_{\text{d, max}}\,, \tag{4.6}$$

where $I_{\text{c, max}}$ is the maximum charge current and $I_{\text{d, max}}$ the maximum discharge current. The `voltage` is a fundamental property of the battery and for the simulation is assumed to be fixed. The off-grid model is not designed to be a detailed electrical design tool, instead framing the simulation from an economic perspective, and so a higher level energy focussed approach can be justified (mirroring commercially available tools, e.g. HOMER).

For `BatteryBase` the maximum discharge current is set arbitrarily using the `discharge_current_limit` attribute. In reality, and for more realistic battery models, this is an internal property of the battery and would be calculated. The maximum output energy is limited by both this attribute and the battery capacity, which is constrained by the the minimum state of charge. This attribute, `min_state_of_charge`, is introduced in real system controllers to prevent the battery from experiencing deep charging cycles, as this can shorten their lifespan [195]. Considering these aspects, as there is no minimum energy output, the energy output that can be achieved at time step t can be expressed as:

$$E_{\text{max, out}}(t) = \begin{cases} E_d(t) & \text{if } q(t) - E_d(t) > q_{\min} \\ \Delta t P_{\text{max, out}} & \text{otherwise}\,, \end{cases} \tag{4.7}$$

where Δt is the length of time, $q(t)$ is the initial battery capacity and q_{min} the minimum allowed capacity, the product of the nominal battery capacity q_0 and the minimum state of charge S_{min} :

$$q_{\text{min}} = q_0 \times S_{\text{min}} \,. \tag{4.8}$$

There is a second lower threshold, `cycle_charge_threshold`, which was introduced in Section 4.2.4. This is only relevant in the context of the "cycle charge" management strategy. If the battery SOC drops below this percentage then the battery output is disabled (the `output_active` attribute set to false). This means that the battery can only accept energy, until the capacity exceeds the `setpoint_soc` threshold (at this point it can operate as an energy source once more).

The maximum energy that the battery can receive is considered in a similar manner to the output. It is constrained by an upper limit, the maximum capacity of the battery q_{max} :

$$E_{\text{max, in}}(t) = \begin{cases} E_i(t) & \text{if } q(t) + E_i(t) > q_{\text{max}} \\ \Delta t P_{\text{max, in}} & \text{otherwise} \,, \end{cases} \tag{4.9}$$

where $E_i(t)$ is the energy that is trying to be put into the battery. For `BatteryBase` the maximum battery capacity is set equal to the nominal capacity (typically the capacity at the 20 hour discharge rate), although it is calculated for the `KineticBattery` child class.

Putting the above equations together means that the battery capacity can never exceed the maximum or fall below the minimum state of charge. The private methods `capacity_above_min_threshold` and `capacity_headroom` calculate the limits on energy extraction for the `present_capacity` of the battery. This attribute defines the capacity of the battery at the present time being considered, and is set at each time step within the off-grid simulation so that the battery capacity is updated and monitored throughout the simulation. This is achieved using the `set_final_charge` method. This takes in a desired current and constrains it to the maximum that is allowed, by converting the current to power and hence energy (using the `modelling_time step` attribute) and using the above inequalities. This energy is then added to the `present_capacity`, permanently modifying it. The function is compatible with both input and output currents, applying the sign convention introduced in Section 4.4. The battery can be reset to its initial, fully charged state, by using the `set_initial_capacities`

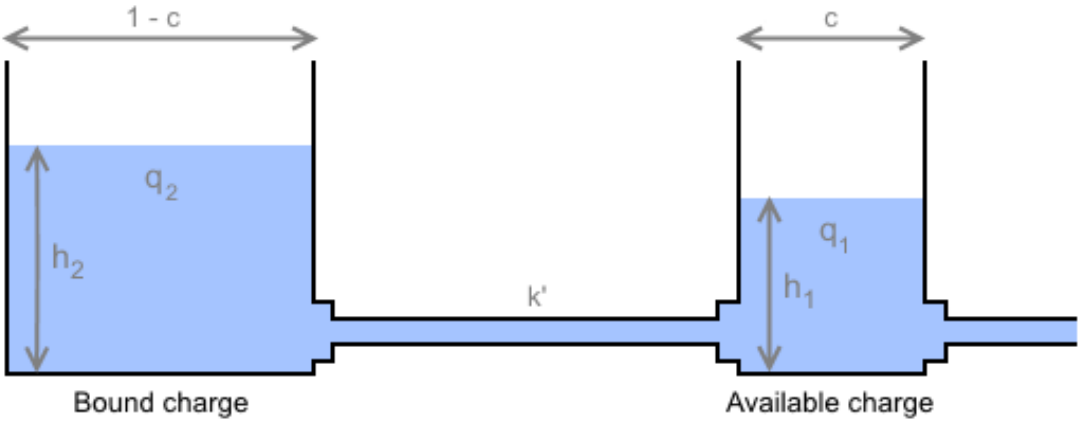

Figure 4.6: The two tank analogy, which is used as the basis of the kinetic battery model. The battery is essentially split into two halves: the right "available charge side" which contains charge which is immediately available to the system, and the left "bound charge" side. This energy is only available after it has propagated to the right tank. Diagram based on [196].

method, which simply reassigns the `nominal_capacity` value to the present capacity attribute. It should be noted that all of the quantities concerned with capacity are defined within the class twice: in units of AH and kWh. While AH is the standard unit, kWh is the unit considered for the load profile and so is the default output in the hybrid simulation. Conversion to kWh is easily achieved by the following:

$$q[kWh] = \frac{q[AH]V}{1000} \,. \tag{4.10}$$

Lastly, the input and output efficiencies of this class are defined by the `roundtrip_efficiency`. Mimicking the approach taken in HOMER, this assumes that the same efficiency is applied in each direction:

$$\eta_o = \eta_i = \sqrt{\eta_{rt}} \ , \tag{4.11}$$

where η_{rt} is the round trip efficiency.

4.4.3.2 Kinetic battery

The `KineticBattery` class builds on `BatteryBase` class by providing more realistic estimates of the energy input and output. While these are essentially defined by the user for the base class and only constrained by the state of charge, within `KineticBattery` the values are also dependent on the time history of the battery.

The main theory and calculations behind the battery model can be found in [196]. The underlying principle, displayed in Figure 4.6, is that the battery

is modelled by two connected tanks. The "available charge" side contains energy which is immediately available to the system, and also initially holds energy put into the battery. The "bound charge" side contains energy which is not available to the system in the immediate term. This energy must be transferred into the available tank before it can be used; this has the effect of limiting the amount of energy that the battery can provide or take in. The relative head difference between the tanks, $h_1 - h_2$ impacts the energy that can be transferred, the theoretical basis meaning that charging regime more closely follows that of a real battery. If the battery capacity is low then it will charge more quickly (bulk charging), levelling off as the head reduces and the battery reaches its maximum capacity.

To find the maximum power that can be transferred Equations 4.5 and 4.6 can be used, however this time the current values are calculated:

$$I_{d,max} = \frac{kq_{1,0}e^{-k\Delta t} + q_0 kc(1 - e^{-k\Delta t})}{1 - e^{-k\Delta t} + c(k\Delta t - 1 + e^{-k\Delta t})} \tag{4.12}$$

$$I_{c,max} = \frac{-kcq_{\max} + kq_{1,0}e^{-k\Delta t} + q_0 kc(1 - e^{-k\Delta t})}{1 - e^{-k\Delta t} + c(k\Delta t - 1 + e^{-k\Delta t})} \,. \tag{4.13}$$

Here $q_{1,0}$ and q_0 are the initial capacities in the available tank and the battery as a whole and Δt is the length of the time step, as before. There are also three constants present: k, c and $q_{\max}$. These are referred to as the kinetic model constants and are based on the physical properties of the battery. The first two essentially define the ratio of the two tanks and the rate that charge can be transferred between the tanks. The third, $q_{\max}$, is the maximum charge as seen previously, and with c defines the size of the two tanks:

$$q_{1,\,\max} = cq_{\max} \tag{4.14}$$

$$q_{2,\,\max} = (1 - c)q_{\max} \,. \tag{4.15}$$

While for `BatteryBase` $q_{\max}$ was set equal to the nominal capacity, for this class it is calculated (along with the other two constants) by using battery discharge capacity data. This process is described in [196]. These constants only need to be calculated once, at the beginning of the simulation.

To integrate all of the new theory and calculations required, the class contains a number of additional attributes to its parent. The actual kinetic model equations are defined in a separate module, `kinetic_battery_model.py`, to keep the theory separate from the implementation. First, to set up the battery the kinetic model constants need to be calculated. This can be achieved using the

`set_kinetic_model_constants`, however this requires the `capacity_data` attribute to be defined. This attribute is a dictionary, linking the battery discharge hour rates to capacities at those rates. These data are commonly specified on the battery datasheet, provided by the manufacturer, an example of which is shown in Table 4.4. The capacity column denotes the charge that can be extracted from

Hour rate	Capacity (AH)	Discharge current (A)
100-hr	250	2.50
20-hr	225	11.25
10-hr	207	20.70
5-hr	185	37.00

Table 4.4: Example battery capacity data, in this case for the Trojan T-105. The full datasheet for this battery can be found in Appendix E.

the battery over the number of hours defined by the hour rate. The discharge current can be implied by dividing the capacity by the hour rate.

Once the kinetic constants are obtained, they can be visually checked by comparing the discharge profile estimated from the constants to that calculated at the specified data points. This is can be done using the `plot_discharge_curve` function, which calculates the discharge current across the capacity range and allows it to be plotted. An example of the output for the battery from Table 4.4 is shown in Figure 4.7.

The kinetic constants are stored in a dictionary within the `kinetic_model_constants` attribute. As defined in Equations 4.14 and 4.15 they define the battery capacity in terms of the two tanks, which can be returned via the `model_tank_sizes` function. This defines the maximum charge that can be stored in each tank. Whereas for `BatteryBase` the capacity was just stored as a single number, for this class the capacity is stored as a tuple of two numbers: the bound charge and the available charge in the battery. Given a current, the final charge in the two tanks can be calculated using the function `final_charge_amounts`. This first constrains the current to the limits as described in Section 4.4.3.1 and then, given the present tank capacities, calculates the final amount of charge in each tank using the kinetic battery model and the methodology from [196]. The outputs from this are new charge values for each tank, which can be assigned to the object by setting them to the `present_capacity` attribute.

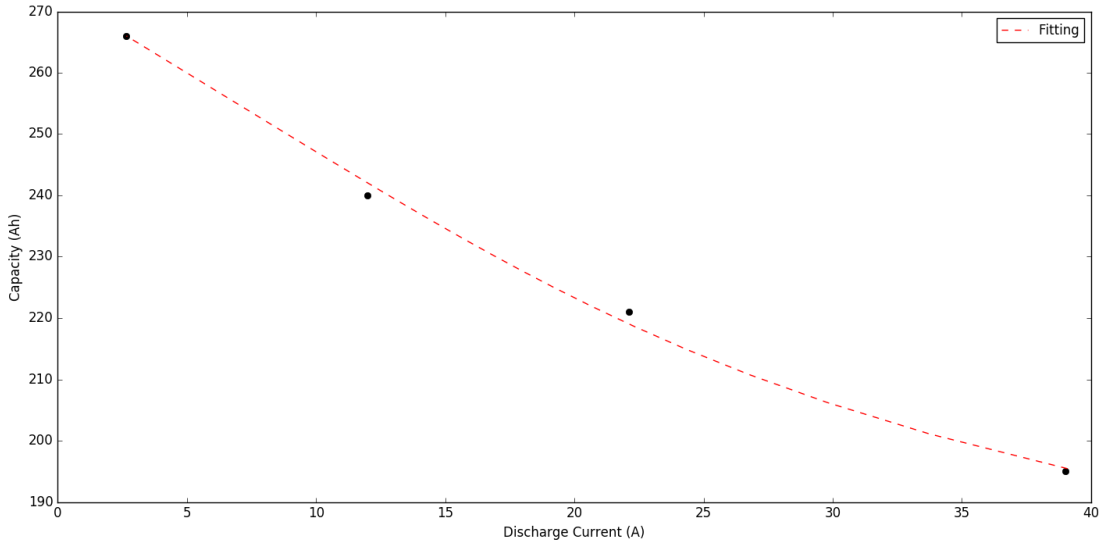

Figure 4.7: Capacity curve for the battery from Table 4.4. Plotted are the discharge currents at 100, 20 10 and 5 hour rates against the fitting as calculated using the kinetic battery model.

4.4.3.3 The Battery bank

While the two individual battery classes previously mentioned might be suitable for very small systems, these are of little use in the majority of kW scale systems where larger storage is required. This is resolved with the `BatteryBank` class, which allows larger systems of batteries to be modelled.

The relationship between the `BatteryBank` and individual battery classes is composition based, in a similar way to the`WaveDevice` and `WaveEnergyArray` classes described in Section 3.6.2. This is because a battery bank can be thought of as a large single battery, subject to the same underlying physical principles. The `unit_battery` attribute is an embedded `BatteryBase` or `BatteryKinetic` instance. In the code, the battery bank parent class is chosen dynamically: set to the class of the unit battery (this is not shown in the UML diagram in Figure 4.2 to improve the diagram readability). This is to keep consistency in the methods and functionality of the unit battery, as there are subtle differences between the two unit battery classes. Most commonly the unit battery is `BatteryKinetic`, making the battery bank a child of `BatteryKinetic`.

The quantity of batteries is not set directly but is the product of the number of batteries connected in series, `batteries_per_string` and the number of parallel strings, `parallel_strings`. The former number relates to the battery voltage, and is chosen to match the DC bus voltage (typically 24 or 48 V). Adding more strings increases the capacity of the battery bank; this is taken into account in the overwritten `capacity_data` method, where each individual capacity and current value is multiplied by the string quantity. The overall battery quantity

is calculated and set to the unit battery's `quantity` property, ensuring that the correct quantity is used for the cost analysis. As the battery bank inherits from `ItemBase`, additional costs can also be set at the battery bank level, within the `local_costs` attribute. This means that costs that are independent of the battery model only need to be defined once, allowing different battery models to be easy swapped in and out. Examples could be the cost to inspect or install the battery bank.

4.5 Limitations and Assumptions Summary

This section highlights the main limitations and assumptions that are present in the off-grid sub-model. These are presented in Table 4.5. While the main functionality draws from the commercial HOMER software, not all of the desired features could be implemented due to the time constraints of the project. The most significant limitations concern the battery. While the kinetic battery approach does provide some realism to the battery model, the model does not include calculation of the battery lifetime or account for degradation of the battery capacity over time or due to operating temperature. As the former aspect is linked to the energy flow through the battery, a geospatial property when paired with a WEC, it means that the battery bank cost calculated in the model is always static over the spatial domain. This means that the spatial cost profile will not reflect reality. The main reason why they were not included was due to the time constraints of the project; there is nothing in the model implementation that would prevent them from being added in future. As the relative cost of the battery bank is low relative to the typical WEC and fuel costs it is not thought that these missing aspects will have much impact on the final LCOE. Also, with careful system design and examining background literature, the battery life could be estimated and replacement included using a `FutureCost` local cost with a recurring time component (see Section 3.4.2). This process is carried out in Chapter 6 for the off-grid case study sensitivity analysis.

The second main limitation compared to the literature is that the algorithm does not optimise for cost. If implemented, this would allow energy sources to provide variable energy and operate "out of turn", to minimise the overall system cost. While this is sometimes seen, for example in HOMER and [158], it was considered too complex for this project. There are more significant factors which impact cost, for example the WEC costs, which can be examined and are sufficient for such easy stage feasibility. Cost optimisation of the algorithm would likely to

seen at a higher TRL level, once the working principle is established and more accessible cost reductions have been exhausted.

The other limitations listed are relatively minor by comparison. As the analyses consider relatively long time steps it does not capture short term fluctuations in the wave resource or load profile. It is assumed that the wave power is smoothed by the system (in the case of the Albatern device by using hydraulic accumulators to store and release energy). To simulate a hybrid system on shorter timescales, in a wave to wire way would require different tools and is not the purpose of this economically-focussed research. While only selected components have been coded

Limitation	Justifications	Priority
Battery lifetime and replacement cost not calculated for cost analysis.	• Battery cost is a small part of overall cost for WEC hybrid system and, with suitable management, would not see significant differences across local areas.	H
Energy balancing algorithm does not optimise for cost instead following the same logic across time steps.	• Currently technology in the feasibility stage; cost optimisation and examining new control strategies will be more important once technology is established.	H
Battery temperature impacts on capacity not considered.	• For fish farm application, the battery bank could be kept in enclosed facility (e.g. on a feed barge) and its temperature carefully regulated.	M
Methodology does not consider short term fluctuations in load or resource.	• Purpose of model is for higher level overview in an economic context. Detailed electrical modelling and hybrid system sizing is outside the scope of the study. • Commercial tools consider energy averaged within discrete time periods, so deemed sufficient for this model.	L
Limited selection of components have been created for model.	• The main components in wave energy context are included (WEC, battery bank and diesel generator). • Module coded in flexible way, so additional renewable sources like wind turbines or solar PV could be included in future.	L
Diesel price is fixed to a single value over lifetime.	• Sensitivity in diesel price can be examined using single values over lifetime, considered as averages.	L

Table 4.5: The main assumptions and limitations that exist within the model, why they were not improved and potential ways in which they could be implemented in future work.

into the sub-model, they capture the options available for a small wave energy hybrid system which is the purpose of this study. Fundamentally, the modular nature of the code means that new energy sources could be easily created. For example wind turbines or solar PV classes could inherit from the `DispatchableSupplier` class and would only require a power time series in order to slot directly into the algorithm. The last point, while a limitation, can be incorporated by viewing the diesel price as a discounted lifetime average and conducting sensitivity analysis on the price value.

Grid-connected Wave Energy Systems

The section presents a case study to demonstrate the model capabilities and how it can be used in practice. A grid connected wave energy system is considered, as in the majority of previous literature. First a baseline analysis is described, considering a specific WaveNET array, which serves as a reference point for proceeding analyses. Henceforth this is known as the *baseline scenario*. The input data are described and justified, and the immediate results are discussed. Some sensitivities are then examined, looking at the impact of specific parameters on the overall baseline scenario LCOE. Several of these are combined to form an *Optimistic Scenario* to show how the model can be used to evaluate modified systems.

All of the data in the configuration files that were used to run the baseline scenario can be found in Appendix C.

5.1 Case Study Location and Metocean Data

The metocean dataset that was used for the case studies covers an area off the west coast of Scotland. This area, shown in Figure 5.1, is a rectangle encompassing both the Inner and Outer Hebrides and lies in the range 56.2 to 58.6°N latitude and -7.6 to -5.2°E longitude. The spatial resolution of the data is 1/60° (one arc-minute); this equates to a domain of 145 by 157 points (latitude by longitude).

The metocean data were provided by Albatern, having been previously pur-

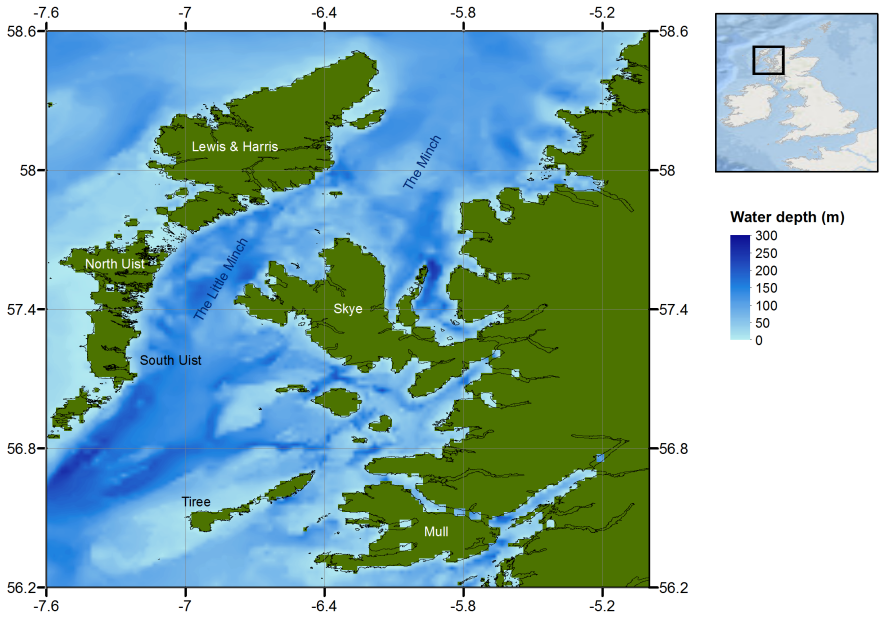

Figure 5.1: The location and extent of the domain that was used for the case study analyses. Labelled locations are those that are made reference to in the proceeding analyses.

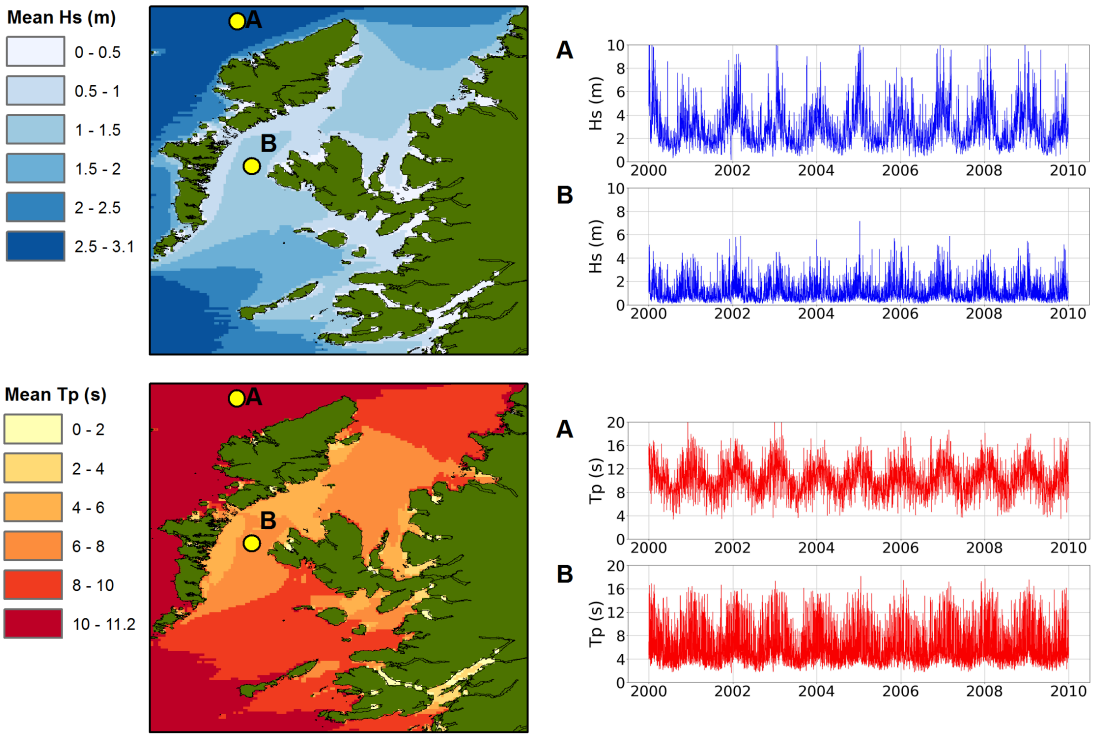

Figure 5.2: Mean H_s and T_p for the ten year metocean dataset. Full time series for the parameters are shown at two arbitrarily chosen points: one exposed to Atlantic swell (A) and one in the more sheltered Little Minch region (B).

chased from Metocean Solutions Ltd. Metocean Solutions is a New Zealand based consultancy who create and distribute metocean data, among other services [197]. The data consist of ten NetCDF files, each made up of a single year of simulated hindcast data, from 2000 to 2009. Included parameters are gridded H_s and T_p, at a temporal resolution of 3 hours, and the water depths that were used to generate the data. The data were created by Metocean Solutions in-house, using SWAN, and validated by them internally using historical buoy data. Figure 5.2 shows the mean H_s and T_p over the ten years of data, as well as time series data at two arbitrarily chosen points.

The west of the domain is dominated by energetic swell waves with a long Atlantic fetch. The mean H_s exceeds 3 m over much of this region, with mean swells up to 11.2 s. As the waves move round the Outer Hebrides a significant amount of this energy is dissipated. Point B in the Little Minch shows similar seasonal trends to the exposed point A but with a much lower mean H_s of 1.1 m. The peak period is also lower, with a more noisy signal that has a higher contribution from locally wind driven waves.

5.2 Baseline Scenario: Early Demonstrator

The baseline scenario is based on best estimates for the current Albatern WaveNET in the present day. As the TRL of the device is behind market maturity (6-7), this represents an early stage demonstrator project. From this starting point, the sensitivity analysis conducted in Section 5.3 aims to demonstrate the model functionality by investigating the key cost drivers for the technology selected.

5.2.1 Input data

5.2.1.1 The device

The baseline scenario considers a small Series-6 WaveNET deployed in the area described in Section 5.1. The array is made up of six Squids arranged in a triangular formation; this is known as a "3-Hex" array. Costs for the devices were obtained from Albatern, with a high level breakdown shown in Table 5.1. The most expensive item is the Anti Node, both per Squid and for the total array. As well as these CAPEX, an insurance cost was included. This proportional cost was set equal to 1% of the total project CAPEX, incurred annually. This value was provided by Albatern, consistent with values quoted to them.

The scenario considers a single PTO unit per Squid in the array. Each PTO unit is rated at 7.5 kW, meaning the whole array is rated at 45.0 kW. The PTO unit is housed in an Anti Node. In theory up to three can be equipped per Squid, although only one per Squid is considered here. It is also assumed that the 3-Hex costs are simply six times the cost of a single Squid, with no discount due to learning or purchasing in bulk.

Component	Cost (£)	Quantity per Squid	Cost per Squid (£)	Quantity per 3-Hex	Cost per 3-Hex (£)
Central node	5,743	1	5,743	6	34,458
Anti-node	7,897	3	23,691	18	142,146
Riser	5,163	1	5,163	6	30,978
Pumping module (central node)	5,335	3	16,005	18	96,030
Pumping module (anti node)	6,936	3	20,808	18	124,848
Link arm	1,523	3	4,569	18	27,414
PTO	6,777	1	6,777	6	40,662
Other	996	1	996	6	5,976
Total			**83,752**		**502,512**

Table 5.1: Current costs for the Series-6 Squid and 3-Hex array (made up of six Squids) that were used for the baseline scenario analysis. The components correspond to the Squid that was depicted in Figure 1.1.

Figure 5.3 shows the power matrix that was used to represent the device. It was generated by Albatern from time domain simulations in Ansys Aqwa. They modelled the array as a series of rigid cylindrical bodies, hinged together to allow movement in the appropriate degrees of freedom that the actual device would experience. The software uses the Morison equation to calculate the hydrodynamic loading. To model the PTO, an external force is considered that opposes the device motion. This is a function of the pressure in the hydraulic system. To obtain the power values, simulations were run at a series of different pressures for each irregular sea state, with the pressure yielding the maximum power taken. The matrix does not include losses, such as hydraulic losses in the rams, mechanical losses due to friction in the bearings or conversion losses.

Power entries in the matrix that are higher than the rated power are curtailed to the rated power value. A 85% efficiency factor was applied to the device, across all sea states, to account for the conversion efficiency of the energy producing

Hs (m) \ Tp (s)	3	4	5	6	7	8	9	10	11	12	13	14	15
7	0.0	0.0	0.0	0.0	0.0	0.0	45.0	45.0	45.0	39.9	33.4	27.3	22.8
6	0.0	0.0	0.0	0.0	0.0	45.0	45.0	45.0	43.5	32.3	26.6	22.1	18.4
5	0.0	0.0	0.0	0.0	45.0	45.0	45.0	35.3	29.9	25.0	20.6	16.7	13.6
4	0.0	0.0	0.0	45.0	45.0	45.0	34.7	25.5	21.1	17.8	14.4	11.3	8.8
3.5	0.0	0.0	0.0	45.0	45.0	38.2	27.6	20.3	17.2	14.2	11.3	8.6	6.4
3	0.0	0.0	45.0	45.0	40.3	29.4	21.6	15.7	13.2	10.6	8.2	5.9	4.4
2.5	0.0	0.0	45.0	38.9	29.3	22.2	16.0	11.4	9.2	7.1	5.2	3.6	2.7
2	0.0	43.4	37.4	27.4	20.3	14.9	10.5	7.1	5.5	4.0	2.8	2.0	1.4
1.5	0.0	29.1	24.3	17.4	12.3	8.3	5.3	3.4	2.7	1.7	1.2	0.8	0.6
1	17.8	13.2	12.0	7.8	4.9	2.9	1.6	1.0	1.2	0.5	0.3	0.2	0.1
0.8	10.7	8.1	7.4	4.4	2.6	1.6	0.8	0.5	0.7	0.2	0.1	0.1	0.1
0.6	5.3	4.2	3.5	2.0	1.1	0.8	0.3	0.2	0.2	0.1	0.1	0.1	0.1
0.4	2.1	1.7	1.2	0.7	0.4	0.2	0.1	0.1	0.1	0.0	0.0	0.0	0.0
0.2	0.4	0.3	0.1	0.1	0.1	0.1	0.0	0.0	0.0	0.0	0.0	0.0	0.0

Figure 5.3: The power matrix representing the 3-Hex Series-6 Device [199]. It was created by Albatern internally, by performing time domain simulations in Ansys Aqwa. Power values are in kW.

systems. This value was provided by Albatern and, due to lack of operating experience, is yet to be verified. It is in line with the literature, for example [92] and [198]. An availability factor of 80% was also assumed, applied over the whole domain. As a benchmark availability has not yet been verified for the device, due to lack of data resolution as noted by Kenny et al. [81], this was informed by the literature and represents an early stage commercially ready product (for example 75% is assumed in [57] and 90% in [34] for other wave devices).

A discount rate of 10% was chosen for the project. This was because the value is characteristic of an early market device and follows typical values used in the literature (for example [32, 57, 97]). The lifetime of the device was set to twenty years, targeted by Albatern and a value again common in the literature (for example [76]). An issue is that the lifetime exceeds the ten years of metocean data available. This means that the model replicates the data twice to form a twenty year time series, as described in Section 3.6.4. Costs for development and decommissioning were not included, assumed to be negligible as is common in the literature (see Section 2.3.3).

5.2.1.2 Mooring system

The mooring system is the triangular WaveNET mooring system, as introduced in Section 3.9.3. Table 5.2 summarises the main system components and costs. These costs were obtained from quotations supplied to Albatern by Gael Force, a manufacturer of marine equipment based in Scotland [200]. The cost for shackles and connectors has been rounded and include a number of minor components.

The ground chain and riser chain are calculated as a function of water depth, as described in Section 3.9.2. The ground chain is 38 mm in diameter, weighing

Component	Unit cost (£)	Unit	Quantity	Total cost (£)
Anchor (1500 kg)	1,995	per unit	3	5,985
Ground chain (38 mm)	29.50	per metre	variable	variable
Riser chain (24 mm)	23	per metre	variable	variable
Grid line (32mm)	1.88	per metre	440	827.20
Corner buoy	760	per unit	3	2280
Shackles & connectors	500	per array	1	500

Table 5.2: Mooring system components that were considered for the analysis. The ground chain and riser (catenary) chain quantities, and hence costs, vary spatially.

34 kg/m in air. A ground chain ratio of three was considered for each leg, as used by Albatern on previous projects (i.e. three metres of ground chain for every metre of water depth). The riser chain is smaller and lighter, at 24 mm diameter and 13 kg/m in air. The grid line is 32 mm polysteel multiplait. A line tension of 20,000 N was assumed as this gave suitable looking catenary shapes for the riser chain over the range of water depths considered. As this only impacts the cost of the riser cable, a negligible part of the overall system, its value is of minimal consequence.

5.2.1.3 Export cable and grid connection

To demonstrate the model as an early stage scoping tool, no landing points are defined for the export cable. Hence, the assumption is made that the cable travels to the nearest point on land. A cable cost of £20 per metre is assumed; this matches the cost that Albatern paid for a 1kV cable for their recent Mingary Bay project. As the device is small, usage of a low cost cable can be justified, however this value is deemed to be optimistic. At further distances from shore, a more costly cable would likely be required to keep transmission losses low. This is not considered for the model, as only one export cable can be assumed over the analysis locations.

A value of £10,000 was included to account for the cost of an onshore grid connection, assuming that this could be made at the cable landing point. This cost is explained by the low power rating of the array (of the same order as domestic solar PV), the assumption being that it could be connected into the distribution network without needing any grid upgrade. The cost itself was estimated from correspondence with Albatern and sense checked by a contact at the University of Edinburgh.

5.2.1.4 Vessels

Table 5.3 shows the vessels that were considered for the baseline operational tasks. Up to now Albatern have used their own vessels, which are essentially small workboats. This assumes that, for a future project, more capable vessels are utilised to allow more exposed sites to be accessed. Data for these vessels were provided by Leaske Marine and represent price estimates as of August 2017. Leaske Marine are a marine contractor who specialise in vessel charter for the marine renewable industry, among other business activities [201].

Type	Speed (kt)		Charter (£/day)			Hs limit (m)		Fuel (l/hr)
	Transit	Tow	Work	Standby	Mob	Transit	Tow	
A. Workboat	9	4.5	1,500	1,000	900	3.0	1.5	40
B. Cable lay	10	-	7,730	5,800	4,640	3.0	-	280
C. RHIB	25	-	1,200	0	0	-	-	30

Table 5.3: Vessels that were considered to carry out the operations in the baseline scenario. The mobilisation (mob) rate is equal to demobilisation (hence it is not shown). The cable lay vessel is a multicat.

Leaske Marine charge a standby rate equal to 75% of the charter day rate. The mobilisation rate is variable in reality, dependent on the distance the vessel needs to travel. For this scenario it it assumed to be 60% of the charter, the average that Leaske Marine charge. The vessel tow speed was assumed to be 50% of the transit speed, the values consistent with previous research conducted with Albatern [10]. The transit H_s limit was obtained from [88], which was again assumed to be 50% for the towing operation. As RHIBs are readily available and do not require crew on standby, no standby or mobilisation costs were included. As the vessel is small and relatively common, one day of mobilisation and one day of demobilisation were applied.

The cable laying vessel is assumed to be a multicat, with base charter cost of £4,000 per day, that is modified to handle the cable laying equipment. The additional costs that are included in the charter rate are summarised in Table 5.4. These indicative costs were obtained from Fraser Hydraulic Power (FHP) Ltd. [202], part of the Royal IHC group. The onshore personnel cost is applied to both the mobilisation and demobilisation cost. Again the standby rate is set to 75% of the charter rate and includes the equipment hire. The price for the cable trencher is at the low end of the estimate that was provided, suitable for softer sediments (sand and mud). As the vessel is more specialised, mobilisation and demobilisation times were assumed to be two days each.

Equipment	Cost (£/day)
Linear cable engine	550
Powered spooler	300
Overboarding chute	30
Cable trencher	2,000
Offshore personnel for operations	850
Total addition to charter	3,730
Onshore personnel for mob/demob	650

Table 5.4: Additional costs for export cable installation equipment. These are included in the overall day rate and mob/demob cost shown in Table 5.3.

5.2.1.5 Installation

Table 5.5 summarises the installation tasks. The tasks can be categorised according to three systems: the mooring system, the export cable and the device itself. The export cable is installed in September 1999, followed by the other systems in October. The device starts to produce power on the 1st of January 2000 (consistent with the metocean data start point). As the year 1999 is not present in the metocean dataset, September and October from the year 2000 were used to represent the months.

Task	Month	Vessel	Hs (m)			Time (h)	Other (£)	Support
			To	At	From			
Cable	9	B	3	1.5	3	calculated	400	-
Mooring	10	A	3	1.5	3	6.0	-	C
Device	10	A	1.5	1.5	3	3.0	-	C

Table 5.5: The installation task properties that were considered for the baseline scenario. The letters in the Vessel column correspond to the vessels defined in Table 5.3. H_s limits are defined for the transit to site, at site for the operation and the transit from site.
Metocean data from the year 2000 were used to represent the month.

The cable installation is achieved using the vessel described in Section 5.2.1.4 above. The time to complete the task is site specific and calculated within the model as described in Section 3.8.2. A maximum working time of 36 hours was set, an arbitrary limit to demonstrate the model over the domain and prevent too many locations from being excluded. The installation rate was set to 500 m/hr which, along with the H_s limit of 1.5, were recommended by Leaske Marine for a typical project. A one off cost of £400 is included to account for servicing cost of

the cabling equipment, the estimate provided by FHP.

Both the mooring and device installations are carried out using the workboat, assisted by a RHIB. The time to complete the mooring install, including deployment of the drag embedment anchors and assembly of the mooring grid, is estimated at six hours. In reality this must be installed before the devices, however this assumption is not captured due to the frequency-based OPEX method. For the device, the installation of each Squid module is considered as a distinct operation. Installation of a single device is quicker than the mooring grid because most of the work is carried out above the water surface and does not require much heavy lifting (the devices are floated and towed to site). For both the device and mooring system, the maximum H_s to carry out the task was estimated at 1.5 m, based on Albatern's experience.

To serve as a base for the installation and subsequent operations, ten ports were designated as potential options. The locations of these are displayed in Figure 5.4. The ports were chosen using Marine Scotland's NMPI digimap, a freely available online portal which allows the user to see a variety of data related to the Scottish marine environment [203]. The layer "Ports, harbours, marinas, and slipways" categorises the ports into major shipping ports, harbours and simple access ramps. Overall 50-100 of these exist over the case study geographic area. The ten ports were arbitrarily chosen from the harbour category to evenly cover the domain. As the devices are small, no specialised equipment is required, save for cranes which could be hired, and so it was assumed that any of the harbours would be suitable. No port usage costs were included in the analysis, deemed to

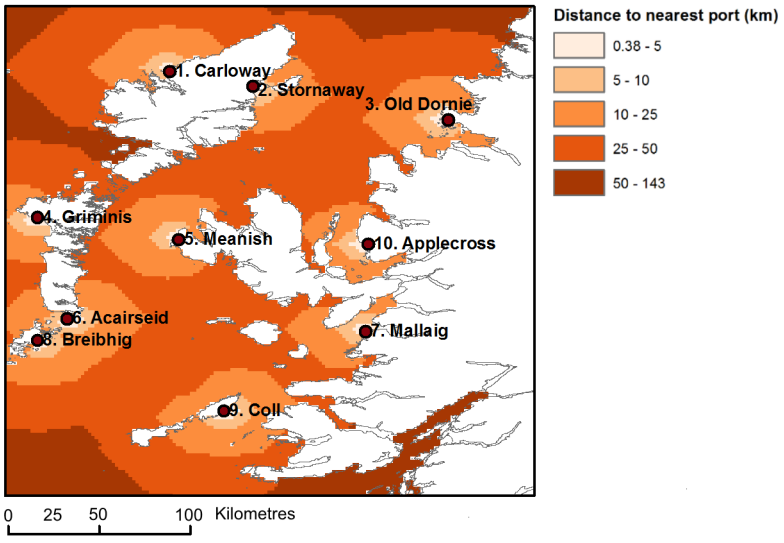

Figure 5.4: The ten ports chosen for O&M, along with the distances to the points in the domain. These distances are an output of the model.

be negligible relative to the other costs. It is also assumed that Albatern would move their main workshop from Roslin to this location, factoring it out of the analysis and into the general business activities.

5.2.1.6 Operations and maintenance

Three planned O&M tasks are considered: annual inspection of the mooring system, bi-annual maintenance of the devices and a mid-life refit. For a given Squid unit, the two latter tasks involve bringing the device into port to carry out the work and subsequent redeployment; these are hence represented by the `MaintenanceAtPort` class, as discussed in Section 3.7.5. The three O&M tasks are summarised in Table 5.6. As the technology concept is still in its infancy, with limited operating experience, the tasks and costs are estimates based on the engineering expertise at Albatern.

Operation	Month	Vessel	H_s (m)	Duration		Other (£)
				On site (h)	Onshore (d)	
Mooring inspection	3	A	1.5	3.0	0	1,500
Device maintenance	3, 9	A	1.5	2.0	1.0	1,600
Mid-life refit	3 (yr 10)	A	1.5	2.0	2.0	43,600

Table 5.6: The planned O&M tasks, carried out at regular intervals over the operating lifetime. The device maintenance and mid-life refit involve towing the device back to port and are displayed on a per device basis. The "other" costs are incurred for each operation.

The mooring inspection requires divers which makes up the additional cost, and occurs annually. The device maintenance is carried out twice per year, with additional costs for tooling and parts. March and September were chosen, to avoid having to carry out the maintenance in the winter months. For a single device, the operation involves towing it back to port, a day to carry out the inspection and then a tow back to site. The mid-life refit cost is set equal to the cost of the pumping modules and PTO from Table 5.1, which assumes that replacement of the structural components is not necessary. For this operation, two days at port are required.

The unplanned O&M cost was modelled as a proportional cost: 2% of the initial project cost per year. This is at the lower end of the literature (as described in Section 2.4.1), as the literature estimates tend to include both planned and

unplanned together.

For all operational tasks, including installation, the vessels were modelled on a "vessel per quantity" basis (see Section 3.7.4.2 for a description of this). The maximum working times were set to 24 hours. Whilst unrealistic, this was to allow the analysis to be demonstrated over the wider domain and not confined to small localities around the ports.

5.2.1.7 Constraints

Table 5.7 summarises the deployment constraints that were considered. The minimum water depth condition is a result of the physical size of the device and represents the clearance required to prevent the device from colliding with the seabed. The maximum water depth is more arbitrary in nature and is specified to represent the difficulties of installing the device in deeper water. The data were provided by Metocean Solutions along with the metocean data.

Constraint condition	Data required	Data source
Water depth ≤ 20 m	Water depths	Metocean Solutions Ltd.
Water depth ≥ 100 m	Water depths	Metocean Solutions Ltd.
Location is in a marine SPA	Marine SPA locations	Joint Nature Conservation Committee [204]
Seabed sediment is rock	Seabed sediments	British Geological Survey [205]

Table 5.7: The constraint conditions, defining invalid device deployment locations in the analysis domain.

Marine SPA areas are included to illustrate how locational constraints are applied in practice. While being located in a SPA would not automatically prevent a project from being developed [206], it is assumed that the additional EIA and consenting processes required for a marine license are grounds to initially rule out these sites in favour of other locations.

The final constraint considered is the seabed sediment; locations are ruled out if the seabed is rock. This is because the current WaveNET mooring system uses drag embedment anchors. While in theory an alternative anchoring method could be devised at these locations, this would require redesign and hence is not considered (as for the SPA consideration, it is assumed that the developer would reject these for more straightforward options).

No constraints on the export cable installation are considered in the baseline scenario, so that the visualisation can be seen in its raw form across the full

domain.

5.2.2 Model execution

Each class instance was defined in a text file, using the method described in Section 3.3. The majority of these were kept in the same directory, with a naming convention to ensure a logical ordering. The exception to this were the O&M files. These were kept in a sub directory: the schedules at the first level, the actual O&M tasks at the second level and ports and vessels at the third level. This was due to the relatively large number of files needed for this model aspect, to make them easier to access. Cost categories were defined at the class level, as well as for some local costs, to ensure that the costs could be suitably aggregated.

The analysis was then executed using the `spatial_analysis` function, as described in Section 3.1. The model took approximately two hours to run, owing to the large size of the domain. The energy, cost and LCOE results, outputted as raster files, were then exported into ArcGIS for visualisation. These are presented in the next section.

5.2.3 Results

5.2.3.1 Energy

Figure 5.5 shows the energy produced by the device over the domain, in terms of both total discounted energy and capacity factor.

The most promising areas for energy production are seen to the west of Lewis and Harris; within the Minches, particularly the Little Minch, and in the south west of the domain. The higher energy production in the west of the domain fits expectation; the wave resource is notably strong due to prevailing westerly winds and the long Atlantic fetch. In contrast the Minches is relatively sheltered, making the hotspot in the Little Minch somewhat counter-intuitive.

The reason why such a hotspot occurs is due to the scale of the device. Out to the west of Lewis and Harris the waves are characteristically longer swell waves, with the resource dominated by powerful high period waves. As can be seen from the power matrix in Figure 5.3, the device does not respond as well to the higher peak period sea states, with the power tailing off. This is because the array tends to heave as a unit in these sea states with less relative motion between the power producing components. The waves in the Minches are primarily wind driven, hence the sea states are higher frequency and better suited to the array scale.

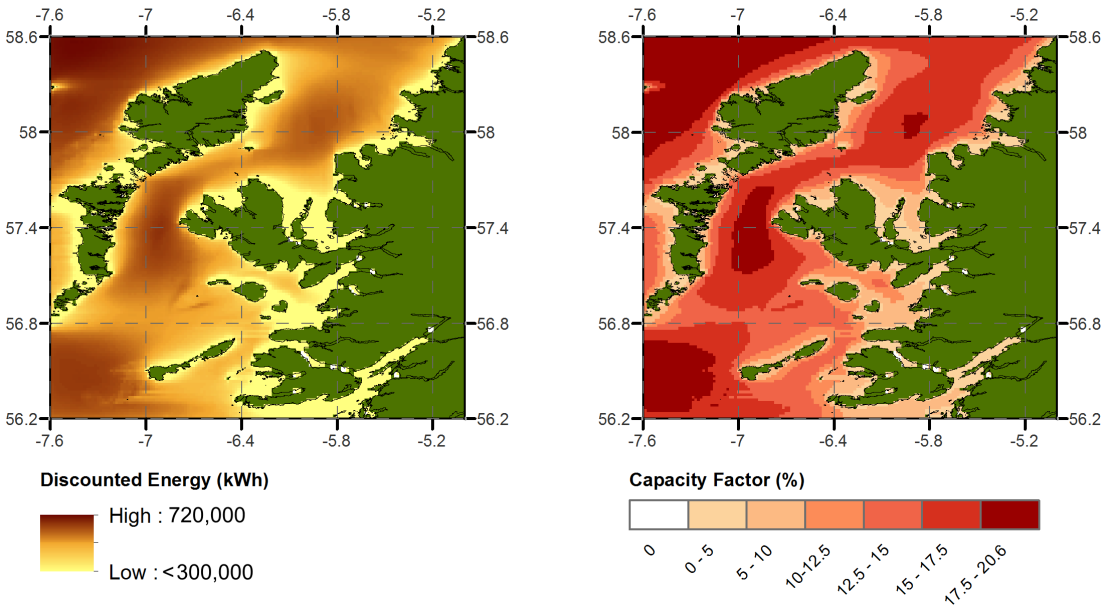

Figure 5.5: The energy production of the device over its lifetime for the baseline scenario, in terms of total energy (left) and capacity factor (right).

Lastly, something to note is that the capacity factor values are relatively low, with a maximum of 20.6% in the north west of the domain. This is especially true in the more sheltered nearshore regions, between the islands. This indicates an issue, as these are the locations that Albatern is generally targeting for the technology scale. The low capacity factors indicate that the device is overrated, and cost savings could potentially be made by down-rating the device: either by removing PTO modules or using a smaller generator.

5.2.3.2 Costs

Figure 5.6 shows the NPC for the total project and the three high level sub-systems: the device, the export cable and the mooring system.

The overall costs exceed £1.5m over the full domain, with certain areas over £2m. These tend to be the further from shore locations, where the export cable cost is very high, but also to the west as these exposed locations make operations difficult and costly (e.g. west of South Uist). As can be seen from the other three maps, the device cost is the dominant factor, not dropping below £1m. As the capital cost of just over £0.5m is static over the domain (from Table 5.1), this implies that the device operational costs must be very high. As discussed in Section 3.7.4.4, the operations also have the effect of constraining the domain of valid locations, when the time in the month is too short for the operation to take place. These areas, coloured grey and denoted as "Operation constrained" in the maps, show that a large amount of the domain is not accessible for all of the time

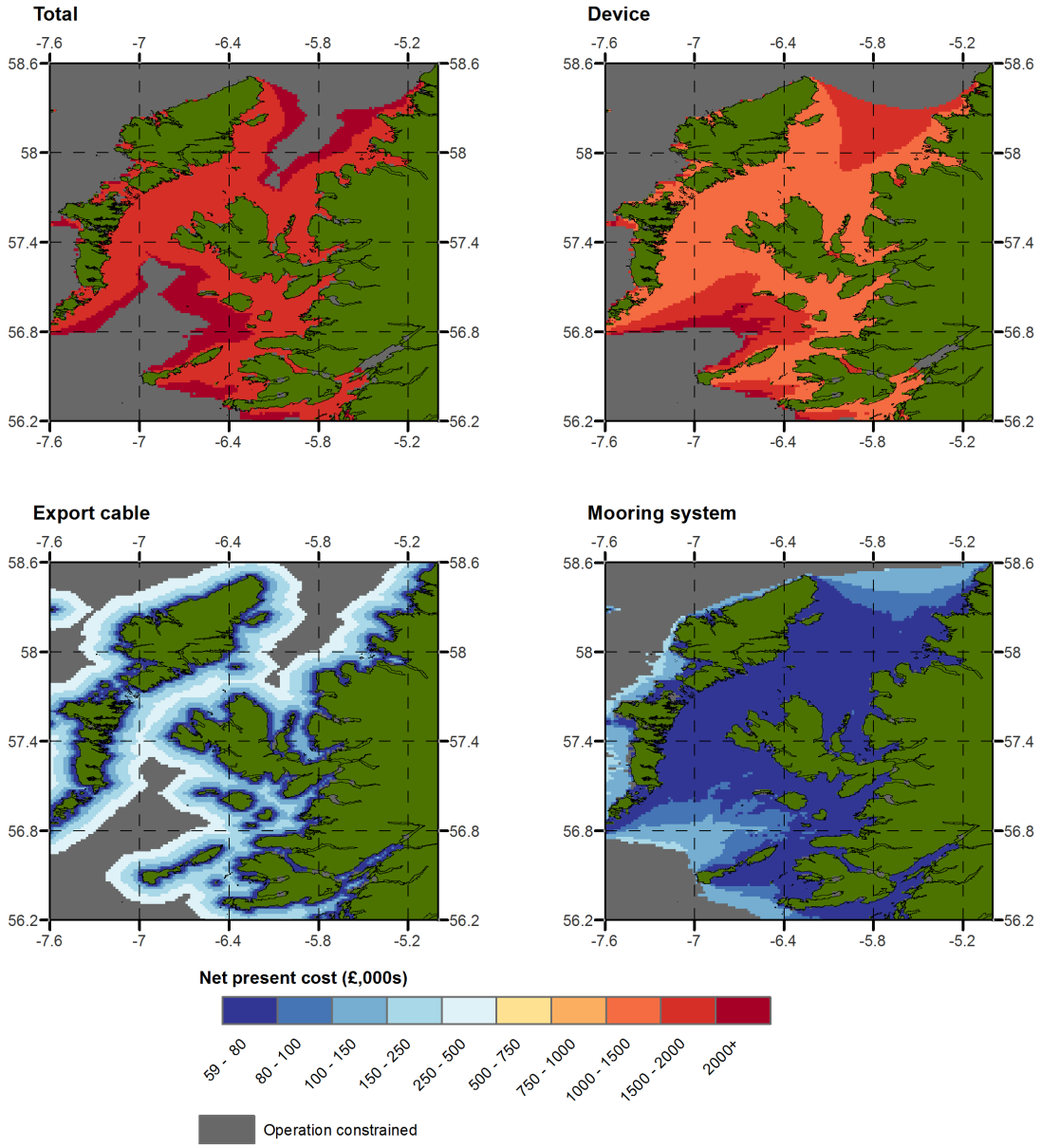

Figure 5.6: NPC values for the whole project (top left), the device system (top right), export cable system (bottom left) and the mooring system (bottom right).

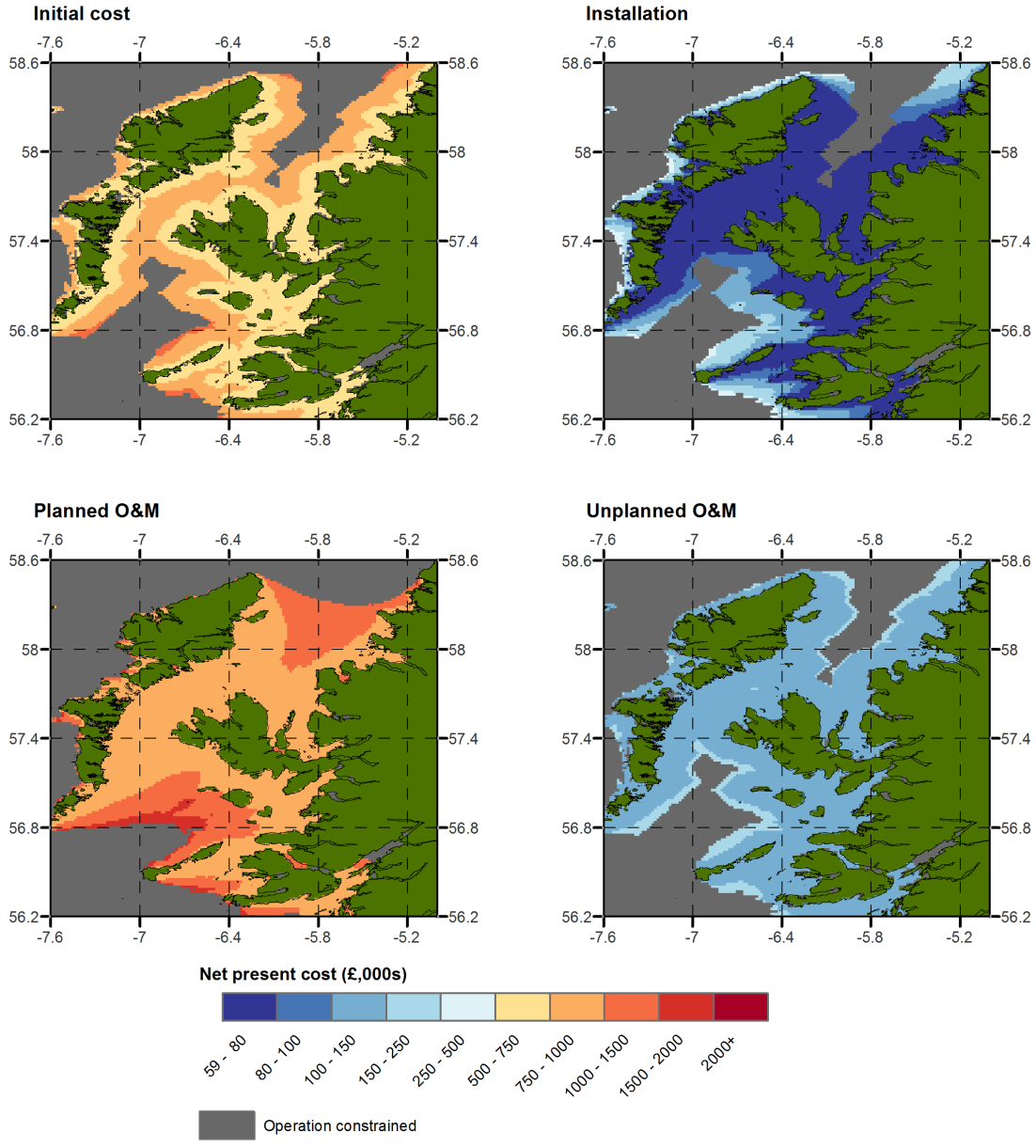

Figure 5.7: The total NPC broken down into the four main cost types: initial cost (CAPEX and installation), installation, planned O&M and unplanned O&M.

periods required. The west of the Outer Hebrides is particularly affected, with only points very close to shore accessible over the desired time periods. As the months of March and September were picked fairly arbitrarily for the purpose of the baseline, this gives scope for improvement.

The export cable cost in Figure 5.6 covers the cable capital cost and installation. Again, like the device, the majority of the expense is incurred in the capital cost. As both capital cost and installation cost are dependent on the distance to the shoreline, this is the overriding factor. Very close to the shore the cable can be bought and installed for about £40,000, however this increases very quickly. The domain is limited to locations around the coast by the cable installation speed and maximum working time available. The representative month chosen, September 2000, proved favourable, with minimal waiting time.

The mooring system cost is typically very low over the domain. Albatern regard the mooring system as one of the major strengths of the WaveNET concept, a fact that these case study data would support (albeit merely from a cost perspective). In some sheltered shallower regions the system can be purchased, installed and inspected over twenty years for just under £60,000, about 12% of the array CAPEX and less than a single Squid. The cost does rise for offshore locations to the west of Lewis and Harris. However in relative terms these costs are still much lower than the other systems.

The costs are categorised by type in Figure 5.7. The initial cost shows a clear trend with the distance from shore, driven by the export cable. The installation costs are low in relative terms across the domain, especially in the Minches where the sum is generally under £80,000. The planned O&M cost is very high, generally exceeding the initial cost over the domain. This is particularly the case to the west, accompanied by a shrinking of the domain size relative to the initial costs. Even the points in the direct vicinity of Carloway Port (see Figure 5.4) are curtailed, indicating that some of the operations coincide with very bad conditions.

As the unplanned O&M cost is just a proportion of the initial cost the trends are the same. In reality these costs would show spatial trends more similar to the planned O&M: higher values in more extreme locations, where accessing the devices is more difficult and the devices are subjected to higher wave loading. As previously mentioned in Section 3.11, lack of reliability analysis is a limitation of the research.

Figure 5.8 shows the three planned O&M activities that make up the total planned OPEX. As expected the costs are lower in the sheltered regions as the

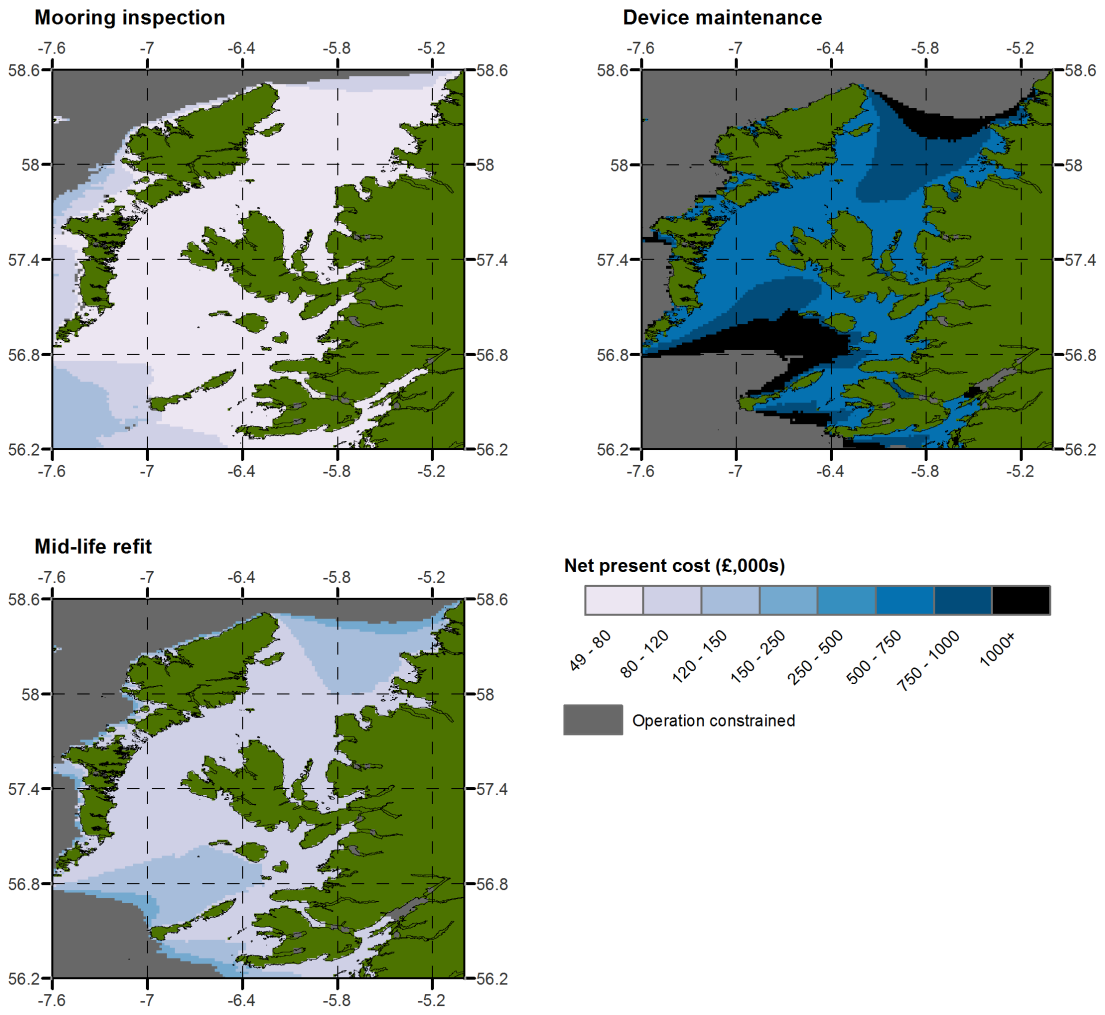

Figure 5.8: Planned O&M costs by task.

waiting times associated with operations are low. The main factor in these areas can actually be the transit weather window, as the time to get to the locations can be more significant than the time to perform the task. The mooring inspection is generally low, with a minimum of £50,000 over the 20 year lifetime. The reason for this is that the task is carried out on site, and is not subject to the same amount of waiting as the other two tasks which require long weather windows for towing the device to and from port. The mid-life refit is also fairly low. The bulk of this is in the replacement parts, although they are heavily discounted to reflect the timing of the operation in the project. The device maintenance is the dominant cost factor. This is mainly due to the fact that it occurs bi-annually, hence requires more days of charter and waiting. The waiting time is high as the device needs towed to and from port. This aspect also heavily constrains the western part of the domain.

The very high planned O&M costs for the device can be attributed in part

to the fact that a vessel was specified for each WEC in the array (as mentioned in Section 5.2.1.6 above, using the `vessel_per_quantity` attribute). This means that the mobilisation and demobiliation costs for the device operations are six times higher than if a single vessel was used, and the charter cost is also higher due to the way that it is rounded. While essentially having one vessel for each array unit is unrealistic, the case study is purely designed to demonstrate the model. Due to the other high system costs, it does also not impact the overall picture significantly.

5.2.3.3 LCOE

The final LCOE calculated across the domain is displayed in Figure 5.9. This is the total energy from Figure 5.5 divided by the total NPC from Figure 5.6. It can be seen that the values are very high. The lowest LCOE in the domain is £2.57/kWh, over twenty times more expensive than offshore wind and much

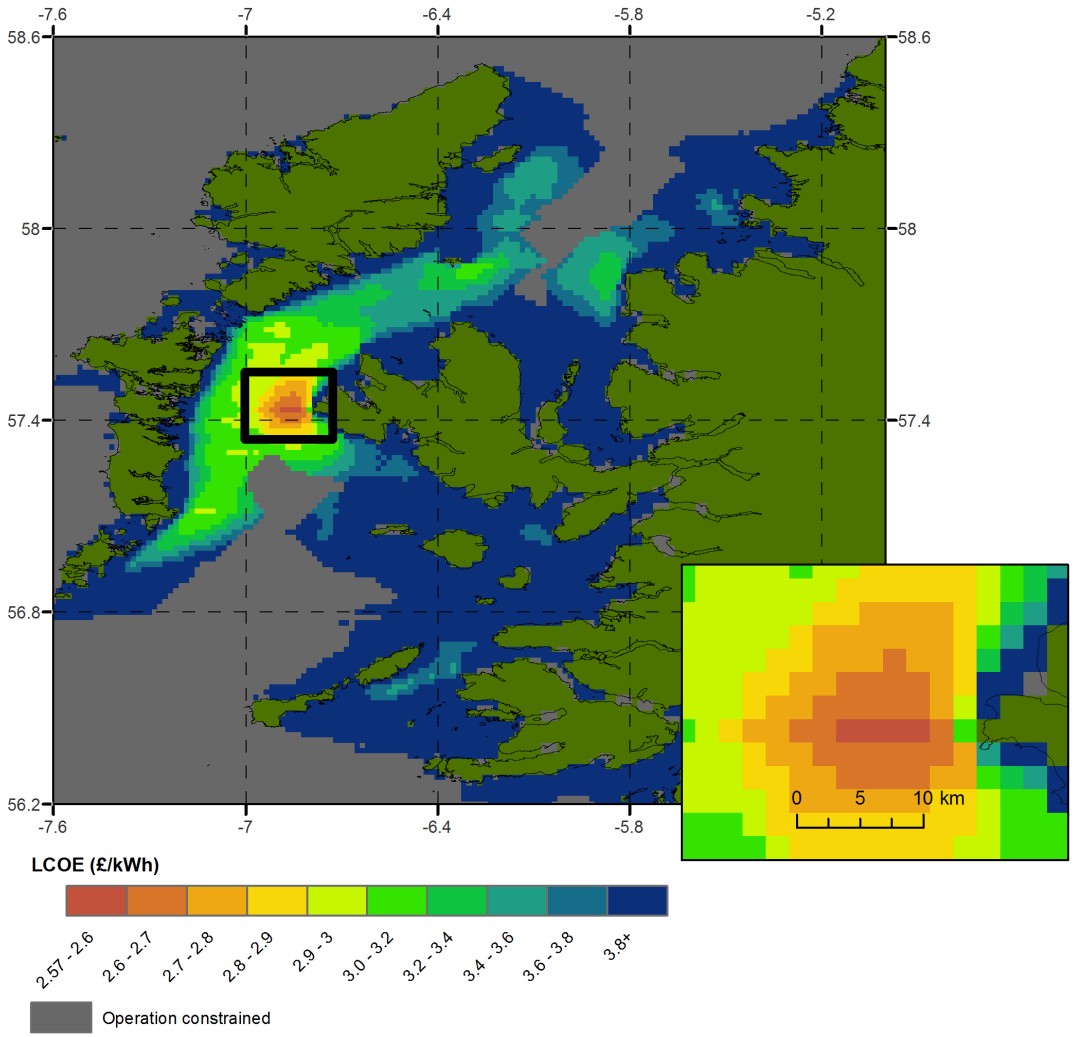

Figure 5.9: LCOE across the domain for the baseline scenario.

higher than the LCOE values that have been calculated in the literature (see Section 2.4.1). The latter can be explained because the baseline considers an early demonstrator project whereas the literature tend to consider large commercial scale devices and projects (tens or hundreds of MW). As the analysis contains some simplifications, for example the unplanned OPEX cost and nearest path to shore for the export cable, there is the possibility that some locations could see higher LCOE in reality.

One major hotspot can be seen, in the Little Minch. This location combines decent energy production with lower spatial costs, a benefit of the nearshore and relatively sheltered site. This reduces the large OPEX cost. The inset figure highlights the large spatial variation that is seen, even on very local scales. Moving the device 3-5 km into the straight can reduce the LCOE by 2-4 times. This really underlines the advantages of the method as a means of site selection, informing locational decisions in a way that conventional studies have been unable to achieve.

There are a few other areas which could hold future promise. They include the south west of South Uist, the south east of Garbh Eilean in the Minches and off the mainland at Melvaig. All of the hotspots share a common trait: they are close to the coastline. While the energy producing potential is decent in the north west and south west of the domain (Figure 5.5), they cannot be accessed for operations. A different operation schedule, combined with a larger device concept to exploit the long period waves, would likely be better suited here.

Section 5.3 expands on these baseline LCOE results by examining sensitivities in different yield and cost drivers.

5.2.3.4 Constraints

Figure 5.10 demonstrates the deployment constraint functionality, laying them over the LCOE results from Figure 5.9. From the four original constraints, eleven unique categories were identified across the domain (four plus seven combinations of constraints). These have been combined in one of the maps within the figure, to improve clarity. From the combined map it is clear that the majority of constrained deployment locations exist in the south west of the domain. This includes South Uist, almost completely excluded by deep water and rocky locations to the west, the west of Tiree and most of the area surrounding Canna and Rum. This latter area lies within a large marine SPA, also containing shallow and deep areas and rocky seabed to the west. Also in the very south west is a large deep trench, although this is located relatively far from the shore and does not coincide with any of the lower LCOE areas. Over the whole domain there are scattered

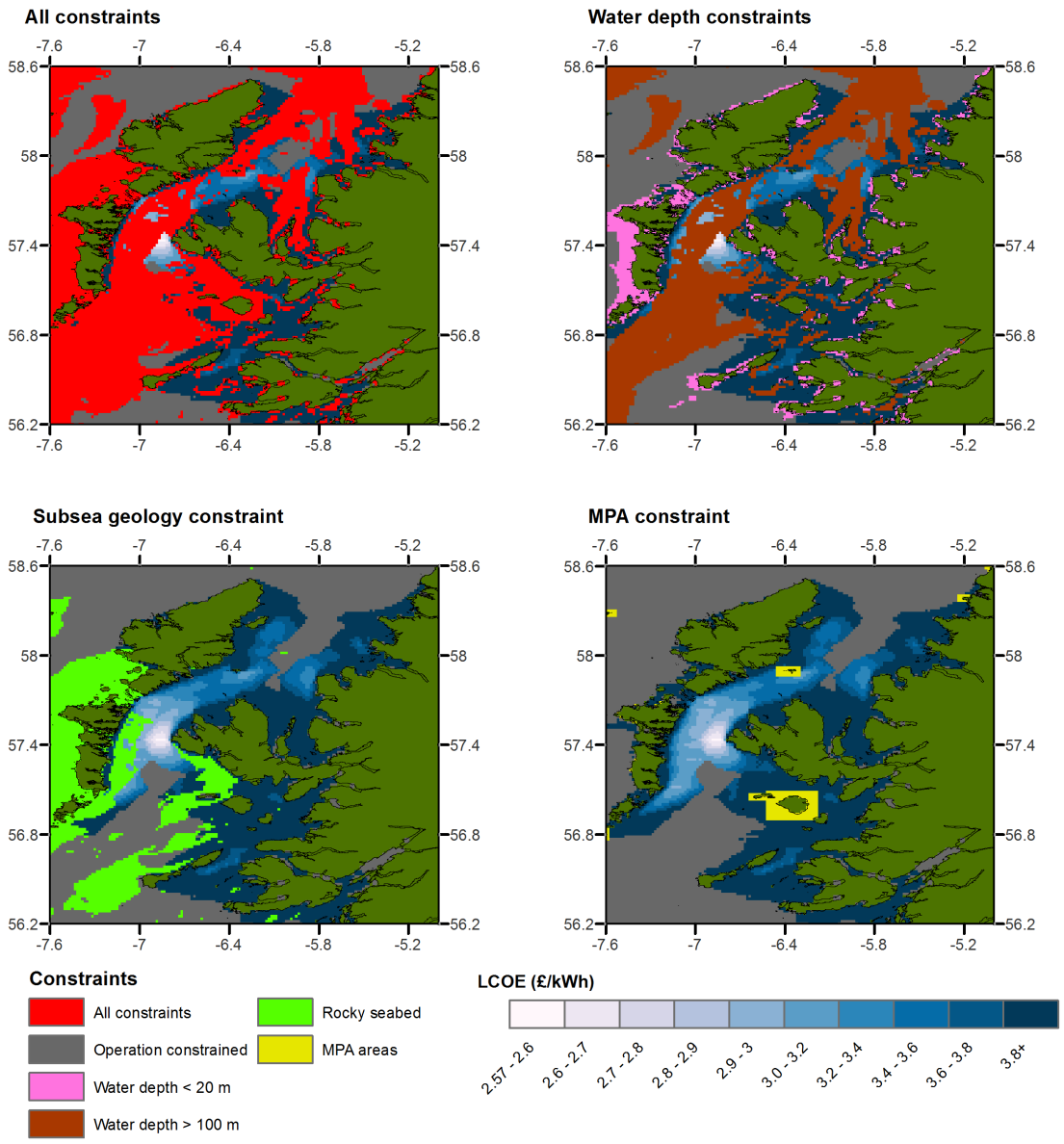

Figure 5.10: The deployment constraints applying to the baseline scenario. The four initial constraints resulted in eleven unique constraint categories: the original four plus seven constraint combinations. These have been combined together for the top left map. The LCOE results from Figure 5.9 are shown underneath, to show how the more economically promising areas would be affected.

areas of shallow water. These tend to be in very sheltered areas where energy production is poor so, like the deep trench, do not encroach very much on the more economically viable locations.

The most significant constraint, other than due to operation time as already discussed, is the deep water constraint. This encroaches on the hotspot in the Little Minch, limiting the potential options for deployment. Unlike the shallow water and rocky seabed constraint, the 100 m water depth limit was somewhat arbitrary in nature. Relaxing this, even slightly, could give more options.

5.3 Sensitivity Analysis

To demonstrate the applicability of the model for more in-depth study of the LCOE drivers, sensitivity analysis was conducted. A smaller area of the domain was considered; this decision was taken to reduce the computation time over the large number of runs required. It excluded the southern part of the domain, shown in Section 5.2.3 to be less suitable from both an LCOE and constraint perspective.

Nine sensitivities were chosen, summarised in Table 6.5, with each examined individually to assess the relative impacts and allow comparisons between them. They are organised into three sub-sections. The first three sensitivities are related to the energy production: the power producing H_s limits of the device and the number of PTO units equipped. The next three are concerned with the operations, a large cost component, and required multiple parameters to be varied. The final three cover the discount rate, reduction in the device CAPEX due to learning and export cable CAPEX.

Sensitivity	Values	Section
Cut-in H_s (m)	0.25, 0.5, 0.75	5.3.1.1
Cut-out H_s (m)	No cut-out, 6.5, 6.0	5.3.1.2
PTO quantity	1 to 8	5.3.1.3
Task duration (h) and H_s threshold (m)	See section	5.3.2.1
Using Albatern's workboat	See section	5.3.2.2
Single device intervention per year	March, September, June, July	5.3.2.3
Discount rate (%)	6, 8, 12	5.3.3.1
Array CAPEX (£)	293,000 to 477,000	5.3.3.2
Export cable CAPEX (£/m)	30, 40, 50	5.3.3.3

Table 5.8: The nine sensitivities that were used for more detailed examination of the spatial variations.

5.3.1 Energy considerations

5.3.1.1 Cut-in Hs

Figure 5.11 shows the increase in LCOE of introducing three different cut-in H_s values. While in reality this might be hard to design for, being a property of the

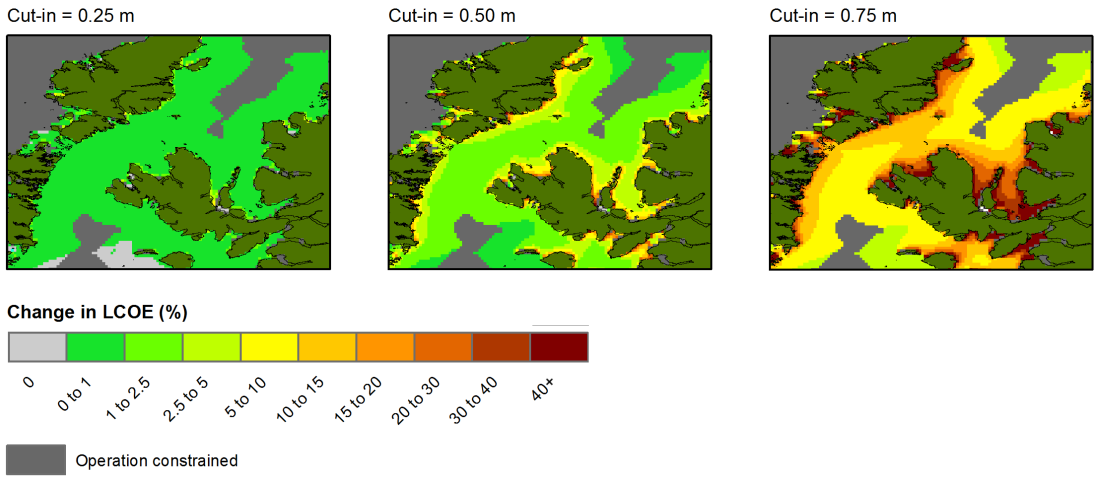

Figure 5.11: The change in LCOE from the baseline after applying three different cut-in H_s limits. Larger change is seen for higher cut-in and in the sheltered areas, as would be expected.

PTO system architecture, the model allows an acceptable limit to be quantified for particular locations. It should be noted that the cost associated with redesigning the device to change the cut-in limit has not been included, the change is purely a theoretical one that examines change in energy only.

At 0.25 m cut-in there is very little change over the domain, with the LCOE increase typically less than 1%. In some of the more exposed locations the change is closer to 0%, as such a small amount of energy comes from the excluded seastates. Increasing the cut-in to 0.5 m sees an increase, as would be expected. This is especially apparent in the sheltered areas, some of which see energy reduction exceeding 20%. The Little Minch hotspot is minimally affected, with increase typically less than 2%. This is increased to around 8% for the 0.75 m threshold. This implies that a significant amount of energy, approximately 6%, is coming from waves between 0.5 m and 0.75 m H_s. The LCOE increase is widespread in the sheltered areas, with a visible amount over 40% higher than the baseline. However, as the LCOE was poor in these areas for the case study, it is of lesser consequence.

5.3.1.2 Cut-out Hs

The cut-out sensitivity, shown in Figure 5.12, sees much less variation than the cut-in over the domain. This is because the majority of energetic, high H_s sites have already been filtered out by the planned operation time constraints. Removing the cut-out limit of 7.0 m sees a very small reduction in LCOE of less than 1%. Having no cut-out was the behaviour of the Pelamis device, which was designed to ride out high energy seastates at its rated power.

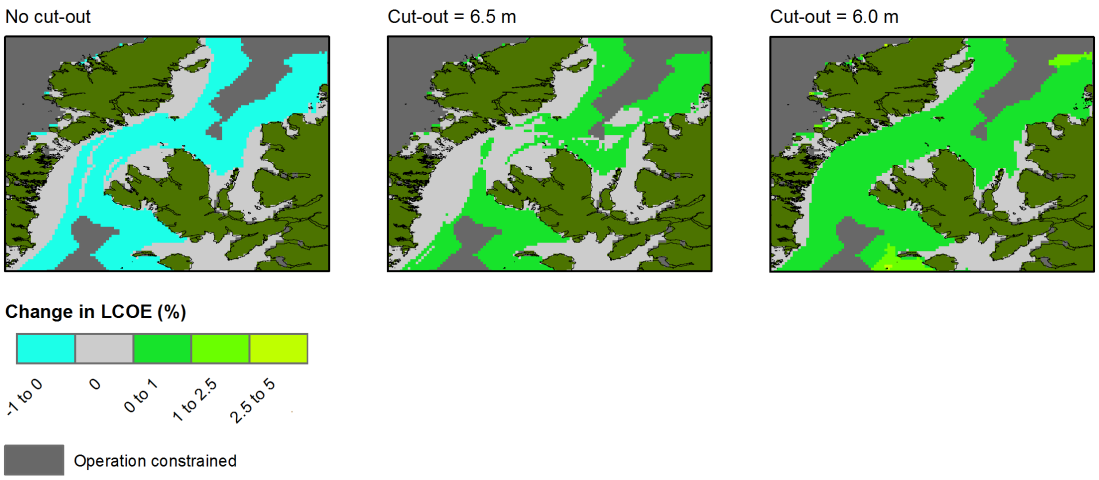

Figure 5.12: The change in LCOE for three cut-out limit cases, the leftmost after removing the baseline limit of 7.0 m and the other two at more extreme cut-out values.

Applying cut-out values of 6.5 m and 6.0 m sees a marginal increase in LCOE, typically 1% although some of the sites out to the west approach a 5% increase at the 6.0 m threshold. At the Little Minch hotspot the reduction seen does not exceed 1%, due to the relatively sheltered nature of the water.

These results imply that the cut-out threshold is a low cost driver for the demonstration case study, and would not have a significant negative impact if the survivability limit was lowered to the values chosen. However this is not the full picture, as for a real device there would be cost implications for the survivability limit. For example, one way that this behaviour could be achieved in practice is by fitting the WaveNET with buoyancy modules. These would fill with water and submerge the device in storms to protect it from extreme wave loading. This would increase CAPEX, potentially raising LCOE further for the 6.0 m and 6.5 m thresholds, however this could be offset by lower insurance premiums or reductions in unplanned maintenance cost. These kind of cost implications and design changes are not considered in this section, as for the cut-in in the previous section, but could be examined by the model if such conceptual design was undertaken.

5.3.1.3 PTO quantity

As stated in Section 5.2.1.1, each Squid can be equipped with between zero and three PTO generators. This means that the 3-Hex array can hypothetically be rated between 7.5 and 90 kW, carrying one to twelve PTO units. As well as the CAPEX contribution from the PTO units, the midlife refit cost was also modified to account for this. Having more PTOs also adds redundancy to the system, improving system reliability. This effect has not been examined due to

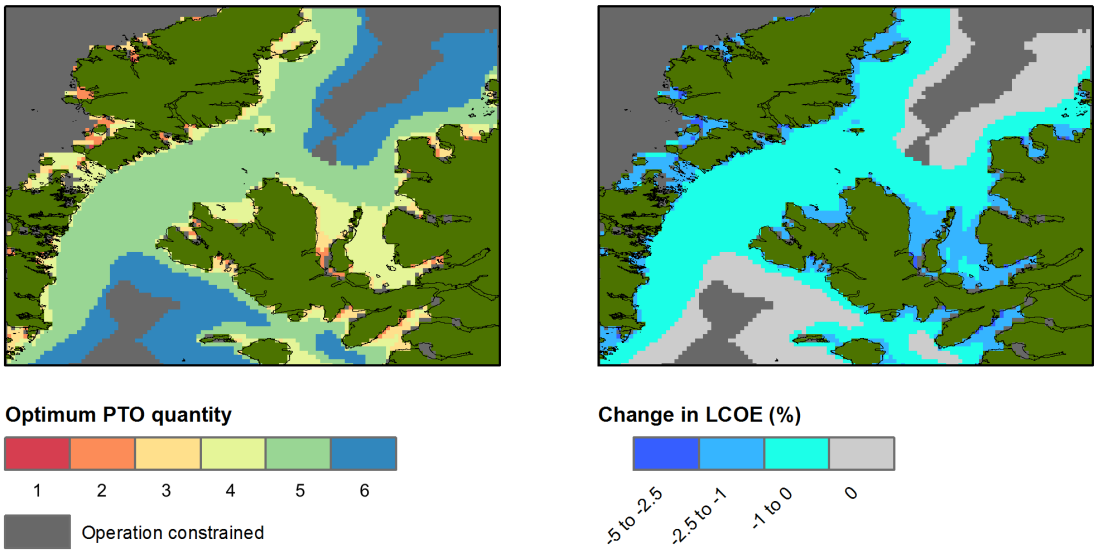

Figure 5.13: The optimum PTO quantity across the domain and the associated reduction in LCOE. The most significant changes were seen in the more sheltered regions, with no site benefiting from more than six PTO modules.

the lack of data and unplanned O&M analysis in the model.

It is clear that the PTO quantity is a design parameter that could be optimised for the location. At sheltered locations lower PTO numbers will be preferable to save cost, as the device will be operating below its rated power for much of the time anyway. The opposite is true at more exposed sites.

The analysis was performed for one to eight PTO units. PTO quantities above eight were not examined as the device is only able to generate power above 60 kW at very few, generally uncommon, sea states. From the results, the minimum LCOE and corresponding PTO quantity was found for each location. This optimum quantity and the decrease in LCOE from the baseline of six PTO units are shown in Figure 5.13. In the figure only PTO quantities of one to six are displayed. This is because the seven and eight PTO configurations were unable to produce the cheapest energy anywhere in the domain, the additional energy produced cancelled out by the extra PTO CAPEX. The optimum PTO quantities tend to be five or six over the domain, with some of the particularly sheltered areas seeing LCOE reductions of up to 4% using fewer PTOs. The top and bottom of the Minch rely on the more extreme seastates for enough of their power to warrant using six PTOs; this is not the case for the Little Minch where five PTOs tends to be the optimum. This implies that only a small amount of energy is coming from elements above 37.5 kW in the power matrix, not enough to justify the cost of an extra PTO. Something interesting to note is the small area to the East of Rum where six PTOs are optimal. This is likely due to local focussing

effects of the terrain, which means that a significant proportion of the energy is coming from seastates in the top left of the power matrix, above 37.5 kW.

5.3.2 Operational considerations

5.3.2.1 Task duration and access thresholds

To demonstrate the sensitivity of the baseline to the planned O&M task parameters, the task duration and H_s access threshold were varied. The timescale was varied by -50% and +200% and the threshold by -33% and +33%. These arbitrary values, summarised in Table 5.9, reflect the wide range of uncertainty due to limited operating experience. The low H_s threshold and high task time represent the pessimistic case.

Adjustment	Device deployment		Device recovery		Mooring inspection	
	H_s (m)	Time (h)	H_s (m)	Time (h)	H_s (m)	Time (h)
Low	1.0	1.0	1.0	1.0	1.0	1.5
Baseline	1.5	2.0	1.5	2.0	1.5	3.0
High	2.0	4.0	2.0	4.0	2.0	6.0

Table 5.9: The lower and higher H_s thresholds and task durations considered for the sensitivity, as well as the baseline for comparison.

Figure 5.14 shows the change in LCOE for the nine parameter combinations. Examining the H_s threshold rows, at the baseline task time there is large impact on the LCOE; for the Minch hotspot this is between 5 and 10%, reaching 20-30% for the more exposed areas. Some of the sheltered areas see little or no change, as there are very few sea states above the H_s threshold. In the optimistic case the biggest reduction in LCOE is found to the west of Lewis and Harris, with some sites in the extremities seeing 10-11% decrease. The Little Minch is only marginally affected, reinforcing the fact that access to this region is not a significant cost driver for the case study. The task timescale parameter has much less impact on the LCOE. At the baseline H_s, the difference between the pessimistic and optimistic is only about 2% for locations in the Little Minch. In the more exposed parts of the domain there is larger variation seen, for example the area to the South of Canna sees a swing of about 5%. In general the task timescale parameter has a greater effect at the lower H_s threshold; this implies that the lower accessibility condition is more sensitive to the length of operation. The domain also slightly shrinks in the north of the Minch as the task time is

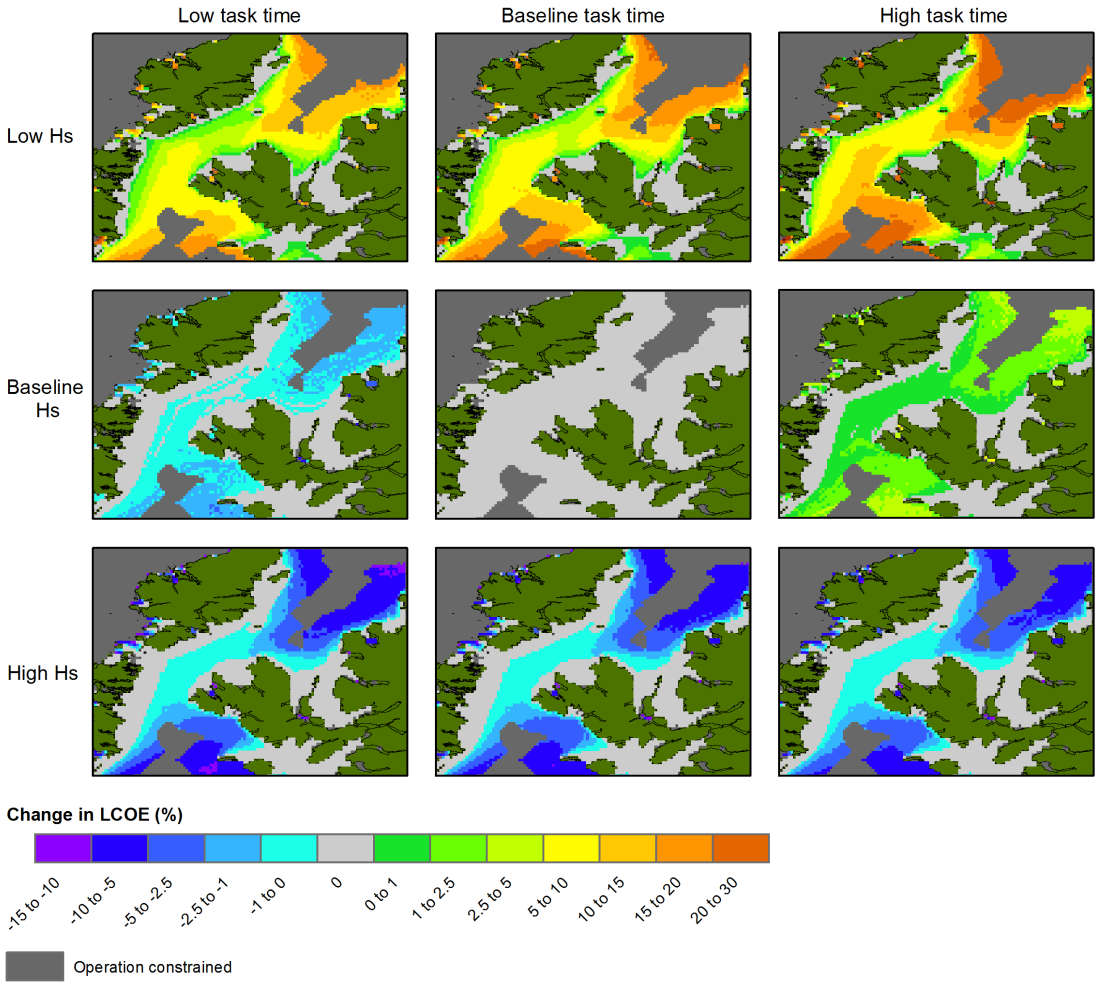

Figure 5.14: The change in LCOE from the combinations of task duration and H_s threshold. The low H_s and high task time is the most pessimistic scenario (top right), with the high H_s and low task time the most optimistic (bottom left).

increased.

The difference between the optimistic and pessimistic cases is emphasised further in Figure 5.15. These are plotted using the same colour scale as the baseline scenario from Figure 5.9. While the optimistic looks broadly similar, with some reductions visible to the north and south of the main hotspot, the pessimistic case is very different: in terms of both the range of colours seen and domain size.

5.3.2.2 Vessel ownership

Rather than chartering a workboat, this sensitivity considered using the smaller vessel owned by Albatern to perform all of the operations except the export cable installation. This is an 8 m length workboat, with three people to perform the task. Table 5.10 summarises the properties of this vessel. The advantage of using this vessel is its low cost. Its disadvantage is that is it slower

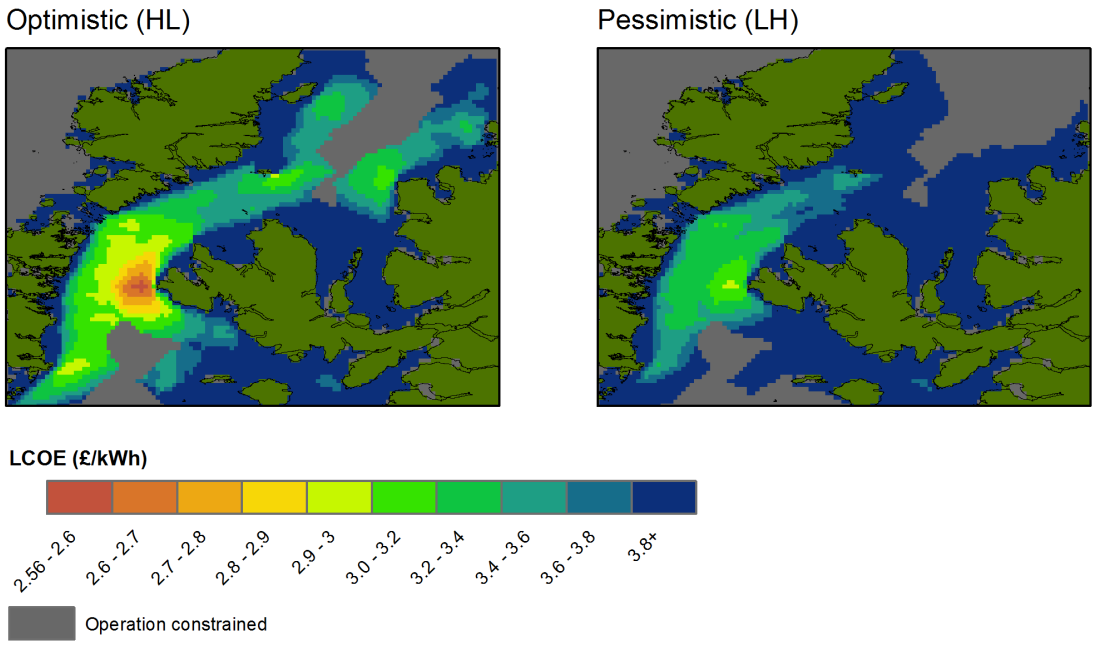

Figure 5.15: Absolute LCOE for the most optimistic and pessimistic cases from Figure 5.14. The optimistic sees slight expansion of the hotspot areas, in contrast to the pessimistic where the domain shrinks.

and less stable at sea than the workboat considered in the baseline, hence lower H_s thresholds have been applied. No additional costs for vessel upkeep or maintenance have been applied as the data were not available, although would have been compatible with the model framework.

Type	Speed (kt)		Charter (£/day)			Hs limit (m)		Fuel (l/hr)
	Transit	Tow	Work	Standby	Mob	Transit	Tow	
Albatern workboat	6	3	300	300	0	2.0	1.0	40

Table 5.10: Modelling properties set for the vessel owned by Albatern.

The day rate is approximated as the wage required by the three members of staff, also incurred in standby. It was assumed that the fuel rate was the same as the baseline workboat, with the H_s limits chosen to reflect Albatern's operating experience. The impact of task time on the operation was also considered. As the workboat is smaller it provides a less stable platform for operations, meaning that tasks might be expected to take longer. Three different task times were considered: the baseline, 150% of the baseline and 200% of the baseline.

Figure 5.16 shows the absolute planned OPEX and the change in LCOE for the three task times. Comparing the planned OPEX with the baseline category from Figure 5.7 two things are apparent. The first is that the domain is significantly

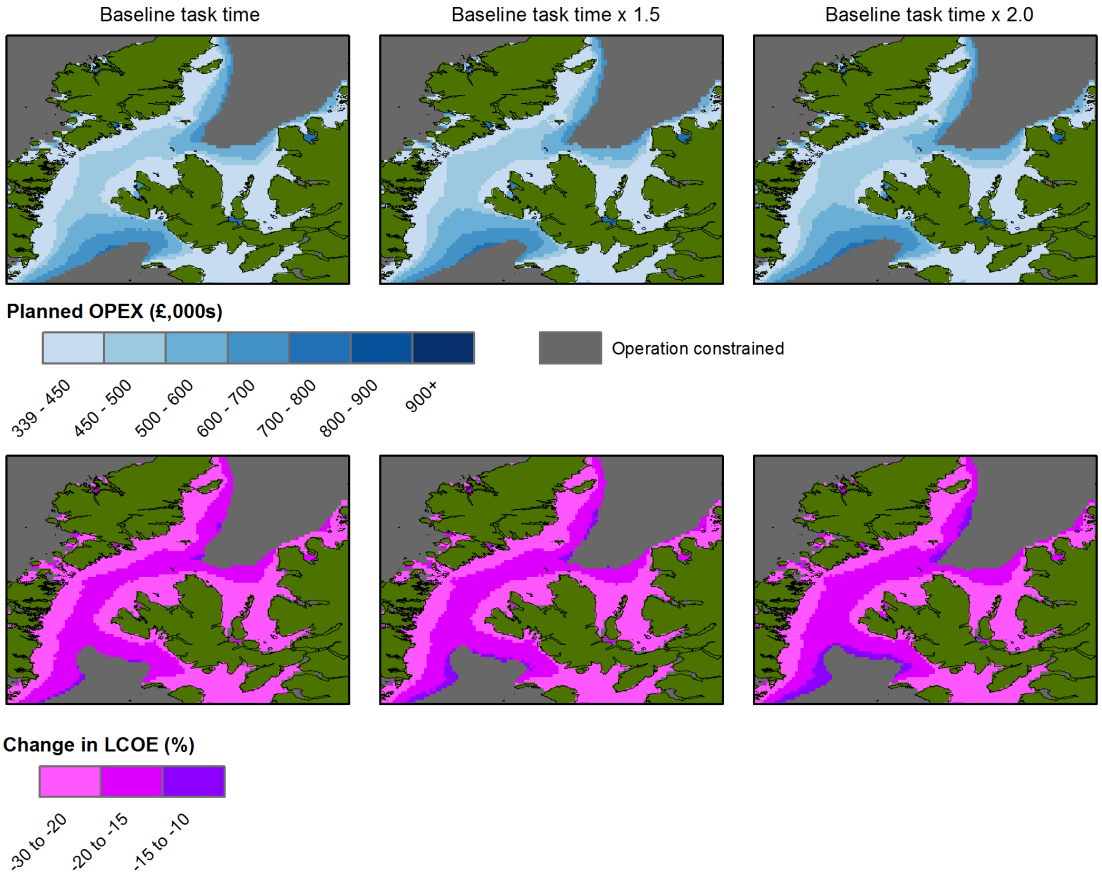

Figure 5.16: Impact of using Albatern's workboat for device installation and operations instead of chartering one.

smaller, the constrained areas cutting into the Minch from both north and south. Areas like the south west of Rum and north west of Melvaig are now barely accessible. The second is that the absolute cost values are far lower in the still accessible areas, including the Little Minch hotspot where the planned OPEX has gone from over £750k to under £450k. This effect is due to the lower costs associated with the vessel, which reduced the LCOE by over 15% across the majority of the valid domain.

There is very little visible impact of increasing the task time. The maximum increase in LCOE seen was 2.3%. This supports the results from the previous section. The general approach of using existing vessels is to improve the situation in the sheltered areas at the expense of exposed ones. As the main hotspot is part of the former, the overall impact can be thought of as a net benefit.

5.3.2.3 Single annual device intervention

For this sensitivity, the planned O&M routine for the device was reduced to a single operation per year. As this cost was one of the most significant factors

for the baseline (see Section 5.2.3.2), this is the kind of hypothetical improvement which could be inferred from using the model.

Four different months were examined: March and September, as used previously, and June and July. To keep consistency within the maintenance schedule, the mooring inspection and midlife refit operations were also scheduled to the same month.

Figure 5.17 shows the total planned OPEX and the change in LCOE from the baseline for each month. Looking at the March and September results, now decoupled from the baseline, it is apparent that the March operation was the larger contributor to cost. The magnitude of LCOE reduction is lower than September and less variable over the domain. The September intervention sees larger LCOE reduction, especially near the fringes of the domain. The planned OPEX cost shows that it is also less constrained to the west and the top right. However this benefit is not seen in the final LCOE results, largely due to the constraining effect from the installation (as can be seen from the shape of the installation component in Figure 5.6).

The June and July intervention months see significantly lower planned OPEX costs to the west of Lewis and Harris as would be expected. The full domain is also accessible. For the planned OPEX the lighter areas coincide with the port locations, again as expected due to the shorter weather window required for transit and lower vessel fuel costs over the lifetime. In the Little Minch there is marginal difference between the September, July and June cases. September is slightly better around the hotspot location, driven by fewer waiting days.

To get an appreciation of the change in LCOE and domain size, the absolute LCOE for July is displayed in Figure 5.18. The domain is slightly larger out to the west in this case, now constrained by the installation activities. While there is a green band out to the west of Lewis and Harris, the LCOE is still relatively high compared to the Minch.

5.3.3 Other considerations

5.3.3.1 Discount rate

The sensitivity of the baseline LCOE to discount rate was explored by examining three additional values: 6%, 8% and 12%. The lower values would typically be reserved for more mature technologies (as noted in Section 2.3.1) and so are included purely on a hypothetical basis.

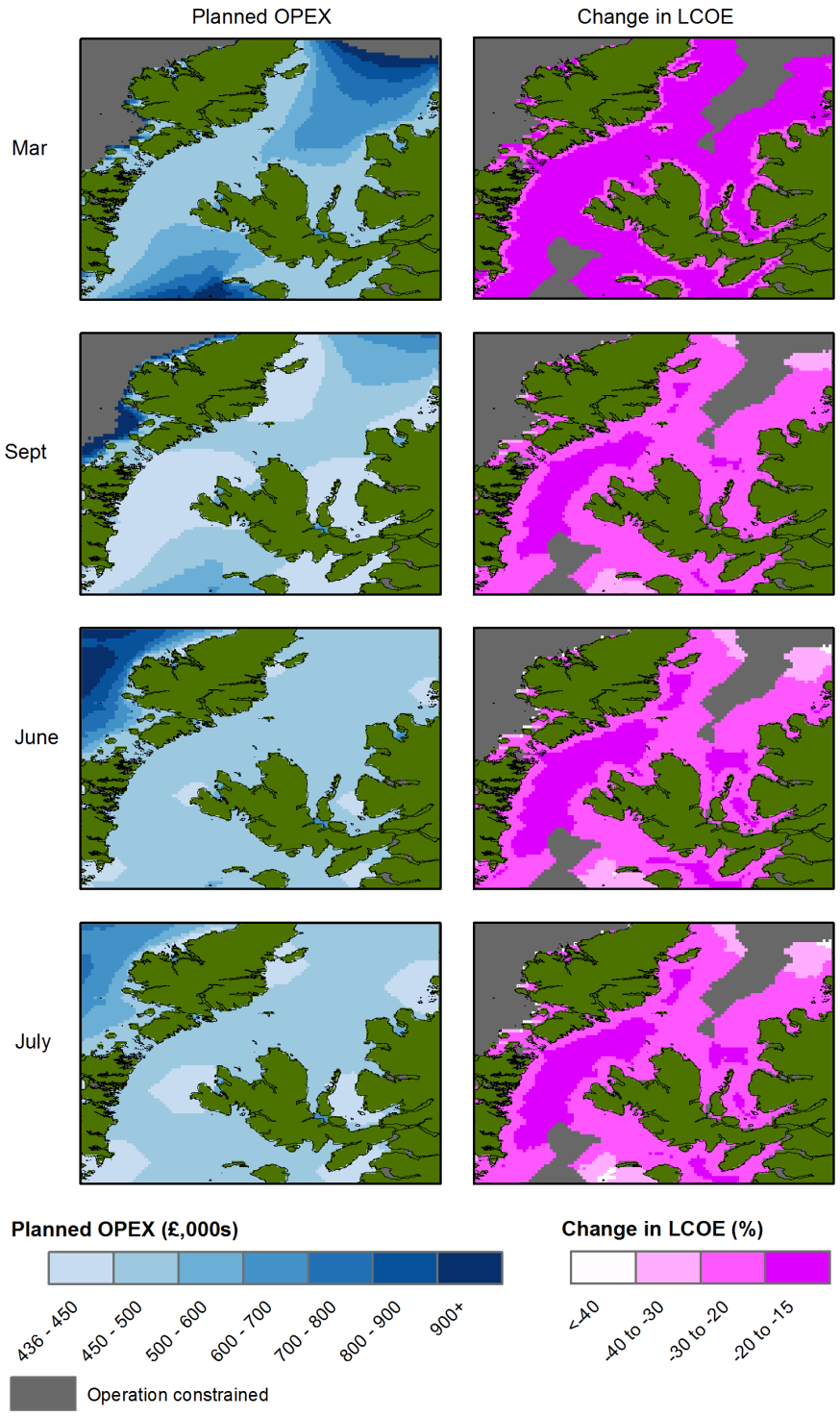

Figure 5.17: The absolute planned OPEX and the change in LCOE from the baseline for the four single intervention scenarios.

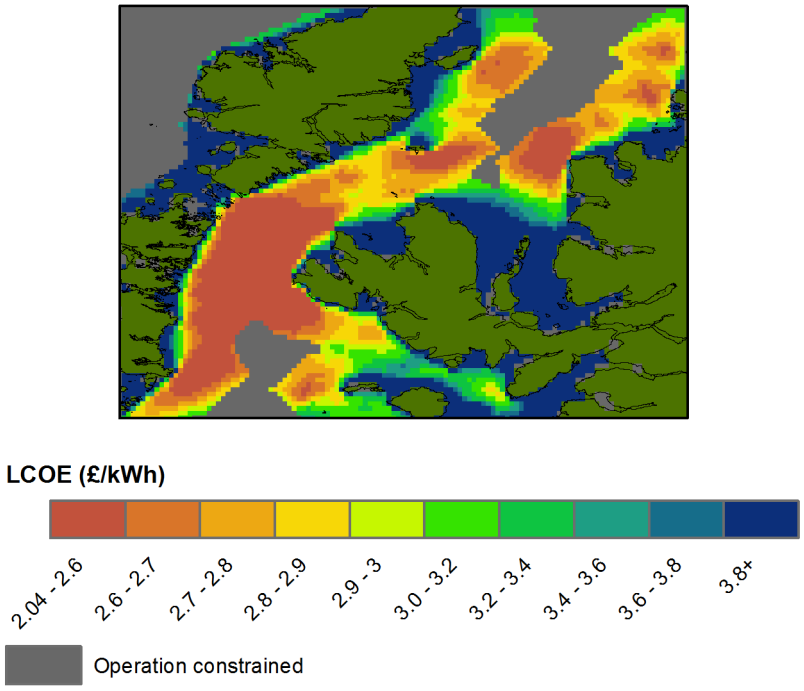

Figure 5.18: The absolute LCOE considering a single annual intervention in July. This is plotted using the same colour scale as the baseline scenario in Figure 5.9

Looking at the changes in LCOE in Figure 5.19, moderate impact on the LCOE can be seen. While there can be subjectivity in the value selected for a LCOE analysis (see Section 2.3.1), across these values the LCOE is still far too high to be competitive with more conventional energy sources and so would not influence the investment decision. Because both the energy and OPEX costs are discounted equally, the change is relatively uniform across the domain. Points closer to the shore, where CAPEX costs are more dominant, generally see a lower

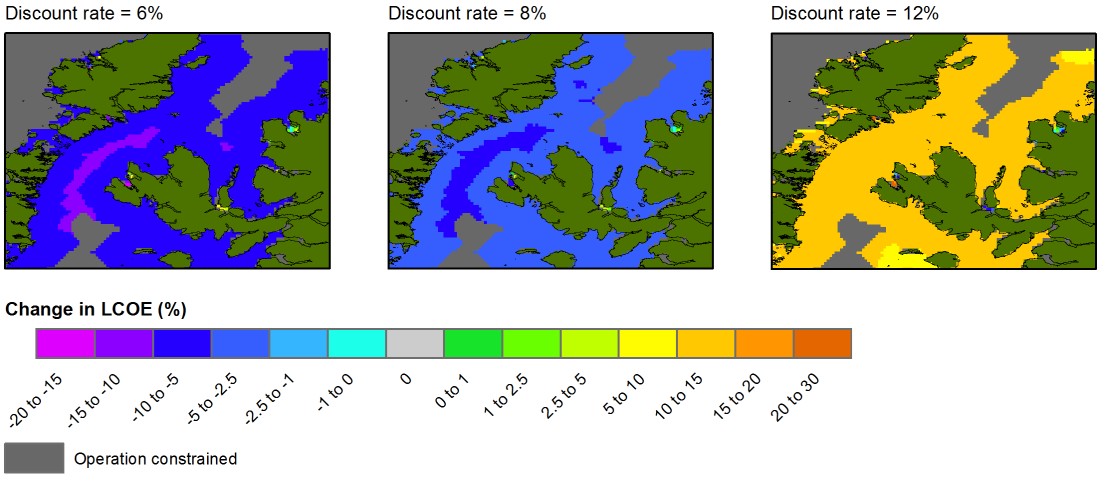

Figure 5.19: The impact of three different discount rates on the baseline LCOE, originally calculated at a discount rate of 10%.

change in LCOE. It should be noted that there are some erroneous points visible in these maps in some of the sheltered regions (for example on the west side of Skye). Here the trend is the reverse that would be expected. The reason for this is due to very low energy yield, which when discounted tends to zero, combined with relatively high OPEX costs due to poor fitting of the Weibull parameters for the very low H_s values. These close to shore locations are very LCOE anyway so the anomalies are not considered further.

5.3.3.2 Device capital cost

As the early stage technology is particularly capital cost intensive, it might be expected that reducing this could see large improvements in LCOE in the near future. This was investigated by scaling the device CAPEX according to two learning rates: 10% and 15%. These are values commonly considered in the literature and reflect the learning rates seen historically in other technologies (see Sections 2.2).

A total of six cost scenarios were examined, considering learning-based reduction after manufacturing one, three and five 3-Hex devices. Learning was applied on the basis of three unit batches of Squids, rather than for single Squid units, as this is the production cycle that was followed for the first six units. Table 5.11 summarises the new array CAPEX values. The cost reduction was also applied to the midlife refit replacement costs.

Learning rate (%)	CAPEX (£)		
	Next device	Third device	Fifth device
10	452,261 (235,386)	382,706 (199,188)	354,114 (184,302)
15	427,135 (222,312)	330,139 (171,828)	292,874 (152,430)

Table 5.11: The six different array CAPEX costs that were examined. The cost reductions were also applied to the midlife refit replacement cost, shown in brackets.

The changes in LCOE due to the CAPEX decrease are shown in Figure 5.20. Both of the learning rates examined see significant LCOE reduction by the fifth 3-Hex device, a maximum of 16.7% seen for the higher rate. The magnitude of decrease tends to be higher in the sheltered regions; this is because at the locations the device CAPEX makes up a larger proportion of the discounted cost. There is visible difference between the learning rates, even for the next device where the higher rate leads to reduction of up to 2.2% over much of the domain.

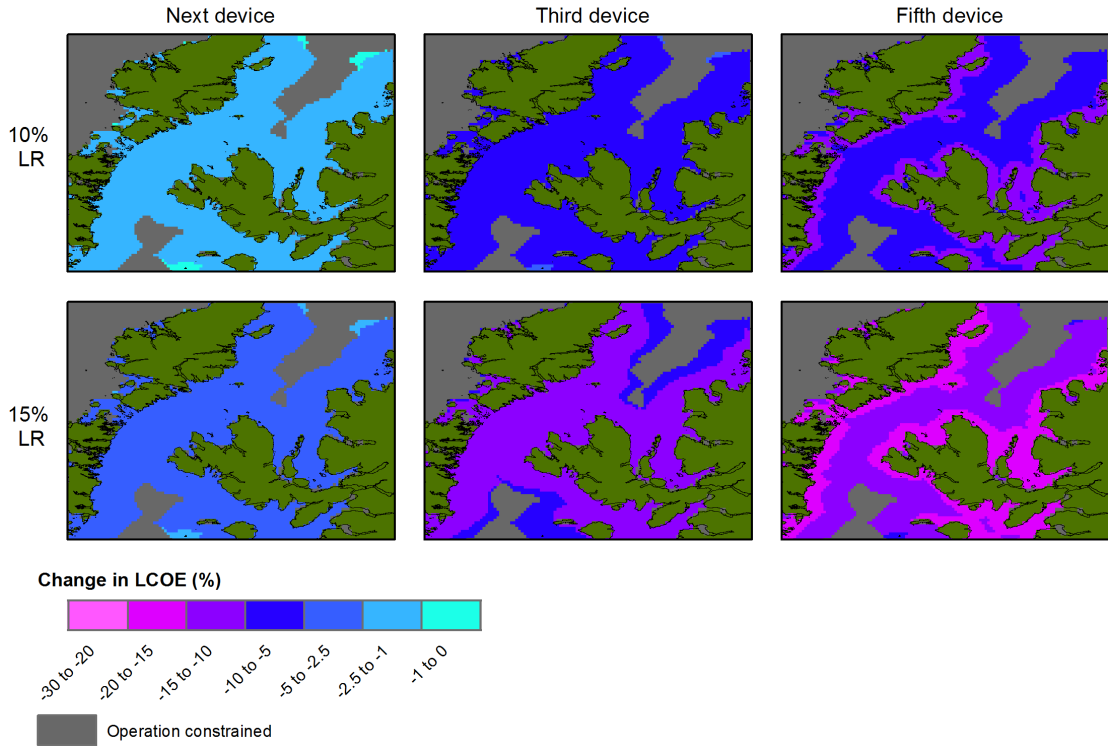

Figure 5.20: Change in LCOE for the six different device CAPEX values considered, obtained from applying learning rates.

5.3.3.3 Export cable capital cost

Figure 5.21 shows the impact of export cable CAPEX on LCOE. Three higher cost values were considered, chosen arbitrarily using the baseline cost estimate as a basis. No lower cost values were examined as the baseline was already deemed to be optimistic (see Section 5.2.1.3). The cable installation was also kept the same as the baseline in all the cases. In reality, more costly and heavier cables might require different cable installation equipment and take longer to install, however these aspects are not considered. Increasing the cost by 50%, to £30/m, sees modest increase across the domain. As would be expected this change is greater for the locations further from shore, seeing LCOE increases of up to 10%. At the Little Minch hotspot the increase is generally less than 5%. As the cost increases this becomes much more significant, exceeding 10% over most of this region. The nearest distance to shore assumption means that this is optimistic compared to reality. The value would be higher still as the cable would need to route around seabed obstacles. One way that a higher cost could be offset is by increasing the number of units, and hence rated capacity of the array, provided that the cable capacity was sufficient. Such a project, with a higher capital cost, would be more difficult to finance.

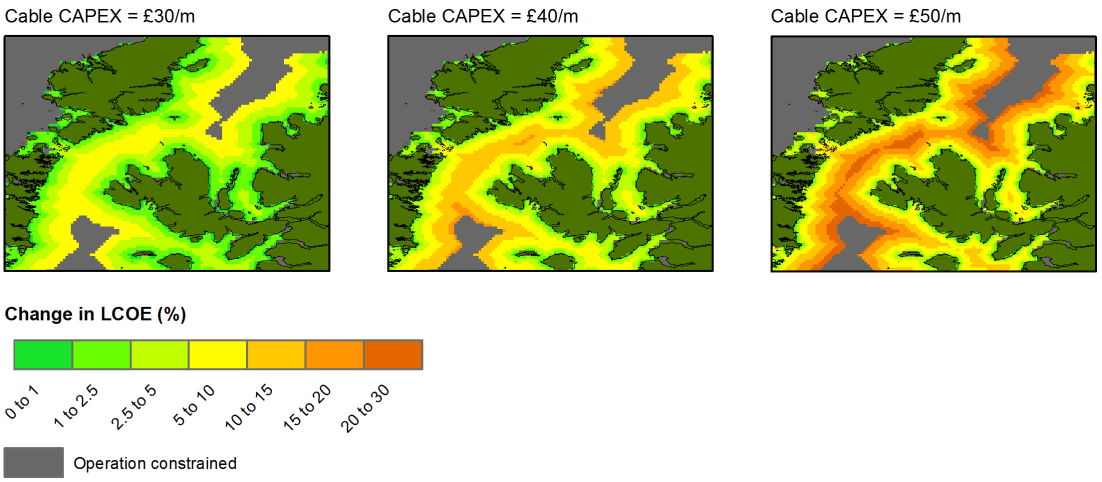

Figure 5.21: The change in LCOE from the baseline for the three new cable CAPEX values considered.

5.3.4 Optimistic combination of sensitivities

While some of the sensitivities in the previous sections showed significant LCOE reduction, the absolute values are still very high. It is apparent that in reality it would take more than one improvement to yield acceptable LCOE.

A short term "optimistic" scenario was modelled, combing four of the positive sensitivities:

- A single intervention, occurring in July.
- Usage of Albatern's vessel, with no impact on task timescale assumed.
- A discount rate of 8%.
- A CAPEX learning rate of 15%, after ten batches of three unit (1-Hex) devices.

These are all sensitivities which, based on the baseline assumptions and previous results, could be deemed as short term targets for improving the LCOE outlook. As for the previous scenarios, this optimistic case is hypothetical and is to illustrate how the model can be used to asses future technology potential. Hence, the financing or research steps required for these improvements to be realised are not examined.

The absolute LCOE and the change from the baseline are presented in Figure 5.22. The four sensitivities can be seen to create a large reduction in the LCOE, by over 50% over much of the domain. In the Minch the areas closer to shore see greater proportional decrease, mainly because the unchanged cable cost is a lower proportion of the overall system cost. The Little Minch region to the

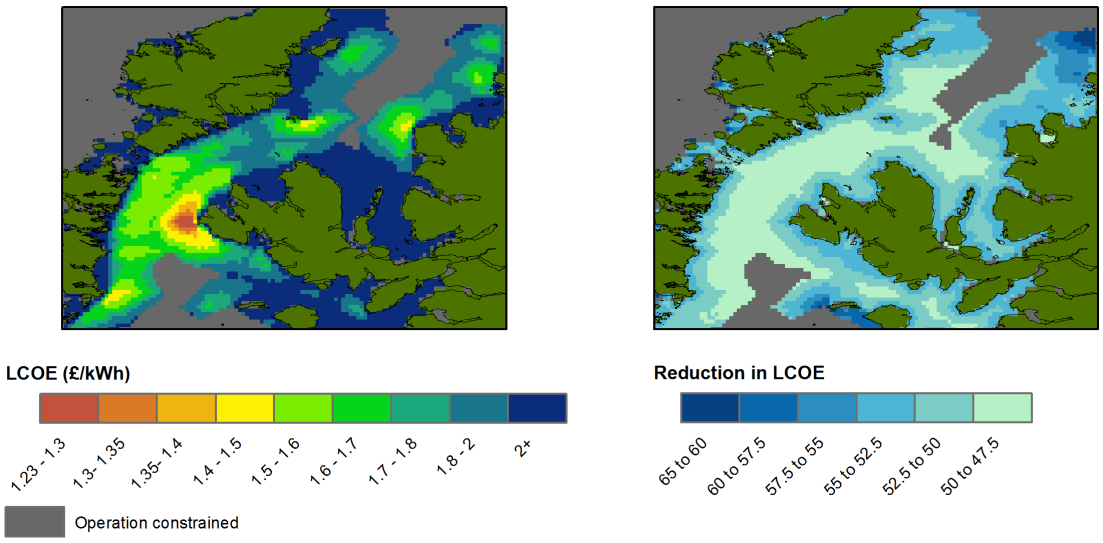

Figure 5.22: The absolute LCOE of the optimistic scenario and change in LCOE from the baseline. Note that both are plotted with different colour maps scales to those seen previously.

East of Skye is still the lowest LCOE region at £1.23/kWh. This is because the starting point was significantly lower than other regions, as the change in LCOE is relatively modest compared to some regions on the map. Hotspots at Garbh Eilean and the west coast at Melvaig are also present, the sensitivities combining to offer large LCOE reduction. Some of the more exposed locations see large LCOE reductions, approaching 65%. However, as these exhibited relatively high LCOE in the baseline case, it is not enough for them to become competitive with the low LCOE regions mentioned.

5.3.5 Summary

The sensitivities that have been presented are compared in Figure 5.23. This shows the lowest LCOE values that were calculated over the domain for each individual simulation within each sensitivity. Including the baseline, 42 unique simulations were run in total: the 41 introduced in Table 6.5 and presented in Sections 5.3.1 to 5.3.3, and the optimistic combination of four sensitivities presented in Section 5.3.4. It should be noted that only the lowest LCOE values are compared, not the wider values across the domain from applying the specific sensitivity. This is deemed a logical parameter for a summary comparison, as in reality a wave developer will be most interested in the lowest LCOE attainable. Table 5.12 accompanies the figure, showing which specific simulations correspond to the points.

Figure 5.23 shows that the optimistic combination causes the largest reduction in lowest LCOE by some margin, reducing it by just over 50%. This is followed

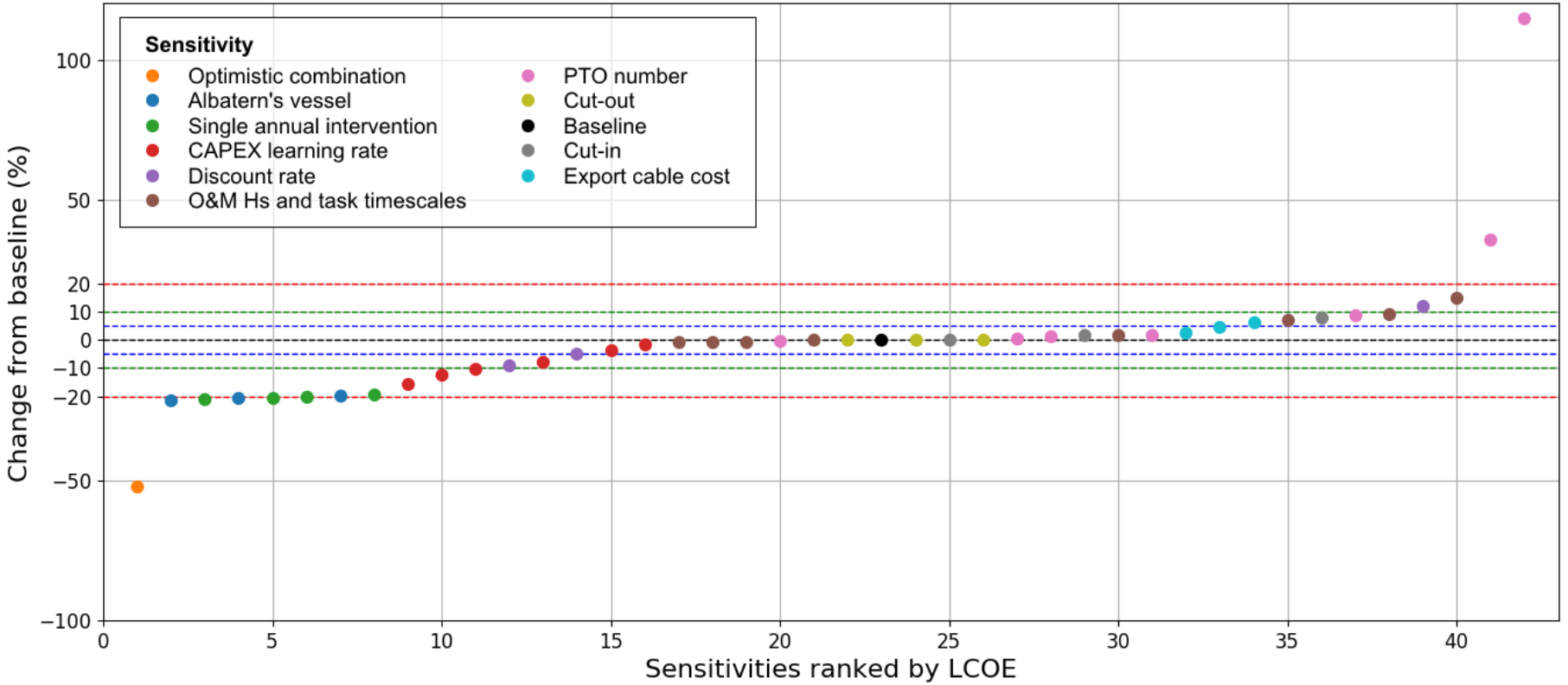

Figure 5.23: The lowest LCOE calculated for all of the simulated sensitivities, relative to the baseline scenario, ranked from largest reduction in LCOE to largest increase. They are coloured according to the sensitivity that was modelled. For example there are three blue dots which correspond to the three simulations used to investigate the option of using Albatern's vessel (Section 5.3.2.2. The dotted horizontal lines represent variations of 0% (black) 5% (blue), 10% (green) and 20% (red) from the baseline.

Sensitivity	Simulations **(ranking)**
Cut-in H_s (m)	0.25 **(27)**, 0.5 **(31)**, 0.75 **(38)**
Cut-out H_s (m)	No cut-out **(22)**, 6.5 **(24)**, 6.0 **(26)**
PTO quantity	5 **(20)**, 7 **(27)**, 8 **(28)**, 4 **(31)**, 3 **(37)**, 2 **(41)**, 1 **(42)**
H_s threshold/task duration	HL **(17)**, HM **(18)**, HH **(19)**, ML **(21)**, MH **(30)**, LL **(35)**, LM **(38)**, LH **(40)**
Using Albatern's workboat	Initial case **(2)**, Task time + 50% **(4)**, task time + 100% **(7)**
Single device intervention per year	September **(3)**, July **(5)**, June **(6)**, March **(8)**
Discount rate (%)	6 **(12)**, 8 **(14)**, 12 **(39)**
Array CAPEX reduction	15% LR, 5th batch **(9)** ; 15% LR, 3rd batch **(10)**; 10% LR, 5th batch **(11)**; 10% LR, 3rd batch **(13)**; 15% LR, next batch **(15)**; 10% LR, next batch **(16)**
Export cable CAPEX (£/m)	30 **(32)**, 40 **(33)**, 50 **(34)**
Optimistic combination	**(1)**

Table 5.12: The rankings of the 42 different simulations, corresponding to the positions of the points in Figure 5.23. Green rankings signify simulations that reduced the lowest LCOE, compared to the baseline (position 23), while red rankings show those that increased the lowest LCOE.

by the sensitivities that consider using Albatern's vessels (Section 5.3.2.2) and a single intervention per year (Section 5.3.2.3). These five all result in reductions of about 20% in the lowest LCOE, with only marginal difference between them. For example the leftmost blue point, signifying using Albatern's vessel in the initial case, only reduces the LCOE by an additional 1.7% on top of the rightmost blue point (using Albatern's vessel but with the task timescales increased by 100%). The next largest reductions in LCOE are found for the CAPEX learning rate reduction (Section 5.3.2.3) and the lower two discount rates of 6% and 8% examined in Section 5.3.3.1. The variation here is much greater, the CAPEX learning rate LCOE ranging from 1.5% (a 10% learning rate after one device batch) to 15.5% in the most optimistic case examined (a 15% learning rate after five device batches).

There are many simulations grouped around the baseline that exhibit very little change in the lowest LCOE. This includes the cut-out H_s, from Section 5.3.1.2) which had a much larger impact in the exposed western part of the domain where the LCOE was already high.

There are some sensitivities that had a notable negative effect on LCOE. The largest are from equipping the array with low numbers of PTOs (Section 5.3.1.3); the two rightmost pink points show the increase in lowest LCOE with one PTO module (115%) and two PTO modules (36%). As illustrated in Figure 5.13 these PTO quantities did reduce the LCOE in some very sheltered parts of the domain. However they increased the LCOE in the most cost-competitive Little Minch region. Increasing the H_s thresholds also resulted in significant increase in the lowest LCOE as shown by the rightmost three brown points

Off-grid Wave Energy Systems for Aquaculture

This chapter presents a case study of the off-grid sub-module as described in Chapter 4. The aim is to demonstrate the model functionality, showing the strengths of the methodology and how it can be applied in practice. It combines the baseline WaveNET system from the previous chapter with hybrid system components, with the aim of supplying power to a fish farm. This is compared to the conventional, diesel generator only case. Sensitivity analysis is also performed to show how the model can guide project decisions.

6.1 Case Study Locations

For the case study two areas were considered: a site to the north east of North Uist and a site to the west of Skye. These are shown in Figure 6.1. They were chosen because they contain active fish farms and coincided with lower LCOE values from the previous analyses in Chapter 5. The fish farm locations were downloaded from the Scotland's Aquaculture website [207]. The five farms enclosed in the analysis domains are active finfish sites.

The same ten years of hindcast metocean data were used as described in Section 5.1. Each analysis domain is approximately ten by twelve kilometres, containing 30 site data points. These areas are significantly smaller than those considered for the grid-connected case study, due to the longer computation time associated with the energy balancing algorithm. One iteration of this algorithm at a single

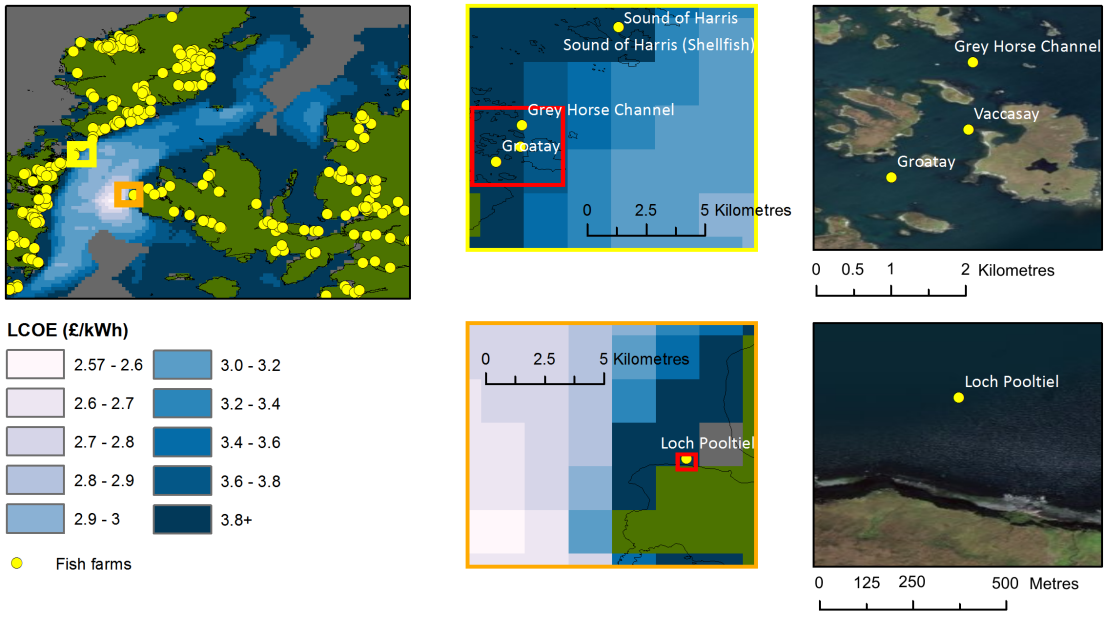

Figure 6.1: The two case study locations considered, relative to fish farm locations in Scotland and the baseline LCOE results from Section 5.2.3.3. Both areas are in the Minch: in the North Uist area (yellow) and the western Skye area (orange). Five fish farms are enclosed: Sound of Harris, Grey Horse Channel, Vaccasay, Groatay and Loch Pooltiel. Satellite images in the vicinity of the fish farms are also shown.

point took almost four minutes for the ten year timeseries, one of the domains thus taking approximately two hours for all of the points. This compares to 45 minutes for most of the sensitivities examined within Section 5.3, which also covered a much larger area.

6.2 Off-grid Baseline Scenario

6.2.1 Input data

6.2.1.1 System and load profile

The system examined was a wave/battery/diesel hybrid system, as depicted in Figure 4.1. The WEC, batteries and diesel generator considered are described in the proceeding sections.

The load profile was obtained from data recorded from a real salmon farm at Gorsten. An electricity meter was installed from December 2014 to January 2017, giving two complete years of data. The meter was connected into the main electrical system, containing an 160 kW diesel generator to power the feed blowers and auxiliary systems on the cages. The domestic load, used to power the on-site office space, is powered by a smaller 10 kW generator. This is a separate electrical

system and hence is not included in this case study

The mean daily energy required by the main system is shown in Figure 6.2, along with the biomass of salmon in the sea pens (obtained from [208]). The profile begins approaching the end of the growth cycle. As the fish reach full size they are harvested and hence less feed, and electricity, is required. The biomass steeply drops off and the energy falls to a minimum in October 2015; by this time all of the fish have been harvested and the cages are restocked. The smaller fish require less feed, and so the energy requirements are less, but quickly build up as the fish grow. The first three months at the start of 2016 are higher than the surrounding trend, despite the low biomass. This is because 24 hour underwater lighting is in operation to make the fish grow more quickly.

Figure 6.3 shows the cumulative probability density of the 24 month load profile. For a large proportion of the time, 44%, no energy is required by the system. This is generally the evening hours, as the fish are fed during daytime. At the 50% probability the load required is 3.5 kW or less, rising to 38.5 kW for 75% of the time. It is in this range that the WEC and battery system is anticipated to provide the most contribution and reduce the diesel input. The load required is 79.5 kW or less 90% of the time. This is below 50% of the generator's rated power of 180 kW, and indicates that the generator at Gorsten is being run somewhat inefficiently.

The seasonal profile from Figure 6.2 can be summarised by four stages:

1. Cages are stocked with adolescent salmon, known as smolts (example October 2015).

2. Winter growth with 24 hour lighting (example February 2016).

3. General growth (example June 2016).

4. Full size fish are being harvested (example July 2015).

Examples of months that fit into these categories are shown in Figures 6.4 and 6.5.

Figure 6.4 shows the raw load profile, as measured, for the four example months above. All four months exhibit a daily peak when the fish are fed. This peak is smaller and narrower for July 2015 as there are less fish to feed, the harvesting process having begun. This occurs around day ten in the month, when the fish are starved prior to being sorted and the fully grown ones removed from the cages.

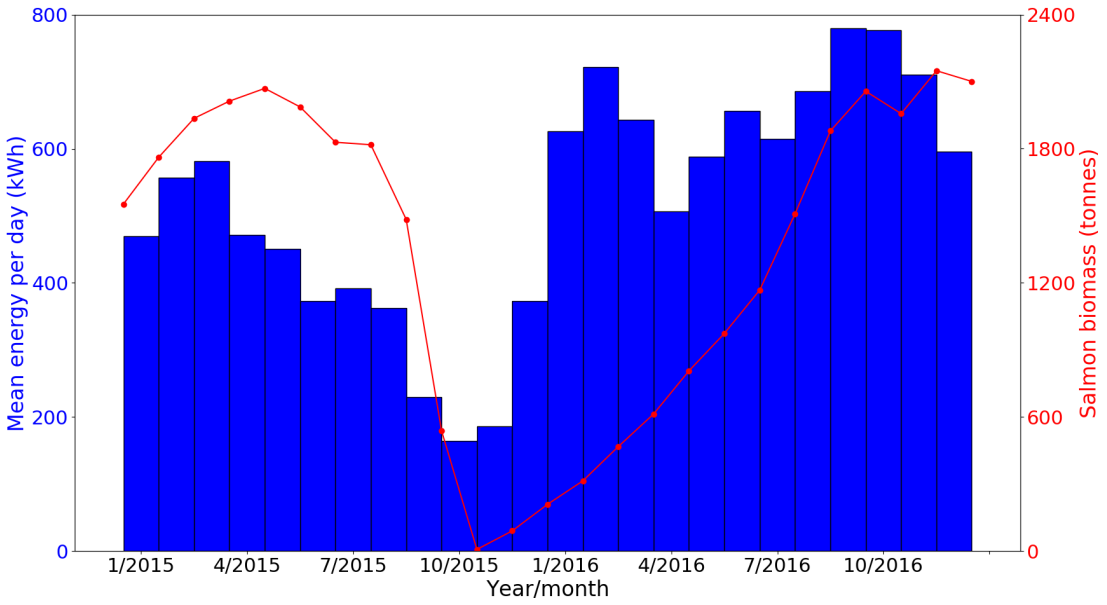

Figure 6.2: The mean daily energy consumed by the feeding system at Gorsten fish farm for each month from January 2015 to December 2016.

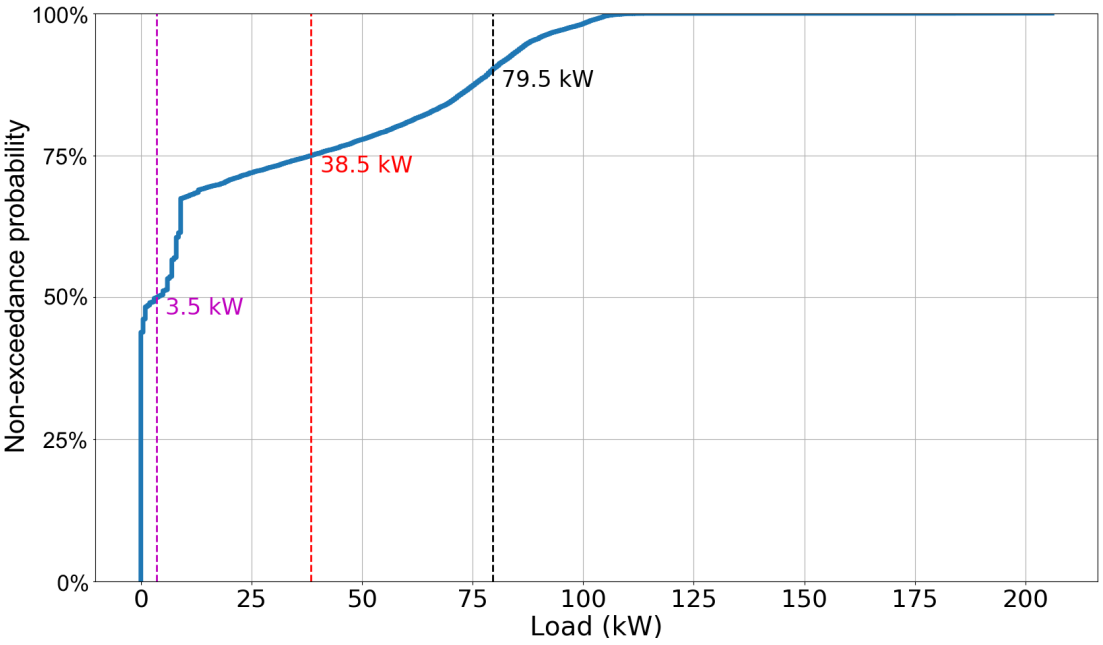

Figure 6.3: Cumulative probability distribution for the load profile. 44% of the profile is zeros, 50% is below 3.5 kW, 75% below 38.5 kW and 90% below 79.5 kW.

This harvesting day is at a regular time in the month, as demonstrated by the October profile. The last of the adult fish are removed and the cages restocked with smaller fish, that only require a small amount of feed. This restocking process is achieved over a number of months. By February 2016, the fish are being fed a substantial amount of feed, and growth lighting is operating 24 hours a day over much of the month. This lighting is no longer being used by June 2016, the load profile taking on a much more regular form.

The daily average profiles for the four months are shown in Figure 6.5. Here the shorter July profile can be seen, as well as the much lower demand in October. The February profile is higher outside the feeding hours because of the growth lighting.

The biomass data from Figure 6.2 indicates that the lifecycle is slightly shorter than 24 months in reality, as the start and end points of the 24 month profile do not match up. To examine a shorter time interval would have meant a somewhat irregular seasonal pattern, which would have been difficult to project over a 20 year lifetime. Hence, the full 24 month profile was chosen in this study as an approximation of the real cyclical behaviour. This profile was duplicated five times to give a ten year profile, this consistent with the amount of metocean data available. No fallowing period between cycles is included, as this was not seen over the 24 month profile. After running the algorithm for ten years, the monthly results are duplicated to cover the 20 year lifetime (as described in Section 3.6.2.2.

No distinction is made between the five fish farms with regard to energy requirements. In reality, each farm will consume a different amount of energy depending on how it is operated (for example some farms might use more feed, some will use more underwater lighting, etc.). These data were not available so the load profile from Gorsten as described above was assumed for all of the farms.

6.2.1.2 Wave energy device

The wave energy device is the same that was chosen for the grid-connected case study from Chapter 5, described in Section 5.2. Valid export cable landing points are assumed to be at the exact fish farm coordinates, as shown in Figure 6.1. Here the cable connects into the hybrid system on the AC side, located close to the diesel generator either onshore or on a feed barge.

6.2.1.3 Diesel generator

Table 6.1 shows the properties of the diesel generator. This is not a backup generator and is actively designed to meet the peak load, due to the scale of the

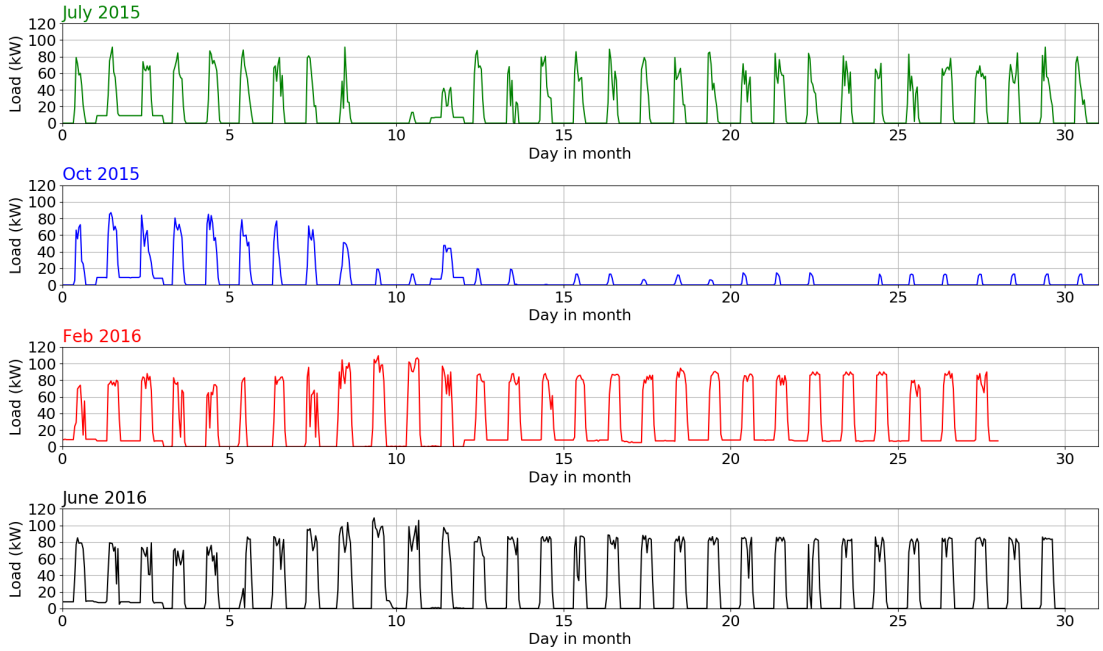

Figure 6.4: Load profile recorded at Gorsten fish farm for four months representative of the main stages of the fish growth cycle: fish harvesting (July 2015), cage restocking (October 2015), winter load with 24 hour growth lighting (February 2016) and general growth (June 2016).

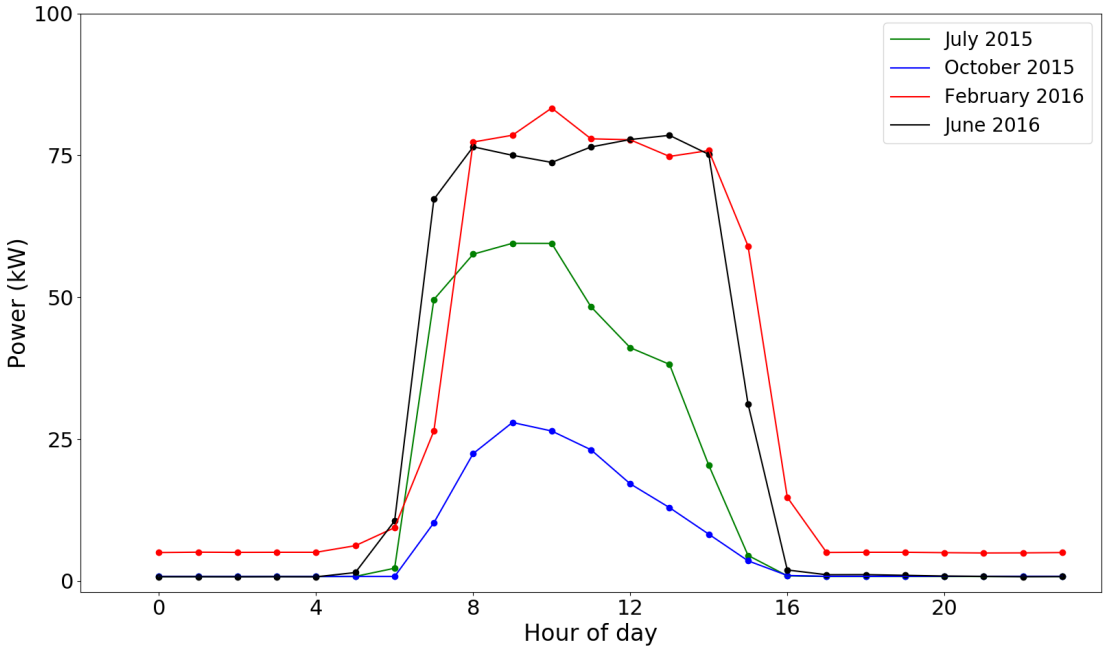

Figure 6.5: Average daily load profile for the four months shown in Figure 6.4.

WEC. A rated power of 160 kW was used, as this matched up with the generator at the site where the load profile data were recorded (see Section 6.2.1.1).

Parameter	Value
Generator model	FG Wilson P220-1
Rating (kW)	160
CAPEX (£)	21,576
Replacement cost	21,576
Generator lifetime (op-hours)	20,000
Minimum load ratio	None
Diesel price (p/l)	60

Load:	100%	75%	50%
Fuel consumed (l/hr)	45.4	34.7	23.4

Table 6.1: Properties of the diesel generator including fuel consumption, a function of the operating load.

The CAPEX and replacement costs were assumed to be equal and estimated from a quotation for a 160 kW diesel generator, the FG Wilson P220-1. The datasheet can be found in Appendix E and includes the fuel consumption properties. A lifetime of 20,000 operating hours was chosen (see Section 2.5.1.2). As the generator needed to run at large load every day for the feeding cycle, wet stacking was not deemed an issue so no minimum load was set. The diesel price was set to 60 p/l. This represents current red diesel price, as of July 2018, and was obtained from correspondence with ValueOils.com Ltd. [209]. The value is deemed to be an annual average over the project, with no time dependence, and does not include the additional cost of transporting the diesel to the remote fish farm locations. These potential higher costs are examined as a sensitivity in Section 6.3.

6.2.1.4 Battery bank

The battery chosen was the Trojan T-105. Its properties are displayed in Table 6.2. It is a FLA battery, chosen because they have a cheaper capital cost than other lead acid battery types (see Section 2.5.1.1). The Trojan T-105 was chosen specifically as it had been identified as being particularly cost effective in a piece of commercial work conducted within Albatern [210]. The T-105 data sheet can be found in Appendix E.

The battery is deep cycle, meaning that it is specially designed for applications

Parameter	Value
Battery model	Trojan T-105
Type	Flooded lead-acid
Nominal voltage (V)	6
Battery capacity (kWh)	1.35
Roundtrip efficiency (%)	90
CAPEX per battery (£)	120
Replacement cost per battery (£)	120
Replacement period (yr)	10

Hour rate	100	20	10	5
Capacity (Ah)	250	225	207	185

Table 6.2: Properties of the battery that was considered for the case study.

which will regularly discharge the battery to a low state of charge. Table 6.2 shows some of the battery input properties. CAPEX and replacement costs were found from prices quoted online [211]. The battery lifetime was an estimate from the literature [34]. It is assumed that all batteries are replaced at the same time.

The overall properties of the battery bank are shown in Table 6.3. It consists of 80 batteries in total: ten strings each made up of eight batteries to get the desired bus voltage. The total capacity at the 20 hour rate is 2250 Ah. A maximum charge current of 340 A was used, about 15% of the battery bank Ah capacity. This is in the range of 10-20% recommended by Rolls, another battery manufacturer [148]. The minimum state of charge was chosen to reflect values seen in the literature. The setpoint SOC was set high enough deemed to avoid excessive numbers of charging cycles. An installation cost of 70% of CAPEX and annual OPEX of 2% of CAPEX per year were assumed. These were estimated from rural generation scenarios defined in [212].

6.2.1.5 Charge controller

Table 6.4 shows the charge controller input parameters. The model chosen was the Sunny Island SI 8.0H, a model that was being considered by Albatern and is designed for off-grid applications. Three units rated at 8 kW can be installed in a cluster, allowing 24 kW to be transmitted to and from the batteries. As the generator is the primary energy source, this level was deemed sufficient in order to supply the times of low loads. It also handles the system control, integrating

Parameter	Value
DC bus voltage (V)	48
Batteries per string	8
Number of strings	10
Battery capacity (kWh)	108
Maximum charge current (A)	340
Minimum SOC (%)	30
Setpoint SOC (%)	80
Installation cost (% of CAPEX)	70
Annual O&M cost (% of CAPEX per year)	2

Table 6.3: The properties of the battery bank selected for the case study.

with the diesel generator and WEC. The efficiency value was approximated from an efficiency curve from the component's datasheet, as listed in Appendix E. As of June 2018 a single unit can be purchased for about £2,500, the final price scaled up to the nearest £10,000 to include installation and logistical costs. The converters are housed in a cabinet (the "Multicluster" box) with a price of about £8,000.

Parameter	Value
Model	Sunny Island SI 8.0H (cluster of 3)
Rating (kW)	24
Efficiency (%)	93
Unit CAPEX (x3)	£10,000
SMA Multicluster box	£8,000

Table 6.4: Charge controller specification.

6.2.2 Model execution

The model was executed using the above inputs, which were written within input text files, as described for the previous case study in Section 5.2.2. As the WEC was the same as considered previously the WEC input files could be reused. Again, a discount rate of 10% and lifetime of 20 years were assumed. As the lifetime is double the amount of data specified (load profile and metocean data) this meant that the output results of the energy balancing algorithm were duplicated, projected forward and discounted within the model.

As well as the baseline, two further scenarios were run. These were:

1. A diesel generator only case.

2. A hybrid system with the optimistic device as considered in Section 5.3.4.

The first demonstrates analysis of a conventional system and allows the impact of moving to a hybrid system to be easily seen. The second is to make comparison with the improvements seen in the grid-connected case.

6.2.3 Results

6.2.3.1 Energy

Figure 6.6 shows the discounted energy that each of the three energy contributing technologies provided to the load over the total lifetime. The WEC output only includes energy transferred to the load or battery bank, not the excess energy dumped. It varies in a similar way to that seen previously, for example Figure 5.2.3.1, with higher output in the more exposed locations. However, because the energy production does not always coincide with times of demand, the useful output is lower than that in the grid-connected case. This is equivalent to effective capacity factors of about 6-10% over the regions.

The battery bank output varies much less than the WEC, with the highest contribution only about 10% greater than the lowest. More energy is provided by the battery bank in the sheltered regions, the inverse trend of the WEC contribution. This is to be expected as the battery has to pick up more of the WEC shortfall. In these regions more of the energy to charge the batteries comes from the diesel generator, which also must provide more energy to the load. The result is higher fuel consumption and hence fuel cost; this is examined in more detail in the next section.

The percentage of energy that is dumped by the WEC is shown in Figure 6.7. This generally matches the energy contribution from Figure 6.6, with a higher proportion lost in the more exposed regions. The result implies that the power profile offered in the sheltered regions better fits the load profile, although this metric will also be a product of the battery bank size. To capture more of the excess a larger battery bank might be better suited. This sensitivity to the baseline case is presented in Section 6.3.

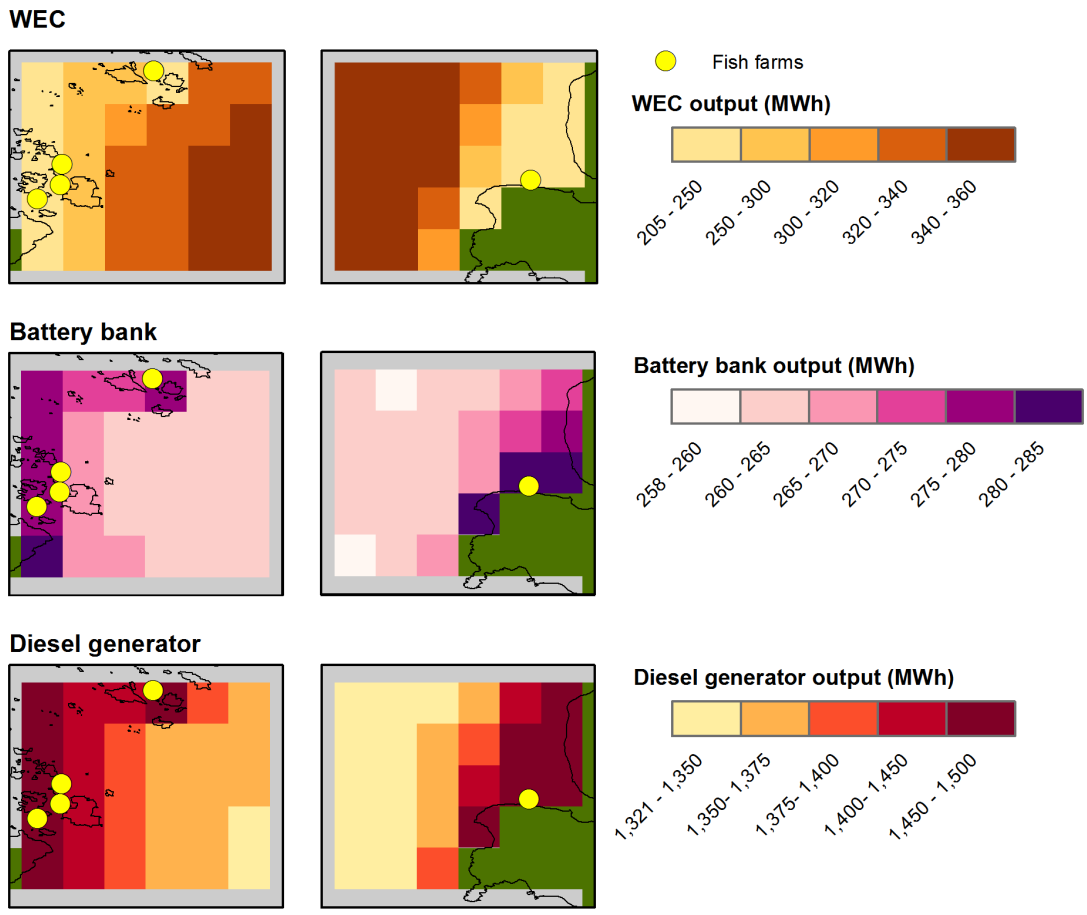

Figure 6.6: The energy provided to the load from the three hybrid system components.

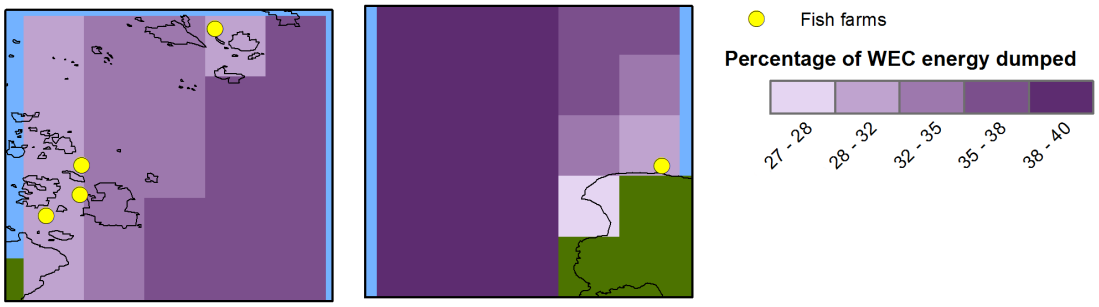

Figure 6.7: The excess energy dumped by the WEC.

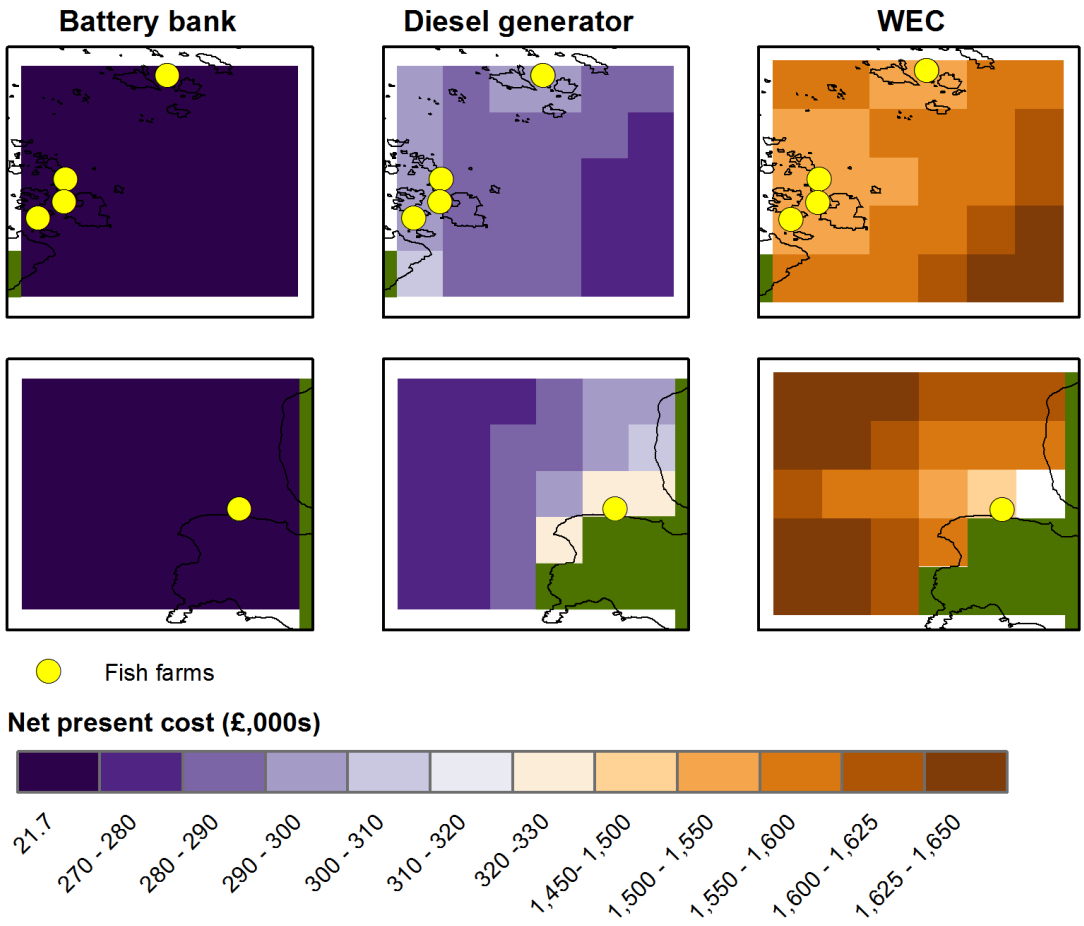

Figure 6.8: Net present cost of the main system components, namely the WEC, battery bank and diesel generator.

6.2.3.2 Total costs

Figure 6.8 shows the NPC broken down by energy sources. The total cost for the WEC system is by far the largest factor, varying between £1.45m and £1.65m. The lowest cost regions coincide with the fish farm locations due to the shorter export cable lengths required. There is also a minor cost reduction from higher availability of weather windows, although the differences point to point are somewhat negligible as both regions are sheltered in the Minch. The total cost of the battery bank is just under £22,000. As explained in Section 4.5 the battery cost is a static quantity over the domain. Despite the simplified approach to battery lifetime inclusion in the model, the relative size of the cost relative to the other systems shows why it was not deemed a priority for this research. The diesel generator cost, including fuel cost, is much lower than the WEC cost. The trend matches that from Figure 6.6, with higher costs in the sheltered areas where more fuel is required.

This fuel cost is more clearly visualised in Figure 6.9, which categorises the

costs by the type of cost. Each plot is given its own colour scale in this figure to help bring out the trends in the individual categories. Also mapped are the CAPEX and OPEX costs. These cost categories are dominated by the WEC, both the absolute values and the spatial trends. The CAPEX trend mainly follows the export cable length, increasing with distance from the fish farm. The OPEX cost includes planned OPEX, unplanned OPEX and the annual insurance. It exceeds the CAPEX at all points, with slightly lower costs in the sheltered regions near to the fish farms. For the North Uist region, the top left cells, somewhat counter-intuitively, see slightly higher OPEX values. This is driven by the unplanned OPEX and insurance as these proportional costs were linked to the CAPEX as in the grid tied case (see Section 5.2.1).

6.2.3.3 LCOE

The LCOE values for the two regions are shown in Figure 6.10. The lowest LCOE sites are found closest to the fish farms; this implies that the additional CAPEX and OPEX costs further from the farms are greater than the fuel cost savings. This trend is mainly driven by the CAPEX, most significantly the export cable cost.

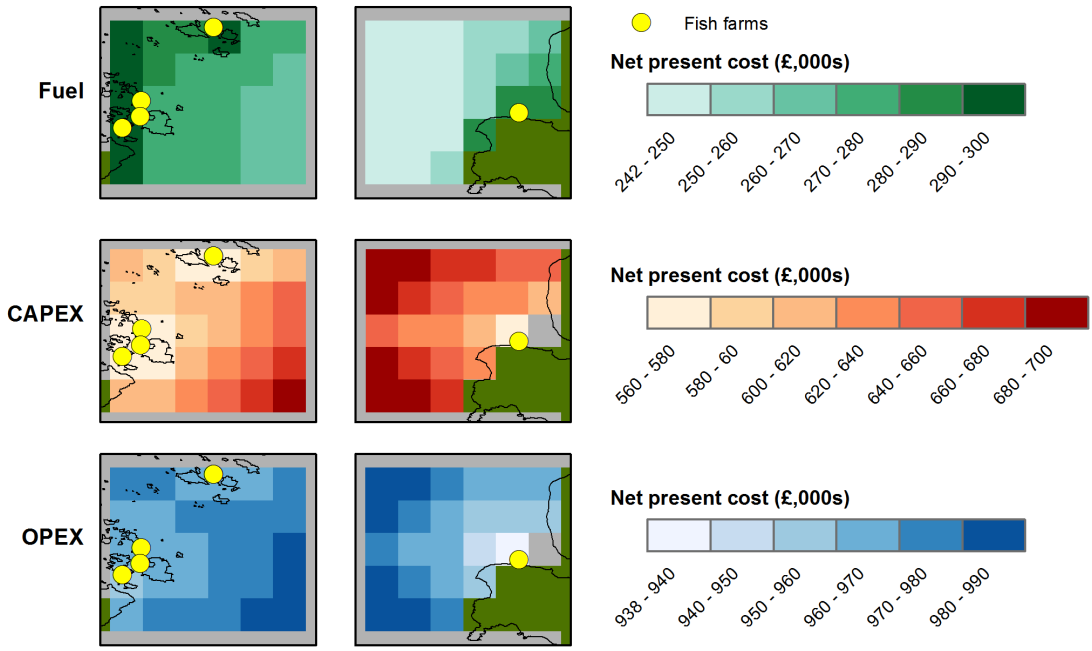

Figure 6.9: Net present cost for the project by type of cost, ordered from minimum to maximum contribution.

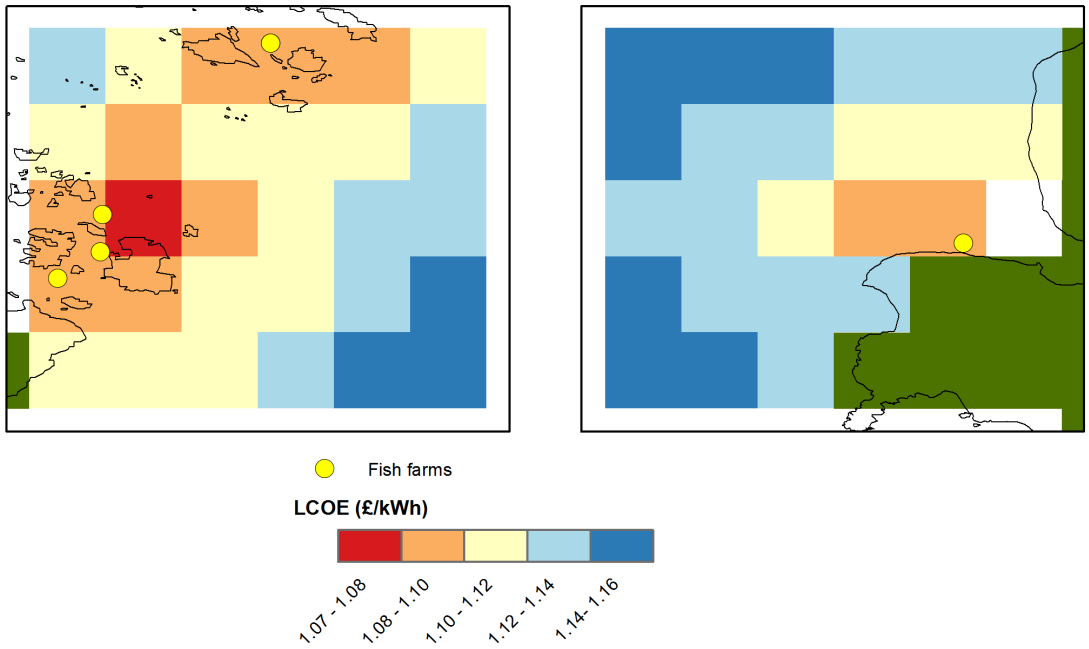

Figure 6.10: LCOE for the baseline hybrid system.

6.2.3.4 Comparison with diesel and optimistic device

Figure 6.11 compares the baseline system with the conventional diesel and optimistic WEC cases, with the different cost categories colour coded. For the hybrid scenarios the lowest LCOE point in the domain is displayed.

The diesel only system is the cheapest, with an LCOE of £0.23/kWh. The majority of this, 84%, is in the fuel cost. The hybrid systems do show marginally lower LCOE for the diesel generator sub-system: £0.17/kWh for North Uist and £0.19/kWh for the Minch. However these savings are dwarfed by the WEC system costs, the CAPEX and OPEX each exceeding this total diesel cost and pushing the LCOE over £1/kWh. The costs for the battery system are incredibly low, the CAPEX and OPEX combined contributing less than £0.02/kWh.

The optimistic WEC cases show the same battery and generator prices as the baseline as these were not modified. The WEC components are greatly reduced, the CAPEX by 43% and OPEX by 62% for both regions. Despite the improvement they still vastly exceed the diesel only case: by 2.57 times in North Uist and 2.60 times in the Minch. The absolute LCOE values and the change from the baseline for these optimistic systems are shown in Figure 6.12. The LCOE shows a similar trend to the baseline in Figure 6.10, with lower values close to the fish farms. These areas also see slightly higher proportional decrease from the baseline, mainly as the unchanged export cable cost is a lower proportion of the cost total.

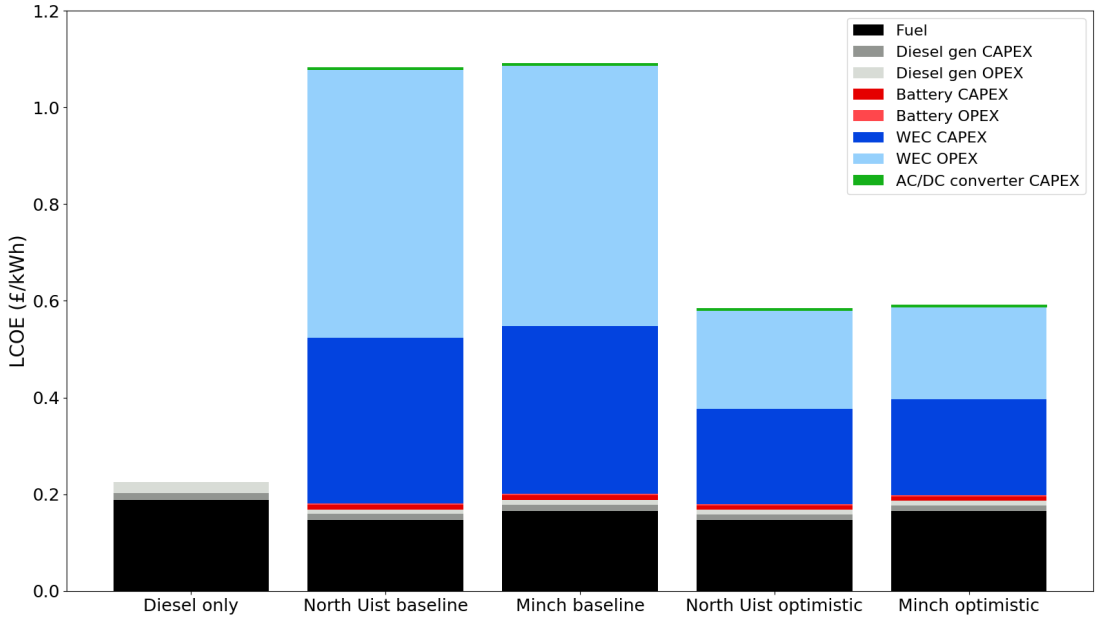

Figure 6.11: Comparison between the baseline, optimistic and conventional diesel only systems. For the hybrid systems the minimum LCOE calculated for the region is displayed.

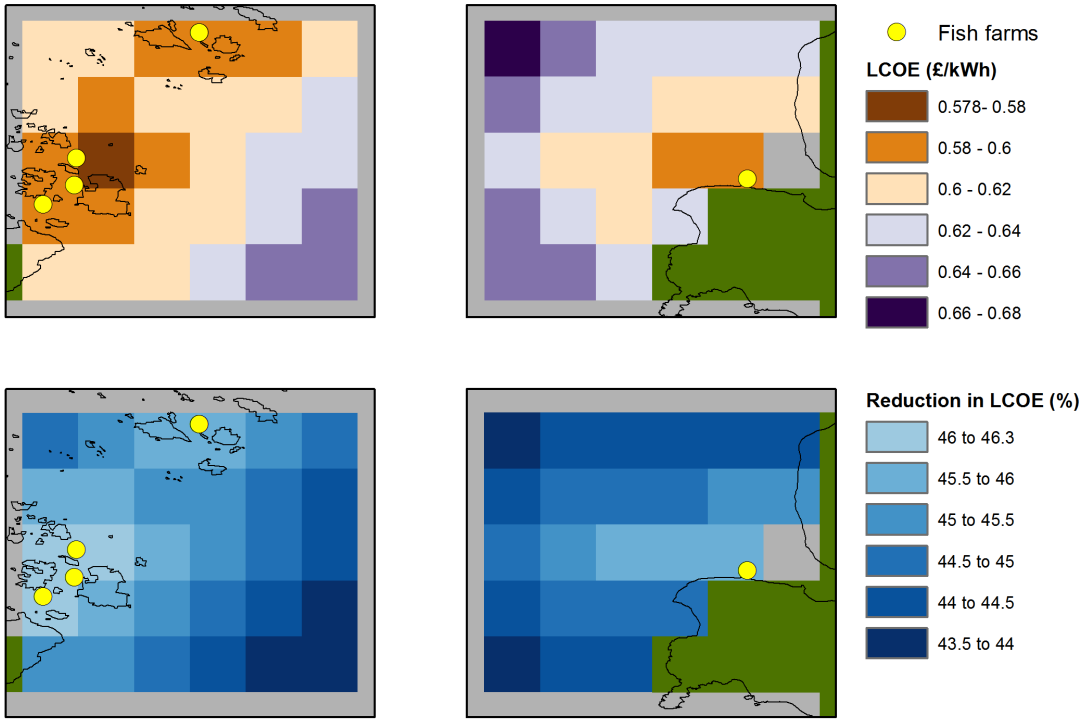

Figure 6.12: Hybrid system LCOE and change from the baseline, considering the optimistic WEC from Section 5.3.4.

6.3 Sensitivities

Four sensitivities were examined, to demonstrate the model usage for more in-depth analysis. These sensitivities were applied to the optimistic WEC case, to allow comparison with the optimistic grid-tied scenario from Section 5.3.4. They are summarised in Table 6.5. Increasing the battery quantity means that

Sensitivity	Values	Section
Battery quantity (strings)	5, 8, 12, 15	6.3.1
Diesel price (p/l)	40, 50, 70, 80, 90, 100	6.3.2
Battery lifetime (years)	2, 3, 5, 8	6.3.3
Smaller array size	1-Hex (three Squid units)	6.3.4

Table 6.5: The four sensitivities that were examined in more detail.

the system has the ability to store more of the excess energy from the WEC and transmit this when required. It also means that the battery bank will need topped up less frequently with energy from the diesel generator. However it does also increase cost, and so in reality there would be a balance which would be linked to the nature of the load profile and wave resource.

The diesel price has been shown to be a significant contributor to LCOE for both conventional and the hybrid systems (Section 6.2.3.4). Six alternative values were chosen, separated in 10 p/l increments (including the 60 p/l baseline). The lower value approximately matches the four year low as shown in Figure 2.9 from Chapter 2. The high value is completely arbitrary, much higher than historical values, and used to demonstrate the effect of high price.

The battery lifetime is chosen to address a main limitation of the off-grid module, as previously noted in Section 4.5. As the ten year lifetime is deemed optimistic, only lower values are chosen; these are consistent with the range as described in Section 2.5.1.1.

Lastly, a smaller array size is considered: the 1-Hex. As the baseline array was found to dump a significant proportion of energy in Section 6.2.3.1, this examines whether a smaller array might be better suited: able to still displace diesel at the low loads but with much lower costs.

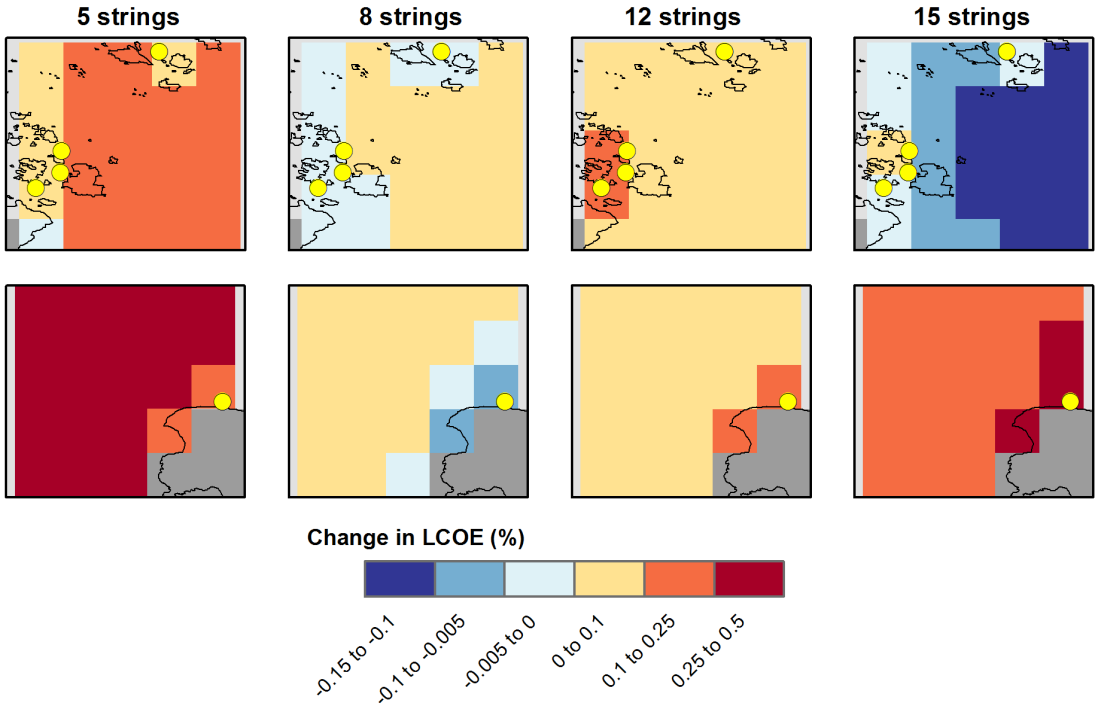

Figure 6.13: Change in LCOE due to different numbers of battery strings.

6.3.1 Battery quantity

Table 6.6 shows the input battery bank parameters for the sensitivity analyses. As for the baseline, the maximum charge current was set to 15% of the battery bank capacity in Ah. Only the number of strings and maximum charge current were directly varied, with the same battery model used as for the baseline.

Strings	Battery quantity	Capacity (kWh)	Max charge current (A)	CAPEX (£)
5	40	54.0	170	4,800
8	64	86.4	270	7,680
12	96	129.6	410	11,520
15	120	162	510	14,420

Table 6.6: The properties of the four battery bank sizes that were examined.

Figure 6.13 shows the change in LCOE from the baseline for the four new battery banks. Overall there is very little variation in the LCOE. For North Uist, a 15 string battery bank sees a maximum LCOE reduction of 0.15%. The largest increase in LCOE is seen for the Little Minch, the 5 string battery bank increasing the LCOE by 0.25-0.5% over most of the area.

The effect of increasing numbers of battery strings is to increase the CAPEX

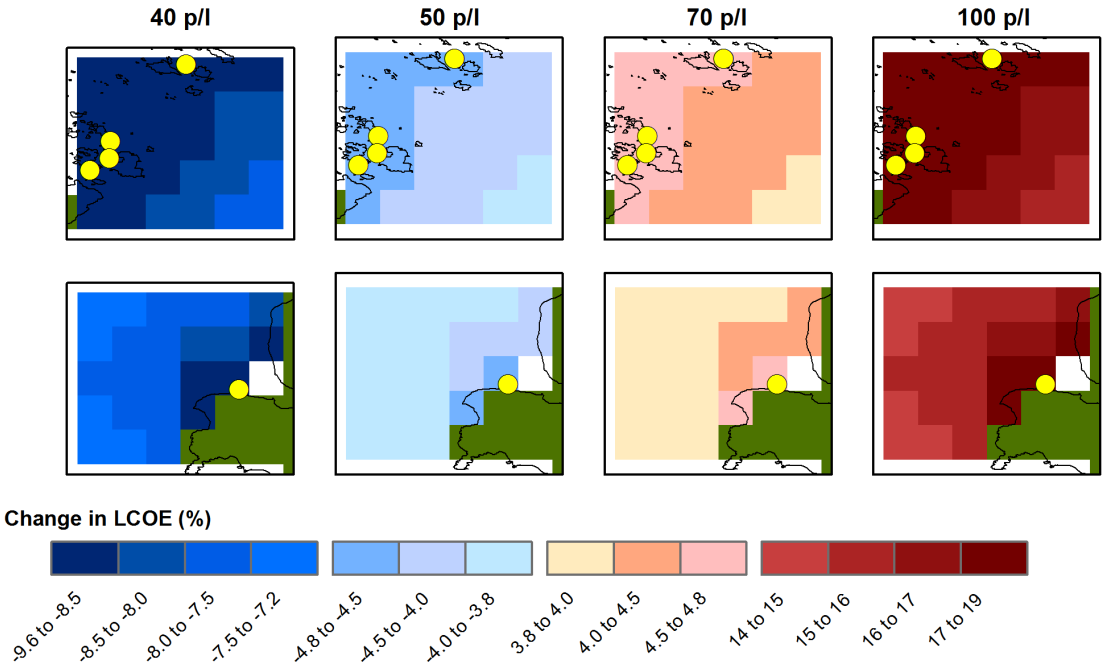

Figure 6.14: Change in LCOE for four different diesel prices.

but also reduce the diesel input for a favourable wave resource that matches the charging profile of the battery. This is apparent for the North Uist domain, where wave energy excess energy coincides more with the battery in a depleted state. The reverse is true for the Little Minch, where the battery excess coincides with a full battery. This means that the diesel generator is used more frequently to charge the battery, resulting in a slight LCOE increase as it does not outweigh the additional battery costs required.

Despite slight variations, overall the LCOE changes are extremely small. This implies that, for this particular case study, the battery quantity could be considered negligible within the range examined.

6.3.2 Diesel price

Figure 6.14 shows the change in LCOE at four different diesel prices. Reducing the price by 10 p/l to 50 p/l sees LCOE reduction between 3.8 and 4.8%. The largest reductions are seen for the more sheltered areas where more diesel is required. Reducing the price further to 40 p/l sees LCOE reduction of 6.8 to 9.1%, a significant amount.

The 70 p/l fuel cost sees the exact inverse trend as the 50 p/l. This is because the fuel price does not change how the hybrid algorithm runs, only the final fuel cost at the end. More sheltered areas see a larger increase, again as more fuel is

required. The maximum price of 100 p/l sees large LCOE increases of 14 to 19%.

As the hybrid system saves fuel compared to the conventional system, a higher fuel cost is desirable to make the system more competitive. Figure 6.15 plots the LCOE against the diesel price for the conventional system and two areas, using the lowest LCOE seen for each area. As the diesel price increases the gap between the conventional and hybrid systems slightly narrows, from £0.364/kWh to £0.339/kWh. The reason why this change is so low is because the sheltered points closest to the fish farms are being used, where the fuel consumption is only marginally reduced. This figure makes it clear that the optimistic system will never be cost competitive in this scenario, even at unrealistically high fuel prices.

6.3.3 Battery lifetime

Figure 6.16 shows the effect of the shorter battery lifetimes on the hybrid system LCOE. In general the effect of the battery lifetime is small. This is because the battery bank is such a low cost component. Even for a pessimistic two year lifetime the increase in LCOE is less than 4%. This is negligible in the context of the overall system.

Something not modelled is the effect of downtime. While the battery bank is being replaced, the energy would have to be supplied by the WEC or diesel generator (more likely the generator if the replacement was carried out in the

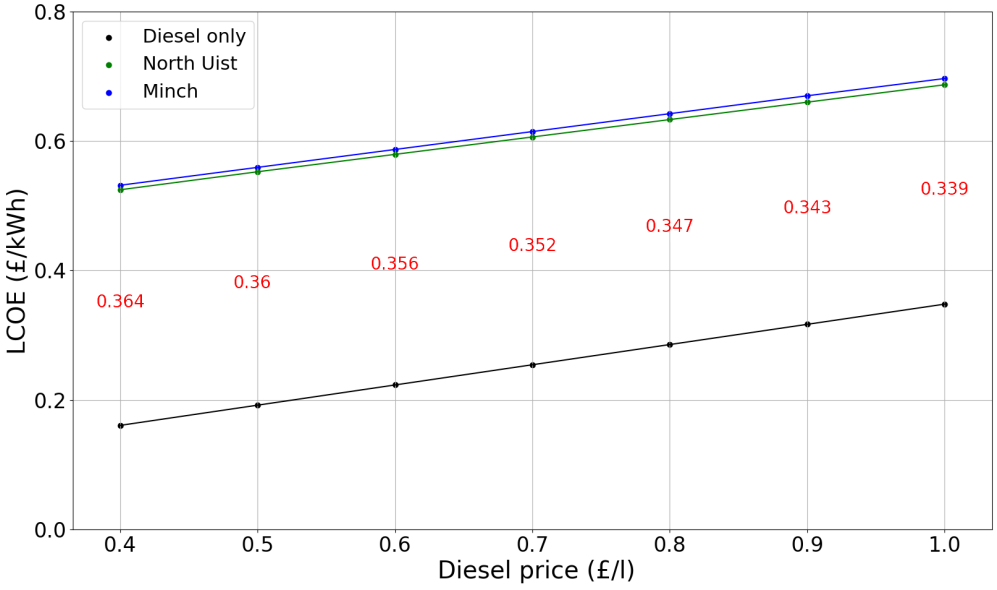

Figure 6.15: LCOE against diesel price for the conventional diesel system and the lowest LCOE points in the North Uist and Minch areas. The red text is the difference between the diesel and North Uist hybrid system.

day). The latter would increase the diesel consumed. For each replacement this time would be of the order of hours, and could be timed to coincide with the feeding time when the diesel generator provides the load anyway. Because of this, the downtime exclusion is not thought to change the overall picture.

Higher battery lifetimes of 3 and 5 years see LCOE increases of about 0.7-3%. These are very small compared to the large impacts previously seen for WEC system sensitivities in Section 5.3, and justifies why a battery lifetime model was not a modelling priority.

6.3.4 1-Hex array size

The 1-Hex is a three unit triangular array. The configuration of this is shown in Figure 6.17. Because there are less devices compared to the six unit baseline array, it means that the overall costs are lower. As the CAPEX and OPEX device costs are considered per Squid, these are effectively halved. The export cable cost and mooring system cost were kept the same as the baseline array, as the export cable cost was already considered optimistic and the mooring system was a negligible proportion of the overall cost anyway. Keeping these components the same would also give the developer more options in reality, to add additional Squid units in the future if desired. This option is not evaluated for the modelling.

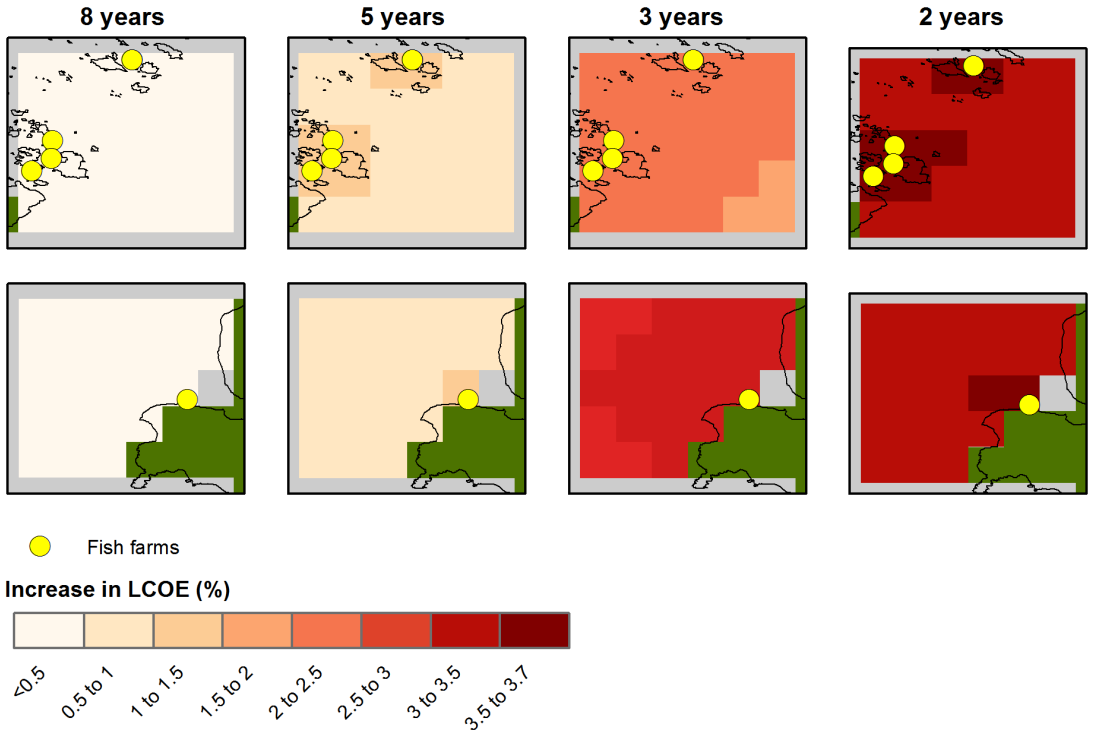

Figure 6.16: Change in LCOE for different battery lifetimes.

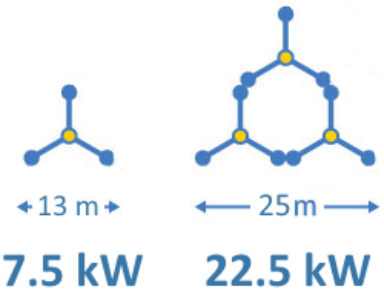

Figure 6.17: Plan view of the 1-Hex array layout (right) compared to a single Squid (left). Image provided by Albatern.

		Tp (s)												
		3	4	5	6	7	8	9	10	11	12	13	14	15
Hs (m)	7	0.0	0.0	0.0	0.0	0.0	0.0	18.1	14.6	12.4	12.3	8.5	7.4	5.6
	6	0.0	0.0	0.0	0.0	0.0	19.6	14.4	12.4	12.6	8.3	7.0	5.2	4.0
	5	0.0	0.0	0.0	0.0	22.5	14.5	12.2	9.5	8.0	6.6	4.6	3.4	2.6
	4	0.0	0.0	0.0	22.5	16.2	11.4	8.5	6.5	5.6	4.1	2.7	1.9	1.5
	3.5	0.0	0.0	0.0	21.8	14.4	9.3	6.6	4.8	4.3	3.1	2.0	1.4	1.0
	3	0.0	0.0	20.4	12.9	9.6	7.0	5.0	3.4	3.2	2.2	1.3	0.9	0.7
	2.5	0.0	0.0	14.7	10.2	6.6	5.4	3.3	2.3	2.2	1.5	0.8	0.5	0.4
	2	0.0	14.5	10.1	6.5	4.8	3.3	2.0	1.5	1.3	0.9	0.4	0.3	0.2
	1.5	0.0	9.0	4.9	4.0	2.5	1.7	1.0	0.8	0.6	0.4	0.2	0.1	0.1
	1	4.7	3.6	2.7	1.6	0.9	0.6	0.3	0.2	0.2	0.1	0.1	0.0	0.0
	0.8	2.7	2.4	1.6	0.9	0.5	0.3	0.1	0.1	0.1	0.1	0.0	0.0	0.0
	0.6	1.7	1.2	0.8	0.5	0.2	0.1	0.1	0.1	0.1	0.0	0.0	0.0	0.0
	0.4	0.6	0.5	0.2	0.1	0.1	0.1	0.0	0.0	0.0	0.0	0.0	0.0	0.0
	0.2	0.1	0.1	0.1	0.0	0.0	0.0	0.0	0.0	0.0	0.0	0.0	0.0	0.0

Figure 6.18: Power matrix for the 1-Hex array, a triangular array of three Squids. This was provided by Albatern [199].

Because the 1-Hex array is physically smaller, it has a different hydrodynamic response to the 3-Hex. It is better suited to shorter waves, as might be expected in shallower areas closer to land. Figure 6.18 shows the power matrix for this array. This was provided by Albatern, who generated it in the same way as described in Section 5.2.1.1. Values of 85% for efficiency and 80% for availability were used, the same as in the grid-connected case study (Section 5.2.1.1).

Figure 6.19 shows the absolute and change in LCOE for the new array. Again the locations close to the fish farm show lower LCOE, because the fuel cost savings in the more exposed locations are exceeded by the increased export cable and OPEX costs. A large reduction in LCOE of 23 to 27% is seen across the domain. The sheltered areas see slightly greater change, as the device CAPEX and OPEX were a greater proportion of the overall NPC.

The breakdown in LCOE is shown in Figure 6.20 for the lowest LCOE values seen in each location. Both regions are very similar, as previously seen. However the CAPEX and OPEX for the WEC are greatly reduced, making the diesel fuel cost the largest contributor to LCOE. Despite the improvements in these costs,

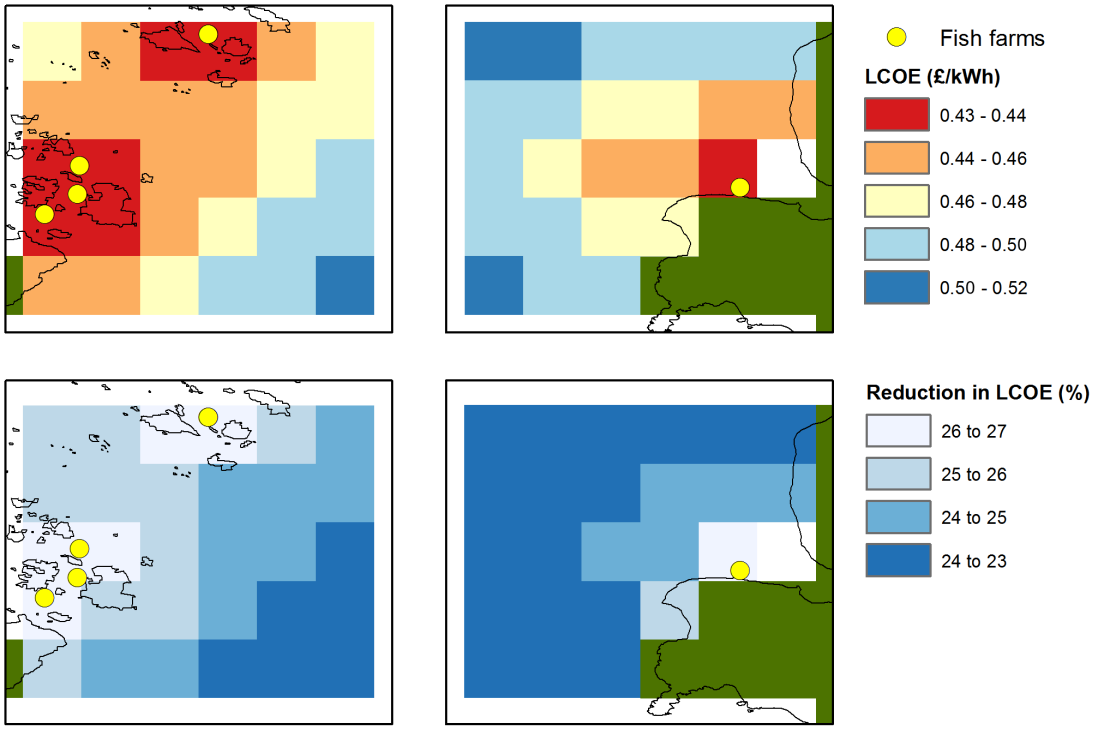

Figure 6.19: Absolute LCOE and change in LCOE from the 3-Hex baseline to the smaller 1-Hex array.

there is now even less diesel cost saving. About 100,000 litres of fuel are saved over the project lifetime, equivalent to £60,000 undiscounted at the baseline diesel price. This is much lower than the additional £158,000 of WEC CAPEX added, not even including OPEX, the export cable or the mooring system.

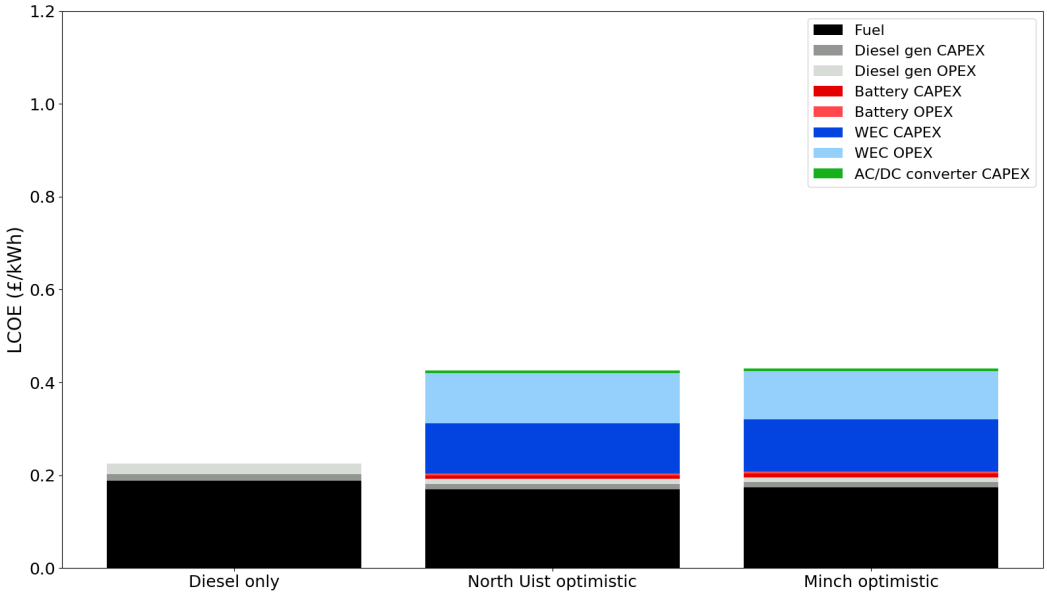

Figure 6.20: LCOE breakdown for the 1-Hex device at the two regions, compared to the conventional diesel system. The lowest LCOE point found for each region is presented.

Discussion

This chapter discusses the performance of the spatial LCOE model as a tool to identify promising locations for wave energy projects. This is framed in the context of the case study results from Chapters 5 and 6, which were used to demonstrate the model functionality and outputs. It includes reflection on both the key capabilities and the areas which would require further improvement to extend its potential.

7.1 Model Summary

An overall assessment of the model should examine two areas:

1. The calculations that are being performed to derive energy, costs and LCOE.

2. The computational structure of the model and how this benefits usability and performance.

The first assessment is necessary to ensure that the model is functioning correctly and providing trustworthy estimates of performance and spatial trends. The second assessment is vitally important to allow the calculations to be checked, bugs to be identified and corrected, runtime to be reduced and to make it possible to expand the model into the future.

7.1.1 Grid-connected array

7.1.1.1 Cost analysis

The cost calculations cover a number of different areas. The model allows a high degree of flexibility in the costs that are specified and how they are categorised. This is made possible by the `ItemBase` class, the most important class for these calculations. It provides a blueprint for any item that has costs associated with it. The `local_costs` attribute means that single and recurring costs are easy to define and are automatically discounted to present values. Multiple and arbitrary cost categories can be defined for `ItemBase` instances or single cost elements which, along with their quantities, are recursively filtered down to nested items and aggregated. The advantage of this approach was seen in Section 5.2.3.2, where cost results were presented both by type (e.g. CAPEX and OPEX) and by system (e.g. device, export cable). Being able to define proportional costs relative to category totals is another useful feature of the model. This was demonstrated in the case study for two recurring costs: the insurance cost and the unplanned OPEX cost. While not a replacement for a dedicated unplanned O&M module, the latter demonstrated how the model can be used to make higher level estimates to account for missing data or functionality.

For the case study results in Section 5.2.3.2, the model allowed the relative proportions of the costs to be easily visualised and compared. From the costs by system results in Figure 5.6, the device cost could be clearly identified as the most significant factor. The smaller costs are also useful to inform business strategy. For example the spatial trends in the total costs are largely driven by the export cable cost behaviour, and so quantifying this for different system designs is shown to be a priority for the company. The mooring system cost is very low, the model is thus able to advise cost reduction and optimisation focus away from this system.

A similar case is seen for the installation cost in Figure 5.7, which is insignificant compared to the initial cost and O&M. Being able to visualise the spatial trends in OPEX is extremely powerful and a key contribution to knowledge from the research. Defining each operation with its own cost category means that the output costs for each are automatically isolated, as shown in Figure 5.8. Again these results can clearly indicate the dominant cost factors, for this case study the device maintenance cost. One might have expected the mid-life refit cost to be more significant due to the high replacement cost involved. The model shows that this is not the case, however, due to the high discounting by project year ten.

Overall the OPEX analysis works well, with the three main parts of the calculation appropriately ordered (calculation of task timescales, waiting times and then vessel costs). The calculation is potentially on the pessimistic side, as the metocean conditions at each point are also used for estimation of transit waiting time. The waiting time has a large impact on the viability of projects at exposed locations, and the methods could be adjusted and improved over time to match the physical reality. The model's ability to automatically constrain the domain size, to exclude points where operations cannot take place, is a useful feature.

The pathfinding abilities coded into the `WaveSite` class are invaluable for the spatial costs. Keeping this benchmark, embedded within all the cost items, ensures consistency in the calculations. Keeping the relevant pathfinding code in a standalone package (the "pathfinding" module, described in Appendix B.3) also means that the functionality is easy to adapt in the future. The locations of ports and export cable landing points in the domain were also demonstrated as influential factors in Figures 5.17 and 6.9 respectively (the latter for the hybrid system). While not included due to lack of data, costs can also be assigned to these points which can provide a finer level of detail in the resulting cost calculations.

7.1.1.2 Energy analysis

The classes used for the power interpolation, `WaveDevice` and `PowerMatrix` are intuitively structured and conveniently combined with the metocean data within the `EnergyAnalysis` class. The `WaveEnergyArray` class gives the flexibility to specify a different power matrix at the array level. While this power matrix modification is somewhat unique to the Albatern interconnected array concept, it is optional and calculating power using power matrices at the device level is also a feature.

The maps in Figure 5.5 show two different measures of the energy production performance. They also show the power of plotting in GIS, as the data visualisation can be fully customised in a straightforward way. To the west of the domain the results were as expected, with energy production increasing further from shore. The sheltered areas between the islands saw very low capacity factors, typically less then 10%. The hotspot in the Little Minch was of particular interest. Because of the multi-dimensional nature of the power production it is more difficult to judge where the best locations will be, especially when confronted with a full timeseries. Being able to map energy production is extremely powerful, and brings attention to areas that would otherwise not be seen.

The modifications that can be applied to the specified power matrix in the

`PowerMatrix` class allow the model to be used as a design tool, to investigate the important factors within the most promising areas. This was seen for the energy based sensitivities in Section 5.3.1, with the cut-in having higher impact than cut-out on the energy production in the Little Minch. The optimisation for PTO quantity in Section 5.3.1.3 had a somewhat negligible impact, reducing the LCOE by up to 5%. As the array only contained six Squids, there were very limited options available. For larger arrays, of tens or hundreds of units, this kind of analysis would be more interesting and generate more variation in the output results. As for the metocean data, this is a limitation of the input data rather than the methods, as Albatern do not have the capability to numerically simulate larger arrays with their current software (Ansys Aqwa). Nevertheless, the model gives an easy way to explore these kind of issues and interpret the geospatial implications.

Validation of the device power matrices will be important for Albatern into the future, to get the best from the model. This is especially the case for larger arrays, which could take advantage of more energetic locations with larger period waves. The limitations in Albatern's numerical modelling means that only arrays of six devices can be simulated in the time domain. This somewhat limits the application of the model to smaller array sizes, although the model is able to consider multiple arrays of 3-Hex devices arrays, or larger arrays using power scaling assumptions.

7.1.1.3 LCOE and sensitivity analysis

Obtaining LCOE from the energy and cost results is straightforward: as the results are stored in dictionaries the categorised costs are just divided by the discounted energy. The LCOE results presented in Section 5.2.3.3 found one significant hotspot in the Little Minch. This location benefited from both a well suited resource and a location close to shore and relatively sheltered for operations. Without the model this location would have been very difficult to identify, as it is not a location renowned for wave energy potential. Focus in the west of Scotland is typically to the west of Lewis and Harris, for example the Harris Demonstrator Zone that is being developed by EMEC [213]. This extends to the literature, for example [51] and [214]. No reference to the Minch as promising for wave energy was found in the literature. This is because previous planned projects have considered larger devices, and because no spatial analyses as demonstrated in this thesis has been conducted for the region. Indeed very few spatial analyses have been conducted at all for wave energy LCOE, especially with the level of detail

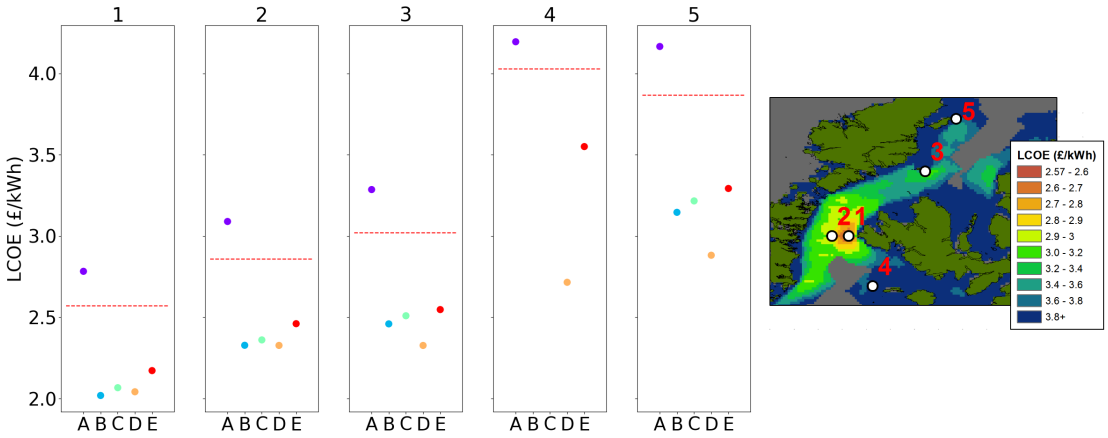

Figure 7.1: The LCOE at five point locations in the domain under five different sensitivities as examined in Section 5.3. These are cut-in of 0.75 m (**A**), using Albatern's vessel (**B**), using Albatern's vessel but at double task times (**C**), a single annual intervention in July (**D**) and reduced device CAPEX with a learning rate of 15% after 5 devices (**E**). The LCOE for the Baseline Scenario is shown by the dashed red line.

demonstrated in this thesis. The model has the capability to identify locations specific to the technology which would be almost impossible by other means. This is also an advantage for wave developers in a pre-commercial industry, who lack the budget and workforce to deploy large quantities of physical measurement apparatus.

The LCOE calculated in the case study was extremely high, even at the hotspot. This was mainly down to the high CAPEX, although the capacity factor did also indicate that the device was also rated too low. This is to be expected for an early stage device concept, and so the results are not worrying from the perspective of the model. The sensitivity analysis demonstrated how the model can be used for more detailed analysis. When four sensitivities were applied together to make up the optimistic case in Section 5.3.4, LCOE reductions of up to 65% were seen over the domain (including about 50% in the Little Minch). This huge decrease shows that the model is capable of providing invaluable insight.

There are various ways that the results can be interpreted and analysed. As well as maps, results at point locations are easy to extract. This is aided by the NetCDF file export, a file format which is generally easier to handle than working with the GeoTiFF files directly. An example of extracting point information is shown in Figure 7.1, where the LCOE change for five of the sensitivities from Section 5.3 are compared at five locations around the domain.

Four positive sensitivities are seen: using Albatern's smaller vessel at the default (B) and double task time (C), moving to a single annual operation in July (D) and reducing CAPEX (E). In the Minch location (points 1, 2 and 3) these

generally have a lower impact on the LCOE and roughly the same magnitude. The negative impact from the 0.75 m cut-in (A) is also plotted and again sees little variation between the three points. For the two more exposed locations, to the west of Canna (4) and south of Coll (5), the impact of a single intervention is very significant, and brings site 4 almost down to the same level as the three Minch locations. Using Albatern's vessel was not valid at this point due to the lower H_s requirements. Site 5 also sees high reductions. However, despite starting off lower than site 4, the single intervention reduction is not as great. This shows that the sensitivities have the ability to alter the relative potential of the points in the domain. The other three benefits are not as significant and mean that the LCOE is still much higher than the other four locations. The analysis allows the relatively low suitability of the site for the device under the examined conditions to be easily seen.

Another example of the geospatial information that the model can provide is shown in Figure 7.2. This plots the LCOE against the distance to shore in the Minch region, for the baseline results from Section 5.2.3. In the results some interesting trends can be seen. For the distances very close to shore, the range of LCOE values is very high. This reflects the large range of energy values seen. Very sheltered areas produce very low energy, however there are also more exposed locations near to the shore. The minimum LCOE value is seen at a distance of about 4 km. Beyond this point there is a slight upward trend in the LCOE, as

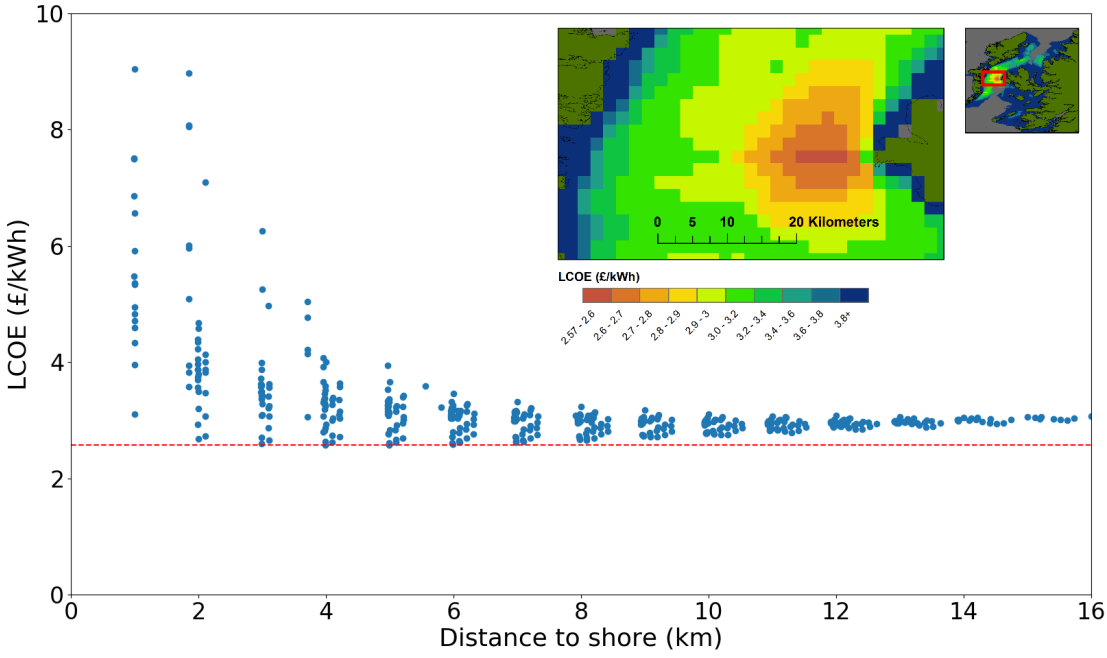

Figure 7.2: LCOE against distance to shore for the baseline Minch hotspot region (inset). The minimum LCOE is indicated by the dashed red line.

any increase in energy production is cancelled out by the export cable and O&M costs. The spread in the results further from shore is also reduced, as there is less variation in the wave climate and hence energy production.

7.1.2 Off-grid array for aquaculture

Overall the off-grid module is well integrated into the model structure. Being able to use many of the same objects for both types of analyses, such as the `WaveSite` object and device child classes, ensures consistency between the analyses. As for the grid-connected case, the case study presented in Chapter 6 demonstrated the analysis principles and the kinds of sensitivities that can be examined.

The case study used a load profile recorded from a real fish farm, along with best estimates of off-grid system component costs. As for the grid-connected case, the model allowed the spatial performance to be assessed; in this case the areas were in the vicinity of actual fish farm locations. The two regions examined performed very similarly, with the North Uist region demonstrating slightly lower LCOE values. As the majority of the load was supplied by the diesel generator, there was low variation in the results. The WEC produced more energy in the more exposed locations away from the fish farm, as would be expected (Chapter 6.2.3.1). However more energy was wasted in these regions, as 44% of the time no energy is required by the system. This meant that the energy production was unable to balance out the higher export cable and OPEX costs, thus the lowest LCOE locations were found closest to the fish farms. In reality cost savings could also be seen in the mooring system, by sharing infrastructure with the fish farm. This was not examined, as detailed design has not been carried out by Albatern, but the model could easily allow it to be included within the cost calculation framework if data were available.

While the case study was demonstrative in nature, the detailed output can be used to gain key insight into the technology. For example, the amount of diesel displaced for the two array sizes examined in Section 6.3 are shown in Figure 7.3. For the smaller 1-Hex array the diesel saved was relatively low at 18-22%. This was higher and more variable for the 3-Hex over the domain, reaching almost 33% in the exposed locations. These are significant numbers and might be favourable to an aquaculture player from a marketing perspective as well as an environmental one.

The case study system was found to be most sensitive to array size and diesel

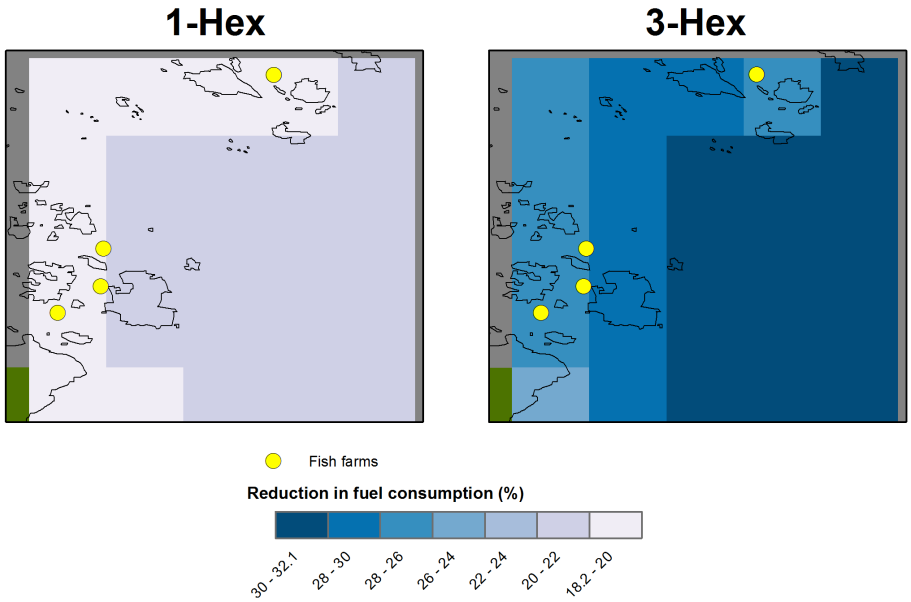

Figure 7.3: Reduction in overall diesel consumption for the 3-Hex and 1-Hex hybrid systems compared to the conventional diesel-only case.

price. The battery quantity had a negligible and somewhat unpredictable impact on LCOE. This could be examined as part of more detailed design, in combination with other aspects.

While the LCOE outputs are higher than the conventional case, as was illustrated in Figures 6.11 and 6.20, the absolute difference was less than for the grid-connected case. The 1-Hex device under the optimistic scenario conditions was approximately twice the price of the conventional case. By contrast, the optimistic grid-connected minimum at £1.12/kWh is over ten times the current LCOE of offshore wind (see Section 2.2). While not the aim of this thesis, with more detailed analysis of the hybrid system components the LCOE could be made more favourable still. The system was not optimised for the load requirement or to minimise the cost. If these aspects were examined, for example by developing a more sophisticated energy balancing algorithm as in software like HOMER, then the system would become even more cost competitive.

While the electricity is more expensive for the hybrid system, it is just one factor that the operator would need to consider in reality. The prices of smolts and feed are also significant factors, as well as the general running costs. If the renewable energy integration could enable a cost premium on the final product then the hybrid system might be viable even at a higher energy price. This is beyond the scope of this research, and would require a full economic assessment from the fish farm operator's perspective.

A factor related to this is the excess energy. This was shown to be high for

the hybrid wave system. Rather than being dumped, this energy could be used for non-critical low power applications. Examples could include environmental monitoring systems or acoustic deterrent devices. The model would easily allow these to be added as additional load profile components, however lacks the ability to distinguish between critical and non-critical applications.

The results from the case study indicate that, for the inputs examined, a 1-Hex system would provide the most competitive LCOE. With less capital deployed in the water, this would also be a lower risk investment and particularly well suited to early R&D activity and proof of concept demonstration. As well as existing fish farms, the model is also able to analyse future fish farm locations by varying the export cable landing location. These locations could offer more beneficial wave climates as the industry is transitioning into more exposed locations (see Section 2.5.3). This spatial functionality is a particularly novel aspect of the research and has not been examined in the literature. The ability to design the hybrid system for specific localised areas is extremely powerful, and could also be applied to off-grid islands communities in the same model framework.

7.1.2.1 Comparison with grid-connected

The output results from the model are well suited to compare the two electrical options. Two examples of the kinds of trends that can be extracted, the LCOE vs export cable length and vs the useful energy produced, are shown in Figure 7.4. For the hybrid system this is the total energy minus the excess. The grid-connected system is defined over the same regions as the hybrid, both systems for the 3-Hex baseline case.

For the off-grid case, on the left of the figure, there is a clear linear relationship between cable length and LCOE. There is also very little difference between the two regions, with both roughly on the same line. This is not seen in the grid-connected case. Here the Minch is significantly cheaper than North Uist, reaching a minimum at about 3 km. The trend is less clear, much more driven by the metocean time series than the hybrid system (where the diesel generator is the dominant factor).

The LCOE against energy production trends are also very different. Somewhat counter-intuitively the hybrid system is cheaper at lower energy production; this is because these points tend to be closer to the fish farm locations with cost benefits. The grid-connected case shows the opposite trend: the lower LCOE values found for higher energy producing points.

7.1.3 Computational performance

Model runtimes for both the grid-connected and off-grid systems are shown in Figures 7.5 and 7.6. These were performed for a number of domain sizes, to visualise the performance and trend. Each time corresponded to a single model run as this was deemed representative of the overall performance. The computer used was a Dell Latitude E6330, running Windows 7, with a 2.7 GHz Intel i5 processor and 12 GB of RAM.

For the grid-connected case the runtimes are reasonable. At the small domain size, where more detailed analysis would be expected to be carried out, the run times were generally less than half an hour. A 5000 point domain, or 70 by 70 points, took 40 minutes in the test. This is approximately a quarter of the domain size examined in the Chapter 5 case study. The largest domain size corresponds to the baseline case study analysis (Section 5.2). This took two hours and ten minutes. While this is a long time, it does not greatly prohibit usage of the model for the purposes previously presented. The time follows a linear trend over the range ("O(N)" in big 'O' notation [215]). Small domain sizes take longer per point due to the overheads associated with loading in the input data and performing pathfinding calculations over the full domain. At the larger domain sizes, sensitivity analysis as carried out in Section 5.3 is slow and could take

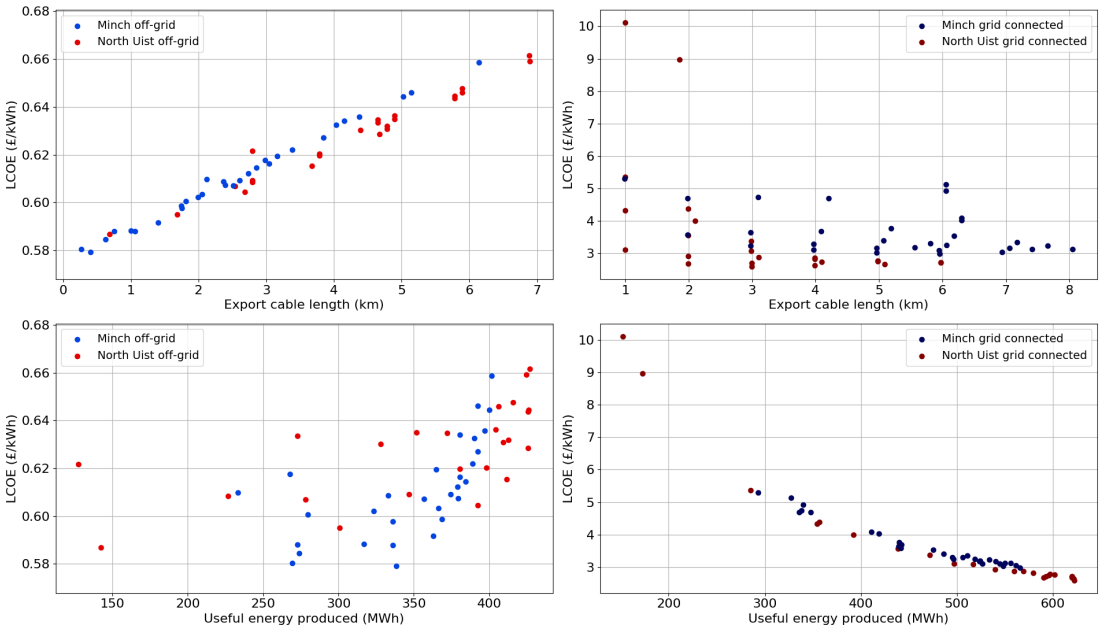

Figure 7.4: LCOE vs distance to shore (top row) and vs useful energy produced by the system (bottom row) for the off-grid energy system from Section 6.2.3 (left) and grid-connected from Section 5.2.3 (right). Both systems are presented over the North Uist and Minch locations, as examined in the hybrid case study.

days. One way that this could be sped up is by saving and loading calculated quantities that will not change between runs. One example is the Weibull fitting parameters, provided the O&M periods of occurrence are not modified between runs. This speed benefit of doing this is shown in the figure in blue. At very small sizes the runtime increases as the method involves loading the whole dataset first from an XML. This could be optimised. At the largest domain size examined, loading rather than calculating the Weibulls reduced the runtime by 12%.

The off-grid module, shown in Figure 7.6, is dominated by the energy balancing algorithm, as it requires iterating through the whole system timeseries and making decisions at every timestep. This means that it also follows an O(N) trend. The

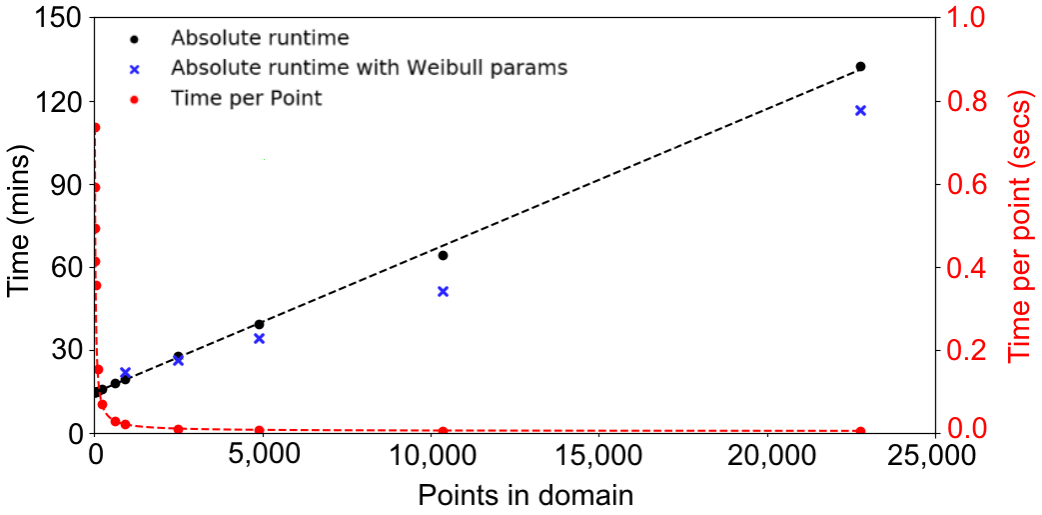

Figure 7.5: Computation time for the grid-connected case study with different domain sizes. The total time (black) and time per point (red) are presented, as well as the total time by loading pre-calculated Weibull parameters rather than calculating them (blue).

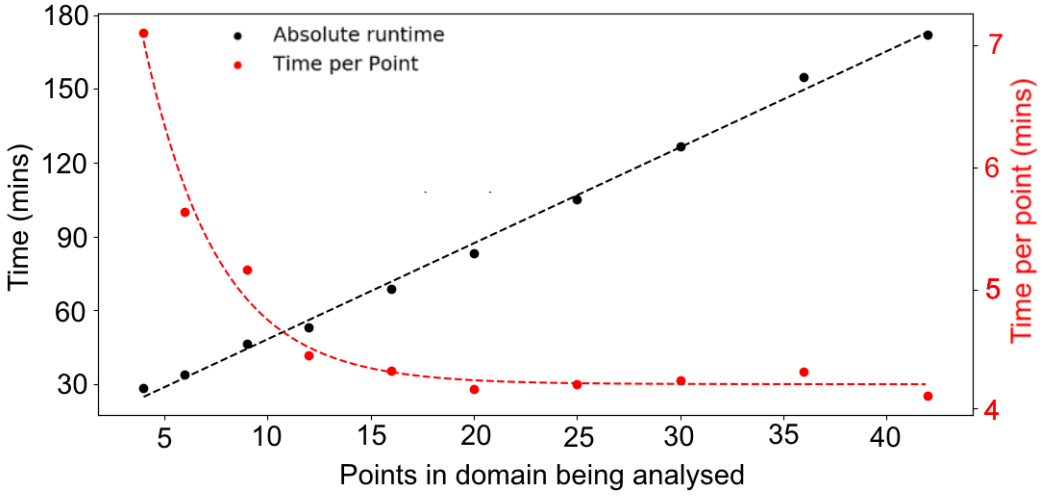

Figure 7.6: Computation time for the off-grid module over different domain sizes for the case study inputs. The total time (black) and time per point (red) are presented.

time per point reduces exponentially over the range examined. As for the grid-connected case this is due to overheads that are applied to the whole domain.

While the linear relationship is reasonable from a computational perspective, the energy balancing algorithm takes far too long per point. For the 42 point domain it represents 93% of the total model runtime. To reduce this, even marginally, would greatly improve the model performance. Ways that this could be achieved could be to reduce the temporal resolution of the simulation, pre-calculating quantities (for example the WEC output at the algorithm model resolution), heavier use of "duck typing" to reduce the number of *if* statements and simplifying the battery logic.

7.2 Areas for Further Improvement

7.2.1 Overall model

The overall model is well structured, with a significant amount of code defined at the top level and filtered down to the various sub modules with inheritance. The main limitations of the model concern the functionality, input data required and performance over larger datasets.

A key limitation of the model is in the lack of validation; it has not been validated against any other approach. This is partly due to a lack of data, preventing it from being compared to a real world case. This is especially the case for O&M, where there have been a limited number of deployments at sea. There are several tools that exist which elements of the model could have been partially validated against, for example DTOcean [135] for the grid-connected case and HOMER for the off-grid energy balancing algorithm. This was not carried out due to time constraints on the project; functionality was prioritised over this kind of detailed evaluation. The model outputs were validated internally, by sense-checking the output numbers and performing checks at individual points to make sure that the calculated costs were being combined properly. This project saw the design of the model completely from scratch, and is designed to be built upon into the future. With this in mind, validation is a key priority going forwards.

Additionally the input data used for the case studies considered a very specific device and geographic area. The data would need to be adapted to consider different locations worldwide. Examples would include a new metocean data set, enclosing the regions of interest, and updated system costs. For the WEC this

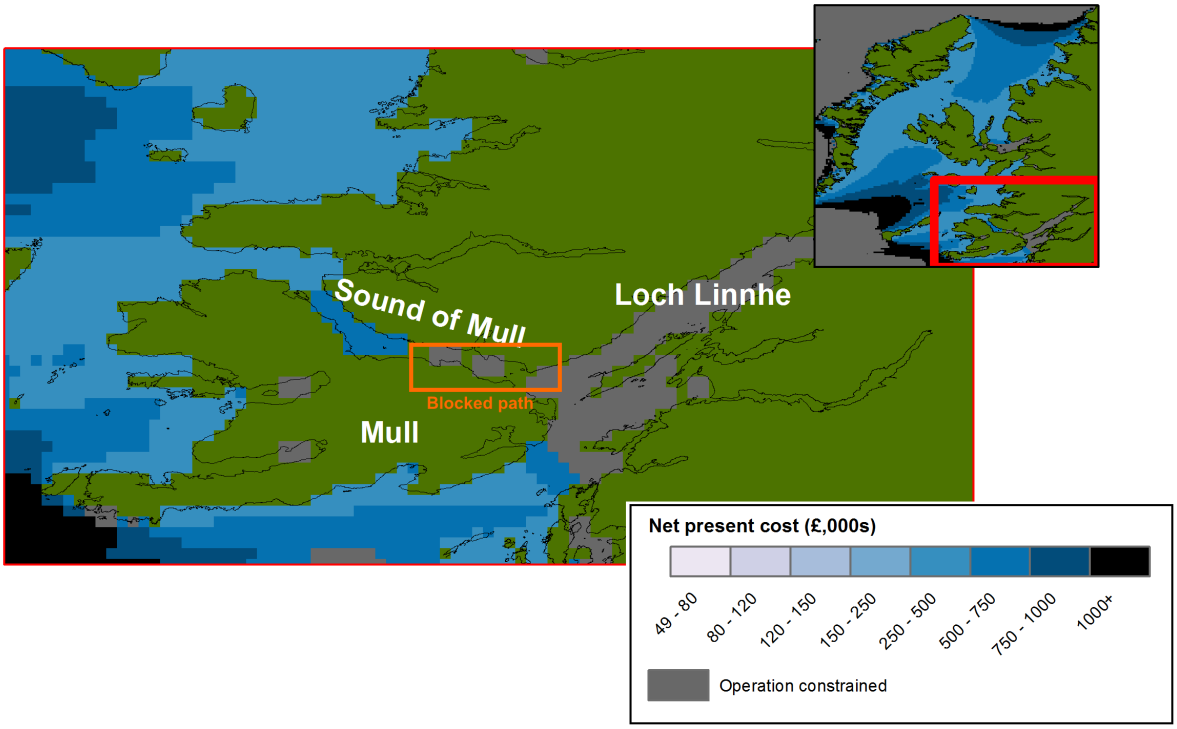

Figure 7.7: The device planned O&M cost from Figure 5.8 around the Isle of Mull. The points in Loch Linnhe are inaccessible as the Sound of Mull is blocked, with bathymetry not defined at several of the points (shown in green).

would need to include a decision about where the units were manufactured.

The most complex part of the model is the O&M module which, as a result, is a source of several issues. The calculated timescales associated with a task are dependent on the distance to the points. As this is calculated directly from the underlying grid, it is very dependent on the spatial resolution and quality. While the dataset used in the case study was at a high resolution, issues can be seen. For example, for the grid-connected case study there was no clear path through the Sound of Mull, as shown in Figure 7.7. This meant that, for the ports selected, the vessels had to go round the Isle of Mull to access locations in Loch Linnhe. The long time to reach these locations made much of this area inaccessible. The area was very poor for energy production in any case so it was not deemed an issue for the case study, however might limit the model in other cases where promising wave climate is cut off due to the grid.

This issue could be mitigated by allowing the option to use a higher resolution bathymetry dataset. A freely available global dataset exists, published by Gebco [216]. This is in NetCDF format, as used in the model, and is at 30 arc-second resolution (0.0083 degrees vs 0.0167 degrees as was used in this thesis).

Constraining areas of the domain with waiting times longer than the time pe-

riod also introduces issues. It means that one extreme month can make large areas appear unviable. A monthly period was coded into the model by default to allow for easier cost discounting. Allowing longer, user defined, time periods by default would allow this issue to be circumvented. In addition, a useful feature would be a standalone metocean analysis class (much in the form of the `CostAnalysis` and `EnergyAnalysis` classes as introduced in Section 3.4.5). This could allow the metocean conditions to be examined prior to executing the model. Output of monthly exceedance statistics would mean that suitable months could be discovered and assigned to the relevant tasks, or optimal solutions chosen from a number of input options.

The weather window analysis is also limited by only including H_s. Other parameters like wind speed and T_p would also be considered in reality and would require a time-series based methodology. The model also assumes a constant vessel charter cost. In reality this will fluctuate with the seasons, with lower rates obtainable in winter as there is less vessel demand [217]. This could benefit sheltered areas like the Minch and make winter operations appear more viable.

While efforts have been made to keep the model and its guiding principles generic, the variation between different device concepts is significant. Larger devices would require more consideration of logistics and port related issues, including having enough space on land to carry out repairs. With more significant energy being exported to the grid there is also the issue of grid stability. The amount that the developer pays for this will depend on the farm size, local environment and government policy [218]. The assumption that the device can feed into the distribution network is not realistic above 20 MW. As larger farms are likely to be more cost competitive, this would need to be addressed to apply the model to situations further in the future.

Also of more relevance to larger scale farms are more complex economic calculations. While LCOE is the most common metric, it is of less interest to investors. The potential return for commercially ready technologies will depend on the subsidy available, and could be calculated from the output energy profile. For the Albatern concept this is more relevant for the hybrid system. A PPA would need to be struck with the fish farm operator above the LCOE for a return to be made. This detail is lacking, and needs expanded for the geospatial and time-dependent trends to inform the business reality.

Lastly, there are other types of analyses that are absent from the model and would help to provide confidence in the results. Unplanned O&M has previously

been mentioned and would be particularly useful for assessing the trade off between cost and survivability over the spatial domain. The mooring module is simplistic, and would benefit from being extended from a cost-based analysis to a more robust design tool. This was not a priority of the research as the Albatern mooring cost is low (as demonstrated in Section 5.2.3.2). Being able to assess the environmental loading on the mooring system, for example through quasi-static methods, would allow extreme wave climates to be factored in as a cost premium or constraint. These kind of cost functions could be defined with a generic spatial formulation and built upon the existing cost methods. This would allow the model parameters to be tuned to conditions seen in the real world, for example the impact of water depth on installation time.

7.2.1.1 Model Usability

The recursive setting of cost categories and quantities works well. However it is not the most transparent process. Particularly at the lower cost levels, where multiple items are embedded, keeping track of these categories can be difficult. A function to visualise the hierarchical item relationship would help to reduce user error and improve the overall model function.

In general, the usability is also hampered by the configuration text file method. While this is convenient and makes the process more widely accessible, it means that many different files need to be being defined and errors can be difficult to track. Rather than this, a fully integrated database would improve the analysis process: ensuring consistency in the input objects and reducing error. A GUI could serve as the model front end, to allow the model to be better understood by users less familiar with Python.

There are also other input data that can be hard to generate. One example is the hybrid module load profile. As there is likely to be a degree of regularity in the profile, Python scripts to generate this from various recurring components would save time and allow different systems to be more easily and quickly examined.

A particularly time consuming part of the process is in formatting the output raster files. Depending on the cost categories specified there can be large numbers of these files, which are then cumbersome to format within ArcGIS. Integration with QGIS using the PyQGIS Python package would allow maps to be automatically formatted according to defined options [219].

7.2.2 Off-grid module

As this module also uses the objects and methods defining the wave energy system, it is subject to the limitations as in Section 7.2.1 above. In addition to these, the main issue with the off-grid module is the slow runtime, as identified in Section 7.1.3, which prohibits sensitivity analysis over larger areas. The impacts of sensitivities are also harder to predict, as was seen for the battery quantity sensitivity in Section 6.3.1, which means that it can take a long time to obtain the necessary results. As the methodology is based on that seen in the literature and HOMER, commercially used software, it is fairly robust. However the algorithm logic is split across a number of functions within the `HybridProject` class and would be difficult to modify for more complex system behaviour.

For getting a higher level spatial estimate of LCOE the module works well, however it is less suitable for detailed hybrid system design due to the prohibitive runtime. For this kind of work, the model would benefit from an optimisation based approach, as achieved in HOMER. Being able to specify different configuration options and determine the most suitable would limit the runtime and allow the various combinations to be considered together. This would be interesting to apply spatially, to see the progression of the design for different site conditions. There are a number of open source Python packages that could be utilised, for example scipy.

Another limitation concerns the available functionality. While suitable for the aquaculture markets Albatern is examining, the range of electrical components is limited for larger scale applications. Examples of these could include island communities which might also contain wind turbines or solar PV. The model is also limited in the storage options available, with only lead acid batteries supported. Different battery models, for example lithium ion or flow batteries, might be better options in reality and would require different governing equations. The weight and space constraints of the battery bank are also not included in the model. For larger numbers of batteries this could restrict the usage in certain locations, for example on a feed barge.

The module is also relatively inflexible when it comes to diesel price. Using a fixed fuel price over the project duration is not realistic; being able to vary this would allow future trends to be examined but with more emphasis on the present day situation. While the uncertainty can be examined by looking at the extreme cases, as was demonstrated in Section 6.3.2, more realistic cases will also be sensitive to the time variation in the resource which a static price does not

capture. Being able to link the price to specific locations in the domain would also make the model able to account for price premiums at particularly remote locations.

Concluding Remarks

8.1 Summary and Achievements

The aim of this research was "To develop an economic model capable of identifying the most suitable geographic locations for localised wave energy projects."

To meet this aim, a sophisticated and detailed computational model has been created. It has been structured using the OOP programming principle, making it modular, scalable, and hence adaptable into the future. This is especially important from the industrial perspective, as it gives Albatern the ability to mould the tool to suit their technology development and commercial requirements.

The research has been broad in focus, the modelling covering a substantial number of aspects. These included energy production estimation from metocean timeseries, manipulation of 2D power matrices, application of pathfinding algorithms, spatial weather window estimation and spatial application of a hybrid system energy balancing algorithm. Eight modules were created, with the interdependencies clearly mapped out and minimised to allow the various calculations to function in isolation. While there are limitations, most notably lack of reliability based unplanned OPEX calculation and the associated downtime, the model offers alternative ways to incorporate these, albeit in a less robust way. The principles defined in the `base_classes` module give the user the flexibility to specify any number of costs, the time periods that they occur in and categorise them in an arbitrary way. In an industry like wave energy, where there are a great many different device concepts made up of different subsystems, this is valuable.

The spatial calculation aspects were a key research need, to help Albatern identify promising locations for their technology and the associated LCOE drivers. These drivers have been shown to vary significantly in the spatial domain, especially for the grid-connected case which was focussed on a larger area. A key example was using Albatern's vessel for the planned O&M procedures, which significantly reduced the number of viable sites to the west of Lewis and Harris but reduced the LCOE by 20-30% in the Little Minch. Being able to apply the calculations over large areas is a huge benefit, with the results easy to visualise and examine further in GIS software.

The off-grid energy simulation was a particularly novel aspect of the research, in particular the application over the spatial domain within the main model framework. This is a market of primary interest of Albatern and thus was a key modelling priority. The model allows easy comparison between the off-grid and grid-connected cases. It also allows sensitivity analysis to be easily conducted, by manipulating the input configuration files. While the case studies were hypothetical, they were deemed to be based on the best data available and indicated significantly more promising LCOE for the hybrid system. There is clearly a case that can be made for pursuing these markets, at least initially until the technology can be proved at a lower cost utility scale.

Both models have been designed with the Albatern device concept in mind. Despite this there are very few, if any, aspects of the model which would not be applicable to other device concepts, or the industry as a whole. The future of wave energy will depend on its ability to optimise performance and reduce costs. This research has presented a model with the capabilities to inform these areas, which will encourage investment in the sector and allow locations and target markets to be established.

8.2 Recommendations for Future Work

The main recommendations for future work are to add in additional model functionality and improve the overall usability.

Unplanned OPEX could be incorporated by creating a class to represent components liable to failures. Multiple failure modes and the associated probabilities could be stored within class attributes. A Monte-Carlo based class method could estimate the times of component failures using an input of timestamps. The time periods, corresponding to the times when vessels need to be mobilised, could then

be used as in the existing `MarineOperation` class as the `period_for_task` attribute. Alternatively a time domain O&M methodology could be integrated, as opposed to the current frequency domain method, which would allow more sophisticated task scheduling to be modelled (for example as seen in [10] or the DTOcean project). This would be built up as an alternative, rather than directly replacing the existing methods, to give more options to the user as both approaches have advantages and disadvantages (as discussed in Section 2.3.3.1).

The Monte-Carlo functionality could also serve a dual purpose: to integrate probabilistic uncertainty analysis. The variables to apply this analysis could easily be marked by a new class type, with attributes to specify the type of distribution and the constants defining it. A new function could run the model for a specified number of iterations, generating new values for the distribution-defined variables for each model run. The resulting energy, cost and LCOE values could be analysed spatially. This would allow standard deviation and uncertainty limits to be determined, as well as confidence levels like the P50 and P90 (as achieved in [57]. This type of analysis would be of particular interest to investors, and give more confidence in the final results.

The main barrier to incorporating such uncertainty analysis is computational performance rather than the implementation, which would be straightforward owing to the structured code development. A run of 1000 iterations is typical for such an analysis. For the grid-connected sensitivity analysis from Section 5.3 this would take 45,000 minutes (assuming 45 minutes per run) or approximately one month. This is not feasible, and so different options would need to be examined. These could include applying parallel computing methods, gaining super computer access, speeding up the existing code and pre-calculating quantities like the energy output and task timescales and varying these rather than the model inputs. Making the model faster to run is of wider interest beyond this additional functionality, and all of these options should be explored.

The off-grid module would particularly benefit from computational performance improvements. Other improvements to the module would be to add to the functionality. Adding in renewable technologies like wind turbines and solar would allow larger hybrid systems to be considered, for example to power island communities. These aspects would also broaden the appeal of the model beyond wave energy and provide wave developers with insight on how to compete in the wider marketplace. Different strategies of dealing with excess energy production from the WEC would also be a good addition. The case study result from Section 6.2.3.1 found that a large proportion of energy was dumped, so incorporating

applications for this would help identify additional markets. This could include desalination, hydrogen production (Power to gas) or displacing energy to heat offices on site in the winter. As well as new capabilities, the existing module could be improved by introducing multi-parameter optimisation of the physical system. This could include aspects like WEC array size, battery quantity and diesel generator size. It would allow the model to be used for more detailed system design and come to more informed choices about the maximum potential for the technology.

For both grid-connected and off-grid functions, the extension beyond LCOE to other financial metrics would enhance the tool. Including the revenue from feed in tariffs or power purchase agreements means that payback time, NPV and IRR could be calculated. These metrics are of particular interest to investors so would improve the model's prospect as a commercial tool to attract funding for the technology.

A key priority going forward should also be in data validation and verification of the theoretical elements. The absence of these elements is a notable limitation of the research project, and mainly due to a lack of available data. This is especially true for O&M, as limited deployments at sea have taken place and developers are apprehensive of sharing data and losing commercial advantage. As an internal tool developed for Albatern, the model can be refined over time by examining the performance and spatial costs against what is seen in the field. Applying the model to larger device sizes and different areas of the world will be particularly beneficial and would open up new possibilities for the company.

Lastly, the usability of the overall model is an area of interest. Full database integration would provide consistency to the modelling, improve performance, reduce user error and ensure that data is responsibly archived. This could be more closely integrated with GIS software, making output maps quicker to format and statistical geospatial analysis more straightforward. The modular nature of the code could also be better utilised. Commonly used sub-module functionality could be grouped into dedicated scripts or tools to make analyses more straightforward, much like the analysis classes described in Section 3.4.5. Examples could include an export cable design tool or O&M simulation tool, which would make it easier and faster to focus on specific elements in isolation.

References

[1] Energy Trends June 2017, Technical report, Department for Business, Energy & Industrial Strategy (BEIS), 2017.

[2] Parliment and Council of European Union, Directive 2009/28/EC of the European Parliament and of the Council on the Production of the use of Energy from Renewable Sources, 2009.
http://data.europa.eu/eli/dir/2009/28/oj, accessed 23/04/18.

[3] Eurostat, Share of renewables in energy consumption in the EU still on the rise to almost 17% in 2015, 2017.
http://ec.europa.eu/eurostat/documents/2995521/7905983/8-14032017-BP-EN.pdf/af8b4671-fb2a-477b-b7cf-d9a28cb8beea.

[4] House of Commons Energy and Climate Change Committee, 2020 renewable heat and transport targets, 2016.
https://publications.parliament.uk/pa/cm201617/cmselect/cmenergy/173/17302.htm.

[5] R. Harrabin, Renewable energy: UK expected to miss 2020 targets, 2016.
http://www.bbc.co.uk/news/science-environment-36710290.

[6] House of Commons Innovation, Universities, Science and Skills Committee, Renewable electricity generation technologies: fifth report of session 2007-08 (Volume 2) 2008.

[7] L. Quesnel, J. Rabe, M. Brommundt, and F. Vorpahl, Task 3.4 Report: State of the art of design tools and standards for offshore renewable energy conversion systems, Technical report, Off-shore Renewable Energy Conversion platforms – Coordination Action (ORECCA) project, 2011.

[8] J. Sandström, J. Griffiths, and T. Svensson, Review of standards on reliability for ocean energy and relation to VMEA, Technical report, Reliability in a Sea of Risk (RiaSoR) project, 2016.

[9] A. O'Hagan, C. Huertas, J. O'Callaghan, and D. Greaves, Wave energy in Europe: Views on experiences and progress to date, *International Journal of Marine Energy*, vol. 14, pp. 180–197, 2016.

[10] A. Gray, *Modelling Operations and Maintenance Strategies for Wave Energy Arrays*. PhD thesis, The Industrial Doctoral Centre for Offshore Renewable Energy (IDCORE), 2017.

[11] D. Mackay, *Sustainable Energy - Without The Hot Air*. UIT Cambridge, 2008.

[12] D. Ross, *Power From Sea Waves*. Oxford University Press, 1995.

[13] S. Kishore, L. Snyder, and P. Pradhan, Electricity from Ocean Wave Energy: Technologies, Opportunities and Challenges, *IEEE Smartgrid Newsletter*, February 2013.

[14] A. F. O. Falcao, Wave Energy Utilisation: A Review of the Technologies, *Renewable and Sustainable Energy Reviews*, vol. 14, pp. 899–918, 2010.

[15] S. Salter, Wave Power, *Nature*, vol. 249, pp. 720–724, 1974.

[16] J. C. Wilson, *A history of the UK renewable energy programme, 1974-88: some social, political, and economic aspects*. PhD thesis, University of Glasgow, 2012.

[17] C. Grove-Palmer, Wave Energy in the United Kingdom: A Review of the Programme June 1975-March 1982 in *Proceedings of 2nd International Symposium on Wave Energy Utilization*, 1982.

[18] A. Mukora, H. Jeffrey, M. Winskel, and M. Mueller, Wave Energy Technology Development Review in the UK: Application of the Learning Curve Concept, 1970-1999 pp. 1036–1042, 2008.

[19] G. Reikard, B. Robertson, and J.-R. Bidlot, Combining wave energy with wind and solar: Short-term forecasting, *Renewable Energy*, vol. 81, pp. 442–456, 2015.

[20] R. W. Furness, H. M. Wade, A. M. C. Robbins, and E. A. Masden, Assessing the sensitivity of seabird populations to adverse effects from tidal stream turbines and wave energy devices, *ICES Journal of Marine Science*, vol. 69, pp. 1466–1479, 2012.

[21] W. J. Grecian, R. Inger, M. J. Attrill, S. Bearhop, B. J. Godley, M. J. Witt, and S. C. Votier, Potential impacts of wave-powered marine renewable energy installations on marine birds, *The International Journal of Avian Science*, vol. 152, pp. 683–697, 2010.

[22] M. Ashley, S. Mangi, and L. Rodwell, The potential of offshore wind farms to act as marine protected areas – A systematic review of current evidence, *Marine Policy*, vol. 45, pp. 301–309, 2014.

[23] E. D. Stoutenburg and M. Z. Jacobson, Reducing Offshore Transmission Requirements by Combining Offshore Wind and Wave Farms, *IEEE Journal of Oceanic Engineering*, vol. 36, pp. 552–561, 2011.

[24] M. Veigas and G. Iglesias, A Hybrid Wave-Wind Offshore Farm for an Island, *International Journal of Green Energy*, vol. 12, pp. 570–576, 2015.

[25] E. D. Stoutenburg, N. Jenkins, and M. Z. Jacobson, Power output variations of co-located offshore wind turbines and wave energy converters in California, *Renewable Energy*, vol. 35, pp. 2781–2791, 2010.

[26] S. Astariz and G. Iglesias, Enhancing wave energy competitiveness through co-Located wind and wave energy farms. a review on the shadow effect, *Energies*, vol. 8, pp. 7344–7366, 2015.

[27] J. Abanades, D. Greaves, and G. Iglesias, Coastal defence through wave farms, *Coastal Engineering*, vol. 91, pp. 299–307, 2014.

[28] B. Hamedni, C. B. Ferreira, and M. Cocho, Generic WEC system breakdown (Deliverable D5.1) 2014. Structural design of wave energy devices (SDWED) project.

[29] A. de Andres, E. Medina-Lopez, D. Crooks, O. Roberts, and H. Jeffrey, On the reversed LCOE calculation: Design constraints for wave energy commercialization, *International Journal of Marine Energy*, vol. 18, pp. 88–108, 2017.

[30] E. Ozkop and I. H. Altas, Control, power and electrical components in wave energy conversion systems: A review of the technologies, *Renewable and Sustainable Energy Reviews*, vol. 67, pp. 106–115, 2017.

[31] J. Cordonnier, F. Gorintin, A. D. Cagny, A. H. Clement, and A. Babarit, SEAREV: Case study of the development of a wave energy converter, *Renewable Energy*, vol. 80, pp. 40–52, 2015.

[32] S. Astariz, A. Vazquez, and G. Iglesias, Evaluation and comparison of the levelized cost of tidal, wave, and offshore wind energy, *Journal of Renewable and Sustainable Energy*, vol. 7, 053112, 2015.

[33] T. Stallard, R. Rothschild, and G. A. Aggidis, A comparative approach to the economic modelling of a large-scale wave power scheme, *European Journal of Operational Research*, vol. 185, pp. 884–898, 2008.

[34] A. B. Sandberg, E. Klementsen, G. Muller, A. de Andres, and J. Maillet, Critical factors influencing viability of wave energy converters in off-grid luxury resorts and small utilities, *Sustainability*, vol. 8, p. 1274., 2016.

[35] L. Margheritini, A. Hansen, and P. Frigaard, A Method for EIA Scoping of Wave Energy Converters: Based on Classification of the used Technology, *Environmental Impact Assessment Review*, vol. 32, no. 1, pp. 33–44, 2012.

[36] S. Viz, C. Adnitt, R. Staniland, J. Everard, A. Sleigh, R. Cappell, S. McNulty, M. Budd, I. Bonnon, and J. Carey, Review of cabling techniques and environmental effects applicable to the offshore wind farm industry, Technical report, Department for Business, Enterprise and Regulatory Reform (BERR), 2008.

[37] R. Bucher and I. Bryden, Overcoming the marine energy pre-profit phase: What classifies the game-changing "array-scale success"?, *International Journal of Marine Energy*, vol. 13, pp. 180–192, 2016.

[38] Energy technology perspectives: strategies and scenarios to 2050, Technical report, International Energy Agency (IEA), 2006.

[39] M. Winskel, N. Markusson, H. Jeffrey, S. Jablonski, C. Candelise, D. Ward, and P. Howarth, Technology Change and Energy Systems: Learning Pathways for Future Sources of Energy, Technical report, Draft paper for UK Energy Research Centre research programme on Energy Technology Learning Rates and Learning Effects, 2008.

[40] D. E. Dismukes and G. B. Upton, Economies of scale, learning effects and offshore wind development costs, *Renewable Energy*, vol. 83, pp. 61–66, 2015.

[41] Trends 2013 in photovoltaic applications, Technical report IEA-PVPS T1-23:2013, International Energy Agency (IEA), 2013.

[42] M. Menicou and V. Vassiliou, Prospective energy needs in Mediterranean offshore aquaculture: Renewable and sustainable energy solutions, *Renewable and Sustainable Energy Reviews*, vol. 14, pp. 3084–3091, 2010.

[43] A. Vögler and V. Venugopal, Wave data analysis for a semi-sheltered site in the Inner Hebrides of Scotland suitable for small scale WEC development, *Ocean Engineering*, vol. 126, pp. 374–383, 2016.

[44] G. Mørk, S. Barstow, A. Kabuth, and M. T. Pontes, Assessing The Global Wave Energy Potential in *Proceedings of OMAE2010*, 2010.

[45] K. Gunn and C. Stock-Williams, Quantifying the Global Wave Power Resource, *Renewable Energy*, vol. 44, pp. 296–304, 2012.

[46] R. Boud, UK Wave Resource Study, Technical report, The Carbon Trust, 2012.

[47] House of Commons Energy and Climate Change Committee, Low Carbon Technologies in a Green Economy: Fourth Report of Session 2009-10 2009.

[48] The Carbon Trust, Focus for success: A new approach to commercialising low carbon technologies, Technical report, The Carbon Trust, 2009.

[49] M. T. Pontes, Assessing the European wave energy resource, *J. Offshore Mech. Arct. Eng*, vol. 120, pp. 226–231, 1998.

[50] UK Wave and Tidal Key Resource Areas Project, Technical report, The Crown Estate, 2012.

[51] G. Lavidas, V. Venugopal, and D. Friedrich, Wave energy extraction in Scotland through an improved nearshore wave atlas, *International Journal of Marine Energy*, vol. 17, pp. 64–83, 2017.

[52] 2020 Routemap for Renewable Energy in Scotland, Technical report, The Scottish Government, 2012.

[53] A. Ilas, P. Ralon, A. Rodriguez, and M. Taylor, Renewable Power Generation Costs in 2017, Technical report, International Renewable Energy Agency (IRENA), 2018.

[54] Lazard's levelised cost of energy analysis - version 11.0, Technical report, Lazard, 2017.

[55] E. S. Rubin, I. M. Azevedo, P. Jaramillo, and S. Yeh, A review of learning rates for electricity supply technologies, *Energy Policy*, vol. 86, pp. 198–218, 2015.

[56] A. MacGillivray, H. Jeffrey, M. reduction for marine analysis, *Technological Forecasting & Social Change*, vol. 87, pp. 108–124, 2014.

[57] N. Farrell, C. O. Donoghue, and K. Morrissey, Quantifying the uncertainty of wave energy conversion device cost for policy appraisal: an Irish case study, *Energy Policy*, vol. 78, pp. 62–77, 2015.

[58] Renewable UK, Offshore wind prices tumble in record breaking auction results - cheaper than nuclear and gas, 2017. `http://www.renewableuk.com/news/362971/Offshore-wind-prices-tumble-in-record-breaking-auction-results--cheaper-than-nuclear-and-gas-.htm`, accessed 20/04/18.

[59] P. Gourley, Tidal power firm Atlantis hits out at funding 'travesty', 2017. `https://www.scotsman.com/news/tidal-power-firm-atlantis-hits-out-at-funding-travesty-1-4557371`, accessed 20/04/18.

[60] ReNews, PTEC slams missing minima, 2017. `http://renews.biz/104867/ptec-slams-missing-minima/`, accessed 20/04/18.

[61] J. Murray, Atlantis warns UK must ensure marine energy prospects not swept away by offshore wind cost revolution, 2017. `https://www.businessgreen.com/bg/analysis/3017049/atlantis-warns-uk-must-ensure-marine-energy-prospects-not-swept-away-by-offshore-wind-cost-revolution`, accessed 20/04/18.

[62] Parliment and Council of European Union, The Paris Protocol - a blueprint for tackling global climate change beyond 2020, 2015. `http://eur-lex.europa.eu/legal-content/EN/TXT/?qid=1425546396765&uri=COM:2015:81:FIN`, accessed 23/04/18.

[63] G. Heal, The Economics of Renewable Energy, Technical report NBER Working Paper No. 15081, National Bureau of Economic Research (NBER), 2009.

[64] A. Myhr, C. Bjerkseter, A. Ågotnes, and T. A. Nygaard, Levelised cost of energy for offshore floating wind turbines in a life cycle perspective, *Renewable Energy*, vol. 66, pp. 714–728, 2014.

[65] M. O'Connor, T. Lewis, and G. Dalton, Operational expenditure costs for wave energy projects and impacts on financial returns, *Renewable Energy*, vol. 50, pp. 1119–1131, 2013.

[66] Ocean Energy: Cost of Energy and Cost Reduction Opportunities, Technical report, Strategic Initiative for Ocean Energy (SI OCEAN), 2013.

[67] S. B. Darling, F. You, T. Veselka, and A. Velosa, Assumptions and the levelized cost of energy for photovoltaics, *Energy & Environmental Science*, vol. 4, pp. 3133–3139, 2011.

[68] L. H. Holthuijsen, *Waves in Oceanic and Coastal Waters*. Cambridge, UK: Cambridge University Press, 2007.

[69] J. P. Pierson and L. Moskowitz, A Proposed Spectral Form for Fully Developed Wind Seas Based on the Similarity Theory of S.A.Kitaigorodskii, *Journal of Geophysical Research*, vol. 69, pp. 5181–5190, 2016.

[70] K. Hasselmann, T. P. Barnett, E. Bouws, H. Carlson, D. E. Cartwright, K. Enke, J. A Ewing, H. Gienapp, D. E. Hasselmann, P. Kruseman, A. Meerburg, P. Muller, D. Olbers, K. Richter, W. Sell, and H. Walden, Measurements of wind-wave growth and swell decay during the Joint North Sea Wave Project (JONSWAP), vol. 8, pp. 1–95, 01 1973.

[71] PELAMIS WEC - CONCLUSION OF PRIMARY R&D, Technical report ETSU V/06/00181/REP, Department of Trade and Industry (DTI), 2003.

[72] D. Dunnett and J. S. Wallace, Electricity generation from wave power in Canada, *Renewable Energy*, vol. 34, pp. 179–195, 2009.

[73] A. Pecher and J. P. Kofoed, eds., *Handbook of Ocean Wave Energy*. Springer Open, 2017.

[74] G. Allan, M. Gilmartin, P. McGregor, and K. Swales, Levelised costs of wave and tidal energy in the UK: cost competitiveness and the importance of "banded" renewables obligation certificates, *Energy Policy*, vol. 39, pp. 23–39, 2011.

[75] G. Dalton, R. Alcorn, and T. Lewis, A 10 year installation program for wave energy in Ireland: A case study sensitivity analysis on financial returns, *Renewable Energy*, vol. 40, pp. 80–89, 2012.

[76] B. Teillant, R. Costello, J. Weber, and J. Ringwood, Productivity and economic assessment of wave energy projects through operational simulations, *Renewable Energy*, vol. 48, pp. 220–230, 2012.

[77] A. Karyotakis and R. Bucknall, Planned intervention as a maintenance and repair strategy for offshore wind turbines, *Journal of Marine Engineering & Technology*, vol. 9, pp. 27–35, 2010.

[78] C. Röckmann, S. Lagerveld, and J. Stavenuiter, *Operation and Maintenance Costs of Offshore Wind Farms and Potential Multi-use Platforms in the Dutch North Sea*, pp. 97–113. Cham: Springer International Publishing, 2017.

[79] M. O'Connor, D. Bourke, T. Curtin, T. Lewis, and G. Dalton, Weather windows analysis incorporating wave height, wave period, wind speed and tidal current with relevance to deployment and maintenance of marine renewables in *Proceedings of the 4th International conference on Ocean Energy (ICOE)*, 2012.

[80] B. Drew, A. R. Plummer, and M. N. Sahinkaya, A review of wave energy converter technology, *Proceedings of the Institution of Mechanical Engineers, Part A: Journal of Power and Energy*, vol. 223, no. 8, pp. 887–902, 2009.

[81] C. Kenny, D. Findlay, P. Thies, J. Shek, and I. Lazakis, Lessons Learned from 3 Years of Failure: Validating an FMEA with Historical Failure Data in *Proceedings of the 12th European Wave and Tidal Energy Conference (EWTEC 2017)*, 2017.

[82] P. R. Thies, J. Flinn, and G. H. Smith, Is it a showstopper? Reliability assessment and criticality analysis for Wave Energy Converters in *Proceedings of the 8th European Wave and Tidal Energy Conference (EWTEC 2009)*, 2017.

[83] A. Ilas, P. Ralon, A. Rodriguez, and M. Taylor, System Performance, Availability and Reliability Trend Analysis – SPARTA 2017/18 Portfolio Review, Technical report, SPARTA, 2018.

[84] S. Astariz and G. Iglesias, The economics of wave energy: A review, *Renewable and Sustainable Energy Reviews*, vol. 45, pp. 397–408, 2015.

[85] M. O'Connor, T. Lewis, and G. Dalton, Weather window analysis of Irish west coast wave data with relevance to operations & maintenance of marine renewables, *Renewable Energy*, vol. 52, pp. 57–66, 2013.

[86] S. Kuwashima and N. Hogben, The estimation of wave height and wind speed persistence statistics from cumulative probability distributions, *Coastal Engineering*, vol. 9, pp. 563–590, 1986.

[87] T. Stallard, J. Dhedin, S. Saviot, and C. Noguera, Deliverables D7.4.1 and D7.4.2: Procedures for Estimating Site Accessibility and Appraisal of Implications of Site Accessibility, Technical report, Equimar, 2010.

[88] R. T. Walker, J. van Nieuwkoop-McCall, L. Johanning, and R. J. Parkinson, Calculating weather windows: Application to transit, installation and the implications on deployment success, *Ocean Engineering*, vol. 68, pp. 88–101, 2013.

[89] K. Anastasiou and C. Tsekos, Persistence statistics of marine environmental parameters from Markov theory, Part 1: analysis in discrete time, *Applied Ocean Research*, vol. 18, no. 4, pp. 187–199, 1996.

[90] T. W. Thorpe, A Brief Review of Wave Energy, Technical report, UK Department of Trade and Industry, 1999.

[91] The World Energy Council, World Energy Resources: Marine Energy 2016, Technical report, The World Energy Council, 2016.

[92] M. Previsic, System level design, performance and costs for San Francisco California Pelamis offshore wave power plant, Technical report, EPRI, 2004.

[93] G. Dalton, R. Alcorn, and T. Lewis, Case study feasibility of the Pelamis wave energy converter in Ireland, Portugal and North America, *Renewable Energy*, vol. 35, pp. 443–455, 2010.

[94] S. Biyela and W. Cronje, Techno-Economic Analysis Framework for Wave Energy Conversion Schemes under South African Conditions: Modeling and Simulations in *Proceedings of World Academy of Science, Engineering and Technology*, 2016.

[95] R. Guanche, A. D. de Andres, P. D. Simal, C. Vidal, and I. J. Losada, Uncertainty analysis of wave energy farms financial indicators, *Renewable Energy*, vol. 68, pp. 570–580, 2014.

[96] G. J. W. van Bussel and M. B. Zaaijer, Reliability, availability and maintenance aspects of large-scale offshore wind farms, a concepts study in *Marine Renewable Energies Conference*, 2001.

[97] M. O'Connor, T. Lewis, and G. Dalton, Techno-economic performance of the Pelamis P1 and Wavestar at different ratings and various locations in Europe, *Renewable Energy*, vol. 50, pp. 889–900, 2013.

[98] C. Beels, P. Troch, J. P. Kofoed, P. Frigaard, J. V. Kringelum, P. C. Kromann, M. H. Donovan, J. D. Rouck, and G. D. Backer, A methodology for production and cost assessment of a farm of wave energy converters, *Renewable Energy*, vol. 36, pp. 3402–3416, 2011.

[99] P. Contestabile, E. D. Lauro, M. Buccino, and D. Vicinanza, Economic Assessment of Overtopping BReakwater for Energy Conversion (OBREC): A Case Study in Western Australia, *Sustainability*, vol. 9, p. 1., 2016.

[100] T. Okamoto, Y. Fukaya, and Y. Higo, Validation of the index to determine design parameters of a WEC for cost optimisation of a wave farm in *Proceedings of OMAE2015*, 2015.

[101] A. Babarit, J. Hals, M. J. Muliawan, A. Kurniawan, T. Moan, and J. Krokstad, Numerical benchmarking study of a selection of wave energy converters, *Renewable Energy*, vol. 41, pp. 44–63, 2012.

[102] A. de Andres, E. Medina-Lopez, D. Crooks, O. Roberts, and H. Jeffrey, Techno-economic related metrics for a wave energy converters feasibility assessment, *Sustainability*, vol. 8, p. 1109., 2016.

[103] D. Mollison and M. Pontes, Assessing the Portuguese wave-power resource, *Energy*, vol. 17, no. 3, pp. 255–268, 1992.

[104] M. G. Hughes and A. D. Heap, National-scale wave energy resource assessment for Australia, *Renewable Energy*, vol. 35, no. 8, pp. 1783 – 1791, 2010.

[105] G. Iglesias, M. López, R. Carballo, A. Castro, J. Fraguela, and P. Frigaard, Wave energy potential in Galicia (NW Spain), *Renewable Energy*, vol. 34, no. 11, pp. 2323–2333, 2009.

[106] E. Rusu and C. G. Soares, Coastal impact induced by a Pelamis wave farm operating in the Portuguese nearshore, *Renewable Energy*, vol. 58, pp. 34–49, 2013.

[107] S. Bozzi, R. Archetti, and G. Passoni, Wave electricity production in Italian offshore: A preliminary investigation, *Renewable Energy*, vol. 62, pp. 407–416, 2014.

[108] L. Rusu and C. G. Soares, Wave energy assessments in the Azores islands, *Renewable Energy*, vol. 45, pp. 183 – 196, 2012.

[109] M. Veigas and G. Iglesias, Wave and offshore wind potential for the island of Tenerife, *Energy Conversion and Management*, vol. 76, pp. 738–745, 2013.

[110] L. Rusu and F. Onea, The performance of some state-of-the-art wave energy converters in locations with the worldwide highest wave power, *Renewable and Sustainable Energy Reviews*, vol. 75, pp. 1348–1362, 2017.

[111] V. Vannucchi and L. Cappietti, Wave Energy Assessment and Performance Estimation of State of the Art Wave Energy Converters in Italian Hotspots, *Sustainability*, vol. 8, no. 12, 2016.

[112] G. Lavidas and V. Venugopal, A 35 year high-resolution wave atlas for nearshore energy production and economics at the Aegean Sea, *Renewable Energy*, vol. 103, pp. 401–417, 2017.

[113] S. Gallagher, R. Tiron, E. Whelan, E. Gleeson, F. Dias, and R. McGrath, The nearshore wind and wave energy potential of Ireland: A high resolution assessment of availability and accessibility, *Renewable Energy*, vol. 88, pp. 494–516, 2016.

[114] S. Pohekar and M. Ramachandran, Application of multi-criteria decision making to sustainable energy planning - A review, *Renewable and Sustainable Energy Reviews*, vol. 8, pp. 365–381, 2004.

[115] S. Ghosh, T. Chakraborty, S. Saha, M. Majumder, and M. Pal, Development of the location suitability index for wave energy production by ANN and MCDM techniques, *Renewable and Sustainable Energy Reviews*, vol. 59, pp. 1017–1028, 2016.

[116] Offshore Wind and Wave Energy Feasibility Mapping for the Outer Continental Shelf off the State of Oregon, Technical report BOEM 2014-658, Bureau of Ocean Energy Management (BOEM), 2014.

[117] F. Flocard, D. Ierodiaconou, and I. R. Coghlan, Multi-criteria evaluation of wave energy projects on the south-east Australian coast, *Renewable Energy*, vol. 99, pp. 80–94, 2016.

[118] J. R. Monds, Multicriteria Decision Analysis for Wave Power Technology in Canada, *Journal of Energy Resources Technology*, vol. 136, 021201-021201-8, 2013.

[119] M. Vasileiou, E. Loukogeorgaki, and D. G. Vagiona, GIS-based multi-criteria decision analysis for site selection of hybrid offshore wind and wave energy systems in Greece, *Renewable and Sustainable Energy Reviews*, vol. 73, pp. 745–757, 2017.

[120] J.-J. Wang, Y.-Y. Jing, C.-F. Zhang, and J.-H. Zhao, Review on multi-criteria decision analysis aid in sustainable energy decision-making, *Renewable and Sustainable Energy Reviews*, vol. 13, pp. 2263–2278, 2009.

[121] I. Galparsoro, P. Liria, I. Legorburu, J. Bald, G. Chust, P. Ruiz-Minguela, G. Pérez, J. Marqués, Y. Torre-Enciso, M. González, and Ángel Borja, A marine spatial planning approach to select suitable areas for installing wave energy converters (WECs), on the Basque continental shelf (Bay of Biscay), *Coastal Management*, vol. 40, no. 1, pp. 1–19, 2012.

[122] L. Cradden, C. Kalogeri, I. M. Barrios, G. Galanis, D. Ingram, and G. Kallos, Multi-criteria site selection for offshore renewable energy platforms, *Renewable Energy*, vol. 87, pp. 791–806, 2016.

[123] A. Martinez, Z. B. Mustapha, R. Campbell, and T. Bouragba, A multi-criteria methodology to select the best wave energy sites in *World Congress on Sustainable Technologies (WCST)*, 2016.

[124] J. Sierra, C. Martín, C. Mösso, M. Mestres, and R. Jebbad, Wave energy potential along the Atlantic coast of Morocco, *Renewable Energy*, vol. 96, pp. 20–32, 2016.

[125] P. Le, A. Fischer, I. Penesis, and R. Rahimi, Aggregating GIS and MCDM to Optimize Wave Energy Converters Location in Tasmania, Australia, *Soft Computing Applications for Renewable Energy and Energy Efficiency*, pp. 141–164, 2015.

[126] K. N. A. Mauluda, W. H. M. W. Mohtara, and O. A. Karima, Spatial Multi Criteria Analysis For the Determination of Areas with High Potential Wave Energy, *Jurnal Teknologi (Sciences & Engineering)*, vol. 65, pp. 113–120, 2013.

[127] S. Astariz and G. Iglesias, The collocation feasibility index – A method for selecting sites for co-located wave and wind farms, *Renewable Energy*, vol. 103, pp. 811–824, 2017.

[128] F. P. de Mendoza, S. Bonamano, G. Stella, M. Giovacchini, D. Capizzi, F. Fraticelli, S. Muratore, C. Burgio, S. Scanu, M. A. Peviani, and M. Marcelli, Where is the best site for wave energy exploitation? Case study along the coast of northern Latium (Italy), *J Coast Conserv*, vol. 20, pp. 13–29, 2016.

[129] R. Prest, T. Daniell, and B. Ostendorf, Using GIS to evaluate the impact of exclusion zones on the connection cost of wave energy to the electricity grid, *Energy Policy*, vol. 35, pp. 4516–4528, 2007.

[130] S. Behrens, J. Hayward, M. Hemer, and P. Osman, Assessing the wave energy converter potential for Australian coastal regions, *Renewable Energy*, vol. 43, pp. 210–217, 2012.

[131] L. Castro-Santos, G. P. Garcia, A. Estanqueiro, and P. A. Justino, The Levelized Cost of Energy (LCOE) of wave energy using GIS based analysis: The case study of Portugal, *Electrical Power and Energy Systems*, vol. 65, pp. 21–25, 2015.

[132] R. Guanche, A. de Andres, I. J. Losada, C. Vidal, and I. J. Losada, A global analysis of the operation and maintenance role on the placing of wave energy farms, *Energy Conversion and Management*, vol. 106, pp. 440–456, 2015.

[133] A. Vazquez and G. Iglesias, Capital costs in tidal stream energy projects - a spatial approach, *Energy*, vol. 107, pp. 215–226, 2016.

[134] S. Cavazzi and A. G. Dutton, An Offshore Wind Energy Geographic Information System (OWE-GIS) for assessment of the UK's offshore wind energy potential, *Renewable Energy*, vol. 87, pp. 212–228, 2016.

[135] DTOcean, *DTOcean User Manual*, 10 2016.

[136] "Advanced design tools for ocean energy systems innovation, development and deployment (dtoceanplus)." `https://cordis.europa.eu/project/rcn/214811_en.html`. Accessed 28/08/18.

[137] The World Energy Council, Off-grid Solar Market Trends 2016, Technical report, World Bank Group, 2016.

[138] R. Kempener, O. L. d'Ortigue, D. Saygin, J. Skeer, S. Vinci, and D. Gielen, Off-grid renewable energy systems: status and methodological issues, Technical report, IRENA, 2015.

[139] J. K. Kaldellis, *Overview of stand-alone and hybrid wind energy systems*, pp. 3–28. Woodhead Publishing, 2010.

[140] U. Datta, A. Kalam, and J. Shi, *Hybrid PV-wind renewable energy sources for microgrid application: an overview*, pp. 1–22. Woodhead Publishing, 2018.

[141] Z. Chmiel and S. C. Bhattacharyya, Analysis of off-grid electricity system at Isle of Eigg (Scotland): Lessons for developing countries, *Renewable Energy*, vol. 81, pp. 578–588, 2015.

[142] H. Aki, Independent hybrid renewable energy systems: Example applications around the world in *Proceedings of IEEE PES General Meeting*, 2010.

[143] Y. Bhikabhai, Hybrid power systems and their potential in the pacific islands, Technical report SOPAC Miscellaneous Report 406, SOPAC Community Lifelines Programme, 2005.

[144] S. Lal and A. Raturi, Techno-economic analysis of a hybrid mini-grid system for Fiji islands, *International Journal of Energy and Environmental Engineering*, vol. 3, no. 1, p. 10, 2012.

[145] G. J. May, A. Davidson, and B. Monahov, Lead batteries for utility energy storage: A review, *Journal of Energy Storage*, vol. 15, pp. 145–157, 2018.

[146] S. P. Ayeng'o, T. Schirmer, K.-P. Kairies, H. Axelsen, and D. U. Sauer, Comparison of off-grid power supply systems using lead-acid and lithium-ion batteries, *Solar Energy*, vol. 162, pp. 140–152, 2018.

[147] N.-K. C. Nair and N. Garimella, Battery energy storage systems: Assessment for small-scale renewable energy integration, *Energy and Buildings*, vol. 42, pp. 2124–2130, 2010.

[148] Rolls Battery Engineering, *BATTERY USER MANUAL*, 3 2017. ver.5.

[149] J. K. Kaldellis, *Feasibility assessment for stand-alone and hybrid wind energy systems*, pp. 102–161. Woodhead Publishing, 2010.

[150] P. Butler, J. Dunleavey, M. Farber-DeAnda, and P. Moseley, Performance of valve-regulated lead-acid batteries in real-world stationary applications - Utility installations, *Journal of Power Sources*, vol. 96, pp. 94–101, 2001.

[151] Fuelling Development: Energy Technologies for Developing Countries, OTA-E-516t, Technical report, U.S. Congress, Office of Technology Assessment, 1992.

[152] V. Nelson, *Wind Energy: Renewable Energy and the Environment.* CRC Press, Florida, 2014.

[153] P. Bolton, Petrol and diesel prices, Technical report, DECC, House of Commons Library, 2014.

[154] S. Sinha and S.S.Chandel, Review of software tools for hybrid renewable energy systems, *Renewable and Sustainable Energy Reviews*, vol. 32, pp. 192–205, 2014.

[155] D. Turcotte and F. Sheriff, Photovoltaic Hybrid System Sizing and Simulation Tools: Status and Needs in *Proceedings of PV Horizon: Workshop on Photovoltaic Hybrid Systems*, 2001.

[156] T. Lambert, P. Gilman, and P. Lilenthal, Micropower system modelling with HOMER in *Integration of alternative sources of energy* (F. Farret and M. Simões, eds.), ch. 15, pp. 379–418, Wiley-IEEE Press, 2006.

[157] HOMER Energy, "Homer energy." `https://www.homerenergy.com/`, accessed 27/08/2018.

[158] E. Hittinger, T. Wiley, J. Kluza, and J. Whitacre, Evaluating the value of batteries in microgrid electricity systems using an improved Energy Systems Model, *Energy Conversion and Management*, vol. 89, pp. 458–472, 2015.

[159] P. O. Oviroh and T.-C. Jen, The Energy Cost Analysis of Hybrid Systems and Diesel Generators in Powering Selected Base Transceiver Station Locations in Nigeria, *Energies*, vol. 11, p. 687, 2018.

[160] A. C. Duman and Önder Güler, Techno-economic analysis of off-grid PV/wind/fuel cell hybrid system combinations with a comparison of regularly and seasonally occupied households, *Sustainable Cities and Society*, vol. 42, pp. 107–126, 2018.

[161] L. M.Halabi, S. Mekhilef, L. Olatomiwa, and J. Hazelton, Performance analysis of hybrid PV/diesel/battery system using HOMER: A case study Sabah, Malaysia, *Energy Conversion and Management*, vol. 144, pp. 322–339, 2018.

[162] R. Rajbongshi, D. Borgohain, and S. Mahapatra, Optimization of PV-biomass-diesel and grid base hybrid energy systems for rural electrification by using HOMER, vol. 126, pp. 461–474, 2017.

[163] J. Bostock, B. McAndrew, R. Richards, K. Jauncey, T. Telfer, K. Lorenzen, D. Little, L. Ross, N. Handisyde, I. Gatward, and R. Corner, Aquaculture: global status and trends, *Phil. Trans. R. Soc. B*, vol. 365, p. 2897–2912, 2010.

[164] The value of aquaculture to Scotland, Technical report, Highlands and Islands Enterprise (HIE), 2017.

[165] W. Kenyon and D. Davies, Salmon Farming in Scotland, Technical report SB 18-12 rev, The Scottish Parliament, 2018.

[166] Salmon Farming Industry Handbook 2015, Technical report, Marine Harvest, 2015.

[167] Scottish Government, "Record levels of salmon and whisky exports." `https://news.gov.scot/news/record-levels-of-salmon-and-whisky-exports`, accessed 19/08/2018.

[168] Aquaculture Growth to 2030, Technical report, Scotland Food & Drink, 2016.

[169] Renewable power generation on aquaculture sites, Technical report ETSU V/06/00181/REP, Scottish Aquaculture Research Forum (SARF), 2014.

[170] F. Cardia and A. Lovatelli, *Aquaculture operations in floating HDPE cages: a field handbook*. FAO, 2015.

[171] M. Ballester-Moltó, P. Sanchez-Jerez, J. Cerezo-Valverde, and F. Aguado-Giménez, Particulate waste outflow from fish-farming cages. How much is uneaten feed?, *Marine Pollution Bulletin*, vol. 119, pp. 23–30, 2017.

[172] L. A. Munro and I. S. Wallace, Scottish Fish Farm Production Survey 2016, Technical report, Marine Scotland Science, 2017.

[173] H. L. Syse, Investigating Off-Grid Energy Solutions for the Salmon Farming Industry, 2016.

[174] D. Whitmarsh and P. Wattage, Public Attitudes Towards the Environmental Impact of Salmon Aquaculture in Scotland, *European Environment*, vol. 16, pp. 108–121, 2006.

[175] A. M. Walker, M. C. Beveridge, W. Crozier, N. . Maoiléidigh, and N. Milner, Monitoring the incidence of escaped farmed Atlantic salmon, Salmo salar L., in rivers and fisheries of the United Kingdom and Ireland: current progress and recommendations for future programmes, *ICES Journal of Marine Science*, vol. 63, pp. 1201–1210, 2006.

[176] "Fish farm loses 155,000 salmon as a result of extreme weather." `http://www.bbc.co.uk/news/uk-scotland-north-east-orkney-shetland-26459825`. Accessed 27/07/2017.

[177] "16,000 salmon escape argyll fish farm after storms." `http://www.scotsman.com/news/16-000-salmon-escape-argyll-fish-farm-after-storms-1-3803325`. Accessed 27/07/2017.

[178] K. Black and A. Hughes, Future of the Sea: Trends in Aquaculture, Technical report NBER Working Paper No. 15081, Government Office for Science, 2017.

[179] J. Bostock, A. Lane, C. Hough, and K. Yamamoto, An assessment of the economic contribution of EU aquaculture production and the influence of policies for its sustainable development, *Aquacult Int*, vol. 24, p. 699–733, 2016.

[180] Steinsvik, "Thermolicer." `https://www.steinsvik.no/en/products/e/seaculture/fish-health/thermolicer`, accessed 20/08/2018.

[181] M. Dumiak, "Lice-hunting underwater drone protects salmon with lasers." `https://spectrum.ieee.org/semiconductors/optoelectronics/licehunting-underwater-drone-protects-salmon-with-lasers`, accessed accessed 20/08/2018.

[182] E. Erwin, T. P. Soemardi, A. Surjosatyo, J. Nugroho, K. Nugraha, and S. Wiyono, Design optimization of hybrid biomass and wind turbine for minapolitan cluster in Domas, Serang, Banten, Indonesia in *IOP Conference Series: Earth and Environmental Science, Indonesia*, 2018.

[183] Python Software Foundation, "The Python Language Reference." Available at http://www.python.org.

[184] M. Lutz, *Learning Python: Powerful Object-Oriented Programming*. O'Reilly Media, 2013.

[185] S. Mount, J. Shuttleworth, and R. Winder, *Python for Rookies.* England: Cengage Learning EMEA, 2008.

[186] Unidata, "The netcdf user's guide." `http://www.unidata.ucar.edu/software/netcdf/docs/user_guide.html`, accessed 19/09/2017.

[187] "N-d labeled arrays and datasets in python." `http://xarray.pydata.org/en/stable/index.html`, accessed 19/09/2017.

[188] N. Marz and J. Warren, *Big Data: Principles and best practices of scalable realtime data systems.* Manning Publications, 2015.

[189] A. Prengère, "Currencyconverter 0.13.2." https://pypi.python.org/pypi/CurrencyConverter, accessed 28/01/18.

[190] O. M. Faltinsen, *Sea Loads on Ships and Offshore Structures.* Cambridge, UK: Cambridge University Press, 1990.

[191] A. Pecher, A. Foglia, and J. P. Kofoed, Comparison and Sensitivity Investigations of a CALM and SALM Type Mooring System for Wave Energy Converters, *J. Mar. Sci. Eng.*, vol. 2, pp. 93–122, 2014.

[192] "Orcaflex documentation; chain: Mechanical properties." `https://www.orcina.com/SoftwareProducts/OrcaFlex/Documentation/`. Accessed 07/07/17.

[193] C. Frost, "Examining the economic potential of hybrid energy systems for fish farms." unpublished, 2016.

[194] FG Wilson, *P220-3.* `http://bellspowersolutions.co.uk/sites/solutions/files/products//P220-3.pdf`, accessed 20/02/2018.

[195] A. Jossen, Battery management in *Valve-Regulated Lead–Acid Batteries* (P. T. Moseley, J. Garche, C. Parker, and D. Rand, eds.), ch. 8, pp. 207–240, Elsevier, 2004.

[196] J. F. Manwell and J. G. McGowan, Lead acid battery model for hybrid energy systems, *Solar Energy*, vol. 50, pp. 399–405, 1993.

[197] Metocean Solutions Ltd. `http://www.metocean.co.nz/`, accessed 15/08/2017.

[198] PELAMIS WEC - CONCLUSION OF PRIMARY R&D: FINAL REPORT, Technical report ETSU V/06/00181/REP, Energy Technology Support Unit (ETSU), 2002.

[199] Albatern Ltd., Albatern Series 6 power matrix. 2015. Data received from Albatern, unpublished.

[200] Gael Force Group, "Gael force group." http://www.gaelforcegroup.co.uk/, accessed 06/09/2017.

[201] Leaske Marine Ltd. http://www.leaskmarine.com, accessed 16/08/2017.

[202] Fraser Hydraulic Power Ltd. http://www.fhpltd.co.uk, accessed 06/05/2018.

[203] Marine Scotland, "Maps nmpi." https://marinescotland.atkinsgeospatial.com/nmpi/, accessed 12/05/2017.

[204] Joint Nature Conservation Committee, Marine SPAs 2009. http://jncc.defra.gov.uk/page-1414, accessed 05/09/2017.

[205] British Geological Survey, "BGS bedrock and superficial geology (WFS service)." http://ogc.bgs.ac.uk/cgi-bin/BGS_Bedrock_and_Superficial_Geology/ows?service=WFS&request=GetCapabilities&, accessed 05/09/2017.

[206] D. Latinopoulos and K. Kechagia, A GIS-based multi-criteria evaluation for wind farm site selection. A regional scale application in Greece, *Renewable Energy*, vol. 78, pp. 550–560, 2015.

[207] Aquaculture site details, 2018. http://aquaculture.scotland.gov.uk/data/site_details.aspx.

[208] Monthly Biomass & Treatment Reports: Gorsten, 2018. http://aquaculture.scotland.gov.uk/data/fish_farms_monthly_biomass_and_treatment_reports.aspx?sepa_site_id=GORS1&ctl00_ctl00_ContentPlaceHolder1_ContentPlaceHolder2_ctl00_gvResultsChangePage=10_15, Accessed 27/07/18.

[209] ValueOils.com.
https://www.valueoils.com/, accessed 23/07/2018.

[210] C. Frost, Economic Feasibility of Integrating a Hybrid Diesel/Battery System into the Domestic Electrical Circuit at Gorsten Fish Farm, Technical report, Albatern Ltd., 2014. unpublished.

[211] "T-105 trojan battery deep cycle." https://www.tayna.co.uk/T-105-Trojan-Battery-Deep-Cycle-T105-P7253.html. Accessed 28/05/2018.

[212] J. Kurtz, G. Saur, S. Sprik, and C. Ainscough, Backup Power Cost of Ownership Analysis and Incumbent Technology Comparison, Technical report, National Renewable Energy Laboratory (NREL), 2014.

[213] "Press release: Emec to take on new development sites in scotland,." http://www.emec.org.uk/press-release-emec-to-take-on-new-development-sites-in-scotland/. Accessed 29/07/18.

[214] S. P. Neill, A. Vögler, A. J. Goward-Brown, S. Baston, M. J. Lewis, P. A. Gillibrand, S. Waldman, and D. K. Woolf, The wave and tidal resource of Scotland, *Renewable Energy*, vol. 114, pp. 3–17, 2017.

[215] ISRD Group, *Data structures using C*. New Delhi, India: McGraw-Hill, 2012.

[216] General Bathymetric Chart of the Oceans (GEBCO), "Gebco 30 arc-second grid." https://www.gebco.net/data_and_products/gridded_bathymetry_data/gebco_30_second_grid/. Accessed 15/08/17.

[217] I. Dinwoodie, D. McMillan, M. Revie, I. Lazakis, and Y. Dalgic, Development of a Combined Operational and Strategic Decision Support Model for Offshore Wind, *Energy Procedia*, vol. 35, pp. 157–166, 2013.

[218] D. O'Sullivan and G. Dalton, Challenges in the Grid Connection of Wave Energy Devices in *Proceedings of EWTEC2009*, 2009.

[219] QGIS, "Pyqgis developer cookbook." https://docs.qgis.org/2.14/en/docs/pyqgis_developer_cookbook/. Accessed 13/08/18.

[220] C. Garrard, *Geoprocessing with Python*. Shelter Island, NY: Manning Publications, 2016.

[221] D. Eppstein, "Dijkstra's algorithm for shortest paths." https://www.ics.uci.edu/~eppstein/161/python/dijkstra.py/, accessed 15/12/2017.

Programming Terminology

A.1 Python

This section describes some common Python terminology that is used in the thesis.

- **Module**: An individual file containing some Python code.
- **Package**: A collection of modules that together form a complete unit. The model examined in this work is an example of a package.
- **String**: A data type defining some text. e.g. `programming = "fun"`
- **Float**: A data type defining numeric data. e.g. `task_length = 10.5`
- **List**: A data type that contains an ordered group of variables.

  e.g. `cute_cats = ['Billy', 'Chuckles', 13.7]`
- **Dictionary** (dict): An unordered data type that maps one variable onto another.

  e.g. `losses = {'hydraulic': 0.03, 'mechanical': 0.05, 'electrical': 0.01}`

A.2 Object-Orientated Programming

In OOP, data variables and the functions that use them can be grouped together in the code into single structures. This is relevant when the variables are related, and together describe some kind of singular entity. In programming terms

this is known as a *class*. It is effectively a blueprint, used to create different objects (or *instances*) that are defined by variables of different values. Variables and functions common to a class are known as class *attributes* and class *methods* respectively.

Classes can be used to represent real, physical objects in code. For example a "car" class might contain attributes like manufacturer, model, engine size and colour. A key advantage of using OOP is the principle of inheritance. This is the idea that a hierarchy of classes can exist, whereby a class instance can be a member of several different class categories. Higher level attributes and functions can be passed down from the super class ("parent") to the subclass ("child"), so that all of the classes share some common variables and methods. This has the advantage that code is only written in a single place, improving organisation and meaning that modifications to code only need to be made once.

A.3 UML Diagrams

UML diagrams are used to visually represent the hierarchy of classes within an OOP framework. In this thesis, three relationships between the classes are represented:

- **Inheritance**: All of the attributes and methods defined for a parent class are passed down to the child, as the child is effectively a sub-type of the parent. For example the `MarineOperation` class is a type of `Operation`.
- **Aggregation**: The parent class contains the child class and the child class can exist independently. The `MarineOperation` class contains a `Vessel`, but the vessel is also an entity in its own right.
- **Composition**: The parent class contains the child class, however the child class cannot exist outside the parent. For example the `ExportCable` class contains landing points (`CableLanding` class instances), however cable landing points do not make physical sense without a cable.

For aggregation and composition, the amount of child classes that exist in the parent are defined with the multiplicity definitions:

- **n**: A specific number are always contained, e.g. 2.
- **0..1**: Zero or one can be contained, i.e a parent does not have to contain the child.
- **0..***: Any number can be contained, including zero.

- **1..***: At least one child must be contained in the parent.

Lastly, the UML diagram shows the visibility of the attributes within each class:

- **Public**: The attribute can be freely set by the user.
- **Private**: The attribute cannot be seen or directly set by the user, instead used within the inner class workings.
- **Derived**: The attribute is not set by the user but is derived or calculated within the class. It is visible to the user.

Supporting Python Modules

This section describes the external modules that are required by the model. These have been coded from scratch, and provide classes and functions to assist in the structuring and operation of the model. They are not solely concerned with the research theme and could, in theory, be applied to other types of projects.

B.1 GIS Utilities

The `gis_utilities` module contains the functions that are used to create and manipulate GIS data. This is required to both import the spatial inputs and results from the model and to extract GIS data from existing files to include in the analysis. The foundation of this module are the *gdal* and *ogr* packages. They are open source and provide the framework for manipulating raster and vector files respectively. The functions are built upon the classes within these modules, each focussing on a specific task and coded in a more readable manner. Much of the code has been created using Garrard as a reference [220].

The first half of the module is concerned with vector data. Functions have been coded to allow different types of shape geometries to be created, including single points, multipoints and polygons. These are typically used to export map layers showing the locations of the geographic input data: examples include the data points being analysed, the full size of the data domain and export cable landing point locations. Fields can be added to these features, providing information and identification, which can be viewed in GIS software. In addition, functions also allow the reading of vector data. This is most useful when exporting geographic data (polygon layers) from external sources into the model in order to create

constraint layers, which are described in Section 3.10. After loading the data into Python, individual coordinates can be cross-referenced against the polygons to determine if they intersect, allowing discrete locations to be categorised.

The functions supporting raster data make up the second half of the module. Like the vector functions, the primary application of these functions is to read and write raster GIS data. Because the hindcast wave data used for the model energy estimation is discrete, time series data given at specific locations, the majority of the GIS data created by the model is raster data. Important to the correct visualisation of the raster data is the *geotransform*. This is an attribute of the underlying *gdal* raster data class, and defines the transformation of the 2D array representing the data to geographic coordinates. By storing the top left pixel position, the resolution in each direction and any rotation angles, the data contained in each raster pixel can be mapped to a geographic position, after also considering the projection. As for the vector functions, attribute tables can be created and added to the data. Raster data imported into Python can not only be read, but also re-sampled. This is desired when the input data of interest is at a different resolution to the hindcast wave data, and allows values to be generated at specified locations not present in the original data.

B.2 MongoDB Utilities

This module was designed to allow MongoDB NoSQL databases to be developed as part of the model. This functionality was desired by Albatern as part of an internal shift towards using a centralised database to keep track of costings and bill of materials. The long term vision is that the model will pull out up to date device costs and feed back into the future design process. The module itself contains some basic classes and functions for performing database queries within Python as well as updating existing databases with new data. It was created using the *pymongo* module, created by MongoDB Inc. to assist Python developers.

Two classes were created. The `MongoDaemon` class allows Python to access the server containing the databases. This is typically achieved using a configuration text file. The second class is a direct representation of a database, `MongoDatabase`. This inherits from the *pymongo DataBase* class, but with additional functions to carry out some common procedures (for example querying and saving items to the database).

The functions within the module use the classes to perform basic operations,

and are linked to the `base_classes` module as was described in Section 3.4. The module was ultimately not used for the research, a configuration text file approach preferred due to project time constraints (see Section 3.3), but is included here for completeness.

B.3 Path Finding

This contains all of the functions used for performing pathfinding operations. The functions can be broadly categorised into three different areas: creating the input graph, performing the actual algorithm on the graph and formatting the output data in a more useful format for general application.

The most basic graph creation function, `get_graph`, takes in an array of data and an obstacle definition. It checks the array points and uses the relevant conditional statement to check whether the point is an obstacle or graph node. It returns a graph as a dictionary type, with each point in the array matched to its nearest neighbours. A more sophisticated function, `get_graph_with_coordinate_distances` takes in this completed graph along with longitude and latitude dimensions corresponding to the array indices. The output graph contains the distances from each node to its nearest neighbours, calculated using the haversine equation. Graphs created with this and the previous method define the nodes by their position in the array, using their (x, y) indices. A third version of the graphing function, `get_graph_with_coordinate_keys`, converts these indices into coordinates by looking up the indices in the latitude and longitude dimensions. The advantage of using coordinate values as keys is that the size and the shape of the array is no longer a factor. An earlier model version using indices required converting between index values defined in the analysis and routing domain, which added complexity and introduced bugs.

For pathfinding algorithms there are two functions based on Dijkstra's algorithm. The first is the classic Dijkstra's algorithm which, given a starting point will calculate distances for all nodes in the graph. This function was downloaded from [221]. A final point can be specified as an optional argument; in this case the algorithm ends when this point is reached. In the default case the algorithm runs until all paths to all graph nodes have been resolved. For the second function, `dijkstra_by_value`, the algorithm is terminated when it reaches a node with a specific data value associated with it. An array with data values accompanying the graph nodes must be included.

The Dijkstra algorithm-based functions return outputs, path distances and the predecessor in the path, in the form of dictionaries, with each node presented by a key in the dictionary. The `distances_to_np_array` function converts the distances dictionary to an array, allowing it to be easily visualised (for example converted to a raster). Lastly, the full paths from the start point to each node can be extracted using another function. This more readable format can be easily stored within a json file, and vectors for individual paths created using the GIS Utilities module described in Section B.1.

B.4 Time Series Manipulation

The purpose of this module is to provide functions to allow time series data to be easily created and modified. It makes use of the *Pandas* module, in particular the *DataFrame* class, which allows data to be easily grouped along specific dimensions. Because of this the *DataFrame* class tends to be the default type used for time series data within the overall model.

Because the three dimensional data arrays (time, latitude and longitude dimensions) can get very large, it is often necessary to group the data along the time dimension, where they can be easily summed or averaged. This is also advantageous as it allows an easily way to examine seasonal trends in the data (for example the power produced by a wave energy device). The function `group_values_by_time` builds on methods in *DataFrame* and allows input time series to be grouped according to a time index (for example by month or year).

A key functionality is the ability to project time series data forward in time. This is required when there is only limited input data to work with (for example metocean data or load profile data) and is achieved using the function `format_and_project_timeseries`. This utilises a number of other functions coded in the module. Given an input *DataFrame* and total periods desired, the function will replicate the *DataFrame* forward, after grouping the data by the time base desired. For incomplete time series, the time series can either be trimmed back or extended forward to a suitable time base prior to replication. This is to ensure that the time periods are consistent with the time index, capturing the seasonal profile. An issue with the data projection is that it simply copies pre-existing data. This means that a projected time series will not see the full inter annual variability that would exist in reality. For larger datasets this is not a significant issue. To handle smaller datasets better, an improvement would be to derive future months based on the data supplied, for example by fitting monthly

normal distributions to the data and using the resulting function to predict future trends. Another option would be to use Markov chains to predict future metocean sea states. This is noted as future work.

B.5 Extra Utilities

Contained within this module are miscellaneous functions which would be suitable for Python applications outside of this research project. They include functions to format and manipulate different object types, conversion functions and functions to read different file formats into Python, among other things.

Grid-connected Case Study Configuration Files

C.1 File Structure

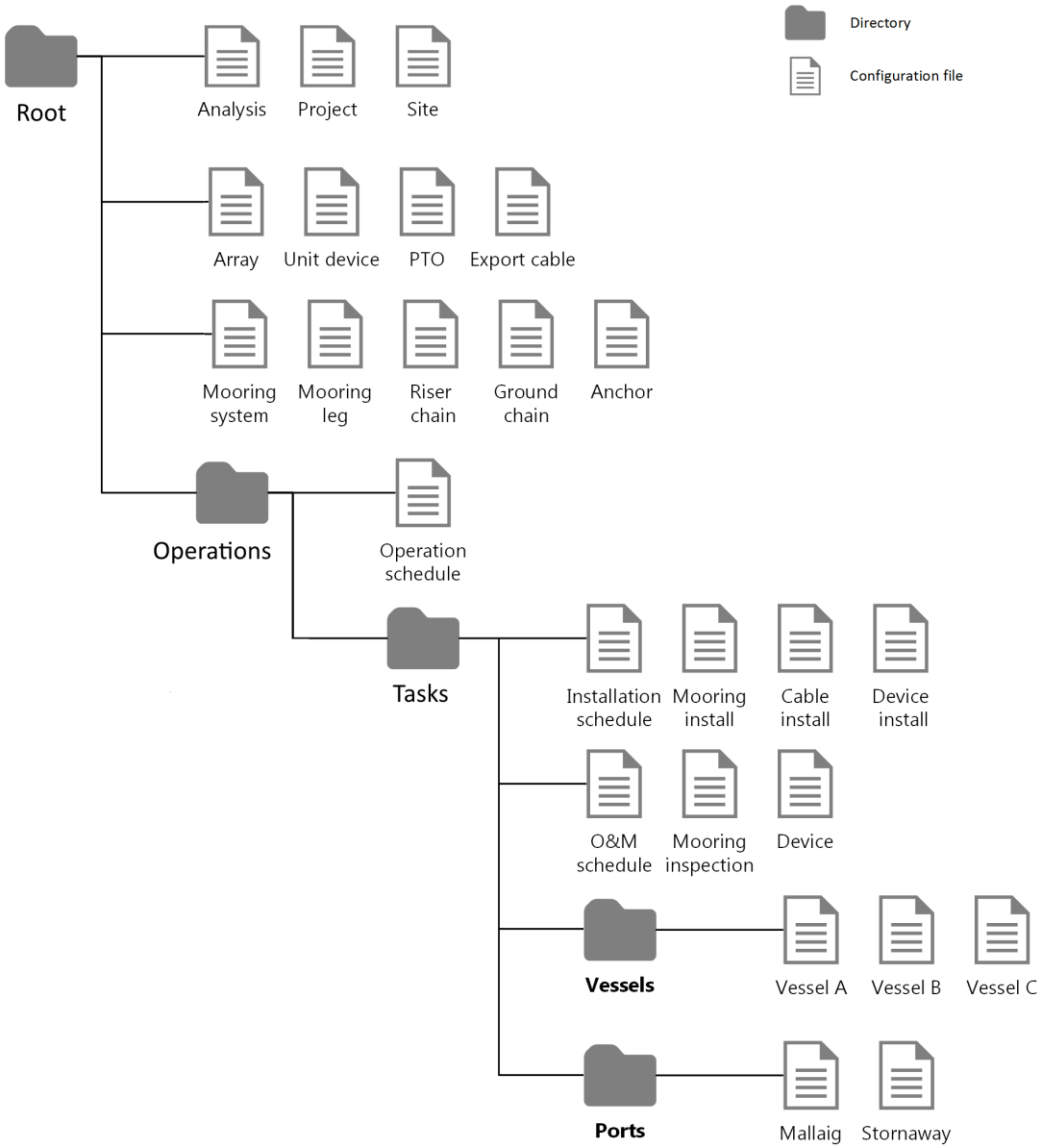

Figure C.1: Example of how configuration files are organised within the directory structure, similar to that used for the grid connected case study.

C.2 Configuration Files

A Project and Site

```
class c_EnergyAnalysis
project b_project.txt
energy_projection_options {'pre_time_trim': '2009-12'}
power_interpolation_options {'chunk_base': 'year', 'sum_to_base':'month'}
```

```
class c_Project
_id project_id
cost_categories PROJECT

# The site
site c1_site.txt
# For testing purposes
#site c2_site_transcend.txt

device d1_wave_device.txt

project_lifetime (20, 0)
power_producing_end (20, 0)

discount_rate 0.10
```

```
class c_WaveSite
_id site_id
start_year 2000

# The analysis area

# Sensitivity area
lat_analysis_extents ((56.95, 58.4), 'coordinates')
lon_analysis_extents ((-7.4, -5.4), 'coordinates')

# Full size
#lat_analysis_extents ((56.2, 58.6), 'coordinates')
#lon_analysis_extents ((-7.6, -5.0), 'coordinates')
```

```
# The data files
site_data_files {'path': 'C:\\Documents\\Albatern\\Data\\Domain
    2\\nwscotlandDom2_MOS_2000_d1.nc', 'time_range':'2000'}
site_data_files {'path': 'C:\\Documents\\Albatern\\Data\\Domain
    2\\nwscotlandDom2_MOS_2001_d1.nc', 'time_range':'2001'}
site_data_files {'path': 'C:\\Documents\\Albatern\\Data\\Domain
    2\\nwscotlandDom2_MOS_2002_d1.nc', 'time_range':'2002'}
site_data_files {'path': 'C:\\Documents\\Albatern\\Data\\Domain
    2\\nwscotlandDom2_MOS_2003_d1.nc', 'time_range':'2003'}
site_data_files {'path': 'C:\\Documents\\Albatern\\Data\\Domain
    2\\nwscotlandDom2_MOS_2004_d1.nc', 'time_range':'2004'}
site_data_files {'path': 'C:\\Documents\\Albatern\\Data\\Domain
    2\\nwscotlandDom2_MOS_2005_d1.nc', 'time_range':'2005'}
site_data_files {'path': 'C:\\Documents\\Albatern\\Data\\Domain
    2\\nwscotlandDom2_MOS_2006_d1.nc', 'time_range':'2006'}
site_data_files {'path': 'C:\\Documents\\Albatern\\Data\\Domain
    2\\nwscotlandDom2_MOS_2007_d1.nc', 'time_range':'2007'}
site_data_files {'path': 'C:\\Documents\\Albatern\\Data\\Domain
    2\\nwscotlandDom2_MOS_2008_d1.nc', 'time_range':'2008'}
site_data_files {'path': 'C:\\Documents\\Albatern\\Data\\Domain
    2\\nwscotlandDom2_MOS_2009_d1.nc'}

# Seabed geology file for constraints and cable routing
seabed_geology 'C:\\Documents\\bathymetry_data\\Seabed
    sediments\\Scotland domain shape\\seabed_sediment.tif'
```

B Device

```
class c_WaveEnergyArray
_id 'device_id'
description '3-Hex, Series 6 array'

# Power properties
# Power matrix must be an absolute path.
power_matrix H:\\Documents\\power_matrices\\S6-3H-6SQ-TS-PM-F1_1_85.csv
hs_limits (None, 7.0)

# Unit device
unit_device_quantity 6.0
```

```
unit_device d2_squid_unit.txt

# Mooring system
mooring_system m0_mooring_system.txt

# Export cable
export_cable e1_export_cable.txt

# Onshore connection
local_costs {'description': 'Onshore connection', 'value': 10000,
    'cost_categories': ['onshore_connection', 'IC_total']}

# Proportional costs (insurance cost)
proportional_costs {'value': 0.01, 'initial':12, 'freq':12,
    'description': 'insurance', 'cost_categories': ['OPEX', 'insurance',
    'ALL_OPERATIONS'], 'master_category': 'IC_total', 'cost_per_parent':
    False}
# Unplanned O&M (% of WEC capex per year). The IC_total is capital +
    installation
proportional_costs {'value': 0.02, 'initial': 12, 'freq':12,
    'description': 'unplanned_om', 'cost_categories': ['OPEX',
    'O&M_UNPLANNED', 'ALL_OPERATIONS'], 'master_category': 'IC_total'}

# Constraints
min_water_depth 20
max_water_depth 100
restricted_locations
    'C:\\Documents\\gis_data\\Environmental\\SPA\\uk_spa_marine_WGS84.shp'

#Availability
efficiencies 0.8
```

```
class c_WaveEnergyDevice
_id 'squid_id'
description 'A single Series-6 Squid unit device'

# Cost categories
cost_categories DEVICE

# Local costs (device subsystems)
```

```
local_costs {'description': 'central node', 'quantity': 1, 'value':
    5743, 'cost_categories':['capex_device', 'IC_total']}
local_costs {'description': 'anti node', 'quantity': 3, 'value': 7897,
    'cost_categories':['capex_device', 'IC_total']}
local_costs {'description': 'riser', 'quantity': 1, 'value': 5163,
    'cost_categories':['capex_device', 'IC_total']}
local_costs {'description': 'pumping module CN', 'quantity': 3, 'value':
    5335, 'cost_categories':['capex_device', 'IC_total']}
local_costs {'description': 'pumping module AN', 'quantity': 3, 'value':
    6936, 'cost_categories':['capex_device', 'IC_total']}
local_costs {'description': 'link arm', 'quantity': 3, 'value':1523,
    'cost_categories':['capex_device', 'IC_total']}
local_costs {'description': 'other', 'quantity': 1, 'value':996,
    'cost_categories':['capex_device', 'IC_total']}

# Operations schedule.
operation_schedule \\operations\\sd1_device_schedule.txt


# PTO
pto_generator d3_squid_pto.txt
pto_generator_quantity 1.0
```

```
class c_PtoGenerator
_id 'pto_generator_id'

cost_categories IC_total
cost_categories capex_device
cost_categories device_pto_unit

description 'The PTO for the Series-6 Squid, rated at 7,5 kW'
local_costs {'description': 'pto', 'quantity': 1, 'value': 6777}
rated_power 7.5
```

C Export Cable

```
class c_ExportCable
_id 'export_cable_id'
cost_per_m 20.0
```

```
# Cost categories
cost_categories EXPORT_CABLE
cost_categories IC_total
cost_categories capex_export_cable

# Operational tasks
operation_schedule \\operations\\tasks\\ti3c_cable_install.txt

# Do for sensitivity, not here.
maximum_depth_for_install None
invalid_seabed_sediments None
#max_cable_length 8000
```

D Mooring System

```
class c_MooringSystemWavenetS6
_id mooring_system_id
description 'WEC mooring system'

# Cost categories
cost_categories MOORING_SYSTEM

# Operation schedule
operation_schedule \\operations\\sm1_mooring_schedule.txt

# Mooring system components
mooring_leg m4_mooring_leg.txt
grid_line {'cost_per_m': 1.88, 'line_material': 'basic_nylon',
    'cost_categories': ['IC_total', 'capex_mooring_system'],
    'line_length_m': 220, 'quantity':2}
corner_buoy {'local_costs': {'description': 'unit', 'value':760},
    'cost_categories': ['IC_total', 'capex_mooring_system']}
local_costs {'description': 'Connectors and shackles', 'value': 500,
    'cost_categories': ['IC_total', 'capex_mooring_system']}

# Other inputs
grid_displacement 5.0
```

```
class c_Anchor
_id anchor_id
description 'Mooring system anchor'
#cost_categories 'mooring_anchor'
local_costs {'description': 'unit', 'value': 1995.0}
weight 1500.0

invalid_seabed_geology 5
```

```
class c_Line
_id ground_chain_id
description 'Mooring system ground chain'
#cost_categories 'mooring_ground_chain'
cost_per_m 29.5
# From
    http://www.sotra.net/products/tables/weight-for-studlink-anchor-chain
dry_mass_per_m 34.0
line_material basic_steel
diameter 38
```

```
class c_CatenaryLine
_id riser_chain_id
description 'Mooring system riser chain'
#cost_categories 'mooring_riser_chain'
cost_per_m 23.0
# From
    http://www.sotra.net/products/tables/weight-for-studlink-anchor-chain
dry_mass_per_m 13.0
line_tension 20000
line_material basic_steel
diameter 24
```

```
class c_CatenaryLeg
_id mooring_leg_id
description 'Mooring system leg'

cost_categories IC_total
cost_categories capex_mooring_system
#cost_categories 'mooring_leg'
```

```
anchor m1_anchor.txt
ground_chain m2_ground_chain.txt
line_to_surface m3_line_to_surface.txt
ground_chain_ratio 3
```

E Operations and Maintenance

E.1 Operation Schedules

```
class c_OperationSchedule
description device_op_schedule_id

cost_categories ALL_OPERATIONS

# The device operational tasks
task_list tasks\\ti2d_device_install.txt
task_list tasks\\to2d_device_port_service.txt
task_list tasks\\to3d_midlife_refit.txt

# The ports
port tasks\\ports\\p1_port_stornaway.txt
port tasks\\ports\\p2_port_mallaig.txt
port tasks\\ports\\p3_port_carloway.txt
port tasks\\ports\\p4_port_griminis.txt
port tasks\\ports\\p5_port_breibhig.txt
port tasks\\ports\\p6_port_acairseid.txt
port tasks\\ports\\p7_port_meanish.txt
port tasks\\ports\\p8_port_coll.txt
port tasks\\ports\\p9_port_old_dornie.txt
port tasks\\ports\\p10_port_applecross.txt
```

```
class c_OperationSchedule
_id o&m_schedule_moorings
description Operation schedule for the mooring system

# Cost categories
cost_categories ALL_OPERATIONS
```

```
# List of tasks
task_list \\tasks\\ti1m_mooring_install.txt
task_list \\tasks\\to1m_mooring_inspection.txt

port tasks\\ports\\p1_port_stornaway.txt
port tasks\\ports\\p2_port_mallaig.txt
port tasks\\ports\\p3_port_carloway.txt
port tasks\\ports\\p4_port_griminis.txt
port tasks\\ports\\p5_port_breibhig.txt
port tasks\\ports\\p6_port_acairseid.txt
port tasks\\ports\\p7_port_meanish.txt
port tasks\\ports\\p8_port_coll.txt
port tasks\\ports\\p9_port_old_dornie.txt
port tasks\\ports\\p10_port_applecross.txt
```

E.2 Tasks

```
class c_MarineOperation
_id inst_mooring_id
description Mooring system install

cost_categories INSTALLATION
cost_categories installation_mooring_system
cost_categories IC_total

# Pre project as installation activity
pre_project True

vessel \\vessels\\v1_workboat.txt
vessel_per_quantity True

vessel_mob_time_days 1
vessel_demob_time_days 1

support_vessels \\vessels\\v2_rhib.txt

hours_to_complete_task 6

max_seastate_transit_out 3.0
max_seastate_task 1.5
```

```
max_seastate_transit_return 3.0

period_for_task '2000-10'

# Scheduling timescale inputs
multiple_trips_allowed False
max_hours_for_single_operation 24
resting_hours_between_operations 0
min_site_time_threshold 1.0
sleep_on_vessel False
```

```
class c_MarineOperation
_id inst_device_id
description Squid_install

cost_categories INSTALLATION
cost_categories installation_device
cost_categories IC_total

# Pre project as installation activity
pre_project True

vessel \\vessels\\v1_workboat.txt
vessel_per_quantity True

vessel_mob_time_days 1.0
vessel_demob_time_days 1.0

support_vessels \\vessels\\v2_rhib.txt

speed_to_site_knots 4.5
speed_from_site_knots None

hours_to_complete_task 3

max_seastate_transit_out 1.5
max_seastate_task 1.5
max_seastate_transit_return 3.0

period_for_task '2000-10'
```

```
# Scheduling timescale inputs
multiple_trips_allowed False
max_hours_for_single_operation 24
resting_hours_between_operations 0
min_site_time_threshold 1.0
sleep_on_vessel False
```

```
class c_ExportCableInstall
_id inst_cable_id
description Cable install

# Cost categories
cost_categories INSTALLATION
cost_categories ALL_OPERATIONS
cost_categories installation_cable
cost_categories IC_total

invalid_cost_categories capex_export_cable

# Pre project as installation activity
pre_project True

vessel \\vessels\\v4_multicat_cable_lay_vessel.txt

vessel_mob_time_days 2
vessel_demob_time_days 2

install_speed (500, 'metre/hour')

max_seastate_transit_out 3.0
max_seastate_task 1.5
max_seastate_transit_return 3.0

period_for_task '2000-09'

local_costs {'description': 'rig servicing', 'value': 400,
    'cost_categories': 'installation_cable_rig_servicing'}

# Timescale properties
```

```
max_hours_for_single_operation 36
multiple_trips_allowed False
min_site_time_threshold 1.0

port ports\\p1_port_stornaway.txt
port ports\\p2_port_mallaig.txt
port ports\\p3_port_carloway.txt
port ports\\p4_port_griminis.txt
port ports\\p5_port_breibhig.txt
port ports\\p6_port_acairseid.txt
port ports\\p7_port_meanish.txt
port ports\\p8_port_coll.txt
port ports\\p9_port_old_dornie.txt
port ports\\p10_port_applecross.txt
```

```
class c_MarineOperation
_id mooring_inspection_id
description Mooring inspection at site

cost_categories OPEX
cost_categories O&M_PLANNED
cost_categories o&m_mooring_inspection

vessel \\vessels\\v1_workboat.txt
vessel_per_quantity True

vessel_mob_time_days 1
vessel_demob_time_days 1

hours_to_complete_task 3

max_seastate_transit_out 3.0
max_seastate_task 1.5
max_seastate_transit_return 3.0

period_for_task ['2001-03', '2002-03', '2003-03', '2004-03', '2005-03',
    '2006-03', '2007-03', '2008-03', '2009-03', '2010-03', '2011-03',
    '2012-03', '2013-03', '2014-03', '2015-03', '2016-03', '2017-03',
    '2018-03', '2019-03']
```

```
local_costs {'description': 'inspection', 'value': 1500, 'initial': 15,
    'freq': 12}

# Scheduling timescale inputs
multiple_trips_allowed False
max_hours_for_single_operation 24
resting_hours_between_operations 0
min_site_time_threshold 1.0
sleep_on_vessel False
```

```
class c_MaintenanceAtPort
_id device_service_in_port_id
description device service in port

cost_categories OPEX
cost_categories O&M_PLANNED
cost_categories o&m_device_routine_service

vessel \\vessels\\v1_workboat.txt
vessel_per_quantity True

pre_maintenance_operation toAd_recover_device_from_site.txt
time_in_port_days 1.0
post_maintenance_operation toBd_deploy_device_at_site.txt

period_for_task ['2000-03', '2000-09', '2001-3','2001-9',
    '2002-3','2002-9','2003-3','2003-9', '2004-3', '2004-9', '2005-3',
    '2005-9', '2006-3', '2006-9', '2007-3', '2007-9', '2008-3',
    '2008-9', '2009-3', '2009-9', '2010-9', '2011-3', '2011-9',
    '2012-3', '2012-9', '2013-3', '2013-9', '2014-3', '2014-9',
    '2015-3', '2015-9', '2016-3', '2016-9', '2017-3', '2017-9',
    '2018-3', '2018-9', '2019-3', '2019-9', '2020-3', '2020-9']

# Pre mid life refit
local_costs {'description':'parts', 'value': 800, 'initial':3, 'freq':6,
    'final':120}
local_costs {'description':'other', 'value': 600, 'initial':3, 'freq':6,
    'final':120}
local_costs {'description':'inspection', 'value': 200, 'initial':3,
    'freq':6, 'final':120}
```

```
# Post midlife refit
local_costs {'description':'parts2', 'value': 800, 'initial':129,
    'freq':6}
local_costs {'description':'other2', 'value': 600, 'initial':129,
    'freq':6}
local_costs {'description':'inspection2', 'value': 200, 'initial':129,
    'freq':6}
```

```
class c_MaintenanceAtPort
_id midlife_refit_id
description midlife refit in port

cost_categories OPEX
cost_categories O&M_PLANNED
cost_categories o&m_midlife_refit

vessel \\vessels\\v1_workboat.txt
vessel_per_quantity True

pre_maintenance_operation toAd_recover_device_from_site.txt
time_in_port_days 2.0
post_maintenance_operation toBd_deploy_device_at_site.txt

period_for_task ['2010-03']

local_costs {'initial': 123, 'description': 'pumping modules',
    'quantity': 3, 'value': 12271}
local_costs {'initial': 123, 'description': 'pto', 'quantity': 1,
    'value': 6777}
```

```
class c_MarineOperation
_id device_service_rtn_id
description device_service_rtn

vessel \\vessels\\v1_workboat.txt

# Assume occurs per 6 devices
vessel_mob_time_days 0.0
vessel_demob_time_days 1.0
```

```
max_seastate_transit_out 3.0
max_seastate_task 1.5
max_seastate_transit_return 1.5

speed_to_site_knots None
speed_from_site_knots 4.5

hours_to_complete_task 2

# Scheduling timescale inputs
multiple_trips_allowed False
max_hours_for_single_operation 24
resting_hours_between_operations 0
min_site_time_threshold 1.0
sleep_on_vessel False
```

```
class c_MarineOperation
_id device_service_out_id
description device_service_out

vessel \\vessels\\v1_workboat.txt

# Assume occurs per 6 devices
vessel_mob_time_days 1.0
vessel_demob_time_days 0.0

max_seastate_transit_out 1.5
max_seastate_task 1.5
max_seastate_transit_return 3.0

speed_to_site_knots 4.5
speed_from_site_knots None

hours_to_complete_task 2

# Scheduling timescale inputs
multiple_trips_allowed False
max_hours_for_single_operation 24
resting_hours_between_operations 0
```

```
min_site_time_threshold 1.0
sleep_on_vessel False
```

E.3 Vessels

```
class c_Fuel
cost_categories vessel_fuel_cost
cost_per_ltr 0.60
```

```
class c_Vessel
_id workboat_vessel_id
description Workboat for smaller operations; Suitable for Series 6
cost_categories vessel_workboat

charter_cost 1500
standby_cost 1000
mob_cost 900
demob_cost 900

average_speed 9
speed_units 'knot'

fuel_consumption_rate_travel 40.0
fuel f0_vessel_fuel.txt

comments 'Based on Leaske Marine's MV Uskmoor
    http://www.leaskmarine.com/vessels/mv-uskmoor'
```

```
class c_Vessel
_id rhib_vessel_id
description Support vessel
cost_categories vessel_rhib

charter_cost 1200
standby_cost 0

mob_cost 0
demob_cost 0
```

```
mob_time_days 0
demob_time_days 0

average_speed 25
speed_units 'knot'

fuel_consumption_rate_travel 30.0
fuel f0_vessel_fuel.txt

comments 'Based on Leaske Marine's MV Explorer
    http://www.leaskmarine.com/vessels/mv-explorer'
```

```
class c_Vessel
_id cable_multicat_vessel_id
description Cable lay vessel
cost_categories vessel_cable_lay_multicat

charter_cost 7700
standby_cost 5800
mob_cost 4600
demob_cost 4600

average_speed 10
speed_units 'knot'

fuel_consumption_rate_travel 280.0
fuel_consumption_rate_working 70
fuel f0_vessel_fuel.txt

comments 'Based on Leaske Marine's MV Uskmoor
    http://www.leaskmarine.com/vessels/mv-uskmoor'
```

E.4 Ports

```
class c_Port
lat 58.20692587839467
lon -6.382697603124509
description Stornaway port
#cost_categories port
#local_costs {'description': 'Port Hire', 'value':1000}
```

```
class c_Port
lat 57.00521880549277
lon -5.827369554384538
description Mallaig port
#cost_categories port
#local_costs {'description': 'Port Hire', 'value':2000}
```

```
class c_Port
lat 58.279
lon -6.791
description Carloway port
#cost_categories port
#local_costs {'description': 'Port Hire', 'value':2000}
```

```
class c_Port
lat 58.20692587839467
lon -6.382697603124509
description Stornaway port
#cost_categories port
#local_costs {'description': 'Port Hire', 'value':1000}
```

```
class c_Port
lat 57.564
lon -7.439
description Griminis port
#cost_categories port
#local_costs {'description': 'Port Hire', 'value':2000}
```

```
class c_Port
lat 56.96
lon -7.441
description Breibhig port
#cost_categories port
#local_costs {'description': 'Port Hire', 'value':2000}
```

```
class c_Port
lat 57.068
```

```
lon -7.294
description Acairseid port
#cost_categories port
#local_costs {'description': 'Port Hire', 'value':2000}
```

```
class c_Port
lat 57.456
lon -6.746
description Meanish port
#cost_categories port
#local_costs {'description': 'Port Hire', 'value':2000}
```

```
class c_Port
lat 56.615
lon -6.522
description Coll port
#cost_categories port
#local_costs {'description': 'Port Hire', 'value':2000}
```

```
class c_Port
lat 58.044
lon -5.421
description Old Dornie port
#cost_categories port
#local_costs {'description': 'Port Hire', 'value':2000}
```

```
class c_Port
lat 57.434
lon -5.814
description Applecross port
#cost_categories port
#local_costs {'description': 'Port Hire', 'value':2000}
```

Sample Results

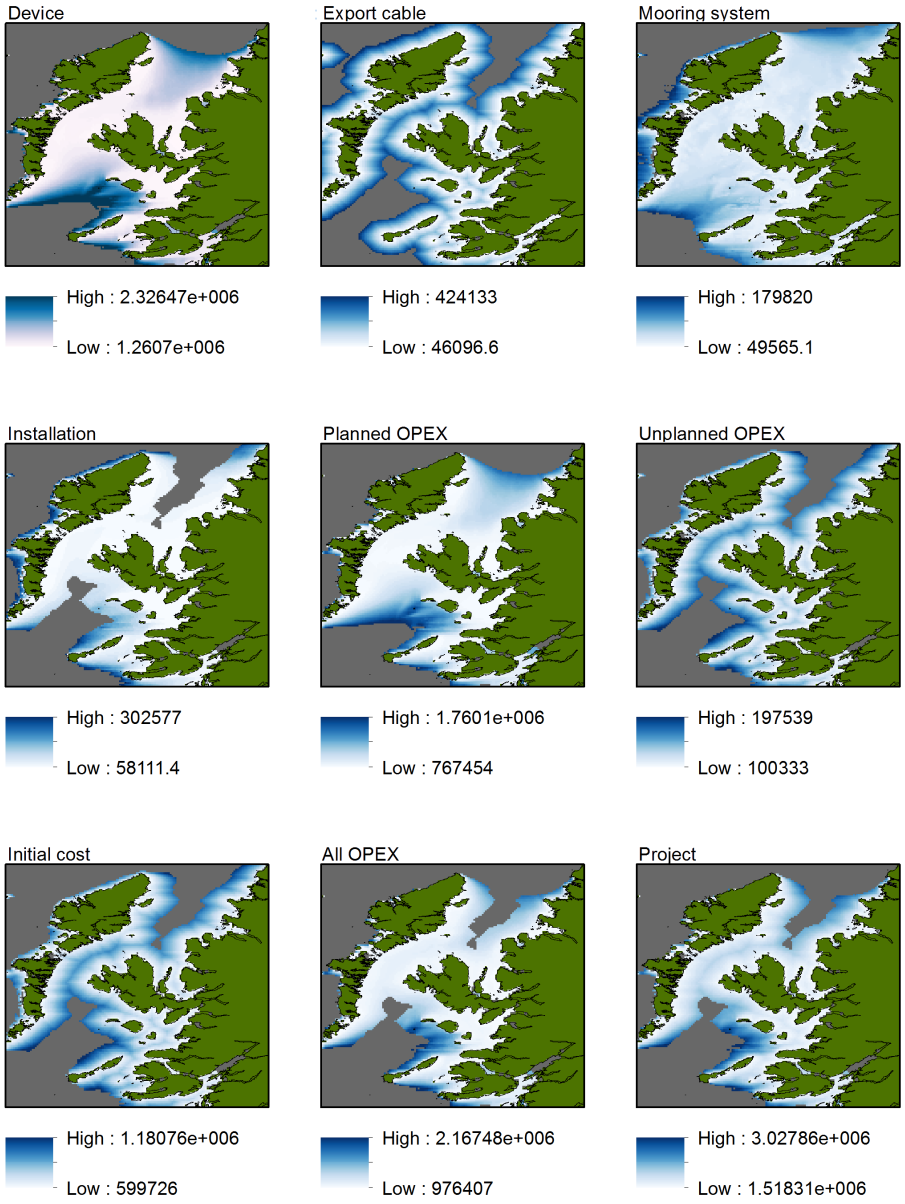

Figure D.1: Examples of categorised cost map outputs from the grid-connected baseline scenario.

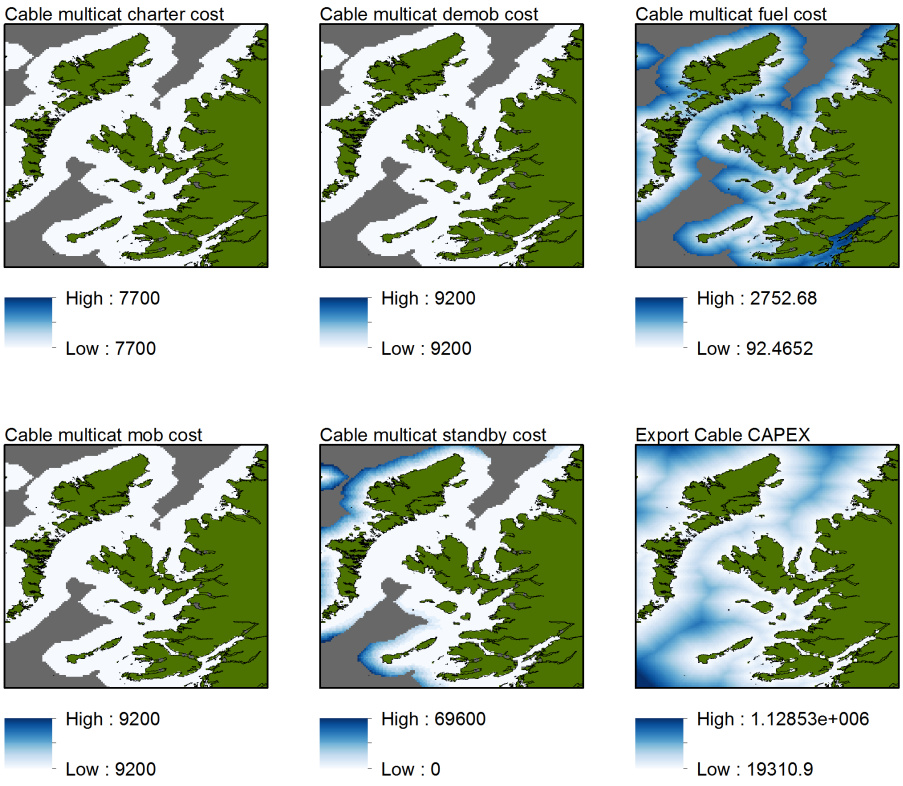

Figure D.2: Costs for the mooring installation task from the grid-connected baseline scenario (Section 5.2).

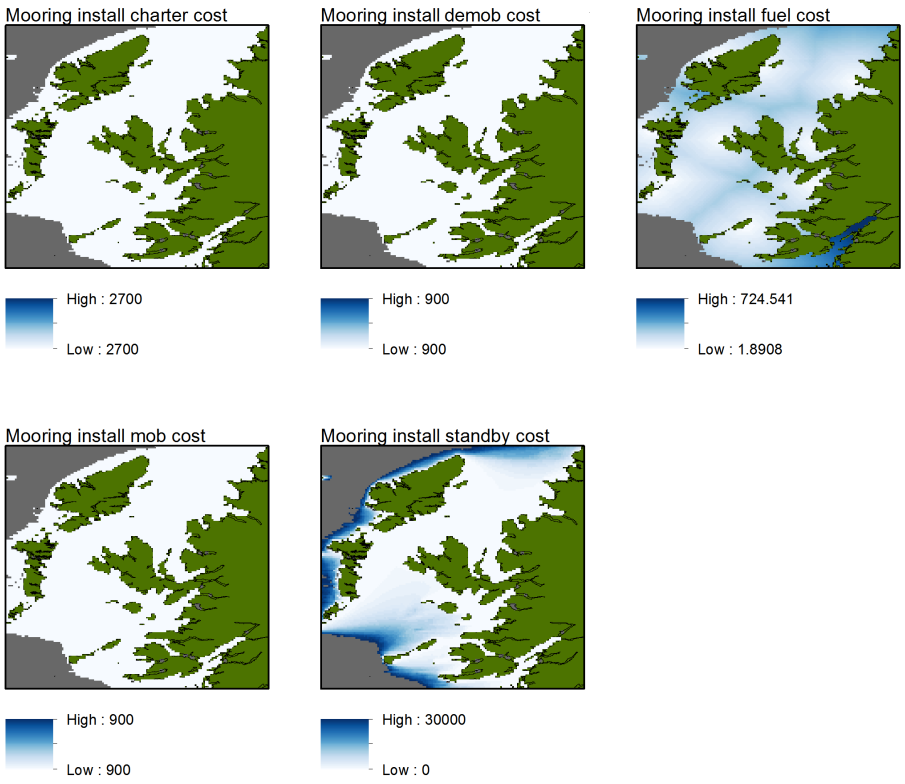

Figure D.3: Costs for the cable installation task from the grid-connected baseline scenario (Section 5.2).

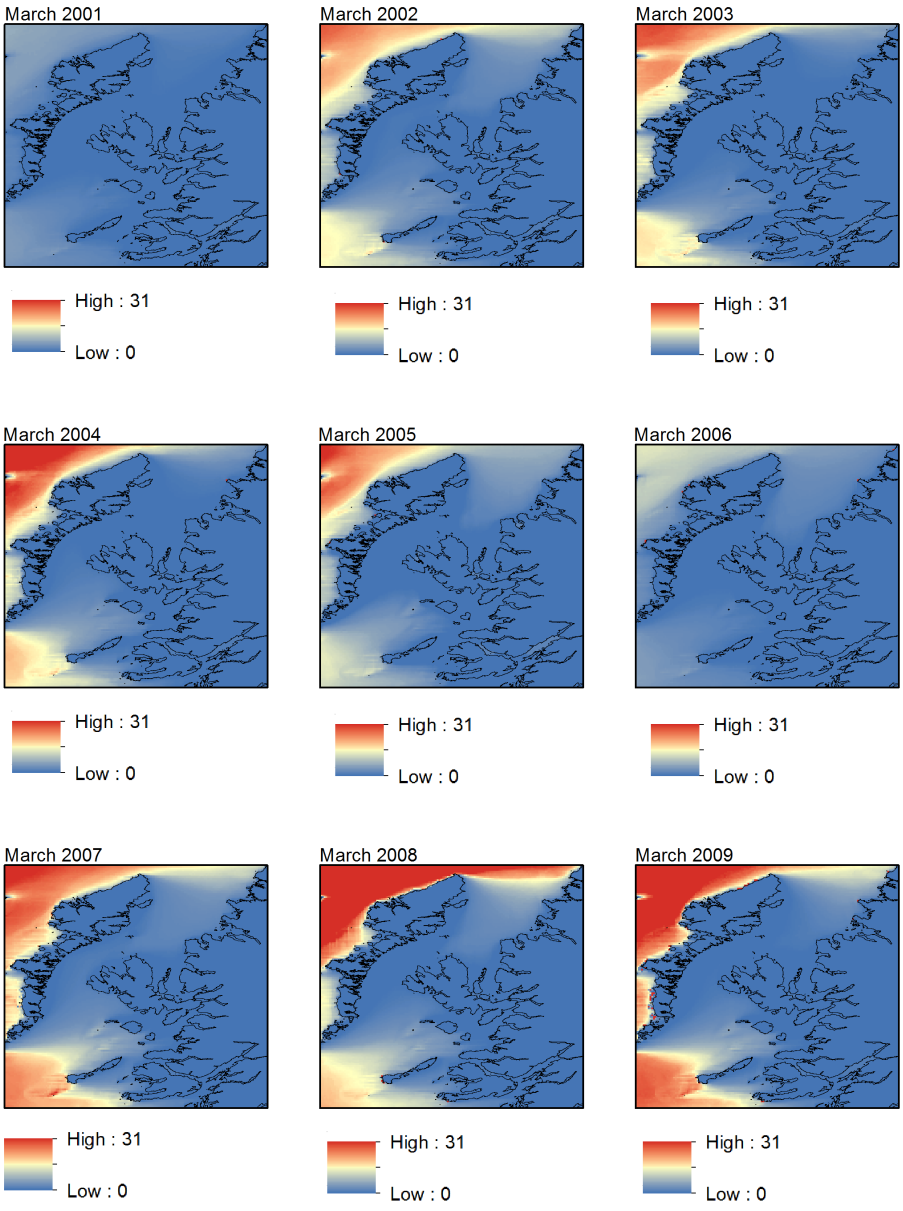

Figure D.4: Weather window durations for the mooring inspection task from the grid-connected baseline scenario (Section 5.2).

Off-grid Case Study Component Datasheets

www.FGWilson.com

P220-1

Image for illustration purposes only.

Output Ratings

Generating Set Model	Prime	Standby
380-415V,50Hz	200.0 kVA / 160.0 kW	220.0 kVA / 176.0 kW
	- / -	- / -

Ratings at 0.8 power factor.

Prime Rating
These ratings are applicable for supplying continuous electrical power (at variable load) in lieu of commercially purchased power. There is no limitation to the annual hours of operation and this model can supply 10% overload power for 1 hour in 12 hours.

Standby Rating
These ratings are applicable for supplying continuous electrical power (at variable load) in the event of a utility power failure. No overload is permitted on these ratings. The alternator on this model is peak continuous rated (as defined in ISO 8528-3).

Standard Reference Conditions
Note: Standard reference conditions 25°C (77°F) Air Inlet Temp, 100m (328 ft) A.S.L. 30% relative humidity.
Fuel consumption data at full load with diesel fuel with specific gravity of 0.85 and conforming to BS2869: 1998, Class A2.

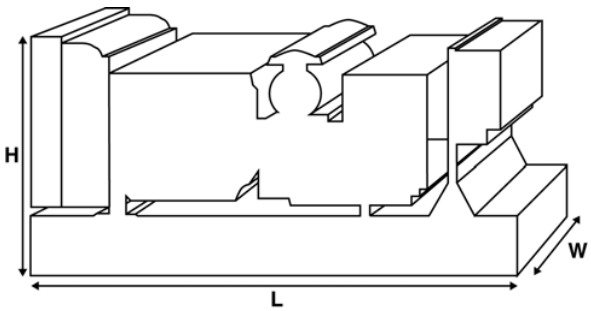

Ratings and Performance Data

Engine Make & Model:		Perkins 1106A-70TAG4	
Alternator manufactured for FG Wilson by:		Leroy Somer	
Alternator Model:		LL5014F	
Control Panel:		DCP-10	
Base Frame:		Heavy Duty Fabricated Steel	
Circuit Breaker Type:		3 Pole MCCB	
Frequency:		**50 Hz**	**60 Hz**
Engine Speed: RPM		1500	-
Fuel Tank Capacity: litres (US gal)		418 (110.4)	
Fuel Consumption: l/hr (US gal/hr)			
(100% Load)	**- Prime**	45.4 (12.0)	-
	- Standby	49.5 (13.1)	-

Available Options

FG Wilson offer a range of optional features to tailor our generating sets to meet your power needs. Options include:

- Upgrade to CE Certification
- A wide range of Sound Attenuated Enclosures
- A variety of generating set control and synchronising panels
- Additional alarms and shutdowns
- A selection of exhaust silencer noise levels

For further information on all of the standard and optional features accompanying this product please contact your local Dealer or visit: www.FGWilson.com

Dimensions and Weights

Length (L) mm (in)	**Width** (W) mm (in)	**Height** (H) mm (in)	**Dry** kg (lb)	**Wet** kg (lb)
2500 (98.4)	1320 (52.0)	1626 (64.0)	1731 (3816)	1758 (3876)

Dry = With Lube Oil Wet = With Lube Oil and Coolant

Ratings in accordance with ISO 8528, ISO 3046, IEC 60034, BS5000 and NEMA MG-1/22.
Generating set pictured may include optional accessories.

FG Wilson has manufacturing facilities in the following locations:
Northern Ireland • Brazil • China • India • USA
With headquarters in Northern Ireland, FG Wilson operates through a Global Dealer Network.

Engine Technical Data	
No. of Cylinders / Alignment:	6 / In Line
Cycle:	4 Stroke
Bore / Stroke: mm (in)	105.0 (4.1)/135.0 (5.3)
Induction:	Turbocharged Air To Air Charge Cooled
Cooling Method:	Water
Governing Type:	Electronic
Governing Class:	ISO 8528 G2
Compression Ratio:	16.0:1
Displacement: l (cu. in)	7.0 (427.8)
Moment of Inertia: kg m² (lb/in²)	1.26 (4306)
Engine Electrical System:	
- Voltage / Ground	12/Negative
- Battery Charger Amps	85
Weight: kg (lb) **- Dry**	788 (1737)
- Wet	822 (1812)

Performance	50 Hz	60 Hz
Engine Speed: rpm	1500	-
Gross Engine Power: kW (hp)		
- Prime	178.9 (240.0)	-
- Standby	196.3 (263.0)	-
BMEP: kPa (psi)		
- Prime	2041.0 (296.0)	-
- Standby	2239.0 (324.7)	-

Fuel System				
Fuel Filter Type:	Replaceable Element			
Recommended Fuel:	Class A2 Diesel			
Fuel Consumption: l/hr (US gal/hr)				
Prime	**110% Load**	**100% Load**	**75% Load**	**50% Load**
50 Hz	49.5 (13.1)	45.4 (12.0)	34.7 (9.2)	23.4 (6.2)
60 Hz	-	-	-	-

Standby	100% Load	75% Load	50% Load
50 Hz	49.5 (13.1)	38.0 (10.0)	25.7 (6.8)
60 Hz	-	-	-

(Based on diesel fuel with a specific gravity of 0.85 and conforming to BS2869, Class A2)

Air Systems	50 Hz	60 Hz
Air Filter Type:	Paper Element	
Combustion Air Flow: m³/min (cfm)		
- Prime	12.6 (445)	-
- Standby	13.2 (466)	-
Max. Combustion Air Intake Restriction: kPa (in H_2O)	8.0 (32.1)	-

Cooling System	50 Hz	60 Hz
Cooling System Capacity: l (US gal)	27.0 (7.1)	-
Water Pump Type:	Centrifugal	
Heat Rejected to Water & Lube Oil:		
kW (Btu/min) **- Prime**	78.2 (4447)	-
- Standby	81.0 (4606)	-
Heat Radiation to Room: Heat radiated from engine and alternator		
kW (Btu/min) **- Prime**	26.0 (1479)	
- Standby	28.3 (1609)	
Radiator Fan Load: kW (hp)	6.3 (8.5)	-
Radiator Cooling Airflow: m³/min (cfm)	307.2 (10849)	-
External Restriction to Cooling Airflow: Pa (in H_2O)	125 (0.5)	-

Designed to operate in ambient conditions up to 50°C (122°F).
Contact your local FG Wilson Dealer for power ratings at specific site conditions.

Lubrication System	
Oil Filter Type:	Spin-On, Full Flow
Total Oil Capacity: l (US gal)	16.5 (4.4)
Oil Pan: l (US gal)	14.9 (3.9)
Oil Type:	API CH4 / CI4 15W-40
Oil Cooling Method:	Water

Exhaust System	50 Hz	60 Hz
Silencer Type:	Industrial	
Silencer Model & Quantity:	SD100 (1)	
Pressure Drop Across Silencer System: kPa (in Hg)	3.50 (1.034)	-
Silencer Noise Reduction Level: dB	10	-
Maximum Allowable Back Pressure: kPa (in Hg)	15.0 (4.4)	-
Exhaust Gas Flow: m³/min (cfm)		
- Prime	34.9 (1232)	-
- Standby	36.8 (1300)	-
Exhaust Gas Temperature: °C (°F)		
- Prime	527 (981)	-
- Standby	580 (1076)	-

Alternator Physical Data	
Manufactured for FG Wilson by:	Leroy Somer
Model:	LL5014F
No. of Bearings:	1
Insulation Class:	H
Winding Pitch Code:	2/3 - 6
Wires:	12
Ingress Protection Rating:	IP23
Excitation System:	SHUNT
AVR Model:	R250

Alternator Operating Data	
Overspeed: rpm	2250
Voltage Regulation: (Steady state)	+/- 0.5%
Wave Form NEMA = TIF:	50
Wave Form IEC = THF:	2.0%
Total Harmonic content LL/LN:	4.0%
Radio Interference:	Suppression is in line with European Standard EN61000-6
Radiant Heat: kW (Btu/min)	
- 50 Hz	15.1 (859)
- 60 Hz	-

Alternator Performance Data:	50 Hz				60 Hz
Data Item	415/240V	400/230V 230/115V 200/115V	380/220V 220/110V	220/127V	
Motor Starting Capability* kVA	414	389	356	457	
Short Circuit Capacity %**	300	300	300	300	
Reactances: Per Unit					
Xd	2.794	3.008	3.330	2.237	
X'd	0.137	0.148	0.163	0.110	
X"d	0.082	0.089	0.098	0.066	

Reactances shown are applicable to prime ratings.
*Based on 30% voltage dip at 0.6 power factor and SHUNT excitation.
**With optional permanent magnet generator.

Voltage Technical Data 50 Hz				
Voltage	**Prime:**		**Standby:**	
	kVA	**kW**	**kVA**	**kW**
415/240V	200.0	160.0	220.0	176.0
400/230V	200.0	160.0	220.0	176.0
380/220V	200.0	160.0	220.0	176.0
230/115V	200.0	160.0	220.0	176.0
220/127V	180.0	144.0	200.0	160.0
220/110V	200.0	160.0	220.0	176.0
200/115V	200,0	160,0	218,0*	174,4*

Voltage Technical Data 60 Hz				
Voltage	**Prime:**		**Standby:**	
	kVA	**kW**	**kVA**	**kW**

*Rating limited by 630A circuit breaker to 218.0 kVA / 174.4 kW.

T-105 DATA SHEET

MODEL: T-105 with Bayonet Cap

VOLTAGE: 6

DIMENSIONS: Inches (mm)

BATTERY: Flooded/wet lead-acid battery

COLOR: Maroon (case/cover)

MATERIAL: Polypropylene

WATERING SYSTEM: HydroLink™ Watering System

T2 Technology

PRODUCT SPECIFICATIONS

BCI GROUP SIZE	TYPE	CAPACITY [A] Minutes		CAPACITY [B] Amp-Hours (AH)				ENERGY (kWh)	TERMINAL Type [E]	DIMENSIONS [C] Inches (mm)			WEIGHT lbs. (kg)
		@25 Amps	@75 Amps	5-Hr Rate	10-Hr Rate	20-Hr Rate	100-Hr Rate	100-Hr Rate		Length	Width	Height [D]	
6 VOLT DEEP CYCLE BATTERY - with T2 TECHNOLOGY™													
GC2	**T-105**	447	115	185	207	225	250	1.50	1, 2, 3, 4	10.30 (262)	7.11 (181)	11.07 (281)	62 (28)

A. The number of minutes a battery can deliver when discharged at a constant rate at 80°F (27°C) and maintain a voltage above 1.75 V/cell. Capacities are based on peak performance.
B. The amount of amp-hours (AH) a battery can deliver when discharged at a constant rate at 80°F (27°C) and 86°F (30°C) for the 5-Hour rate and maintain a voltage above 1.75 V/cell. Capacities are based on peak performance.
C. Dimensions are based on nominal size. Dimensions may vary depending on type of handle or terminal.
D. Dimensions taken from bottom of the battery to the highest point on the battery. Heights may vary depending on type of terminal.
E. Terminal images are representative only.
Trojan's battery testing procedures adhere to both BCI and IEC test standards.

CHARGING INSTRUCTIONS

CHARGER VOLTAGE SETTINGS (AT 77°F/25°C)					
System Voltage	**6V**	**12V**	**24V**	**36V**	**48V**
Absorption Charge	7.40	14.8	29.6	44.4	59.2
Float Charge	6.60	13.2	26.4	39.6	52.8
Equalize Charge	7.75	15.5	31.0	46.5	62.0

Do not install or charge batteries in a sealed or non-ventilated compartment. Constant under or overcharging will damage the battery and shorten its life as with any battery.

CHARGING TEMPERATURE COMPENSATION

.028 VPC for every 10°F (5.55°C) above or below 77°F (25°C) (add .028 VPC for every 10°F (5.55°C) below 77°F and subtract .028 VPC for every 10°C above 77°F).

OPERATIONAL DATA

Operating Temperature	Self Discharge
-4°F to 113°F (-20°C to +45°C). At temperatures below 32°F (0°C) maintain a state of charge greater than 60%.	5 – 15% per month depending on storage temperature conditions.

TERMINAL CONFIGURATIONS

1	ELPT	Embedded Low Profile Terminal
		*Terminal Height Inches (mm)* **1.22 (31)** *Torque Values in-lb (Nm)* **95 – 105 (11 - 12)** *Bolt Size* **5/16"**
2	EHPT	Embedded High Profile Terminal
		*Terminal Height Inches (mm)* **1.50 (38)** *Torque Values in-lb (Nm)* **95 – 105 (11 - 12)** *Bolt Size* **5/16"**
3	EAPT	Embedded Automotive Post Terminal
		*Terminal Height Inches (mm)* **.95 (24)** *Torque Values in-lb (Nm)* **50 – 70 (5.6 - 7.9)**
4	EUT	Embedded Universal Terminal
		*Terminal Height Inches (mm)* **1.10 (28)** *Torque Values in-lb (Nm)* **95 – 105 (11 - 12)** *Bolt* **5/16"**

TRJN_T-105_DS_0315

BATTERY DIMENSIONS (shown with EHPT)

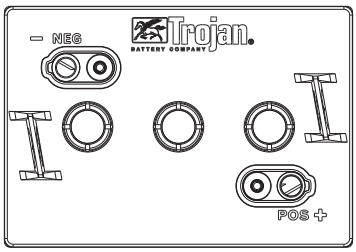

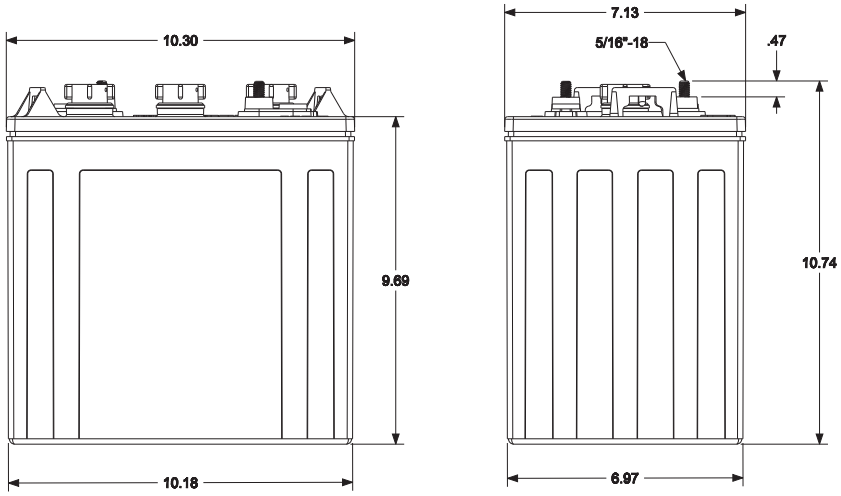

TROJAN T-105 PERFORMANCE

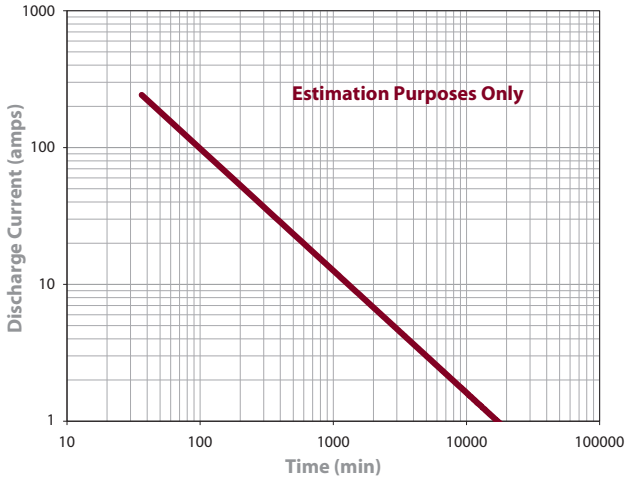

PERCENT CAPACITY VS. TEMPERATURE

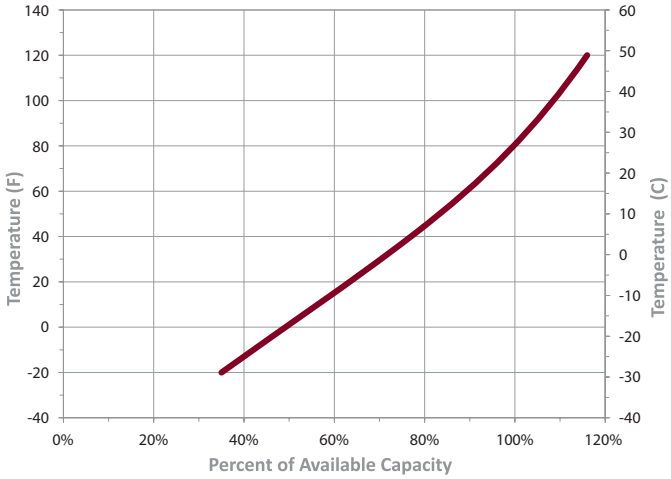

Battery Council International™ IEC MADE IN USA TROJAN BATTERY COMPANY WITH QUALITY SYSTEM CERTIFIED BY DNV =ISO 9001:2008=

Trojan BATTERY COMPANY
Clean energy for life.

Trojan batteries are available worldwide through Trojan's Master Distributor Network.
We offer outstanding technical support, provided by full-time application engineers.

For a Trojan Master Distributor near you,
call 800.423.6569 or + 1.562.236.3000 or visit www.trojanbattery.com

12380 Clark Street, Santa Fe Springs, CA 90670 • USA

© 2015 Trojan Battery Company. All rights reserved. Trojan Battery Company is not liable for damages that may result from any information provided in or omitted from this publication, under any circumstances. Trojan Battery Company reserves the right to make adjustments to this publication at any time, without notices or obligation. Please check the Trojan Battery website (www.trojanBattery.com) for the most up-to-date information.

TRJN_T-105_DS_0315

SUNNY ISLAND 6.0H / 8.0H
FOR OFF-GRID APPLICATIONS

SI6.0H-11 / SI8.0H-11

Easy to use

- OptiUse: fast installation and commissioning, simplified operation
- OptiBat: state of charge calculation keeps you informed at all times

Robust

- IP 54: optimal protection from dust and humidity
- OptiCool: greater temperature range
- OptiPower: secure operation in any situation

Flexible

- For systems from 3 to 300 kW
- Precise design
- Supports Multicluster Technology

SUNNY ISLAND 6.0H / 8.0H

Simple. Robust. Flexible.

More durable than its predecessors: The new Sunny Island impresses with its high protection class and wide temperature range. Moisture, dust and temperature fluctuations won't impair its operation, even after 20 years. Thanks to OptiCool, there's no need to compromise when it comes to overload capacity and economic viability. And there's more: OptiPower, the intelligent load and energy management system, ensures operation even in critical situations. OptiUse makes installation, commissioning and daily use easier than ever with automatic rotary field detection, an optimized quick configuration guide and intuitive operation. And the intelligent OptiBat battery management system automatically controls the most important charging and discharging procedures, which extends the service life of sensitive energy storage. Sunny Island is a truly comprehensive package for a worry-free, reliable and self-sufficient electricity supply.

SUNNY ISLAND 6.0H / 8.0H

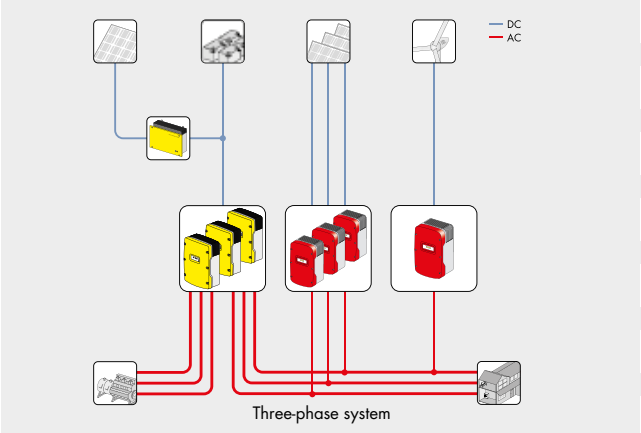

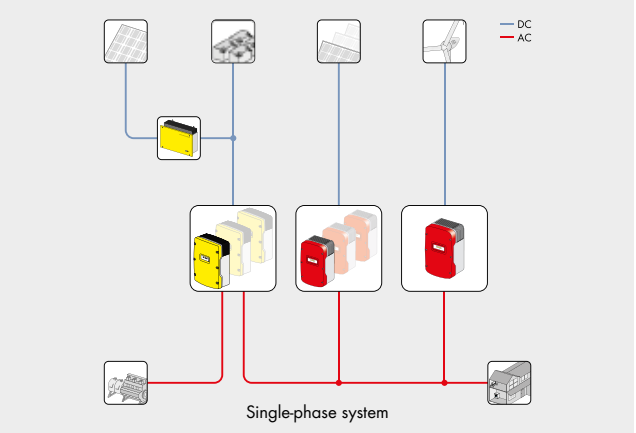

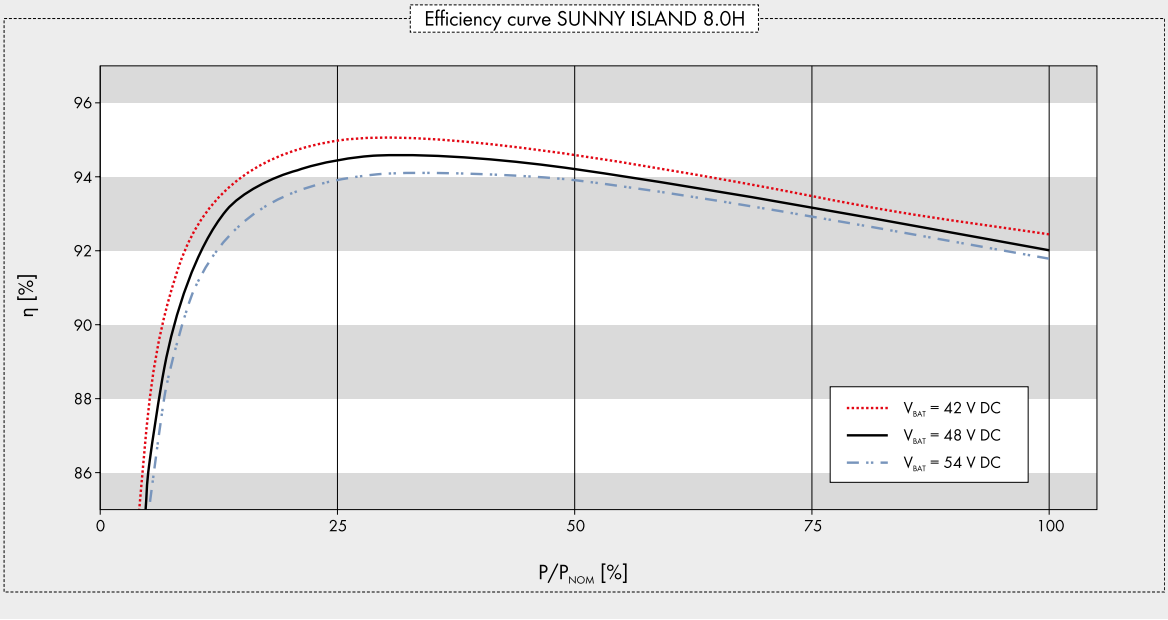

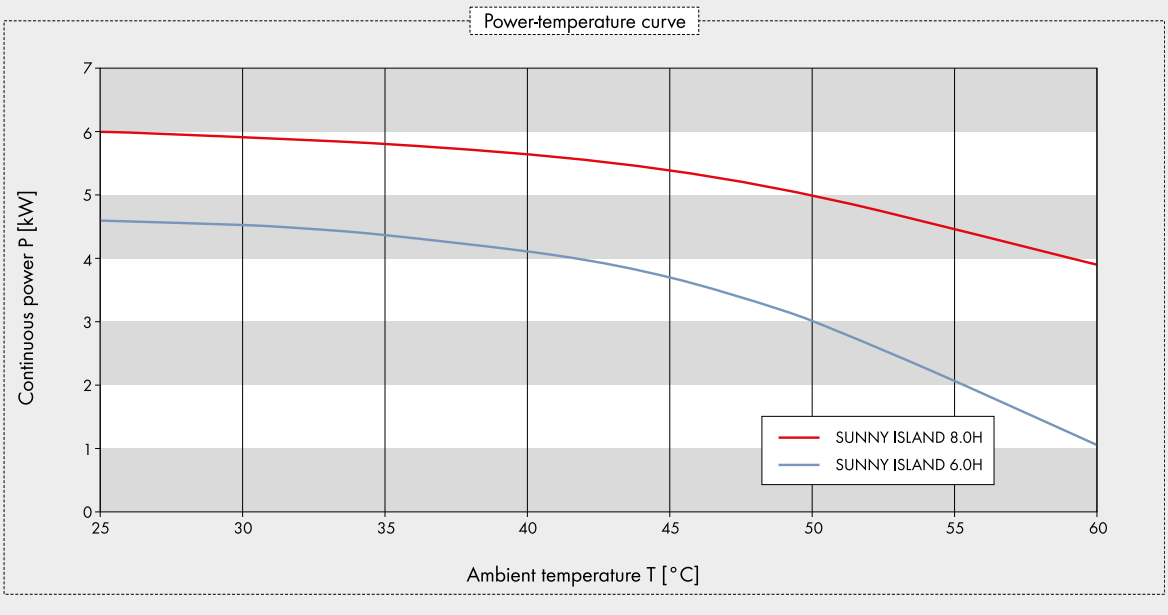

Technical data	Sunny Island 6.0H	Sunny Island 8.0H
AC output (loads / stand-alone grid)		
Rated grid voltage / AC voltage range	230 V / 202 V ... 253 V	230 V / 202 V ... 253 V
Rated frequency / frequency range (adjustable)	50 Hz / 45 Hz ... 65 Hz	50 Hz / 45 Hz ... 65 Hz
Rated power (for Unom / fnom / 25 °C / cos φ = 1)	4600 W	6 000 W
AC power at 25 °C for 30 min / 5 min / 3 sec	6 000 W / 6 800 W / 11 000 W	8 000 W / 9 100 W / 11 000 W
AC power at 45 °C	3 700 W	5 430 W
Rated current / maximum output current (peak)	20 A / 120 A	26 A / 120 A
THD output voltage / power factor with rated power	< 4 % / -1 ... +1	< 4 % / -1 ... +1
AC input (PV array, grid or MC box)		
Rated input voltage / AC input voltage range	230 V / 172.5 V ... 264.5 V	230 V / 172.5 V ... 264.5 V
Rated input frequency / allowable input frequency range	50 Hz / 40 Hz ... 70 Hz	50 Hz / 40 Hz ... 70 Hz
Maximum AC input current	50 A	50 A
Maximum AC input power	11 500 W	11 500 W
Battery DC input		
Rated input voltage / DC voltage range	48 V / 41 V ... 63 V	48 V / 41 V ... 63 V
Maximum battery charging current	110 A	140 A
Rated DC charging current / DC discharging current	90 A / 103 A	115 A / 136 A
Battery type / battery capacity (range)	FLA, VRLA / 100 Ah ... 10 000 Ah	FLA, VRLA / 100 Ah ... 10 000 Ah
Charge control	IUoU charge procedure with automatic full charge and equalization charge.	IUoU charge procedure with automatic full charge and equalization charge
Efficiency / self-consumption		
Maximum efficiency	96 %	96 %
Self-consumption without load / standby	< 26 W / < 4 W	< 26 W / < 4 W
Protective devices (equipment)		
AC short-circuit / AC overload	● / ●	● / ●
DC reverse polarity protection / DC fuse	– / –	– / –
Overtemperature / battery deep discharge	● / ●	● / ●
Overvoltage category as per IEC 60664-1	III	III
General data		
Dimensions (width x height x depth)	467 mm x 612 mm x 242 mm	467 mm x 612 mm x 242 mm
Priority	63 kg	63 kg
Operating temperature range	-25 °C ... +60 °C	-25 °C ... +60 °C
Protection class according to IEC 62103	I	I
Climatic category according to IEC 60721	3K6	3K6
Degree of protection according to IEC 60529	IP54	IP54
Features / function		
Operation and display / multifunction relay	External via SRC-20 / 2	External via SRC-20 / 2
Three-phase systems / parallel connection	● / ●	● / ●
Integrated bypass / multicluster operation	– / ●	– / ●
State of charge calculation / full charge / equalization charge	● / ● / ●	● / ● / ●
Integrated soft start / generator support	● / ●	● / ●
Battery temperature sensor / data cables	● / ●	● / ●
Certificates and approvals	www.SMA-Solar.com	www.SMA-Solar.com
Warranty: 5 years	●	●
Accessory		
Battery cable / battery fuse	o / o	o / o
Interface SI-COMSMA (RS485) / SI-SYSCAN (Multicluster)	o / o	o / o
Extended generator start "GenMan"	o	o
Load-shedding contactor / battery current measurement	o / o	o / o
Type designation	SI6.0H-11	SI8.0H-11

● Standard features o Optional features – Not available

Data at nominal conditions

MULTICLUSTER-BOXES for SUNNY ISLAND 5048

Flexible

- Three different power ranges from 30 kW to 300 kW
- Different generators, PV and load magnitudes

Simple

- Integrated AC distribution for Sunny Island, generator, PV
- Integrated load-shedding contactor

Reliable

- Automatic bypass for the generator
- Active Anti-Islanding
- Reverse current monitoring

Durable

- High protection class IP65
- 5-year SMA warranty

Multicluster Boxes for SUNNY ISLAND 5048

For Easy Set-Up of Stand-Alone and Hybrid Systems

The Multicluster Boxes for Sunny Island 5048 enable the formation of off-grid and hybrid systems with a capacity of between 30 and 300 kW. As the main AC distribution for the connection of generators and to supply loads of up to 300 kW, between two and 12 three-phase clusters, each consisting of three Sunny Island inverters, can be connected in parallel using the Multicluster Box. To simplify installation, all Multicluster Boxes are completely wired and fitted at the factory and have a main connector for PV plants or wind turbine systems. All communication cables required for the installation are included in the delivery.

MULTICLUSTER BOXES for SUNNY ISLAND 5048

Technical Data	SUNNY ISLAND 5048 Multicluster Box 6	SUNNY ISLAND 5048 Multicluster Box 12
General		
Phase number	3-phase	3-phase
Nominal AC voltage	230 V (L, N), 400 V (L1, L2)	230 V (L, N), 400 V (L1, L2)
AC voltage range	172.5 V – 265 V 300 V – 433 V	172.5 V – 265 V 300 V – 433 V
Nominal AC frequency / range	50 Hz / 40 Hz ... 70 Hz	50 Hz / 40 Hz ... 70 Hz
Reliable grid configuration	TN	TN
Dimensions (W / H / D)	760 / 760 / 210 mm	1000 / 1400 / 300 mm
Assembly type	Suspended	Standing on base
Weight	60 kg	140 kg
Terminals for Sunny Island		
Maximum number of devices	6	12
Nominal AC power / nominal AC current at 25 °C	30 kW / 3 x 44 A	60 kW / 3 x 87 A
Nominal AC power / nominal AC current at 45 °C	24 kW / 3 x 35 A	48 kW / 3 x 70 A
AC power (25 °C, 30 minutes)	40 kW	80 kW
AC power (25 °C, 1 minute)	50 kW	100 kW
Fuses	Miniature circuit-breaker C 32A	Miniature circuit-breaker C 32A
Load connection		
Number	1 (3-phase)	1 (3-phase)
Nominal AC power (25 °C, unlimited)	55 kW	110 kW
Nominal AC current (25 °C)	3 x 80 A	3 x 160 A
Fuses	LV / HRC (size 00)	LV / HRC (size 00)
PV plant connection		
Number	1 (3-phase)	1 (3-phase)
Nominal AC power (25 °C, unlimited)	55 kW	110 kW
Nominal AC current (25 °C)	3 x 80 A	3 x 160 A
Fuses	–	–
Generator connection		
Number	1 (3-phase)	1 (3-phase)
Nominal AC power (25 °C, unlimited)	55 kW	110 kW
Nominal AC current (25 °C)	3 x 80 A	3 x 160 A
Fuses	LV / HRC (size 00)	LV / HRC (size 00)
Features		
Warranty (5 / 10 / 15 / 20 / 25 years)	● / ○ / ○ / ○ / ○	● / ○ / ○ / ○ / ○
Certificates	CE	CE
Ambient conditions		
Ambient temperature	-25 °C ... +50 °C	-25 °C ... +50 °C
Degree of protection (according to IEC 60529)	IP65	IP65
Humidity	0 % ... 100 %	0 % ... 100 %
Accessories		
Communication lines	●	●
Multicluster Piggy-Back	○	○
● Standard features ○ Optional – Not available		
Type designation	MC-BOX-6.3	MC-BOX-12.3

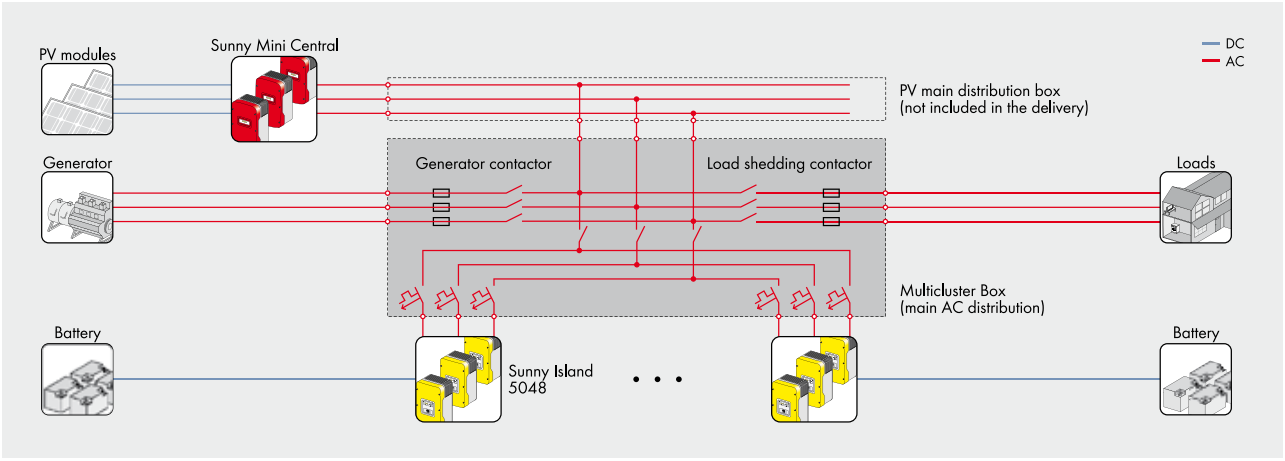

Technical Data	SUNNY ISLAND 5048 Multicluster Box 36	
General		
Phase number	3-phase	
Nominal AC voltage	230 V (L, N), 400 V (L1, L2)	
AC voltage range	172.5 V – 250 V 300 V – 433 V	
Nominal AC frequency / range	50 Hz / 40 Hz ... 70 Hz	
Reliable grid configuration	TN	
Dimensions (W / H / D)	1200 / 2000 / 800 mm	
Assembly type	Standing on base	
Weight	400 kg	
Terminals for Sunny Island		
Maximum number of devices	36	
Nominal AC power / nominal AC current at 25 °C	180 kW / 3 x 260 A	
Nominal AC power / nominal AC current at 45 °C	144 kW / 3 x 209 A	
AC power (25 °C, 30 minutes)	234 kW / 3 x 340 A	
AC power (25 °C, 1 minute)	300 kW / 3 x 440 A	
Fuses	Miniature circuit-breaker C 32A	
Load connection		
Number	1 (3-phase)	
Nominal AC power (25 °C, unlimited)	300 kW	
Nominal AC current (25 °C)	3 x 435 A (AC1)	
Fuses	LV / HRC (size 3)	
PV plant connection		
Number	1 (3-phase)	
Nominal AC power (25 °C, unlimited)	300 kW	
Nominal AC current (25 °C)	3 x 435 A (AC1)	
Fuses	–	
Generator connection		
Number	1 (3-phase)	
Nominal AC power (25 °C, unlimited)	300 kW	
Nominal AC current (25 °C)	3 x 435 A (AC1)	
Fuses	LV / HRC (size 3)	
Features		
Warranty (5 / 10 / 15 / 20 / 25 years)	● / ○ / ○ / ○ / ○	
Certificates	CE	
Ambient conditions		
Ambient temperature	-25 °C ... +60 °C	
Degree of protection (according to IEC 60529)	IP54	
Humidity	0 % ... 100 %	
Accessories		
Communication lines	●	
Multicluster Piggy-Back	○	
● Standard features ○ Optional – Not available		
Type designation	MC-BOX-36.3	